SYLVAIN CHAUVETTE

SLOW-WAVE SLEEP: GENERATION AND PROPAGATION OF SLOW WAVES, ROLE IN LONG-TERM PLASTICITY AND GATING

Thèse présentée
à la Faculté des études supérieures et postdoctorales de l'Université Laval
dans le cadre du programme de doctorat en Neurobiologie
pour l'obtention du grade de Philosophiae Doctor (Ph.D.)

DÉPARTEMENT DE PSYCHIATRIE ET DE NEUROSCIENCES
FACULTÉ DE MÉDECINE
UNIVERSITÉ LAVAL
QUÉBEC

2013

Résumé

Le sommeil est connu pour réguler plusieurs fonctions importantes pour le cerveau et parmi celles-ci, il y a le blocage de l'information sensorielle par le thalamus et l'amélioration de la consolidation de la mémoire. Le sommeil à ondes lentes, en particulier, est considéré être critique pour ces deux processus. Cependant, leurs mécanismes physiologiques sont inconnus. Aussi, la marque électrophysiologique distinctive du sommeil à ondes lentes est la présence d'ondes lentes de grande amplitude dans le potentiel de champ cortical et l'alternance entre des périodes d'activités synaptiques intenses pendant lesquelles les neurones corticaux sont dépolarisés et déchargent plusieurs potentiels d'action et des périodes silencieuses pendant lesquelles aucune décharge ne survient, les neurones corticaux sont hyperpolarisés et très peu d'activités synaptiques sont observées. Tout d'abord, afin de mieux comprendre les études présentées dans ce manuscrit, une introduction générale couvrant l'architecture du système thalamocortical et ses fonctions est présentée. Celle-ci comprend une description des états de vigilance, suivie d'une description des rythmes présents dans le système thalamocortical au cours du sommeil à ondes lentes, puis par une description des différents mécanismes de plasticité synaptique, et enfin, deux hypothèses sur la façon dont le sommeil peut affecter la consolidation de la mémoire sont présentées.

Puis, trois études sont présentées et ont été conçues pour caractériser les propriétés de l'oscillation lente du sommeil à ondes lentes. Dans la première étude (chapitre II), nous avons montré que les périodes d'activité (et de silence) se produisent de façon presque synchrone dans des neurones qui ont jusqu'à 12 mm de distance. Nous avons montré que l'activité était initiée en un point focal et se propageait rapidement à des sites corticaux voisins. Étonnamment, le déclenchement des états silencieux était encore plus synchronisé que le déclenchement des états actifs.

L'hypothèse de travail pour la deuxième étude (chapitre III) était que les états actifs sont générés par une sommation de relâches spontanées de médiateurs. Utilisant différents enregistrements à la fois chez des animaux anesthésiés et chez d'autres non-anesthésiés, nous avons montré qu'aucune décharge neuronale ne se produit dans le néocortex pendant les états silencieux du sommeil à ondes lentes, mais certaines activités synaptiques peuvent

être observées avant le début des états actifs, ce qui était en accord avec notre hypothèse. Nous avons également montré que les neurones de la couche V étaient les premiers à entrer dans l'état actif pour la majorité des cycles, mais ce serait ainsi uniquement pour des raisons probabilistes; ces cellules étant équipées du plus grand nombre de contacts synaptiques parmi les neurones corticaux. Nous avons également montré que le sommeil à ondes lentes et l'anesthésie à la kétamine-xylazine présentent de nombreuses similitudes.

Ayant utilisé une combinaison d'enregistrements chez des animaux anesthésiés à la kétamine-xylazine et chez des animaux non-anesthésiés, et parce que l'anesthésie à la kétamine-xylazine est largement utilisée comme un modèle de sommeil à ondes lentes, nous avons effectué des mesures quantitatives des différences entre les deux groupes d'enregistrements (chapitre IV). Nous avons trouvé que l'oscillation lente était beaucoup plus rythmique sous anesthésie et elle était aussi plus cohérente entre des sites d'enregistrements distants en comparaison aux enregistrements de sommeil naturel. Sous anesthésie, les ondes lentes avaient également une amplitude plus grande et une durée plus longue par rapport au sommeil à ondes lentes. Toutefois, les ondes fuseaux (spindles) et gamma étaient également affectées par l'anesthésie.

Dans l'étude suivante (Chapitre V), nous avons investigué le rôle du sommeil à ondes lentes dans la formation de la plasticité à long terme dans le système thalamocortical. À l'aide de stimulations pré-thalamiques de la voie somatosensorielle ascendante (fibres du lemnisque médial) chez des animaux non-anesthésiés, nous avons montré que le potentiel évoqué enregistré dans le cortex somatosensoriel était augmenté dans une période d'éveil suivant un épisode de sommeil à ondes lentes par rapport à l'épisode d'éveil précédent et cette augmentation était de longue durée. Nous avons également montré que le sommeil paradoxal ne jouait pas un rôle important dans cette augmentation d'amplitude des réponses évoquées. À l'aide d'enregistrements *in vitro* en mode cellule-entière, nous avons caractérisé le mécanisme derrière cette augmentation et ce mécanisme est compatible avec la forme classique de potentiation à long terme, car il nécessitait une activation à la fois les récepteurs NMDA et des récepteurs AMPA, ainsi que la présence de calcium dans le neurone post-synaptique.

La dernière étude incluse dans cette thèse (chapitre VI) a été conçue pour caractériser un possible mécanisme physiologique de blocage sensoriel thalamique survenant pendant le sommeil. Les ondes fuseaux sont caractérisées par la présence de potentiels d'action calcique à seuil bas et le calcium joue un rôle essentiel dans la transmission synaptique. En utilisant plusieurs techniques expérimentales, nous avons vérifié l'hypothèse que ces potentiels d'action calciques pourraient causer un appauvrissement local de calcium dans l'espace extracellulaire ce qui affecterait la transmission synaptique. Nous avons montré que les canaux calciques responsables des potentiels d'action calciques étaient localisés aux synapses et que, de fait, une diminution locale de la concentration extracellulaire de calcium se produit au cours d'un potentiel d'action calcique à seuil bas spontané ou provoqué, ce qui était suffisant pour nuire à la transmission synaptique.

Nous concluons que l'oscillation lente est initiée en un point focal et se propage ensuite aux aires corticales voisines de façon presque synchrone, même pour des cellules séparées par jusqu'à 12 mm de distance. Les états actifs de cette oscillation proviennent d'une sommation de relâches spontanées de neuromédiateurs (indépendantes des potentiels d'action) et cette sommation peut survenir dans tous neurones corticaux. Cependant, l'état actif est généré plus souvent dans les neurones pyramidaux de couche V simplement pour des raisons probabilistes. Les deux types d'expériences (kétamine-xylazine et sommeil à ondes lentes) ont montré plusieurs propriétés similaires, mais aussi quelques différences quantitatives. Nous concluons également que l'oscillation lente joue un rôle essentiel dans l'induction de plasticité à long terme qui contribue très probablement à la consolidation de la mémoire. Les ondes fuseaux, un autre type d'ondes présentes pendant le sommeil à ondes lentes, contribuent au blocage thalamique de l'information sensorielle.

Abstract

Sleep is known to mediate several major functions in the brain and among them are the gating of sensory information during sleep and the sleep-related improvement in memory consolidation. Slow-wave sleep in particular is thought to be critical for both of these processes. However, their physiological mechanisms are unknown. Also, the electrophysiological hallmark of slow-wave sleep is the presence of large amplitude slow waves in the cortical local field potential and the alternation of periods of intense synaptic activity in which cortical neurons are depolarized and fire action potentials and periods of silence in which no firing occurs, cortical neurons are hyperpolarized, and very little synaptic activities are observed. First, in order to better understand the studies presented in this manuscript, a general introduction covering the thalamocortical system architecture and function is presented, which includes a description of the states of vigilance, followed by a description of the rhythms present in the thalamocortical system during slow-wave sleep, then by a description of the mechanisms of synaptic plasticity, and finally two hypotheses about how sleep might affect the consolidation of memory are presented.

Then, three studies are presented and were designed to characterize the properties of the sleep slow oscillation. In the first study (Chapter II), we showed that periods of activity (and silence) occur almost synchronously in neurons that are separated by up to 12 mm. The activity was initiated in a focal point and rapidly propagated to neighboring sites. Surprisingly, the onsets of silent states were even more synchronous than onsets of active states.

The working hypothesis for the second study (Chapter III) was that active states are generated by a summation of spontaneous mediator releases. Using different recordings in both anesthetized and non-anesthetized animals, we showed that no neuronal firing occurs in the neocortex during silent states of slow-wave sleep but some synaptic activities might be observed prior to the onset of active states, which was in agreement with our hypothesis. We also showed that layer V neurons were leading the onset of active states in most of the cycles but this would be due to probabilistic reasons; these cells being equipped with the most numerous synaptic contacts among cortical neurons. We also showed that slow-wave sleep and ketamine-xylazine shares many similarities.

Having used a combination of recordings in ketamine-xylazine anesthetized and non-anesthetized animals, and because ketamine-xylazine anesthesia is extensively used as a model of slow-wave sleep, we made quantitative measurements of the differences between the two groups of recordings (Chapter IV). We found that the slow oscillation was much more rhythmic under anesthesia and it was also more coherent between distant sites as compared to recordings during slow-wave sleep. Under anesthesia, slow waves were also of larger amplitude and had a longer duration as compared to slow-wave sleep. However, spindles and gamma were also affected by the anesthesia.

In the following study (Chapter V), we investigated the role of slow-wave sleep in the formation of long-term plasticity in the thalamocortical system. Using pre-thalamic stimulations of the ascending somatosensory pathway (medial lemniscus fibers) in non-anesthetized animals, we showed that evoked potential recorded in the somatosensory cortex were enhanced in a wake period following a slow-wave sleep episode as compared to the previous wake episode and this enhancement was long-lasting. We also showed that rapid eye movement sleep did not play a significant role in this enhancement of response amplitude. Using whole-cell recordings *in vitro*, we characterized the mechanism behind this enhancement and it was compatible with the classical form of long-term potentiation, because it required an activation of both NMDA and AMPA receptors as well as the presence of calcium in the postsynaptic neuron.

The last study included in this thesis (Chapter VI) was designed to characterise a possible physiological mechanism of thalamic sensory gating occurring during sleep. Spindles are characterized by the presence of low-threshold calcium spikes and calcium plays a critical role in the synaptic transmission. Using several experimental techniques, we verified the hypothesis that these calcium spikes would cause a local depletion of calcium in the extracellular space which would impair synaptic transmission. We showed that calcium channels responsible for calcium spikes were co-localized with synapses and that indeed, local extracellular calcium depletion occurred during spontaneous or induced low-threshold calcium spike, which was sufficient to impair synaptic transmission.

We conclude that slow oscillation originate at a focal point and then propagate to neighboring cortical areas being almost synchronous even in cells located up to 12 mm

apart. Active states of this oscillation originate from a summation of spike-independent mediator releases that might occur in any cortical neurons, but happens more often in layer V pyramidal neurons simply due to probabilistic reasons. Both experiments in ketamine-xylazine anesthesia and non-anesthetized animals showed several similar properties, but also some quantitative differences. We also conclude that slow oscillation plays a critical role in the induction of long-term plasticity, which very likely contributes to memory consolidation. Spindles, another oscillation present in slow-wave sleep, contribute to the thalamic gating of information.

Foreword

The following thesis is presented as a collection of scientific articles published, submitted for publication, or in final steps prior to submission. The first chapter is composed of a general introduction describing the theoretical concepts and experimental strategies that were used in the presented studies. Then the core of this thesis is represented by five scientific articles and the first three articles focus on the slow oscillation found either during natural slow-wave sleep or under ketamine-xylazine anesthesia. We describe the mechanisms of generation and propagation of this type of oscillation. Out of the two other studies composing the core of this thesis, one is about the synaptic plasticity induced by the slow oscillation of slow-wave sleep, and the last article presents a mechanism of thalamic gating during another type of sleep oscillation, namely the spindle, which is also present during slow-wave sleep. A brief review of the main results and a general discussion finalizes this thesis. The bibliography used for both the general introduction and the general discussion is presented at the very end of the thesis, while the bibliography for each articles (chapter II-VI) is presented at the end of the text of the corresponding paper, with a formatting of the reference list in accordance to the rules of the journal where the paper was published or submitted.

I would like to take the opportunity to express my gratitude to my thesis supervisor, Prof. Igor Timofeev, who, about ten years ago, trusted me enough to give me the opportunity to work in his lab as an undergraduate student although my marks were rather low at that time. Since then, a fruitful collaboration developed and our productivity gave me the opportunity to get fellowships from different organisms during both my master [Centre de Recherche en Neuroscience (CRN)] and my PhD [Savoy Foundation (refused) and Canadian Institutes of Health Research (CIHR)], and to publish several studies. It also gave me the opportunity to receive four excellence prices for different poster presentations (2003, 2004, 2007, and 2012) and a travel award for the Federation of European Neuroscience Societies (FENS) forum held in Amsterdam (2010). Without his critics, discussions, and support, these studies would not have been possible.

I would also like to thank Prof. Maxim Volgushev, Prof. Maxim Bazhenov, Josée Seigneur, Sofiane Boucetta, Sylvain Crochet, Mikhail Mukovski, Francis Lajeunesse, Alex

Ferescko, Kriszta Kovacs, Laszlo Grand, Courtney Pinard, and Maxime Lemieux for their great collaboration that resulted in several completed studies that are already published or will be soon submitted for publication. I would like to thank Pierre Giguère (now retired) and Sergiu Ftomov for their excellent technical support. I would also like to thank all my colleagues during these almost ten years in this lab with whom, even if we did not have official scientific collaboration per se, we had several fruitful and nice discussions that really help in improving my studies.

Following, is the chronological list of scientific publications (published or submitted) in which I have contributed during the progress of my postgraduate studies:

1. Crochet S, **Chauvette** S, Boucetta S, Timofeev I (2005) Modulation of synaptic transmission in neocortex by network activities. The European journal of neuroscience 21:1030-1044.

2. Volgushev M, **Chauvette** S, Mukovski M, Timofeev I (2006) Precise long-range synchronization of activity and silence in neocortical neurons during slow-wave oscillations [corrected]. J Neurosci 26:5665-5672.

3. Mukovski M, **Chauvette** S, Timofeev I, Volgushev M (2007) Detection of active and silent states in neocortical neurons from the field potential signal during slow-wave sleep. Cereb Cortex 17:400-414.

4. **Chauvette** S, Volgushev M, Mukovski M, Timofeev I (2007) Local origin and long-range synchrony of active state in neocortex during slow oscillation. In: Mechanisms of spontaneous active states in the neocortex (Timofeev I, ed), pp 73-92. Kerala, India: Research Signpost.

5. Volgushev M, Mukovski M, **Chauvette** S, Timofeev I (2007) Detection of active and silent states in neocortical networks. In: Mechanisms of spontaneous active states in the neocortex (Timofeev I, ed), pp 93-122. Kerala, India: Research Signpost.

6. Boucetta S, **Chauvette** S, Bazhenov M, Timofeev I (2008) Focal generation of paroxysmal fast runs during electrographic seizures. Epilepsia 49:1925-1940.

7. **Chauvette** S, Volgushev M, Timofeev I (2010) Origin of Active States in Local Neocortical Networks during Slow Sleep Oscillation. Cerebral Cortex 20:2660-2674.

8. **Chauvette** S, Crochet S, Volgushev M, Timofeev I (2011) Properties of Slow Oscillation during Slow-Wave Sleep and Anesthesia in Cats. The Journal of Neuroscience 31:14998-15008.

9. Timofeev I, **Chauvette** S (2011) Thalamocortical Oscillations: Local Control of EEG Slow Waves. Current Topics in Medicinal Chemistry 11:2457-2471.

10. Volgushev M, **Chauvette** S, Timofeev I (2011) Long-range correlation of the membrane potential in neocortical neurons during slow oscillation. In: Progress in Brain Research (Van Someren EJW, Van Der Werf YD, Roelfsema PR, Mansvelder HD, Lopes Da Silva FH, eds), pp 181-199: Elsevier.

11. Chen J-Y, **Chauvette** S, Skorheim S, Timofeev I, Bazhenov M (2012) Interneuron-mediated inhibition synchronizes neuronal activity during slow oscillation. The Journal of physiology 590:3987-4010.

12. **Chauvette**, S, Seigneur J, Timofeev I (2012) Sleep Oscillations in the Thalamocortical System Induce Long-Term Neuronal Plasticity. Neuron 75(6): 1105-1113.

13. Boucetta S, Crochet S, **Chauvette** S, Seigneur J, Timofeev I (in press) Extracellular Ca^{2+} fluctuations in vivo affect afterhyperpolarization potential and modify firing patterns of neocortical neurons. Experimental Neurology

14. Ferecsko AS, Seigneur J, **Chauvette** S, Kovacs K, Lajeunesse F, Sik A, Timofeev I (in preparation for submission) Low-threshold calcium spike dependent gating in thalamus.

Cette thèse est dédiée à mon père, Marcel Chauvette, qui a toujours cru en moi et m'a toujours soutenu dans les moments plus difficiles et à ma sœur, Chantal Chauvette, malheureusement décédée beaucoup trop jeune, mais qui malgré tout, demeure encore aujourd'hui une source quotidienne de courage et d'inspiration.

Table of Contents

List of figures

Chapter I

Chapter II

Chapter III

Chapter IV

Chapter V

Chapter VI

Chapter VII

List of abbreviations

ACSF	Artificial cerebro-spinal fluid
AMPA	alpha-amino-3-hydroxy-5-methyl-4-isoxazolepropionic acid
EEG	Electroencephalogram
EMG	Electromyogram
EOG	Electro-oculogram
EPSP	Excitatory postsynaptic potential
FRB	Fast-rhythmic-bursting
FS	Fast-Spiking
GABA	Gamma-amino butyric acid
IB	Intrinsically-bursting
I_h	Hyperpolarization-activated cation current
I_{leak}	Potassium leak current
IPSP	Inhibitory postsynaptic potential
I_T	Low-threshold calcium current
LDT	Laterodorsal tegmental nucleus
LFP	Local field potential
LTD	Long-term depression
LTP	Long-term potentiation
LTS	Low-threshold calcium spike
NMDA	N-Methyl-D-aspartic acid
PPT	pedunculopontine tegmental nucleus
RE	Thalamic reticular nucleus
REM	Rapid eye movement
RS	Regular-spiking
sAHP	Short afterhyperpolarization
SWS	Slow-wave sleep
TC	Thalamocortical

Chapter I

1.0 General introduction

This first chapter is a general introduction to the concepts and findings that will be described in the following chapters. First a description of the architecture of the thalamocortical system, which is composed of the thalamus, the thalamic reticular nucleus, and the neocortex, will be provided. Then the electrographic activities during the three states of vigilance (wake, rapid-eye-movement sleep, and slow-wave sleep) will be briefly described with a focus in describing the thalamocortical oscillations occurring during slow-wave sleep. Subsequently, a section will be dedicated at describing the different forms of synaptic plasticity, and finally, the last section will be presenting two hypotheses about the mechanisms of plasticity related to states of vigilances, their possible role in learning and memory.

1.1 Architecture of thalamocortical system

The thalamocortical (TC) system is the site of generation of many different types of oscillatory rhythms with distinct mechanisms. The TC network is organised in a loop (Fig. I.1) where three structures are implicated: the dorsal thalamus, the thalamic reticular nucleus (RE), and the neocortex. The complete organisation will be discussed in details in the following sections, but briefly, the thalamus receives information from ascending pathway and gives glutamatergic projections to both the neocortex and the thalamic reticular nucleus. The neocortex processes the information received and send glutamatergic axons to both TC and RE neurons, but with a greater impact on RE neurons. Then RE neurons send GABAergic projections to TC cells.

1.1.1 Thalamus

The thalamus of different mammals is composed of TC relay neurons, some (20-30 %) local inhibitory interneurons, and glial cells, however for rodents, interneurons would be present only in the lateral geniculate nucleus (visual thalamus). It is composed of *specific* and *non-specific* nuclei. The *specific* nuclei relay information from periphery and

project mainly to a given cortical region, while *non-specific* nuclei have widespread cortical projections.

The dorsal thalamus is composed of multiple *specific* nuclei and it receives information from ascending sensory pathway such as medial lemniscus for somatosensory information, optic tract for visual information, inferior colliculus for auditory information, brachium conjunctivum for motor information from cerebellum. The dorsal thalamus also receives information from the brainstem modulatory systems (cholinergic, norepinephrinergic, serotoninergic, etc.) (reviewed in (Steriade et al., 1997)). Typically, for thalamic relay neurons, ascending pathways (driving inputs) form large synapses with multiple release sites on proximal dendrites, while cortico-thalamic projections (modulator inputs) preferentially arrive to distal dendrites (Liu et al., 1995a; Sherman, 2005). The same logic applies for higher order thalamic nuclei, however with an inverse role where corticothalamic inputs from cortical layer V become the driving inputs that project on proximal dendrites and other inputs arriving mainly on distal dendrites (Sherman, 2005). An example of that is seen for layer Vb neurons of somatosensory (barrel) cortex that form giant synapses on proximal dendrites of thalamic neurons of the posteromedial nucleus (POm) (Groh et al., 2008). Two different chemically defined types of TC neurons have been described, which are the calbindin and parvalbumin containing TC neurons (reviewed in (Jones, 2001)). Parvalbumin-containing TC neurons project in a topographically ordered fashion to layer IV of the cortex and form the thalamic *core* projections, while calbindin-containing TC neurons have widespread projections to superficial cortical layers (mainly layer I) which are not limited by cortical areas boundaries; these projections represent the thalamic *matrix* projections (reviewed in (Jones, 2001)). While calbindin-positive TC neurons are found in all thalamic nuclei, parvalbumin-positive are found in much higher concentration in specific TC nuclei (Jones, 2001).

Thalamocortical neurons are not interconnected by chemical synapses, but one study suggests the presence of gap junctions (electrical synapses) between TC neurons in cats (Hughes et al., 2002). Electrophysiologically, TC neurons possess some characteristic features. They are equipped with low-threshold calcium current (I_T) which needs

hyperpolarisation for a certain amount of time (80-150 ms) to deinactivate (Llinas and Jahnsen, 1982; Jahnsen and Llinas, 1984). TC neurons also possess a hyperpolarisation-activated depolarizing current (I_h) (McCormick and Pape, 1990). Those currents are important for the generation of intrinsic delta rhythm (described in a following section). They are also important to characterise the two firing mode of TC neurons, which are tonic firing and bursting. When TC neurons are depolarised either by a current injection or by the presence of some neuromodulators (acetylcholine, noradrenaline, serotonin), they start to fire action potential, and the more these neurons are depolarised, the more they fire; this is the tonic mode (McCormick, 1992). However, when TC neurons are hyperpolarised sufficiently, either via intracellular current injection or by active inhibition, I_h is activated and the neuron starts to depolarise to a point where I_T is also activated. The activation of this current leads to low-threshold calcium spike (LTS) and on top of this calcium spike, usually many sodium action potentials (up to 7) take place at high frequencies (up to 250 Hz). Thus TC neurons can transmit information following either excitation, where they fire in tonic mode or at the end of inhibition where they respond with a LTS in the bursting mode.

1.1.2 Thalamic reticular nucleus

The thalamic reticular nucleus is composed exclusively of GABAergic neurons (Houser et al., 1980; Oertel et al., 1983), all of them projecting to the correspondent thalamic nucleus after giving one or two collaterals (Scheibel and Scheibel, 1966; Yen et al., 1985; Liu et al., 1995b). These neurons are also equipped with I_T and I_h, however I_h is much weaker in RE neurons than in TC cells (Blethyn et al., 2006). As for TC cells, RE neurons fire in a tonic mode when depolarised and in a bursting mode when hyperpolarised. However they can generate more action potential during a LTS (up to 40) and with much higher frequency (up to 500 Hz) than TC neurons can do. RE neurons are interconnected with gap junction (Landisman et al., 2002; Fuentealba et al., 2004; Blethyn et al., 2008). The sources of afferents to the RE thalamic nucleus are the collaterals of TC and corticothalamic fibers (Fig. I.1), all of which pass through the RE nucleus (Jones, 1985). Both of these projections are glutamatergic and thus excitatory. The vast majority of corticothalamic fibers originate from layer VI small pyramidal neurons and project exclusively to relay (specific) nuclei and to the RE nucleus (Fig. I.1); other corticothalamic

fibers originate from layer V pyramidal neurons and these projections target both specific and non specific thalamic nuclei, but not RE neurons (reviewed in (Jones, 2007)). Layer VI terminals form 60% and TC terminals form 30% of synapses on RE thalamic neurons. However, EPSCs originating from TC neurons are faster rising and larger in amplitude as compared to those originating from corticothalamic fibers (Liu and Jones, 1999). Minimal stimulations of corticothalamic fibers evoked EPSCs that are 2.4 times greater in RE than in relay neurons; and the quantal size of EPSCs is also 2.6 times greater in RE neurons than in TC neurons. Also, GluR4 subunits labeled at corticothalamic synapses on RE neurons outnumbered those on relay cells by 3.7 times (Golshani et al., 2001). Thus, the excitatory influence of corticothalamic fibers on RE neurons is much larger than their influence on TC neurons. Therefore, both TC and corticothalamic axons produce efficient activation of RE neurons.

1.1.3 Neocortex

The neocortical tissue is composed of neuronal and glial cells commonly called neurons and glia or neuroglia. Neocortical neurons are the principal elements of neocortex. They receive information from periphery, integrate the received signals, and send the received information to executive structures. Two major groups of neurons compose neocortex. These are pyramidal cells and interneurons.

1.1.3.1 Pyramidal neurons

In fixed tissue, pyramidal neurons have a pyramidal shape; in the unfixed tissue they usually look ovoid. Pyramidal neurons constitute about 80 % of all cortical neurons (DeFelipe and Farinas, 1992). All pyramidal neurons are projecting neurons with long axons. Their distinct morphological feature is the presence of a long apical dendrite that arise from the upper pole of the neuronal body toward cortical surface giving rise to several oblique branches, which in turn give second, third, (etc.) order of branches. In most of pyramidal neurons, their apical dendrite reaches cortical layer I. The base of the neuronal body gives rise to several basal dendrites oriented either horizontally or downward. Basal dendrites produce also branches. In large pyramidal cells, the diameter of the basal dendritic field covers up to 500 μm wide. Usually the peri-somatic dendrites of pyramidal neuron is not covered with spines, but tens of microns away from cellular body the density

of spines dramatically increases, and it fades away toward the distal portions of the dendritic arbor. The axon of pyramidal cells is oriented downward; it originates from the base of neuronal body or from the very proximal part of basal dendrites. Giving off several short-range local branches within the surrounding tissue, the axon leaves neocortex to innervate other cortical and subcortical structures (DeFelipe and Farinas, 1992).

Figure I- 1 The thalamocortical system

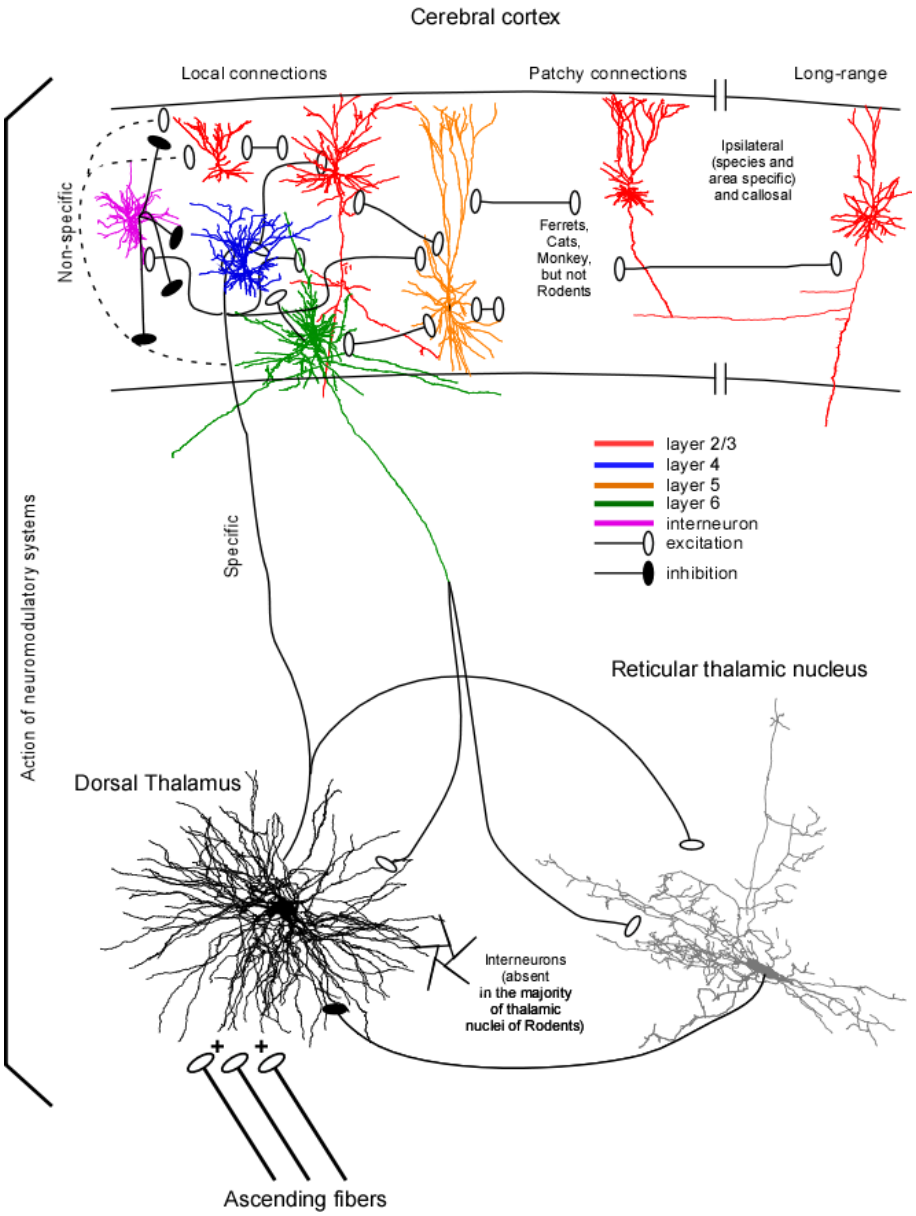

(Figure modified from (Timofeev and Chauvette, 2011))

1.1.3.2 Non-pyramidal neurons, interneurons

All non-pyramidal neurons are also called interneurons and most of them exert an inhibitory action on their target. Interneurons are a very heterogeneous population of neocortical cells with diverse morphological, physiological, and molecular features. Detailed description of interneurons morphological and physiological types could be found in recent reviews (Somogyi et al., 1998; Markram et al., 2004). All known neocortical interneurons are local-circuit cells with axon arborizing within neocortex either in vertical direction forming a neocortical column or horizontally. Different types of interneurons form synapses at different locations on their target: proximal dendrites, distal dendrites, soma, axon initial segment, etc. Out of all known cortical interneuronal types, only the spiny stellate cells, which have a star-shaped dendritic arbor and are located in layer IV, possess spines and exert a glutamatergic excitatory action. The major inputs on these spiny stellate neurons are from axons of *specific* thalamic nuclei. Spiny stellate neurones project preferentially to cortical layers II-III (Fig. I-1).

1.1.3.3 Electrophysiological types of cortical neurons

There are billions of neurons composing the neocortex, and they can be classified in at least four electrophysiological groups: Regular-Spiking (RS), Intrinsically-Bursting (IB), Fast-Spiking (FS), and Fast-Rhythmic-Bursting (FRB, also called chattering cells) neurons (Connors and Gutnick, 1990; Gray and McCormick, 1996; Steriade et al., 1998c; Steriade et al., 2001). All these electrophysiological types of neurons can be observed in vitro (FRB can be seen only with artificial cerebrospinal fluid that contains physiological levels of extracellular calcium (Brumberg et al., 2000)) as well as in vivo under anesthesia, or in vivo without anesthesia in any state of vigilance (Steriade et al., 2001). However, their electrophysiological type is dynamic as it might change according to the extracellular milieu or states of vigilance (Steriade, 2001b; Steriade et al., 2001; Boucetta et al., (in press)). In addition, they can all be observed in all cortical layers (Steriade et al., 1998c; Timofeev et al., 2000a; Cardin et al., 2005; Chauvette et al., 2010). RS cells are the most common type of cells recorded in neocortex (Connors and Gutnick, 1990). These cells are characterized by spike frequency adaptation in response to depolarizing current pulses and

by the absence of burst response (McCormick et al., 1985). IB cells are characterized by the presence of an initial burst that can be followed either by other bursts or by single spikes (McCormick et al., 1985; Connors and Gutnick, 1990; Nunez et al., 1993). Within a burst, spikes tend to decrease in amplitude and bursts occur at 5-15 Hz (Connors and Gutnick, 1990). The intraburst frequency could reach up to about 200 Hz (Nunez et al., 1993). The intraburst frequency of FRB cells is between 300 and 600 Hz, and the interburst frequency ranges from 20 to 50 Hz, but is mainly between 30 and 40 Hz (Gray and McCormick, 1996; Steriade et al., 1998c; Steriade et al., 2001; Cardin et al., 2005). The FRB cells differ from IB cells by their regular interspike intervals within a burst while the IB cells generally display a longer first interspike interval. In addition, the spikes of FRB cells show a much larger short afterhyperpolarization (sAHP), while spikes of IB and RS show only a slight sAHP (Steriade et al., 1998c). The spikes of FS and FRB cells are thin, while spikes of RS and IB are wider (Steriade et al., 2001). The FS cells are characterized by a linear current-frequency response to depolarizing current pulses with tonic firing reaching up to 800 Hz, and they don't show spike frequency adaptation (Connors and Gutnick, 1990; Gray and McCormick, 1996).

1.1.3.4 Correlation between electrophysiology and morphology

Many authors have tried to correlate electrophysiology with neuronal morphology (McCormick et al., 1985; Chagnac-Amitai et al., 1990; Connors and Gutnick, 1990; Gray and McCormick, 1996; Timofeev et al., 2000a; Steriade, 2004). RS cells were thought to be either pyramidal cells or spiny stellate cells while FS were thought to be aspiny non-pyramidal neurons, thus interneuron (Connors and Gutnick, 1990; Gray and McCormick, 1996). There was also a study that showed that in layer V, IB cells are large pyramidal cells (Chagnac-Amitai et al., 1990). FRB, also called chattering cells, were initially thought to be layer II/III pyramidal cells (Gray and McCormick, 1996), but later they were identified as pyramidal cell of any layer or basket cell (Steriade et al., 1998c; Steriade, 2004). Further studies showed that electrophysiological properties of neurons can be modulated by a change in the network activity (Boucetta et al., (in press)) (Fig. I-2) or by changing the extracellular calcium concentration (Boucetta et al., (in press)) (Fig. I-3). The proportion of

IB cells observed in cortical slab preparation was increased with 39% of cells recorded being IB, while 15 to 20% are usually observed in intact cortex of anesthetized animals (Timofeev et al., 2000b). The presence of norepinephrine and acetylcholine also transforms the burst firing mode of a cell into a tonic firing mode (Wang and McCormick, 1993). Thus cells are able to change their firing pattern. In addition, by injecting slight sustained depolarization in the cells, some neurons converted their burst firing into a RS pattern. It is also important to note that these depolarisations can occur naturally with transition from slow-wave sleep to wakefulness or to REM sleep, and thus, the change in state of vigilance can change the firing pattern of neurons (Steriade, 2001a, b, 2004). This could be an explanation for the increased proportion of IB cells in cortical slabs (Timofeev et al., 2000b) or in slices (40-60%) (Nishikawa and MacIver, 2000) in which cells are more hyperpolarized, and it could also explain the lower percentage (4 %) of IB cells during wakefulness, a state in which the neurons are more depolarized (Steriade et al., 2001). The change in extracellular calcium concentration to a physiological range (1.0 to 1.2 mM) in artificial cerebrospinal fluid (ACSF) allowed to record cells with FRB pattern (Brumberg et al., 2000) while with traditional ACSF, no FRB cells were reported in vitro. Also, in vivo, with microdialysis technique, a diminution in the extracellular calcium concentration to approximately 0.8 mM transformed RS cells into IB cells (Fig. I-3). It is worth to note that extracellular calcium concentration naturally varies in this range during slow oscillation (Heinemann et al., 1977; Massimini and Amzica, 2001; Crochet et al., 2005). Transitions from RS to FRB to FS were also described (Steriade et al., 1998c) and these transitions were ascribed to the persistent sodium current ($I_{Na(p)}$) and to a reduction in fast voltage- and calcium-dependant potassium conductances (Traub et al., 2003). Up to now, all FS cells recorded and stained were found to be interneurons, but for the three other types, no association between morphology and electrophysiology can be made since the firing pattern is modulated by different factors including the extracellular potassium concentration, the membrane potential, the network activity/state, the presence of neuromodulators, and the extracellular calcium concentration.

Figure I- 2 Neuronal firing pattern could be modulated by the network activity.

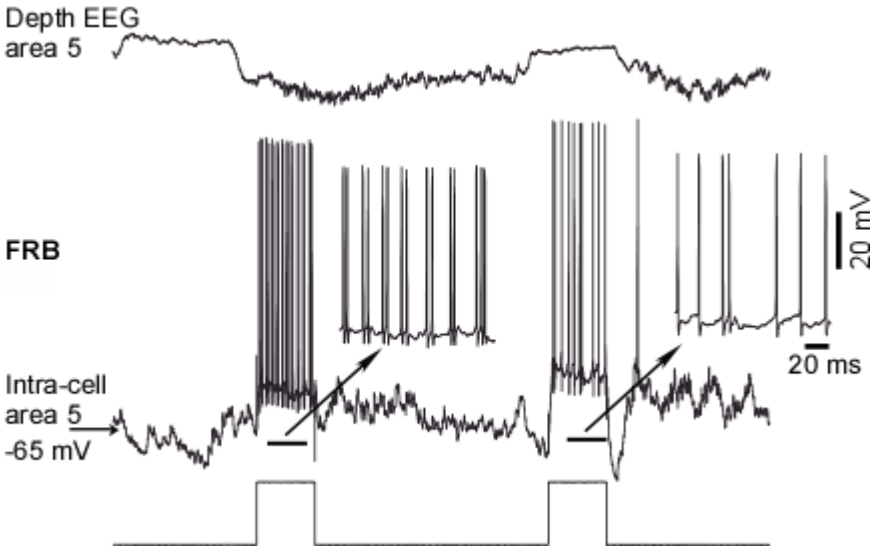

Local field potential and intracellular recording performed in cortical area 5 of a cat anesthetized with ketamine-xylazine. Depolarizing current pulses of 1.0 nA were applied to the fast-rhythmic-bursting neuron during active and silent network states. Note that FRB pattern of firing was seen only during active network states. (Figure from (Boucetta et al., (in press)))

Figure I- 3 Modulation of extracellular calcium concentration affects intrinsic excitability and firing patterns.

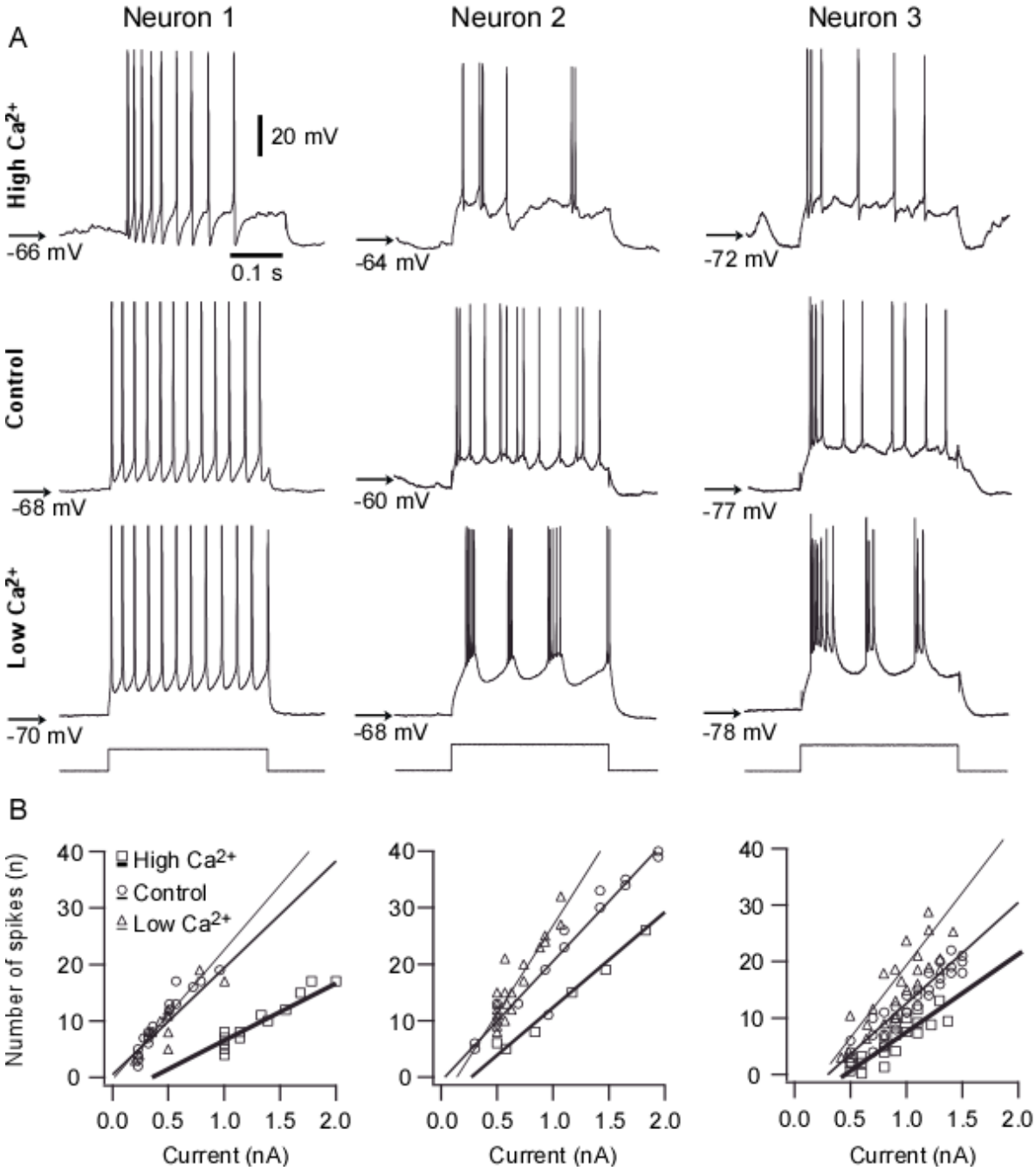

A, neuronal excitability was tested by injection of depolarizing current pulses of variable intensity. Examples of responses shown for three different neurons during high, control, and low conditions of $[Ca^{2+}]_o$. B, plots showing the number of action potentials elicited by intracellularly applied current pulses of different intensity. Note a decrease in the number of action potentials as $[Ca^{2+}]_o$ increases and the bursting response during low $[Ca^{2+}]_o$ conditions for the second (middle column) and third neuron (right column). (Figure from (Boucetta et al., (in press)))

1.1.3.5 Laminar and columnar organisation of cortex

Despite a large complexity, neocortex has a stereotyped organization. The normal cortex has a specific cytoarchitecture, being horizontally organized into six laminae (Baillarger, 1840) and vertically into groups of synaptically linked cells, called neocortical minicolumns, that represent the basic processing units of the mature neocortex, and which are further grouped together by short-range horizontal connections into cortical columns (Mountcastle, 1957, 1997; Buxhoeveden and Casanova, 2002a, b; Kaas, 2012).

Similar laminar cortical organization is found across multiple species. In cats the total thickness of neocortex in somatosensory and parietal areas in fixed and dry sections was estimated to be around 1.7-1.8 mm (Hassler and Muhs-Clement, 1964). However, neuronal recordings in vivo demonstrated the presence of neuronal activities until the depth of 2.3 mm (Mountcastle, 1957) suggesting that unfixed normal cortical tissue in cats could have a thickness of about 2.3 mm. Multiple original studies and reviews provided a description of cortical layers. We provide here only a brief version of such description done by (Creutzfeldt, 1995).

The molecular layer I contains almost exclusively GABAergic (mainly Cajal-Retzius) neurons (more than 90%) (Winer and Larue, 1989) and consists mainly of extensions of apical dendrites from pyramidal neurons and horizontally oriented axons.

The external granular layer II contains small pyramidal neurons and numerous interneurons.

The external pyramidal layer III contains predominantly small and medium sized pyramidal neurons, as well as non-pyramidal neurons with vertically oriented intracortical axons. Layers I through III are the main target of interhemispheric corticocortical afferents, and layer III is the principal source of corticocortical afferents including callosal projections. Layers II and III are not easily distinguishable even from dried and fixed sections and many authors refer to layer II/III without any distinction between the two.

The internal granular layer IV contains different types of stellate and pyramidal neurons, and is the main target of thalamocortical afferents as well as intra-hemispheric corticocortical afferents.

The internal pyramidal layer V contains large pyramidal neurons (as the Betz cells in the primary motor cortex), as well as interneurons, and it is the principal source of efferent to tectum, brainstem and spinal cord. A subgroup of layer V pyramidal neurons is callosaly projecting, another group of neurons forms large and efficient synapses on thalamocortical neurons from higher order thalamic nuclei.

The multiform layer VI contains few large pyramidal neurons and many small spindle-like pyramidal and multiform neurons. The layer VI sends efferent fibers to the thalamus establishing a very precise reciprocal interconnection between the cortex and the thalamus and primarily modulating the activity of thalamocortical neurons (see thalamocortical oscillations).

The cortical firing is generally sparser in supragranular layers as compared to infragranular ones (see figure III-3, also reviewed in (Barth and Poulet, 2012)).

1.1.3.6 Synaptic connections in neocortex

The synaptic connectivity in the neocortex is very dense. Each pyramidal cell receives 5000 to 60000 synapses (Cragg, 1967; DeFelipe and Farinas, 1992; Mountcastle, 1998; Somogyi et al., 1998). Local-circuit synapses have been estimated to account for as many as 70 % of the synapses present in some areas of the cortex (Szentagothai, 1965; Gruner et al., 1974; Douglas and Martin, 2007) and pyramidal cells constitute about 80 % of the total number of neocortical neurons (DeFelipe and Farinas, 1992). Most of inhibitory synapses are located in the perisomatic region and most of excitatory synapses are located on dendrites and dendrites spines (DeFelipe and Farinas, 1992). According to the cable theory of neuron (Rall, 1977), synapses that are located closer to the place of generation of action potential (axon hillock in most of the cases, but in some occasions in dendritic triggering zones) have a stronger influence on action potential generation than synapses located remotely. However, the influence of remotely connected synapses on the generation of action potentials might be significantly facilitated by a variety of dendritic intrinsic currents (Spencer and Kandel, 1961; Wong et al., 1979; Benardo et al., 1982; Llinas, 1988; Turner et al., 1991; Amitai et al., 1993; Magee and Johnston, 1995; Schwindt and Crill, 1995; Crill, 1996; Huguenard, 1996; Pape, 1996; Larkum and Zhu, 2002) and simultaneous or close time-related activation of several synapses (Markram et al., 1997a; Azouz and

Gray, 2000; Palva et al., 2000; Wang et al., 2000; Stuart and Hausser, 2001). Shunting effects of network activities on cortical neurons (Borg-Graham et al., 1998; Hirsch et al., 1998) and in particular on their dendrites might significantly influence the expression of the abovementioned phenomena. In addition to thalamic inputs (see above), corpus callosum neurons, connecting the two hemispheres of the cerebrum, provide inputs to neocortical areas. These neurons are located mainly in cortical layers II/III but also in infragranular layers, among them layer V, in different neocortical areas (Porter and White, 1986; Barbaresi et al., 1989; Barbaresi et al., 1994; Cisse et al., 2003). The other inputs to a given cortical area come from multiple ipsilateral cortical fields. For example associative cortical area 5 receives ipsilateral cortical inputs from anterior parietal cortex, motor cortex, somatosensory cortex, visual cortex, posterior to area 5 fields of suprasylvian gyrus, and to a lesser extent projections from dorsolateral prefrontal cortex, cingular, retrosplenial, insular cortices (Avendano et al., 1988). A given intracortical excitatory presynaptic axon forms from one to eight synaptic contacts with postsynaptic neurons (Markram et al., 1997b; Krimer and Goldman-Rakic, 2001) that elicit excitatory postsynaptic potentials from 0.1 to 10 mV, with a total mean of about 1 mV (Thomson et al., 1995; Buhl et al., 1997; Markram et al., 1997b; Feldmeyer et al., 1999; Krimer and Goldman-Rakic, 2001; Crochet et al., 2005). Similarly to RE neurons, a network of inhibitory interneurons in the neocortex is coupled via electrotonic synapses (Galarreta and Hestrin, 1999; Gibson et al., 1999).

The vertical cortical organization is complex and basically each layer is connected to each layer. However, some connections are more numerous and more powerful than others (reviewed in (Thomson and Lamy, 2007)). Briefly, when sensory inputs from thalamus arrive to layer IV, layer IV neurons excite layer III, which in turn excite layer III, layer IV and layer V neurons. Layer V neurons excite other layer V neurons, layer III neurons, and layer VI neurons. Layer VI neurons excite layer IV neurons (Thomson and Bannister, 2003; Douglas and Martin, 2004; Wester and Contreras, 2012) (Fig. I-1). This morphological background is reflected in consecutive pattern of activation of cortical tissue (Contreras and Llinas, 2001).

There are important species related differences in intracortical organization among species of mammals. These differences include basic features that are determinant of the emergent activity such as the density of neurons, patterns of connectivity, density of synaptic connections, cell types, proportion of inhibitory / excitatory cells, etc (Thomson et al., 2002). There are also differences in horizontal connectivity. Intracortical network forms horizontal patchy connections in cats, ferrets and primates, but not in rodents (Fig. I-1, Reviewed in (Sanchez-Vives et al., 2007).

1.2 States of vigilances

There are three states of vigilance, which are wake, rapid eye movements (REM, also called paradoxical) sleep, and slow-wave sleep (SWS, also called non-REM). The earliest electrophysiological study of brain activities demonstrated that the waking state is characterized by low amplitude fast waves, sleep is dominated by large amplitude slow waves, but a part of sleep (called fair sleep in that study) was characterized by low amplitude fast waves (Blake and Gerard, 1937). Modern formal electrophysiological description of states of vigilance requires the evaluation of three criteria: electroencephalogram (EEG) or local field potential (LFP), electromyogram (EMG), and electro-oculogram (EOG). These states are also characterized by the presence or the absence of different neuromodulatory systems in different states of vigilance. At the neuronal level, the membrane potential of cortical neurons during waking state and REM sleep is relatively depolarized (around -62 mV); during SWS cortical neurons oscillate between depolarizing (mean around -62 mV) and hyperpolarizing (mean around -70 mV) states (Steriade et al., 2001; Timofeev et al., 2001a).

1.2.1 Wake

From an electrophysiological point of view, the waking state is characterized by activated cortical LFP and/or EEG recordings (low amplitude fast waves), by the presence of a muscle tone (usually irregular), and might show eye movements. Physiologically, wake is characterized by the activation of brain ascending activating systems which is composed of several neuromodulators. Among major contributors are cholinergic, serotoninergic, and

norepinephrinergic systems, but, dopamine, glutamate, histamine, and orexin are also involved in promoting wakefulness (Wright et al., 2012). Cholinergic neurons located in the pedunculopontine (PPT) and laterodorsal tegmental nuclei (LDT) project to the thalamus and excite thalamocortical cells facilitating arousal and information transfer to the cerebral cortex (McCormick and Bal, 1997). Cholinergic neurons located in the BF, project to the cortex to promote behavioral and cortical arousal (Metherate et al., 1992; Steriade, 1992; Alam et al., 1999; Strecker et al., 2000). Activation of dopaminergic neurons located primarily in the substantia nigra and in the ventral tegmental areas which project to the striatum and frontal cortex, are important for behavioral arousal, reward seeking, and movement (reviewed in (Wright et al., 2012)). The locus coeruleus is composed of norepinephrine (noradrenergic) neurons that project to the forebrain and the cerebral cortex and are involved in attention, enhancing cortical activation, and behavioral and emotional arousal (Greene et al., 2009; Tully and Bolshakov, 2010). During slow-wave sleep, locus coeruleus neurons were recently shown to fire preferentially during the frontal cortex transition from silent to active states (Eschenko et al., 2012). Norepinephrine neurons also project to motor neurons providing excitatory drive to the motor neuron pool and therefore enhanced neuromuscular activity. Serotonin neurons, localized in the brain stem raphe nuclei project to the cortex and spinal cord to promote brain, emotional, and neuromuscular arousal (Hale and Lowry, 2011).

1.2.2 Rapid eye movement sleep

Rapid eye movement sleep, also referred as paradoxical sleep, is also characterized by low amplitude fast waves in cortical LFP and/or EEG recordings (similar to wake). However, a key electrophysiological feature is the absence of muscle tone in EMG recordings (except muscles of respiratory system and occasional twitches) and the presences of rapid ocular saccades in EOG recordings. Serotoninergic and norepinephrinegic systems are not activated during REM sleep, but cholinergic system is active (reviewed in (Steriade and McCarley, 2005)).

1.2.3 Slow-wave sleep

Slow-wave sleep (SWS) is characterized by the presence of large amplitude slow waves in cortical LFP and/or EEG recordings, a steady muscle tone, and the absence of eye movements. Intracellular recordings of neocortical neurons show a bimodal distribution of the membrane potential due to the presence of active (depolarized, Up) and silent (hyperpolarized, Down) states, which are present only during SWS and under certain types of anaesthesia. SWS properties will be largely discussed throughout this thesis.

Figure I- 4 Oscillations in thalamocortical system.

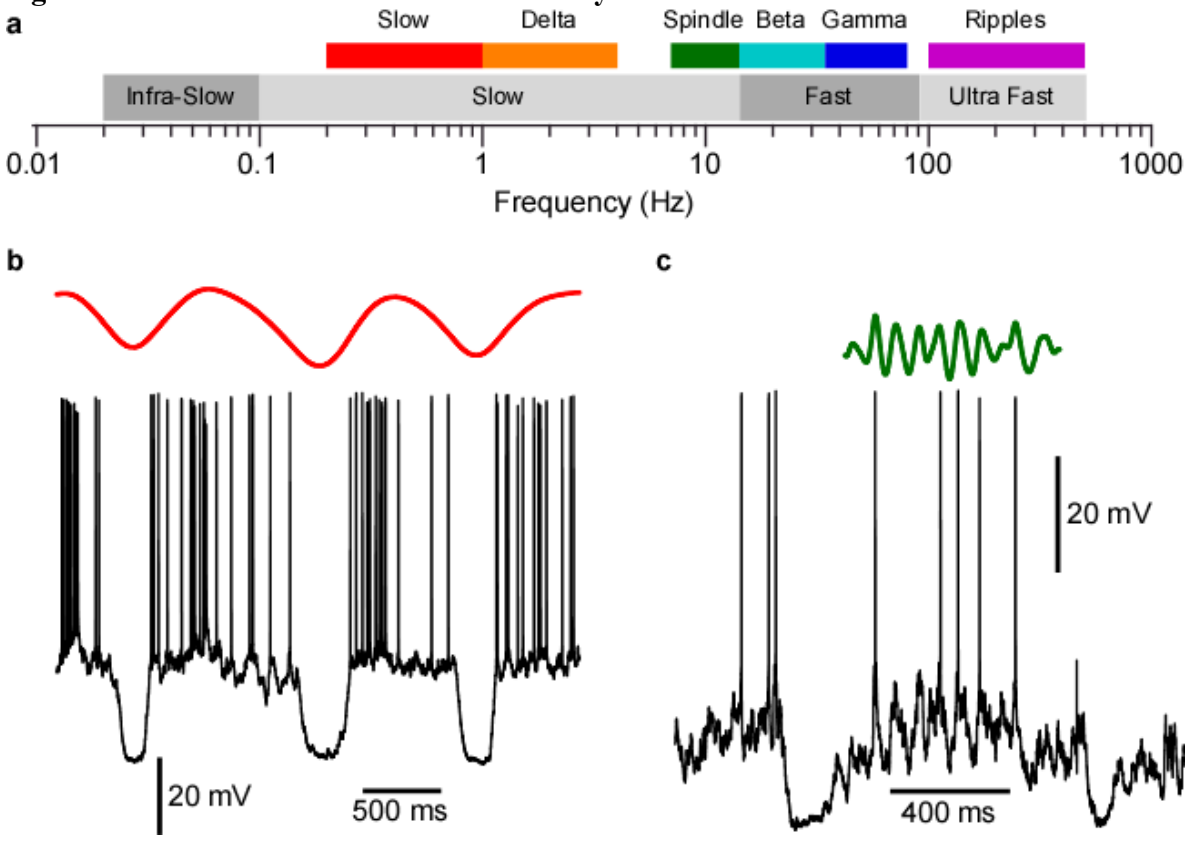

a. Frequency band of oscillations recorded in the thalamocortical system. b. Segment of intracellular recording (black) recorded during slow-wave sleep in cat's associative cortex. The signal was then filtered for slow oscillation (0.1-1 Hz, red trace). c. Segment of intracellular recording (black) recorded during slow-wave sleep in cat's somatosensory cortex. A segment filtered for spindle (7-15 Hz, green). From (Timofeev and Chauvette, 2011)

1.2.4 Thalamocortical oscillations during slow-wave sleep

The frequencies of thalamocortical oscillations range from as slow as 0.02 Hz to as fast as 500 Hz (Fig. I-4). These different rhythms and their functionality were largely reviewed previously (Timofeev and Bazhenov, 2005; Bazhenov and Timofeev, 2006; Timofeev and Chauvette, 2011). Therefore, thalamocortical oscillations are grouped in several frequency bands, for some of which the mechanisms of generation are known.

1.2.4.1 Infra-slow oscillation

This type of oscillatory activity has a period within the range of tens of seconds to a minute (Aladjalova, 1957). Very little is known about the underlying mechanisms of these oscillations but at least some of the factors responsible for their generation could depend on non-neuronal dynamics, such as changes in CO_2 concentration (Nita et al., 2004). Infra-slow activities likely have a cortical origin given that they can be recorded from neocortical slabs (Aladjalova, 1962). Infra-slow oscillation is correlated with the magnitude of faster EEG oscillations, and infra-slow oscillation might be implied in controlling the gross cortical excitability (Vanhatalo et al., 2004).

1.2.4.2 Slow oscillation

During slow-wave sleep (SWS) and some types of anesthesia the dominant activity is generated with a frequency (0.3 - 1 Hz), termed slow oscillation (Steriade et al., 1993b; Steriade et al., 1993a; Steriade et al., 2001; Timofeev et al., 2001a). In both, anesthetized (Metherate and Ashe, 1993; Contreras and Steriade, 1995) and naturally sleeping animals (Steriade et al., 2001; Timofeev et al., 2001a; Okun et al., 2010), during slow oscillation the entire cortical network (both excitatory and inhibitory neurons) alternates between silent (Hyperpolarizing, or Down) and active (Depolarizing, or Up) states that correspond to depth-positive and depth-negative waves of local field potentials, respectively (Fig. I-4 b). Active states are characterized by cellular firing and faster frequencies (Mukovski et al., 2007; Volgushev et al., 2007). Silent states are periods of disfacilitation and are mediated mainly by a potassium current, likely the leak current (Timofeev et al., 2001a). During

silent states, both RE and TC neurons are hyperpolarized like cortical neurons; during active states RE neurons are depolarized and either fire in tonic mode or reveal spindle-like high frequency spike-bursts (Contreras and Steriade, 1995; Contreras et al., 1996a; Fuentealba et al., 2005). By contrast, TC neurons display rhythmic IPSPs with spindle frequency and occasional rebound spike-bursts (Contreras and Steriade, 1995; Timofeev and Steriade, 1996; Timofeev et al., 2001b).

Most studies point to a cortical origin of slow oscillation because slow oscillation is present in cortical slab in vivo (Timofeev et al., 2000b), in cortical brain slice with modified ACSF (Sanchez-Vives and McCormick, 2000; Sanchez-Vives et al., 2007), in animals with kainic acid thalamic lesion (two days after the lesion) (Steriade et al., 1993a), and absent in decorticated cats (Timofeev and Steriade, 1996). Inactivating a small cortical region disrupt the synchrony between sites on each side of the inactivation site (Amzica and Steriade, 1995), and layer V was shown to be critical for the lateral propagation of slow oscillation in thalamocortical slice preparations (Wester and Contreras, 2012).

Intracellular recordings from cortical neurons during states of vigilance demonstrated that an alternation of active and silent states occurs only during SWS and not in any other state of vigilance (Steriade et al., 2001; Timofeev et al., 2001a; Mukovski et al., 2007; Rudolph et al., 2007). Similar alternations of active and silent states in neocortical neurons were recorded in associative, motor, somatosensory, and visual cortices (see chapter IV; (Chauvette et al., 2011)). Waking state and REM sleep show a single mode distribution of membrane potential and silent states were absent during these states of vigilance (Matsumura, 1979; Steriade et al., 2001). In contrast to these observations, large amplitude fluctuations of membrane potential (unlikely states) were found during quiet wakefulness in mice barrel cortex (Crochet and Petersen, 2006; Poulet and Petersen, 2008; Gentet et al., 2010). In these studies, states of vigilance were not identified formally. However, in the available example [(Poulet and Petersen, 2008), see their Fig. 2B], the large amplitude membrane potential fluctuations occur only when slow waves are present in local field potential recordings, suggesting that at this time the mice was either in the

state of SWS or drowsiness. A more speculative alternative explanation is that slow waves in mice somatosensory cortex can occur during waking state.

Propagation of slow oscillation

High density EEG study in humans demonstrated that each individual cortical wave can start at any location and then propagate to other cortical regions, however, in adult human, slow waves preferentially start in frontal cortical areas and propagate from there to more posterior regions (Massimini et al., 2004). It was recently shown that the preferred site of origin of slow waves was age-dependent in humans moving from very posterior cortical regions in the first years of life to frontal regions when becoming adult (Kurth et al., 2010). It was unclear from these scalp EEG recordings what component of slow waves (active or silent states or both) starts and propagates. Multisite intracellular recordings associative cortex of cats anesthetized with ketamine-xylazine showed that active states start in some point of the neocortex and propagate to other regions (see chapter II; (Volgushev et al., 2006; Chauvette et al., 2007; Volgushev et al., 2011)). Surprisingly, the onset of silent states occurred almost simultaneously (more than for active state onset) in cortical regions separated by up to 12 mm, which suggests the presence of a global mechanism. Although silent states are mediated by potassium conductance (Timofeev et al., 2001a), a recent computational model suggested a role for active inhibition at the onset of silent state (Chen et al., 2012).

Origin of active states

I will not describe here the whole rationale about the mechanism of active state generation because a whole chapter of this thesis is dedicated to this subject (see chapter III). Briefly, our results showed that active states may start in any cortical layer, but large layer V pyramidal neurons having the largest dendritic tree are better suited to receive more spike-independent mediator releases that would summate and initiate the active state when the whole thalamocortical network is silent (see chapter III; (Chauvette et al., 2010)).

1.2.4.3 Delta oscillation

The delta oscillation occurs with frequencies of 1 Hz to 4 Hz. The fact that delta and slow oscillation represent two distinct phenomena was demonstrated by Achermann and Borbély (Achermann and Borbely, 1997) who showed differences in the dynamics between the slow and the delta oscillations, as the latter declines in activity from the first to the second non-REM sleep episode, whereas the former does not. Cortically recorded delta oscillation has likely two components: one of which originates in the neocortex and the other in the thalamus. Both surgical removal of thalamus (Villablanca and Salinas-Zeballos, 1972; Ball et al., 1977), and neocortical slabs in chronic conditions result in the significant enhancement of neocortical delta activity. Little is known about the cellular mechanisms mediating cortical delta oscillation. One of the hypotheses suggests that cortical delta activity could be driven by the discharge of IB neurons (Amzica and Steriade, 1998). This is unlikely, because in order to induce a burst, intrinsically bursting neurons have to be driven by either intrinsically or synaptically generated depolarization (Connors et al., 1982). Therefore, it is unclear what would drive these neurons, in conditions of decreased activity of neuromodulatory systems, which removes the depolarizing drive in the majority of cortical neurons. If IB neurons are implicated in the generation of delta oscillation, they have to be driven by some other active neurons or neuronal properties. On the other hand, the thalamic delta (1-4 Hz) is a well known example of rhythmic activity generated intrinsically by thalamic relay neurons as a result of an interplay between their low-threshold Ca^{2+} current (I_T) and hyperpolarization-activated cation current (I_h). As such, the delta oscillation may be observed during deep sleep when thalamic relay neurons are hyperpolarized sufficiently to deinactivate I_T (McCormick and Pape, 1990; Leresche et al., 1991; Soltesz et al., 1991; Dossi et al., 1992). It was also shown that at a certain level of leak current (I_{leak}), the 'window' component of I_T in thalamocortical neurons, may create oscillations similar in frequency to the intrinsic thalamic delta oscillation (Williams et al., 1997). However, multisite unit recordings demonstrated that TC neurons generate delta oscillations in an asynchronous manner (Timofeev and Steriade, 1996). Asynchronous firing of TC neurons cannot produce an effect appearing as large amplitude synchronized slow waves. Therefore, it is unlikely that intrinsic delta oscillation of TC neurons is implicated in the generation of cortical delta rhythm.

1.2.4.4 Spindle oscillation

Sleep spindle oscillations consist in a group of rhythmic waves characterized by a progressively increasing, then gradually decreasing field potentials amplitude (waxing-and-waning) of 7-15 Hz which last 1-3 sec and recur every 5-15 sec. Spindles were first observed by Berger in 1933 (Berger, 1933) but their name "spindle" was given two years later (Loomis et al., 1935). In vivo, spindle oscillations are typically observed during light stages of sleep or during active phases of slow-wave sleep oscillations (Fig. I-3 c). In cats, the maximal occurrence of sleep spindle was found in motor, somatosensory, and to a lesser extent in associative cortical areas (Morison and Dempsey, 1942). In humans, spindles are rather fast (13–15 Hz) in centroparietal regions while they appear with slightly slower frequencies (11–13 Hz) in frontal regions (Jankel and Niedermeyer, 1985; De Gennaro and Ferrara, 2003; Andrillon et al., 2011). Fast centroparietal spindles occur mainly at the active state onset while slow frontal spindles occur later during active state often at the transition toward silent state (Molle et al., 2011). The thalamus is separated in a core pathway in which thalamocortical cells projects focally to cortical layer IV, and in a matrix pathway that have diffuse projections to layer I (Jones, 2001, 2002).The difference in spindle frequency was previously attributed to intrinsic properties of the thalamic reticular nucleus with longer hyperpolarisation leading to longer spike-bursts and a lower frequency of spindles (Steriade and Amzica, 1998). However, a recent modelling study suggested that spindles are initiated in the core pathway, but the widespread cortical synchronization was achieved by the matrix pathway (Bonjean et al., 2012).

In vivo, in vitro, and modeling studies suggest that the minimal substrate contributing to the generation of spindle oscillations is the thalamus (Steriade and Deschenes, 1984; Steriade et al., 1985; Steriade and Llinas, 1988; Steriade et al., 1990; von Krosigk et al., 1993; Destexhe et al., 1994). A presence of spindle oscillations after decortication (Morison and Bassett, 1945; Contreras et al., 1996b; Timofeev and Steriade, 1996; Timofeev et al., 2001b) provides strong evidence to the thalamic origin of this activity. Spindle-like activity was found in thalamic LGN (lateral geniculate nucleus) slice preparations of ferrets with preserved interconnections with perigeniculate nucleus (Bal and

McCormick, 1993; von Krosigk et al., 1993; Kim et al., 1995). The well accepted mechanism of spindle oscillation is following: the reticular thalamic inhibitory neurons fire a spike burst that elicit IPSPs in TC neurons, at the end of IPSPs the TC neurons generate a rebound spike-burst that excite RE neurons, which then generate spike-burst starting the next cycle of spindle oscillation.

There are at least two sets of data, which demonstrate that this hypothesis does not represent all spindle generating mechanisms. (a) Spindles are generated in isolated RE nucleus (Steriade et al., 1987) and spindles are absent in the dorsal thalamus that is disconnected from RE nucleus (Steriade et al., 1985). (b) During the early 3-4 IPSPs composing the spindle, TC neurons do not display rebound spike-bursts (Bazhenov et al., 2000), suggesting that the positive feedback from TC to RE neurons does not contribute to the early phase of a spindle sequence. Generally, the early part of spindles is not seen or less marked at the neocortical level. A more complex model suggests the presence of at least three phases with different underlying mechanisms that contribute to the spindle generation (Timofeev et al., 2001b). Cortical firing can trigger the onset of spindles by exciting hyperpolarized RE neurons that generate low-threshold calcium spikes accompanied with high frequency spike bursts. During an early phase of spindles, the RE nucleus is driving the spindles by its own mechanisms. The membrane potential of RE neurons during network silence is hyperpolarized by about 8-10 mV below the reversal potential for IPSP mediated by chloride. An initial spike-burst in RE neurons generate depolarizing IPSPs in their synaptically connected targets and RE neurons drive low-threshold spike in those target neurons (Bazhenov et al., 1999). The second part of spindles primarily develops as a result of interactions between RE and TC neurons as described above, but the cortical firing contributes to the spindle synchronization via the firing of corticothalamic neurons imposing simultaneous excitation of RE and TC neurons. Given the robust cortical influence on RE neurons (Golshani et al., 2001), the inhibitory projections of RE neurons onto TC neurons reinforce the spindle. The waning phase occurs as a result of Ca^{2+} induced cAMP up-regulation of hyperpolarization-activated cation current, I_h, in TC cells (Bal and McCormick, 1996; Budde et al., 1997; Luthi et al., 1998) and network desynchronization (Timofeev et al., 2001b). The active role of neocortex in

spindle generation is emphasized by the fact that in cats anesthetized with ketamine-xylazine, the overall length of spindles constitutes less than 400 ms, while after decortications, in the same anesthesia conditions the spontaneous or evoked by electrical stimulation spindles last more than 1 second. Therefore, the neocortex does not only reflect spindle activities originating in thalamus (Fig. I-2. c), but actively contribute to the initiation and termination of spindles (Bonjean et al., 2011).

1.2.4.5 Beta-Gamma activities

The waking state of the brain is characterized by low correlation of spike discharges across neighboring neurons (Noda and Adey, 1970) and the predominance of the frequencies in the beta (15-30 Hz) and gamma (30-60 Hz) ranges (Bressler, 1990; Freeman, 1991). Studies have indicated that cortical gamma activity is associated with attentiveness (Rougeul-Buser et al., 1975; Bouyer et al., 1981), focused arousal (Sheer, 1989), sensory perception (Gray et al., 1989), and movement (Murthy and Fetz, 1992; Pfurtscheller and Neuper, 1992). It has been proposed that the synchronization in the gamma frequency range is related to cognitive processing and to the temporal binding of sensory stimuli (Llinas and Ribary, 1993; Joliot et al., 1994; Singer and Gray, 1995). The fast rhythms are also synchronized between neighboring sites during deep anesthesia, natural SWS, and REM sleep (Steriade et al., 1996a; Steriade et al., 1996b; Mukovski et al., 2007), when consciousness is either suspended or bizarre. During slow-wave sleep the fast rhythms follow the onset of depth-negative EEG wave. Large-scale network simulations revealed that coherent gamma range oscillations may appear through occasional increases in spiking synchrony within local groups of cortical neurons (Rulkov et al., 2004; Bazhenov et al., 2008).

At least two non-exclusive basic mechanisms have been proposed to explain the origin of beta-gamma oscillations. One of them emphasizes an extracortical origin and another one point to intracortical origin of these activities. A transient feed-forward synchronization to high-frequency peripheral (retinal, lemniscal or cerebellar) oscillations (Timofeev and Steriade, 1997; Castelo-Branco et al., 1998) could impose peripheral fast activities onto thalamocortical system. Intracortical mechanism itself includes several

possibilities. The first one is based on the intrinsic property of fast-rhythmic-bursting (FRB) neurons to fire fast spike-bursts at frequencies of 20-60 Hz. These neurons were first described as fast pyramidal tract neurons from somatosensory cortex (Calvin and Sypert, 1976), later found in layer II-III of visual cortex (small pyramids called "chattering cells" (Gray and McCormick, 1996)). Later studies demonstrated that FRB neurons could be found in most of cortical layers (they are seemingly absent in layer I) and they could be both aspiny non-pyramidal and pyramidal cells (Steriade et al., 1998c; Timofeev et al., 2000a). Experimental and modeling studies provide two possible mechanisms of fast-rhythmic-burst generation. The first depends on the interplay of Na^+ and K^+ currents (Wang, 1999; Brumberg et al., 2000) and the second requires a reduction of intracellular Ca^{2+} concentration (Traub et al., 2003). This second mechanism of gamma activity generation was described both in vitro and in computational models. According to this mechanism, the activity of inhibitory interneurons is essential to obtain oscillations at gamma range (Lytton and Sejnowski, 1991; Traub et al., 1996; Traub et al., 1998; Traub et al., 1999). One way to describe this process is that after excitatory input, the network of inhibitory interneurons generates rhythmic and synchronized inhibition onto the entire local network. Pyramidal cells will be able to respond to excitatory input only during the time window of fading inhibition. If one assumes that all pyramidal neurons of a local population receive a similar amount of phasic inhibition, then only those pyramidal neurons receiving the strongest excitatory drive will fire first. Because pyramidal cells provide the major excitatory drive to interneurons, interneurons will discharge with some phase delay relative to pyramidal cells and the resulting network inhibition terminates the firing of both pyramidal cells and interneurons. This results in an inhibition of the whole network and the next gamma cycle is ready to begin (Fries et al., 2007).

Lastly, the FRB neurons hypothesis may function by providing a large-scale input to an axon plexus consisting of gap-junctionally connected axons from both FRB neurons and their anatomically similar counterparts, regular-spiking neurons (Cunningham et al., 2004). The resulting network gamma oscillation demonstrated in computational model shares all of the properties of gamma oscillations and shows a critical dependence on multiple spiking in FRB cells.

1.2.4.6 Ripples (very fast oscillations, >100 Hz)

Fast oscillations (>100 Hz), termed ripples, were described in CA1 hippocampal area and perirhinal cortex, where they were associated with bursts of sharp potentials during anesthesia, behavioral immobility, and natural sleep (Ylinen et al., 1995; Chrobak and Buzsaki, 1996; Collins et al., 1999; Csicsvari et al., 1999b, a). In the neocortex, fast oscillations (>200 Hz, up to 600 Hz) have been found in sensory-evoked potentials in rat barrel cortex (Jones and Barth, 1999; Jones et al., 2000), during high-voltage spike-and-wave patterns in rat (Kandel and Buzsaki, 1997). During natural states of vigilance in cats, ripples were generally more prominent during the depolarizing component of the slow oscillation in slow-wave sleep than during the states of waking and REM sleep (Grenier et al., 2001). Around epileptic foci in humans and cats the amplitude of ripples is dramatically enhanced (Allen et al., 1992; Fisher et al., 1992; Steriade et al., 1998b; Grenier et al., 2003b; Grenier et al., 2003a). Studies in epileptic patients have revealed the presence of high-frequency oscillations also in the hippocampus and entorhinal cortex (Bragin et al., 1999b; Bragin et al., 1999a; Bragin et al., 2002).

The high-frequency field potential oscillations during ripples are phase-locked with neuronal firing (Draguhn et al., 1998; Jones et al., 2000; Grenier et al., 2001, 2003a). The dependence of ripples on neuronal depolarization was shown by their increased amplitude in field potentials in parallel with progressively more depolarized values of the membrane potential of neurons (Grenier et al., 2001). Of all types of electrophysiologically identified neocortical neurons, FRB and fast-spiking cells displayed the highest firing rates during ripples and the inhibitory processes controlled the phase precision of ripple-dependent neuronal firing (Ylinen et al., 1995; Grenier et al., 2001). As ripples can be generated within small isolated slabs of cortex, the neocortical network seems to be sufficient to produce them (Grenier et al., 2001). In addition to active inhibition, the electrical coupling mediated by gap junctions contributes to the ripple synchronization (Draguhn et al., 1998; Traub et al., 1999; Grenier et al., 2003a). The electrical coupling may occur between axons of principal cells (Schmitz et al., 2001) or via a network of inhibitory interneurons (Galarreta and Hestrin, 1999; Gibson et al., 1999; Galarreta and Hestrin, 2001a, b; Gibson

et al., 2005). The field potentials increase neuronal excitability, and by a positive feedback loop they could be also involved in the generation of neocortical ripples (Grenier et al., 2003b). Since ripples are recorded also in glial cells, the electrical coupling between glial cells could also play a role in the synchronization of ripples (Grenier et al., 2003a).

1.3 Synaptic plasticity

Synaptic plasticity is the ability of a connection, or synapse, between two neurons to change its strength in response to either use or disuse of transmission over synaptic pathways. Heterosynaptic plasticity occurs when the neuronal activity involving one synapse of a neuron causes a change in the strength of another synapses of the neuron (reviewed in (Chistiakova and Volgushev, 2009)). Homosynaptic neuronal plasticity is the ability of neurons to modify their responses to incoming stimuli due to previous activities (reviewed in (Timofeev, 2011)). Unless specified, mechanism of plasticity described in the following sections will refer to homosynaptic processes. Most of the neuronal plasticity is due to the synaptic plasticity that could be either of short-term duration (milliseconds to seconds scale) or of long-term duration (tens of minutes and more). However, neuronal output is also modified by intrinsic currents, which also reveal several forms of plasticity. In addition to short- and long-term plasticity, neuronal plasticity also includes mid-term plasticity that occurs in the seconds to minutes scale.

1.3.1 Short-term synaptic plasticity

Changes in responses occurring at a sub-second scale are referred to as short-term plasticity. Facilitation or potentiation refers to an increase in the response, while a reduction in the response strength is called depression. The short-term plasticity may depend on both pre- and postsynaptic mechanisms, although much of known mechanisms have a presynaptic mechanism.

1.3.1.1 Short-term depression

The synaptic short-term depression is a decrease in the response to a same stimuli delivered shortly after the previous one. Among presynaptic mechanisms, vesicle depletion, high release probability, and an inactivation of release sites could all contribute to short-term synaptic depression (Zucker and Regehr, 2002).

One of the key factors in short-term depression is the readily releasable pool, which consist in the pool of vesicles that can be immediately released by a spike (Rizzoli and Betz, 2005). Usually, hundreds of vesicles are associated with an active zone, but typically, less than 5% of these vesicle are readily released with repeated stimulations (Rizzoli and Betz, 2005). The time required to fully replenish this readily releasable pool was estimated to be as long as few seconds (Neher and Sakaba, 2008), thus any subsequent stimuli arriving before the full replenishment of the readily releasable pool will result in fewer vesicles released (Zucker and Regehr, 2002). Another key factor for short-term depression is the release probability, which is the probability that a synaptic active zone release one (or more) vesicle following an action potential. Both the size of readily releasable pool and the probability of release will account for the number of vesicles released by an action potential (Fioravante and Regehr, 2011). Using in vitro techniques, the release probability was estimated to be as high as 0.5 (Branco and Staras, 2009), however in vivo it was estimated to be around 0.1 (Borst, 2010). The possible reasons to explain this major difference between in vivo and in vitro studies will be discussed in a next section. Having a high release probability and a rather slow kinetic to replenish the readily releasable pool will undoubtedly lead to short-term depression.

Another possible presynaptic mechanism of short-term synaptic depression is the inactivation of release sites (Fioravante and Regehr, 2011). The fusion of a vesicle at a release site can inhibit subsequent fusion events at that site even if the readily releasable pool is not depleted (Neher and Sakaba, 2008). This site inactivation would lasts for seconds following exocytosis and could reflect the time it takes to clear vesicular membrane proteins, which get incorporated into the plasma membrane upon vesicle fusion, from the release site (Neher and Sakaba, 2008).

One of the postsynaptic mechanisms of short-term depression is the desensitization of receptors (Trussell et al., 1993; Jones and Westbrook, 1996; Chen et al., 2002; Sun et al., 2002; Xu-Friedman and Regehr, 2003), another one would be the receptor saturation (Wadiche and Jahr, 2001; Chen et al., 2002; Foster et al., 2002), reviewed in (Blitz et al., 2004). Desensitization may take tens of milliseconds or even minutes to recover, but desensitization does not play a widespread role in short-term plasticity (reviewed in (Zucker and Regehr, 2002)). Receptor saturation was mainly described at climbing fibers in the cerebellum where saturation of the postsynaptic receptors would render the Purkinje cell less sensitive to changes in the amount of glutamate that is released by the climbing fibers, which then reduces the effects of depression at this synapse (reviewed in (Blitz et al., 2004)).

1.3.1.2 Short-term facilitation

The synaptic short-term facilitation is an increase in the response to a same stimuli delivered shortly after the previous one. Short-term facilitation is associated with a presynaptic increase in intracellular calcium concentration, often referred to as the calcium residual hypothesis. In a synapse with a low release probability, a first spike will open calcium channel that will increase the intracellular calcium concentration. If a second spike arrives shortly after the first one, the increased calcium concentration will largely increase the release probability and might even increase the quantum release, which both lead to facilitation. A possible complementary mechanism for short-term facilitation is the saturation of endogenous calcium buffer in the presynaptic terminal (Fioravante and Regehr, 2011). Present in the terminal, calcium-binding proteins capture calcium and reduces the initial release probability (Neher, 1998; Matveev et al., 2004), if a second stimulus arrives quickly after the first one and that calcium still occupies some of these calcium-binding proteins, then more calcium will reach the release site and consequently, the release probability will be increased (Fioravante and Regehr, 2011).

1.3.1.2 Differences between in vivo and in vitro studies

Most of in vitro studies conclude that synapses are depressing, while in vivo studies show much less depression and often facilitation. These discrepancies might be due to several different causes, however among them, differences in neuronal maturity, differences in the level of tonic activity, and differences in extracellular calcium concentrations likely play a major role (Borst, 2010). Because of technical reasons, neuronal culture are produced from immature neurons and slice recordings are performed mainly on young animals, while in vivo recordings are generally performed on adult animals. While brain slices are generally not active, recordings made in vivo are from active networks. Reducing the level of extracellular calcium concentration in the artificial cerebrospinal fluid (ACSF) (and increasing extracellular potassium) in ferret prefrontal cortical slice preparation made the slice active and oscillating in a way that resemble to the slow oscillation present during slow-wave sleep (Sanchez-Vives and McCormick, 2000; Sanchez-Vives et al., 2007). The level of extracellular calcium in vivo is of 1-1.2 mM (Heinemann et al., 1977; Massimini and Amzica, 2001; Crochet et al., 2005), while most of in vitro studies are conducted with an extracellular concentration of calcium of 2 mM or more. Both the presence of "in vivo-like" ACSF and the presence of network activity in in vitro preparations were shown to have an impact on short-term plasticity mainly by decreasing the release probability (Reig et al., 2006; Reig and Sanchez-Vives, 2007; Sanchez-Vives et al., 2007). Increased network activity was also shown to favor facilitation over depression with in vivo preparations (Crochet et al., 2005; Crochet et al., 2006).

1.3.2 Mid-term plasticity

Mid-term plasticity refers to plasticity occurring at a scale of seconds to minutes (Timofeev, 2011). Mid-term plasticity might be implicated in the formation of short-term memory including learning and forgetting. In active cortical network less than half of synapses show mid-term plasticity, but in cortical silent networks most of synapses show mid-term synaptic depression (Crochet et al., 2006). In experiments using control stimuli applied at 1 Hz followed by rhythmic train of stimuli (5-10 pulses) of different frequencies

(10 Hz, to mimic spindles, 40 Hz to mimic gamma, and 100 Hz to mimic ripples) repeated every two seconds to mimic the grouping induced by sleep slow waves, the amplitude of responses during extinction could be either facilitated or depressed at the same synapse (Cisse et al., 2004; Crochet et al., 2006), and at least a part of the facilitation was NMDA-dependent because it could be blocked by AP5 microdialysis (Cisse et al., 2004).

1.3.3 Long-term synaptic plasticity

Synaptic changes that last for tens of minutes to hours are referred to as long-term synaptic plasticity that could be either long-term depression in the case of a reduced response, or long-term potentiation in the case of an increased response. These changes can be physiological (functional modification of existing synapses and neurons) or structural (physical rewiring by synapse formation, elimination, and morphological change). In the following sections, some of the known mechanisms for long-term plasticity will be described.

1.3.3.1 Long-term depression

Long-term depression (LTD) is a decrease in response and is mainly associated with low frequency stimulation, which is called homosynaptic LTD. Long-term depression can also be induced as result of inactivity in synapses on a neuron that have active synapses (heterosynaptic LTD) (reviewed in (Chistiakova and Volgushev, 2009; Timofeev, 2011)). In NMDA receptor–dependent LTD (NMDA-LTD), calcium from postsynaptic NMDA receptors activates protein phosphatases including calcineurin, leading to dephosphorylation of specific sites on the AMPA receptor GluR1 subunit and internalization of synaptic AMPA receptors (Feldman, 2009). A second major form is metabotropic glutamate receptor–dependent LTD (mGluR-LTD), of which several subforms exist (Egger et al., 1999; Renger et al., 2002; Barbara et al., 2003; Czarnecki et al., 2007).

A third form of LTD involves cannabinoid type 1 (CB1) receptors (Chevaleyre et al., 2006). In CB1-LTD, postsynaptic calcium elevation and activation of group I mGluRs

drive postsynaptic endocannabinoid synthesis, which signals retrogradely to presynaptic CB1 receptors, driving a long-lasting decrease in release probability (Chevaleyre et al., 2006), this is considered a presynaptic mechanism.

1.3.3.2 Long-term potentiation

Long-term potentiation (LTP) is mainly associated with high frequency tetanic stimulations that are purely non-physiological, typically 100 Hz for one second. Some other stimulation protocols are more physiological, for example the theta-burst stimulations. It usually consists in trains of 3-4 stimuli delivered at 100 Hz and recurring every 200 ms (5 Hz). This type of activity is common in the hippocampus (Kandel and Spencer, 1961), although not common in the thalamocortical system.

The classical mechanism of LTP in neocortex is NMDA-LTP, which occurs because calcium from postsynaptic NMDA receptors activates different kinases including αCaMKII, which then drives specific AMPA receptor phosphorylation, and insertion of GluR1-containing AMPA receptor into synapses (Malinow and Malenka, 2002; Lisman et al., 2012).

A second form of neocortical LTP is expressed presynaptically by an increase in release probability, which also alters short-term synaptic dynamics (Markram and Tsodyks, 1996; Buonomano, 1999; Eder et al., 2002). This enhancement would be achieved by an increased level of calcium concentration in the presynaptic terminal leading to an increased activity of cAMP and to activation PKA, which would be necessary for this type of LTP (reviewed in (Castillo, 2011)).

1.3.4 Augmenting responses, a form of plasticity

Other form of plasticity includes intrinsic plasticity and network plasticity. Augmenting responses for example, is a form of network plasticity. It consists in a particular form of short-term neuronal plasticity that requires both synaptic dynamics and activation of some types of intrinsic neuronal currents (Timofeev, 2011). Augmenting

responses can be reliably elicited by applying rhythmic stimuli with a frequency of about 10 Hz in diverse experimental preparations including in intact TC system (Bazhenov et al., 1998b; Steriade et al., 1998a), in the thalamus of decorticated animals (Bazhenov et al., 1998a; Timofeev and Steriade, 1998; Houweling et al., 1999), and in isolated cortical preparation (Castro-Alamancos and Connors, 1996b, a; Houweling et al., 2002; Timofeev et al., 2002).

Intracortical augmentation is generally weak and occurs with weak depression of inhibitory synapses and stronger depression at excitatory synapses (Houweling et al., 2002). In the intact thalamocortical system, augmenting responses are primarily due to a low-threshold mechanism (Bazhenov et al., 1998b; Steriade et al., 1998a). The first stimulus elicits EPSPs in thalamocortical and thalamic reticular neurons. Thalamocortical firing elicit EPSPs in cortical neurons and the corticothalamic feedback reinforces the depolarisation of thalamic reticular neurons. Then due to the burst firing of thalamic reticular neurons, the EPSP in thalamocortical neurons is followed by a strong IPSP. The second and following stimuli arrive when the thalamocortical neuron is hyperpolarized and the EPSP evoked in these neurons triggers a low-threshold calcium spike that augment the response (Timofeev, 2011). Therefore, augmenting responses is a form of short-term neuronal plasticity that is based on an interaction of synaptic response and intrinsic currents.

1.4 Plasticity in different states of vigilance, learning, and memory

An early study demonstrated that the rate of forgetting is low during sleep as compared to wakefulness, suggesting, at least that sleep is important for memory retention (Jenkins and Dallenbach, 1924). There is a current debate on the role of different states of vigilance in plasticity, learning, and memory. One of the views is that synapses are potentiated by long waking periods and slow-wave sleep relieves synapses from their potentiated state by a general synaptic downscaling; this will be presented as the “sleep and synaptic homeostasis hypothesis”. An alternative point of view is that memory is encoded during wake but its consolidation occurs during slow-wave sleep by a reactivation of

circuits involved in the learning; this will be presented as the "memory consolidation during slow-wave sleep hypothesis". Both hypotheses point to a critical role of slow-wave sleep in learning and memory formation with however, a very different mechanism.

1.4.1 Sleep and synaptic homeostasis hypothesis

The first hypothesis is referred to as the sleep and synaptic homeostasis and is defined as follow: (1) wakefulness is associated with synaptic potentiation in several cortical circuits; (2) synaptic potentiation is tied to the homeostatic regulation of slow wave activity; (3) slow wave activity is associated with synaptic downscaling; (4) synaptic downscaling is associated with the beneficial effect of sleep on performance (Tononi and Cirelli, 2003, 2006; Tononi, 2009). Among arguments for synaptic potentiation during wake are the high level of expression of genes associated with LTP such as *Arc*, *BDNF*, *NGFI-A*, *Homer*, *Narp*,... (Wallace et al., 1995; Ying et al., 2002; Silva, 2003), and the expression of these genes is strongly reduced or abolished during sleep (Cirelli and Tononi, 2000a, b; Cirelli et al., 2004). Noradrenaline is important for the LTP induction (Walling and Harley, 2004), and noradrenergic lesions lead to a decrease in *P-CREB*, *Arc*, *BDNF*, *NGFI-A*, *Homer*, and *Narp* to a level similar to what is seen during sleep (Cirelli et al., 1996; Cirelli and Tononi, 2000a).

Although slow-wave sleep seems to suppress globally the molecular signalling that mediate LTP-related synaptic remodelling and to enhance LTD-related signalling (Cirelli and Tononi, 2000a; Cirelli et al., 2004; Vyazovskiy et al., 2008), it does not preclude that LTP occurs in specific regions during sleep (Diekelmann and Born, 2010). Actually, in rats exposed to a novel tactile experience during waking or in which LTP was induced in hippocampus were shown to have an increased expression of the plasticity-related immediate early genes *Arc* and *Egr1* (which are implicated in LTP) during subsequent sleep, mainly in cortical areas that were the most activated by the novel experience, and this effect seemed to be mediated by REM sleep (Ribeiro et al., 1999; Ribeiro et al., 2002; Ribeiro et al., 2007).

The sleep and synaptic homeostasis hypothesis also predicts that the more synaptic potentiation occurs during wakefulness, the higher will be the increase in the subsequent sleep (Tononi and Cirelli, 2006). A 24h stimulation of a whisker resulted in a net increase in synaptic density by about 35% on cortical neurons in the corresponding barrel cortex (Knott et al., 2002). Cutting whiskers on one side led to an increase in slow wave activity in the contralateral cortex of the intact whiskers (Vyazovskiy et al., 2000). Increasing the duration of wakefulness by few hours produced an increase in the expression of synaptic potentiation markers (Cirelli and Tononi, 2000b) and was followed by an increase in slow wave activity (Tononi and Cirelli, 2006). In animals with a lesion of the noradrenergic system, the amount and timing of sleep was unaffected, but the peak in slow wave activity seen in the morning hours after the nocturnal activity phase was dampened, so was the slow wave activity response to sleep deprivation (Cirelli et al., 2005).

The downscaling is different from LTD because the latter affects a select group of specific synapses, while the former would affect all synapses in a similar manner without any fine-tuning at the level of individual synapses (Tononi and Cirelli, 2003, 2006).Thus the relative difference in synaptic strength is preserved, and presumably memory traces as well. This downscaling would be brought about by the dephosphorylation and subsequent internalization of AMPA receptors (Turrigiano, 2000; Malinow and Malenka, 2002). The synaptic downscaling would benefit learning by increasing the signal to noise ratio (Tononi and Cirelli, 2006). This downscaling would ensure to restore the brain's ability to learn by preventing synaptic saturation.

Slow wave activity was found to be modulated in a use-dependent manner; both peripheral experimentally induced stimulation and the spontaneous use of circumscribed cortical areas led to regionally more intense slow waves (Kattler et al., 1994; Vyazovskiy et al., 2000; Vyazovskiy et al., 2004). In addition, learning of a motor task was shown to increase locally slow wave activity (Huber et al., 2004; Vyazovskiy and Tobler, 2008; Hanlon et al., 2009), while unilateral arm immobilization led to a decrease in slow waves (Huber et al., 2006). The proportion of high-amplitude slow waves decreased from early to late sleep (Riedner et al., 2007). The slope of slow waves is determined by the speed of

recruitment/decruitment of neurons in the population. The steeper is the slope, the quicker is the recruitment (higher synchrony) and the efficacy of cortical connections would be a key factor in determining the slope (Vyazovskiy et al., 2011a). Slow waves slope was found to be steeper in early sleep as compared to late sleep (Riedner et al., 2007; Vyazovskiy et al., 2007). High firing synchrony was associated with steep slopes of simultaneously occurring EEG slow saves, whereas low synchrony was associated with decreased slopes (Vyazovskiy et al., 2009). Early sleep was also characterized by short ON (active, UP) periods that alternated with frequent OFF (silent, Down) periods, while late sleep was characterized by longer ON periods and by less synchronized transitions between periods of activity and inactivity (Vyazovskiy et al., 2009; Vyazovskiy et al., 2011a). Moreover, sleep deprivation resulted in an increase in the number of high-amplitude slow waves, steeper slopes, and fewer multipeak waves, suggesting that changes in SWA are likely to be the result of homeostatic sleep regulation and not circadian time (Vyazovskiy et al., 2007).

Slow wave activity increases after periods of wakefulness and decreases after periods of sleep (Achermann and Borbely, 2003). Cortical firing rate was found to increase with duration of wakefulness, while it was found to decrease with the duration of slow-wave sleep (Vyazovskiy et al., 2009).

As described in a previous section, at the molecular level the best established mechanism of LTP and LTD involves the trafficking of postsynaptic glutamatergic AMPA receptors containing the GluR1 subunit, with adding receptor at the membrane being linked to potentiation and their removal to synaptic depression (Malinow and Malenka, 2002; Collingridge et al., 2004; Malenka and Bear, 2004; Lisman et al., 2012). It was recently found that GluR1-containing AMPA receptor levels are higher by about 40% during wakefulness as compared to sleep and changes in the phosphorylation states of AMPA receptors, CamKII, and GSK3β were consistent with synaptic potentiation during wake and synaptic depression during sleep (Vyazovskiy et al., 2008).

A local BDNF infusion in a small cortical region induces a local slow wave activity increase in the same region while blocking BDNF expression during waking results in a local decrease in slow wave activity decrease in the subsequent sleep (Faraguna et al., 2008; Hanlon et al., 2011).

1.4.2 Memory consolidation during slow-wave sleep hypothesis

The two-stage memory model consists in a first step occurring during wake in which the memory is encoded and a second step occurring during sleep in which the memory is replayed and consolidated. The memory consolidation during sleep relies on a reactivation of circuits implied in the memory task and depending on the type of memory, different structures could be implicated. Memory can be defined as declarative memory (also referred to as explicit or relational memory) and non-declarative memory (also referred to as procedural or implicit memory). The declarative memory can be consciously recalled (facts, knowledge), while the non-declarative memory refers to unconscious memories such as skills. The declarative memory is further divided into episodic memories (specific events, for example: what you had for dinner last night) and semantic memories (general information, for example: Ottawa is the capital of Canada), while non-declarative memories are divided into several subcategories such as procedural skills, conditioning, non-associative, and priming (reviewed in (Stickgold, 2005)).

The encoding and short-term retrieval of declarative memory essentially rely on the hippocampus and associated medial temporal lobe structure (Squire, 1992), however with time, its retrieval becomes independent of the hippocampus presumably due to a gradual transfer to neocortical networks (Sutherland and McNaughton, 2000; Diekelmann and Born, 2010). Non-declarative memories would rely primarily on striato-cortical circuitry (Doyon and Benali, 2005).

The improvement in declarative memory, which is hippocampus-dependent, is enhanced by the slow oscillation of slow-wave sleep, while the non-declarative memory would benefit more from REM sleep (Plihal and Born, 1997; Gais and Born, 2004b; Peigneux et al., 2004; Stickgold, 2005), although the non-declarative memory may also

benefit from slow-wave sleep (Huber et al., 2004; Holz et al., 2012). For example, a motor learning task (non-declarative memory) was shown to increase locally the slow wave activities in the human brain areas implicated in the task (Huber et al., 2004). This might be due to the fact that encoding of declarative memories is typically explicit, whereas procedural memory encoding can involve both implicit and explicit processes (Diekelmann and Born, 2010). Also, a recent study showing that pharmacological suppression of REM by administration of anti-depressant drugs (selective noradrenalin or serotonin re-uptake inhibitors) did not impair the consolidation of procedural memory (Rasch et al., 2009). Recent studies showed that REM sleep was particularly important for the consolidation of emotional aspect of a memory (Wagner et al., 2001; Payne et al., 2008; Nishida et al., 2009). The blockage of NMDA receptors or of the AMPA receptors in humans was shown to prevent the improvement on a visual skill learning task (Gais et al., 2008).

Enhancing slow oscillation by transcranial electrical stimulation during early slow-wave sleep improved the declarative memory retention even more than for slow-wave sleep alone, which suggests an important role for slow oscillation in memory formation (Marshall et al., 2006). In humans, even a short nap of about an hour is very profitable for memory retention improvement of a visual texture discrimination task (Mednick et al., 2002; Mednick et al., 2003), for a motor learning task (sequential finger-tapping task) (Nishida and Walker, 2007), and for declarative memory (Takashima et al., 2006). However, sleep fragmentation in human patients suffering of obstructive sleep apnea (no significant difference in total sleep time, sleep efficiency or sleep stage as compared to control group) was shown to impair off-line consolidation of a non-declarative procedural task (motor sequence learning task) (Djonlagic et al., 2012). Compared with a period of wake of equal length, a period of post-learning sleep enhances the retention of declarative memory (Plihal and Born, 1997; Born et al., 2006; Tucker et al., 2006; Rasch et al., 2007; Lahl et al., 2008; Born and Wilhelm, 2012) and improves performance in procedural skills (Plihal and Born, 1997; Stickgold et al., 2000; Fischer et al., 2002; Gais et al., 2002; Mednick et al., 2003; Walker et al., 2003a; Walker et al., 2003b; Born et al., 2006; Korman et al., 2007). Improvements in declarative memory was shown to be stronger if the sleep occurred

shortly after the learning task than if the sleep occurred after a full day of wakefulness (Payne et al., 2012).

Role of spindles:

An object recognition task for rats, which uses the declarative memory system without any stressful procedures, was shown to increase the power in slow oscillation and spindles frequency ranges in a subsequent sleep episode, and rats only showed significant memory for the target object place in the Test trial after a sleep episode (Binder et al., 2012). Both declarative and non-declarative learning tasks in humans (learning of paired-associate lists of 336 unrelated words, episodic memory of a virtual city maze, learning face-scene association, motor procedural learning,…) were also shown to increase the spindle density in the following sleep episode in regions involved in the learning of task (Meier-Koll et al., 1999; Gais et al., 2002; Fogel and Smith, 2006; Morin et al., 2008; Bergmann et al., 2012; Holz et al., 2012). The overnight memory retention is highly correlated with the number of spindle detected (Clemens et al., 2005). A reward-association task in rats, which is believed to be analogous to paired-associate learning task in humans, was shown to increase spindle density after learning (Eschenko et al., 2006). Sleep spindles are likely associated with a dendritic calcium increase (Contreras et al., 1997; Sejnowski and Destexhe, 2000; Waters and Helmchen, 2004; Destexhe et al., 2007), and natural spindle stimulation pattern applied to a cortical slice led to both short-term facilitation and long-term potentiation (Rosanova and Ulrich, 2005).

Role of sharp-wave ripples:

Hippocampal sharp waves are fast depolarizing events that are generated in the CA3 region, on which high-frequency oscillations (100-300 Hz, ripples) originating from an interaction between inhibitory interneurons and pyramidal cells in CA1 are superimposed (Buzsaki, 1989). Sharp-wave ripples are recorded in CA1 and in the deep layers of the entorhinal cortex. They occur during slow-wave sleep and also during wake, and they accompany the reactivation of neuron ensembles that are active during a preceding wake experience (Buzsaki, 1989; Wilson and McNaughton, 1994; Nadasdy et al., 1999; Peyrache et al., 2009; O'Neill et al., 2010). Selective disruption of ripples by electrical stimulation

during the post-learning rest period in rats impaired the formation of long-lasting spatial memories, suggesting that ripples have a causal role in sleep-associated memory consolidation (Girardeau et al., 2009; Ego-Stengel and Wilson, 2010).

Hippocampal sharp-wave ripples were shown to be time-locked to a specific phase of spindles and slow oscillation (Sirota et al., 2003; Battaglia et al., 2004; Molle et al., 2006; Clemens et al., 2011). It is known that slow oscillation groups other sleep rhythms such as spindles, delta waves, and hippocampal sharp-wave ripples (Steriade and Amzica, 1998; Steriade and Timofeev, 2003; Steriade, 2006). Transcranial electrical stimulation applied above the frontal cortex at low frequency to boost slow wave activity not only induced an increase in slow waves, but also in frontal spindle activity (Marshall et al., 2006; Mölle and Born, 2011). Both spindles and hippocampal sharp-wave ripples occur during the neocortical active state of the slow oscillation (Molle et al., 2002; Sirota et al., 2003; Isomura et al., 2006; Molle et al., 2006; Steriade, 2006), and sharp-wave ripples are also temporally coupled to sleep spindles troughs (Siapas and Wilson, 1998; Sirota et al., 2003; Wierzynski et al., 2009). Thus ripples and associated hippocampal memory reactivations feed the cortex exactly into the excitatory phases of the spindle cycle (Buzsaki, 1998; Sirota et al., 2003; Born et al., 2006; Marshall and Born, 2007; Molle and Born, 2009; Mölle and Born, 2011). Spindle–ripple events that contain reactivated memory information and arrive at neocortical networks during the slow oscillation up-state represent a putative mechanism which serves the effective transfer and storage of hippocampal memory information within neocortical networks (Mölle and Born, 2011).

Also, re-activation in hippocampal networks seems to be enabled by the low level of acetylcholine that characterizes slow-wave sleep (Hasselmo, 1999; Gais and Born, 2004a; Hasselmo and McGaughy, 2004). The high cholinergic activity during wakefulness is inhibiting feedback synapses within the hippocampal CA3 region and efferent projections from CA3 to CA1, the entorhinal cortex, and the neocortex, thus leading to a reduced flow of information from the hippocampus to the neocortex (reviewed in (Hasselmo, 1999)). Consequently, during wakefulness, the primary direction of information flow is from the neocortex to the hippocampus, which allows the encoding of new memories (Hasselmo,

1999; Born et al., 2006). In contrast, minimal cholinergic activity during SWS enables a feedback of information from the hippocampus to neocortical networks (Born et al., 2006). Reactivations have also been observed in other brain regions such as striatal and neocortical networks (Ribeiro et al., 2004; Euston et al., 2007; Ji and Wilson, 2007).

1.5 General objectives of the thesis and experimental approaches

A large part of this thesis is dedicated to the understanding of the slow oscillation: how and where is it generated? How does it propagate? How similar is ketamine-xylazine anesthesia and natural slow-wave sleep? To answer those questions, we performed multiple simultaneous intracellular, local field potential or multiunit recordings in the neocortex of cats either under ketamine-xylazine anesthesia or during natural sleep-wake transitions in head-restrained conditions. Performing these studies gave us the opportunity to compare our results obtained under ketamine-xylazine anesthesia with those obtained during natural sleep, to establish similarities and to quantify some differences between the two approaches. Those questions are treated in chapters II-III-IV. In the last two chapters, we wanted to know how is modified the synaptic communication as a function of states of vigilances. In chapter V, we asked if slow waves that are so characteristic of slow-wave sleep could play a role in long-term potentiation, since sleep and LTP are thought to play a major role in memory. To answer this question, we performed local field potential and intracellular recordings in non-anesthetized animals in different states of vigilance, and we studied how evoked potentials were modified by states of vigilances. Then to characterize the mechanism of this plasticity, we performed different experiments using natural pattern of stimulation in brain slices. Finally, in chapter VI, we specifically asked what could be the effect of spindles, a natural sleep rhythm, on synaptic transmission at the thalamic level. To answer this question, we used several technical approaches including intracellular recordings in the thalamus of anesthetized (with barbiturates) cats, cortical local field potential and intracellular recording in non-anesthetized cats through sleep/wake cycles, intracellular recordings and calcium measurements in cortical slices, computational modelling of calcium depletion, immune-staining, and electron microscopy.

Chapter II

2.0 Precise long-range synchronization of activity and silence in neocortical neurons during slow-wave oscillation

Maxim Volgushev[1,2], Sylvain Chauvette[3], Mikhail Mukovski[1], Igor Timofeev[3]

[1]Department of Neurophysiology, Ruhr-University Bochum, D-44780, Germany
[2]Institute of Higher Nervous Activity and Neurophysiology, Moscow, 117485, Russia
[3]Department of Anatomy and Physiology, Laval University, Québec, G1K 7P4, Canada

Published in the Journal of Neuroscience, 2006

Complete citation: Volgushev M, Chauvette S, Mukovski M, Timofeev I (2006) Precise long-range synchronization of activity and silence in neocortical neurons during slow-wave oscillations [corrected]. J Neurosci 26:5665-5672.

Titre en français:

2.0 Synchronisation précise de l'activité et du silence dans des neurones néocorticaux distants pendant l'oscillation lente.

2.1 Résumé en français

Le sommeil à ondes lentes est caractérisé par une alternance de périodes actives et silencieuses dans le réseau cortico-thalamique. Tant l'activité que le silence sont des états stables du réseau, mais les mécanismes de leur alternance demeurent inconnus. Nous montrons, en utilisant des enregistrements intracellulaires simultanés chez le chat, que les rythmes lents impliquent tous les neurones néocorticaux, et que tant l'activité que le silence débutent de façon presque synchrone dans des cellules situées jusqu'à 12 mm de distance. L'activité apparaissait principalement à la bordure des aires 5/7 et se propageait dans les deux directions, antérieure et postérieure. L'activité débutait plus tôt dans les cellules à décharges rapides ainsi que dans les cellules à décharges par bouffées de potentiels d'action, puis dans les neurones à décharges régulières. Ces résultats fournissent une évidence directe pour deux mécanismes de génération de l'état actif : la propagation de l'activité à partir d'un foyer local, et la synchronisation de faibles activités débutant à plusieurs endroits. Étonnamment, les déclenchements des périodes silencieuses étaient synchronisés de façon plus précise que les déclenchements des périodes actives, ne montrant aucun biais pour l'endroit ou pour le type de cellule. Cette découverte intrigante expose une lacune majeure dans la compréhension de la nature des alternances d'états. Nous proposons que ce soit la terminaison synchrone de l'activité et l'occurrence des périodes silencieuses du réseau neuronal qui font de l'EEG une image si caractéristique du sommeil à ondes lentes. Le déclenchement synchronisé des périodes de silence dans des neurones distants ne peut reposer exclusivement sur les propriétés individuelles des cellules et des synapses, comme l'adaptation des décharges neuronales ou la dépression synaptique; ceci implique plutôt l'existence d'un mécanisme de réseau. Parvenir à révéler ce mécanisme à grande échelle qui assure la transition d'une période active du réseau vers une période silencieuse, nous permettrait d'améliorer grandement notre compréhension de l'origine des rythmes du cerveau lors de fonctions normales ou lors de pathologies.

2.2 Abstract

Slow-wave sleep is characterized by alternating periods of activity and silence in cortico-thalamic networks. Both, activity and silence are stable network states, but the mechanisms of their alternation remain unknown. We show, using simultaneous multisite intracellular recordings in cats, that slow rhythm involves all neocortical neurons, and that both, activity and silence started almost synchronously in cells located up to 12mm apart. Activity appeared predominantly at the area 5/7 border, and spread in both, anterior and posterior directions. The activity started earlier in fast-spiking cells and intrinsically-bursting cells, than in regular-spiking neurons. These results provide direct evidence for two mechanisms of active state generation: spread of activity from a local focus, and synchronization of weaker activity, originated at multiple locations. Surprisingly, onsets of silent states were synchronized even more precisely than the onsets of activity, showing no latency bias for location or cell type. This most intriguing finding exposes a major gap in understanding the nature of state alternation. We suggest that it is the synchronous termination of activity and occurrence of silent states of the neuronal network that makes the EEG picture during slow wave sleep so characteristic. Synchronous onset of silence in distant neurons cannot rely exclusively on properties of individual cells and synapses, like adaptation of neuronal firing or synaptic depression; instead, it implies the existence of a network mechanism. Revealing this yet unknown large-scale mechanism, which switches network activity to silence, will aid our understanding of the origin of brain rhythms in normal function and pathology.

2.3 Introduction

A signature of the slow-wave sleep in the electroencephalogram (EEG) are large amplitude fluctuations (Blake and Gerard, 1937), which reflect alternating periods of activity and silence in thalamocortical networks (Steriade et al., 1993a, b; Contreras and Steriade, 1995; Steriade et al., 2001; Timofeev et al., 2001; Petersen et al., 2003). The active states are associated with neuronal depolarization, firing, and rigorous synaptic activity, while during the silent states neurons are hyperpolarized and the network is inactive (Contreras et al., 1996; Timofeev et al., 1996; Wilson and Kawaguchi, 1996; Timofeev et al., 2001; Shu et al., 2003). The alternation of states is of intracortical origin since active and silent states are self-generated in the isolated cortical preparation (Steriade et al., 1993a; Sanchez-Vives and McCormick, 2000; Timofeev et al., 2000) and absent in the thalamus of decorticated animals (Timofeev and Steriade, 1996). Both, activity and silence are stable states of the network, but the mechanisms of state alternation remain an enigma. One possibility is the origin of activity in a specific focus, or group of cells, with sequential lateral propagation (Sanchez-Vives and McCormick, 2000; Cossart et al., 2003). In its most conservative formulation, the propagation hypothesis predicts a reiterating pattern of activity initiation and spread, with systematic site-specific onset delays. For this scenario, focal activity must be strong enough to evoke discharges in target cells and thus to spread. Alternatively, weaker activity may originate occasionally at multiple locations, and involve further parts of the network, if it appears to be sufficiently synchronous (Timofeev et al., 2000; Massimini et al., 2004). The synchronization hypothesis predicts a variable spatial pattern of activity initiation, no systematic delays between sites, and occurrence of occasional local episodes of activity at any site. To trigger a generalized active state by this mechanism, sufficient number of sites must become active within an integration period of postsynaptic responses. These hypotheses propose two mechanisms which, either alone or in combination, underlie the origin of active states. Termination of activity and onset of silent states is ascribed to the intrinsic cellular properties and currents (Bazhenov et al., 2002; Compte et al., 2003; Hill and Tononi, 2004; Milojkovic et al., 2005). However, a mechanism relying exclusively on single-cell properties, might lead to a high variability of silent state onsets in individual cells, since each neuron has a unique set of intrinsic currents. To test these predictions, we recorded simultaneously local field

potentials (LFP) and intracellular activity of 2-4 neurons in cat neocortex. We show that slow rhythm involves all neocortical neurons, and that onsets of both, activity and silence, occurs with high temporal precision in cells located up to 12 mm apart. Our results provide direct evidence for two mechanisms of active state generation: spread of activity from a restricted local, and synchronization of weaker activity, originated at multiple locations. Most surprisingly, onsets of silent states were synchronized even more precisely than onsets of activity. We suggest that the synchronous termination of activity and occurrence of silent states of the neuronal network are what make the EEG picture during slow wave sleep so characteristic.

2.4 Materials and Methods

Surgery and recording

All experimental procedures used in this study were performed in accordance with the Canadian guidelines for animal care and were approved by the committee for animal care of Laval University.

Experiments were conducted on adult cats under a mixture of ketamine-xylazine and thiopental anesthesia (i.m. injection of 10-15 mg/kg ketamine, 2-3 mg/kg xylazine and i.v. injection of 10 mg/kg thiopental). We opted for this type of anesthesia as it reproduces closely the typical natural sleep EEG patterns, including the slow-wave oscillations. Specifically, under this anesthesia both the slow-wave oscillations, spindles and beta-gamma activities are reliably observed in the EEG. Details of the experimental procedures are described elsewhere (Crochet et al., 2005; Rosanova and Timofeev, 2005). Briefly, surgery was started after the EEG showed typical signs of general anesthesia and complete analgesia was achieved. Additional doses of anesthetics were administrated when the EEG showed changes towards activated patterns. A craniotomy was made at coordinates AP –5 to +18, L 3 to 12, to expose the suprasylvian gyrus. Brain pulsations were reduced by bilateral pneumothorax, hip suspension, and drainage of the cisterna magna. End-tidal CO2 was held at 3.5-3.7% and body temperature at 37°-38°C. To avoid possible respiration deficiency during deep anesthesia and improve further the stability of the recordings, animals were paralyzed with gallamine triethiodide (2 mg/kg, i.v.), and artificially ventilated.

Simultaneous recordings of the local field potential (LFP) and intracellular activity of 2-4 neurons were performed. Intracellular recordings were made with sharp electrodes, filled with 2.5 M potassium acetate and 2% neurobiotin and beveled to a resistance of 55-80 MOhm. Four electrodes for intracellular recording were positioned along the suprasylvian gyrus at 4 mm intervals, around the following coordinates: *Electrode 1*: AP +12, area 5; *Electrode 2*: AP +8, border between area 5 and area 7; *Electrode 3*: AP +4, area 7; *Electrode 4*: AP 0, border between area 7 and area 21. Lateral coordinates of all intracellular electrodes were between 8 and 9. LFP's were recorded with a coaxial bipolar

tungsten electrode (SNE-100, Rhode Medical Instruments, Summerland, USA), positioned between intracellular electrodes 2 and 3, at coordinates anterior +6, lateral between 7 and 8.

After electrode positioning, the craniotomy was filled with 3.5-4% agar (Sigma). With each intracellular electrode, several cells were sequentially recorded in one experiment. Some of the recorded cells were injected with neurobiotin. To facilitate the morphological/electrophysiological correlation, we selected for injection only cells which were recorded for longer than 30 min, and were separated well by cortical depth when recorded with the same electrode.

Intracellular signals were amplified with Neurodata IR-283 amplifiers (Cygnus Technology, PA, USA). Both intracellular and LFP signals were digitized at 20 kHz and recorded on a Vision data acquisition system (Nicolet, WI, USA).

Morphological procedures

After experiments animals were perfused, with 0.9% saline, followed by 3% paraformaldehyde. The brain around recorded sites was placed in 30% sucrose, sectioned and then processed by standard procedures (Horikawa and Armstrong, 1988). Reconstruction of stained cells was done with a computerized Neurolucida system.

Data processing

Offline data processing was done with custom-written programs in MatLab (Mathworks Inc) environment.

Clusters of states

We defined as "clusters" groups of states, which fulfill two criteria. First, they occur in all simultaneously recorded cells. Second, their onsets are separated by less than 200 ms. Thus, number of states in one cluster is equal to the number of simultaneously recorded cells. Within each cluster we calculated delays of state onset in each cell relative to the cluster mean. After completing these calculations, we had: (i) for a set of simultaneously recorded cells, number of clusters; (ii) for each cell, delays of state onsets in that cell relative to the cluster mean, and (iii) for each cell, we calculated the proportion of the states contributed to clusters out of the total number of states in this cell.

Statistical analysis

For statistical analysis we used subroutines of the MatLab Statistics Toolbox and SPSS for Windows (SPSS Inc.). Throughout the text, mean values are given together with SD (mean + SD).

2.5 Results

We recorded simultaneously the LFP and intracellular activity of 2-4 neurons in cat neocortex. Data sample consists of 89 neurons, recorded in 10 sets of 4 cells, 13 sets of 3 cells and 5 pairs. For the pair-wise analysis, 104 pairs were composed of this data.

In membrane potential traces of 4 simultaneously recorded cells (Fig. II-1, A), the active, depolarized states are unambiguously distinguishable from the silent, hyperpolarized states. Two features are immediately apparent in the simultaneously recorded cells. First, all cells are involved in the rhythm of the slow LFP oscillations. Membrane potential traces of all 4 cells showed clear relation to the LFP signal, although occasionally a cell may skip few activity cycles (Fig. II-1, B, shadowed period). Second, all simultaneously recorded neurons showed a very similar pattern of membrane potential changes. In all 4 cells, the alternation between active and silent states was synchronized on a coarse time scale, with common periods of activity or silence.

To compare the timing of the onsets of activity and silence quantitatively, we detected active and silent states in the membrane potential traces of the 89 cells. We used two methods to detect and separate active and silent states.

The first method was based on clear bimodality of the membrane potential distributions during slow wave oscillations. Two levels were set in the bimodal distribution of membrane potential values, which divided the interval between the peaks in three equal parts (Fig. II-2, A,B). The upper level was used as a threshold for the detection of active states, and the lower level for the detection of silent states. “States” were defined as periods during which the membrane potential remained above the threshold for active states, or below the threshold for silent states. To avoid disturbances by transient membrane potential peaks, level crossings for periods shorter than 40 ms were not considered as states. Further, if two active or two silent states were separated by less than 40 ms, the two states were extended to fill the gap and pasted together. During active states, cells were depolarized by 10.4±4.94 mV (mean ± SD) relative to the silent states. Moreover, active states were also associated with stronger fluctuations of the membrane potential, as indicated by significantly higher values of its standard deviation (SD), 3.18±1.27 mV during active states vs. 1.11±0.43 mV during silent states ($n=89$, $p<0.001$).

Our second method of state detection exploits this difference, using two parameters; by which active and silent state differ: (i) membrane potential value and (ii) variability of the membrane potential. We calculated the mean membrane potential and its SD in a running window of 25 ms, and plotted a 3D distribution of the occurrence of pairs of mean and SD values (Fig. II-2, C,D). In this 3D plot, silent states formed a sharp peak at hyperpolarized potentials and low SD values. Active states are represented in this plot by a broader hill at more depolarized potentials and higher SD values. Two regions, one containing the sharp peak representing silent states, and another containing the peak representing active states, were delimited on the top view of this plot. Those periods, which were represented by data points within these regions, were classified as respective, active or silent, states. Since the location of the two peaks differs along both axes, the use of a combination of these two parameters improves detection and separation of active and silent states. For example, occasional periods of strong inhibition during active state of the network may hyperpolarize a cell below the membrane potential threshold of active state. But since the network remains active, fluctuations of the membrane potential during such periods would still be strong, and this period will be correctly assigned as an active state. After this initial separation of active and silent states, the procedures against disturbances by occasional membrane potential peaks were applied: periods shorter than 40 ms were not considered as states, and two active or two silent states separated by less than 40 ms were extended to fill the gap and pasted together.

The two methods gave close results, with high coincidence of the states, detected in the same membrane potential traces. In 19 cells, in which results of state detection with both methods were compared quantitatively, coincidence indexes (calculated, for two state sequences, as percent of the time of their intersection from their mean total length, see (Mukovski et al., 2006) for details) were 92.0±4.9% for the active, and 82.2±7.0% for the silent states (n=19). Since results of the second method, which exploited both, the mean value of the membrane potential and its SD, corresponded better to the expert assessment, was used for the analysis presented below. Averaged duration of active states detected in 89 cells was 266±121 ms, range from 82 to 671 ms; average duration of silent state was 183±57 ms, range from 101 to 385 ms.

Having detected the onsets of active and silent states, we could now address the question: Were there specific temporal patterns of involvement of neurons from different locations in active or silent states? Two strategies were used to investigate this.

First, we searched for possible patterns during generalized states, in which all simultaneously recorded cells, separated by 4 mm intervals in antero-posterior direction were involved (Fig. II-3A). Such groups of active (or silent) states in simultaneously recorded cells will be referred to as "*clusters*" (Fig. II-3, B). We defined as "*clusters*" groups of states, which fulfill two criteria: (i) they should occur in all simultaneously recorded cells, (ii) their onsets should be separated by less than 200 ms. Thus, number of states in one cluster is equal to the number of simultaneously recorded cells. When searching for clusters, states in one cell were taken as reference, and all other simultaneously recorded cells were assessed for state onsets within 200 ms from state onsets in the reference cell. During this search, only near-by-neighbors were considered.

After detecting clusters of states, we calculated for every cluster the delays of state onset in each cell relative to the cluster mean. If an active state would typically originate in a specific focus and then spread, as the propagation hypothesis predicts, the cell which is closest to that focus would be leading in the clusters and thus have a negative delay. Data in Figure 3, c for the active state clusters supports this scenario. Cell-2 had a strong tendency to lead (averaged delay -22.5±27.5 ms), while cell-4 had a strong tendency to follow (averaged delay +20.2 ±46.1 ms, $p<0.001$, $n=138$). In cell-3, located between the neurons 2 and 4, the clustered active states had intermediate delays (average -1.9±49.7 ms). However, the above relation was not absolute, and active state clusters with a "reversed" order, with cell-4 leading and cell-2 following, were occasionally observed (Fig. II-3, B4). Furthermore, the dispersion of the delays was high in every cell and all distributions covered zero, implying that any cell could be leading in some clusters (negative delays), while following in others (positive delays). Despite these reservations, the results strongly suggest that active states originated most often at, or close to, the cell-2 location, and then spread in both directions. Population analysis of the sets of simultaneously recorded cells further supports this scenario (Fig. II-3, D1). In 21 neurons recorded at the border between area 5 and area 7 (position 2), averaged delays of clustered active states were negative (-

14.6±12.9 ms, n=21) and significantly different from the positive delays in more posteriorly recorded cells (6.1±14.8 ms, n=17, $p<0.0016$ at position 3 and 11.9 ±8.8 ms, n=23, $p<0.001$ at position 4). Moreover, the delays in neurons recorded at position 2 were more negative than the delays in more anteriorly recorded cells (position 1, -3.6±12 ms, p=0.0015).

In another approach we analyzed state onset in 104 pairs of simultaneously recorded cells (Fig. II-3, E). Since more states contribute to a pair-wise comparison, we consider it a useful supplement to the analysis of clusters. The pair-wise analysis confirmed the results obtained for clustered states. When all possible pairs were pooled together the cells, located 8-12 mm more posteriorly, were involved in active states with a delay of 7.8±7.9 ms (8 mm, n=33) and 6.1±7.2 ms (12 mm, n=18) relative to more anteriorly-located reference cells (Fig. II-3, E1). At 4 mm distance, the delays were not significantly different from zero (1.4±9.0 ms, n=53), apparently because active states did not originate from the most anterior position. To test for this latter possibility, and to take into account the results of cluster analysis, which revealed preferential beginning of activity at recording position 2, we segregated the pairs of cells in two groups. The first group consisted only of pairs which contained cells recorded at the position of activity origin or more anterior to it (positions 1 and 2). The average delay of active state onsets in these pairs was negative, –5.1+8.6 ms (difference from zero: p=0.022, n=18 pairs), indicating that activity started earlier at position 2. The second group consisted only of cells recorded at or more posterior to the preferential site of activity origin, at positions 2, 3 and 4. For these pairs, the delays at either 4 or 8 mm distance were positive, and significantly different from zero (4.7±7.3 ms, p=0.001, n=35 and 10.5±6.8 ms, $p<0.001$, n=21). Moreover, there was a significant correlation between the anterio-posterior distance and delay of the active state onsets (r=0.386, p=0.003, n=57 pairs). This result supports our conclusion, that activity starts earlier at position 2, and spreads in the anterior direction, to position 1.

Did active states originate in cells of a specific type? We classified cells into 4 electrophysiological classes with differential intrinsic membrane properties (Connors and Gutnick, 1990; Gray and McCormick, 1996; Steriade et al., 1998; Steriade, 2004): regular-spiking (RS), fast-rhythmic-bursting (FRB), intrinsic-bursting (IB) and fast-spiking (FS, Fig. 4, A). This simplistic classification was made primarily on the basis of firing patterns in response to depolarizing current pulses. As additional criteria, action potential shape, and

firing pattern without stimulation were taken into account. For example, during both, current evoked firing and occasional spiking without stimulation, FS neurons generated very short action potentials, FRB cells generated characteristic duplets or triplets of action potentials, and IB cells produced typical bursts.

Comparison of the timing of state onset in different electrophysiological cell classes revealed an interesting pattern of involvement of neurons in active states. On average, active states in clusters appeared first in the FS cells, then in IB neurons and only later in the RS cells (Fig. II-4, B1). In FS cells, active states appeared with an averaged delay of –8.15±16.2 ms, (n=14), which was significantly different from delays in cells of all other types ($p=0.051$) and from delays in RS cells ($p=0.023$). In IB neurons, active states appeared with an average delay of –4.42±19.79 ms (n=16). This delay was significantly different from the delay in RS neurons ($p=0.047$) but not from FS cells or all other cell-types pooled together ($p>0.1$ for both comparisons). Pair-wise comparison confirmed the results of analysis of state clusters. In the pairs consisting of an FS and an RS cell the active states in the FS neurons started earlier, with an average delay of –6.14±13.5 ms ($p=0.028$, n=26 pairs, consisting of 14 FS and 26 RS neurons). Also in IB-RS pairs, the IB cells were leading with averaged delay of –11.5±7.9 ms ($p<0.01$, n=27 pairs, consisting of 16 IB and 27 RS neurons).

In marked contrast to the above results, similar analyses of silent state onsets provided no evidence for preferential origin at specific locus or specific cell type. The averaged delays of clustered silent states in cells 1-4 in Figure II-3, A-C were 5.3±31.7 ms; –2.5±23.4 ms; 3.9±40.0 ms; and –6.7±37.2 ms ($p>0.1$ for all pairs). Population analysis of silent state onsets in 23 sets and 104 pairs of simultaneously recorded neurons did not reveal any significant latency bias for any particular location (Fig. II-3, D2) or relative position of recorded cells (Fig. II-3, E2; 0.14±11.0 ms at 4 mm distance, 2.3±7.6 ms at 8 mm and 1.9±8.6 ms at 12 mm) or cell type (Fig. II-4, B2). For the silent states, the FS neurons had only a non-significant tendency to lead in clusters (–3.93±16.4 ms) and in the FS-RS pairs (–1.53±14.3ms, $p>0.1$ in both cases).

Comparison between active and silent states revealed the most interesting point, namely, that silent states begin in simultaneously recorded cells more synchronously than

active states. Several lines of evidence corroborate this conclusion. In state clusters, the SD of onset delays was lower for the silent states than for the active states (34.4±11.2 ms vs. 39.8±11.0 ms, $p<0.001$, n=89, Fig. II-4, D), showing that the silent states started with a higher temporal precision in different cells. This point is further stressed by the absence of significant dependencies of the onset of silent states on location (Fig. II-3, D2, E2) or cell type (Fig. II-4, B2). The proportion of states, which formed clusters in simultaneously recorded neurons was higher for the silent than for the active states (52.5±17.7% vs. 46.0±17.1%, $p<0.001$, n=89, Fig. II-4, C). The higher percent of clustered states implies that the cases when all simultaneously recorded cells entered the silent state were encountered more often than those cases when all cells became active together. Finally, the pair-wise analysis also revealed lower SD of silent states onset than of the active states (28.7±7.4 ms vs. 33.6±7.8 ms, $p<0.001$, n=104 pairs).

2.6 Discussion

Our analysis of slow sleep oscillation with simultaneous multisite intracellular recordings in cats showed, that (i) all neocortical neurons are involved in the slow rhythm of alternating periods of activity and silence. (ii) Both, activity and silence started almost synchronously in cells located up to 12 mm apart. (iii) Most surprisingly, onsets of silent states were synchronized even more precisely than the onsets of activity.

The results provide direct evidence for both suggested mechanisms of active state generation: spread of activity from a specific focus (Sanchez-Vives and McCormick, 2000; Cossart et al., 2003; Massimini et al., 2004), and synchronization of weaker activity, originated at multiple locations (Timofeev et al., 2000; Massimini et al., 2004). The focal origin and spread hypothesis is supported by the finding that active states appear predominantly at the border between areas 5 and 7, and spread from there in both directions. Together with recent analysis of high-density EEG in humans (Massimini et al., 2004), our data suggests the presence of cortical regions with enhanced intrinsic excitability, which could primarily generate active states during sleep oscillations. Despite the difference in both, experimental subjects and recording techniques, there are clear parallels between the results of Massimini et al. (2004) and our data. In both studies, activity was found to spread preferentially, although not exclusively, in anterio-posterior direction. Moreover, both studies report that activity originates predominantly at certain locations, although occasionally it may start at almost any location. These points indicate a possible similarity between the basic mechanisms underlying slow oscillations in higher mammals and in humans.

Earlier onset of activity in FS and IB cells than in other neurons shows, that a specific cell type may underlie the origin of active states in cat neocortex (Sanchez-Vives and McCormick, 2000). The possibility that activity originates in IB cells, many of which are layer V large pyramids neurons, is consistent with earlier in vitro results (Sanchez-Vives and McCormick, 2000). Moreover, bursts of action potentials generated by these cells may facilitate successful activation of further cells and thus switching of the entering of the whole network into the active state. Earlier onset of activity in FS cells, which are inhibitory interneurons, is more difficult to interpret. Possible factors, contributing to the

earlier onset of active states in FS cells could be larger amplitude and faster onset dynamics of excitatory postsynaptic potentials in the FS cells than in pyramidal neurons (Povysheva et al., 2006). Occasional spontaneous release, which could be one of the reasons for the origin of active states (Timofeev et al., 2000) may depolarize the FS cells more effectively than neurons of other types. An additional factor could be the presence of electrical coupling among FS neurons (Galarreta and Hestrin, 1999; Gibson et al., 1999), which may facilitate detection of activity in electrically coupled neurons. One factor which could have led to an apparently earlier onset of active states in FS cells is a bias in our sample – of 14 FS cells, 8 were recorded at the border between area 5 and 7, where activity started most often. Definite resolution of the question, which of the two factors – recording position versus cell type – contributed stronger to the relative timing of activity onset needs further investigation.

Two observations cannot be explained by activity spread from a local focus, but lend support to the hypothesis on multiple sources and synchronization of activity. At any recording site we have observed local activity episodes, not accompanied by activity in the other simultaneously recorded neurons. Moreover, "typical" sequences of involvement of cells in generalized active states occurred in line with alternative sequences, including "reversed" order. One important implication of the direct evidence for two mechanisms of active state generation is that the necessary requirements for both are fulfilled. Hence during slow-wave sleep, thalamocortical networks can support both, spread of activity from a local focus (Sanchez-Vives and McCormick, 2000; Cossart et al., 2003), as well as synchronization of activity originating from different foci (Timofeev et al., 2000; Massimini et al., 2004). It is tempting to speculate, that the efficacy of these mechanisms may increase in pathology, eventually leading to seizures.

The most intriguing finding of our study is the high synchrony of the silent state onsets. It exposes a major gap in understanding the nature of state alternation. We suggest that it is the synchronous termination of activity and occurrence of silent states in the neuronal network, which produces the characteristic EEG pattern of the slow wave sleep. Our results allow the exclusion of several candidate mechanisms of activity termination. One candidate mechanism would be alternating activity of two mutually inhibiting neuronal sub-populations. Neurons belonging to one of these subpopulations would be active during

active states and silent during silent states, but cells in the other subpopulation should express the opposite pattern, i.e. being active while the rest of the network is silent. This latter requirement is at odds with our results: we found, that all cells, excitatory as well as inhibitory, were involved in the same slow rhythm, and we never observed a cell to be systematically active while other neurons were silent. Another candidate mechanism could be silencing of the network at a particular local focus, followed by a spread of silence in a kind of spreading depression. However, since we did not find evidence for preferential onset of silent states at any specific location, this possibility could be excluded as well. Finally, some recent hypotheses ascribe termination of activity and onset of silent states to the intrinsic cellular properties and currents or synaptic depression (Bazhenov et al., 2002; Compte et al., 2003; Hill and Tononi, 2004; Milojkovic et al., 2005). However, a mechanism relying exclusively on properties of individual cells and synapses, might lead to a high variability of silent state onsets in neurons, since intrinsic properties are extremely non-uniform in different cells and synapses (Thomson and Deuchars, 1994; Markram et al., 2004). This allows to exclude intrinsic membrane properties of neurons or synaptic depression as major reasons for synchronous activity termination. Even not being the major players, intrinsic membrane currents and synaptic properties may nevertheless be instrumental in the organization of the slow EEG rhythm. For example, similarities in the properties of individual cells may facilitate synchronization of their activity.

The high synchrony of the silent state onsets implies the existence of a network mechanism which switches activity to silence. One possibility is synchronization among a sub-population of inhibitory cells, which eventually discharge synchronously enough to silence the whole network. This would lead to termination of activity of both excitatory as well as inhibitory cells, including those cells which have generated the silencing discharge. Following considerations suggest several possible mechanisms, which are compatible with and may contribute to the above scenario. Fast spiking and low-threshold spiking cortical interneurons are electrotonically coupled (Galarreta and Hestrin, 1999; Gibson et al., 1999). During slow-wave oscillation, neuronal activity leads to a decrease of extracellular calcium concentration (Massimini and Amzica, 2001), thus facilitating electrotonical coupling of neurons and glial cells (Thimm et al., 2005). Finally, cortical activity can recruit intrinsic oscillatory mechanisms in thalamocortical neurons (Hughes et al., 2002), which could

increase synchrony among inhibitory interneurons. Indeed, synchrony in silent state onset is disrupted in neocortical slabs (Timofeev et al., 2000). The above hypothesis predicts an increase of synchrony in membrane potential fluctuations of inhibitory interneurons towards the end of an active state. This could lead to the higher incidence of strong IPSPs in neocortical cells. Further, if inhibitory neurons exert a synchronizing effect on activity in the neocortex, as they do in the hippocampus (Cobb et al., 1995), synchrony of the membrane potential fluctuations in all cells might also increase. Experimental testing of these predictions is technically an extremely challenging task, but it will lead to further insights into the mechanisms of slow-wave sleep and the origin of brain rhythms.

2.7 Acknowledgements

Acknowledgements: We are grateful to Marina Chistiakova for comments and discussions and Dimitrios Giannikopoulos for improving the English. We thank Pierre Giguere for technical assistance. This work was supported by grants from CIHR and NSERC of Canada (to IT) and the DGF to MV. IT is CIHR scholar.

2.8 References

Bazhenov M, Timofeev I, Steriade M, Sejnowski TJ (2002) Model of thalamocortical slow-wave sleep oscillations and transitions to activated states. J Neurosci 22:8691-8704.

Blake H, Gerard RW (1937) Brain potentials during sleep. Am J Physiol 119:692-703.

Cobb SR, Buhl EH, Halasy K, Paulsen O, Somogyi P (1995) Synchronization of neuronal activity in hippocampus by individual GABAergic interneurons. Nature 378:75-78.

Compte A, Sanchez-Vives MV, McCormick DA, Wang X-J (2003) Cellular and network mechanisms of slow oscillatory activity (<1 Hz) and wave propagations in a cortical network model. J Neurophysiol 89:2707-2725.

Connors BW, Gutnick MJ (1990) Intrinsic firing patterns of divers neocortical neurons. Trends Neurosci 13:99-104.

Contreras D, Steriade M (1995) Cellular basis of EEG slow rhythms: a study of dynamic corticothalamic relationships. J Neurosci 15:604-622.

Contreras D, Timofeev I, Steriade M (1996) Mechanisms of long-lasting hyperpolarizations underlying slow sleep oscillations in cat corticothalamic networks. J Physiol 494:251-264.

Cossart R, Aronov D, Yuste R (2003) Attractor dynamics of network UP states in the neocortex. Nature 423:283-288.

Crochet S, Chauvette S, Boucetta S, Timofeev I (2005) Modulation of synaptic transmission in neocortex by network activities. Eur J Neurosci 21:1030-1044.

Galarreta M, Hestrin S (1999) A network of fast-spiking cells in the neocortex connected by electrical synapses. Nature 402:72-75.

Gibson JR, Beierlein M, Connors BW (1999) Two networks of electrically coupled inhibitory neurons in neocortex. Nature 402:75-79.

Gray CM, McCormick DA (1996) Chattering cells: superficial pyramidal neurons contributing to the generation of synchronous oscillations in the visual cortex. Science 274:109-113.

Hill SL, Tononi G (2004) Modeling sleep and wakefulness in the thalamocortical system. J Neurophysiol 93:1671-1698.

Horikawa K, Armstrong WE (1988) A versatile means of intracellular labeling: injection of biocytin and its detection with avidin conjugates. J Neurosci Methods 25:1-11.

Hughes SW, Cope DW, Blethyn KL, Crunelli V (2002) Cellular mechanisms of the slow (<1 Hz) oscillation in thalamocortical neurons in vitro. Neuron 33:947-958.

Markram H, Toledo-Rodriguez M, Wang Y, Gupta A, Silberberg G, Wu C (2004) Interneurons of the neocortical inhibitory system. Nat Rev Neurosci 5:793-807.

Massimini M, Amzica F (2001) Extracellular calcium fluctuations and intracellular potentials in the cortex during the slow sleep oscillation. J Neurophysiol 85:1346-1350.

Massimini M, Huber R, Ferrarelli F, Hill S, Tononi G (2004) The sleep slow oscillation as a traveling wave. J Neurosci 24:6862-6870.

Milojkovic BA, Radojicic MS, Antic SD (2005) A strict correlation between dendritic and somatic plateau depolarizations in the rat prefrontal cortex pyramidal neurons. J Neurosci 25:3940-3951.

Mukovski M, Chauvette S, Timofeev I, Volgushev M (2006) Detection of active and silent states in neocortical neurons from the field potential signal during slow-wave sleep. Cereb Cortex DOI 10.1093/cercor/bhj157.

Petersen CCH, Hahn TTG, Mehta M, Grinvald A, Sakmann B (2003) Interaction of sensory responses with spontaneous depolarization in layer 2/3 barrel cortex. Proc Natl Acad Sci U S A 100:13638-13643.

Povysheva NV, Gonzalez-Burgos G, Zaitsev AV, Kroner S, Barrionuevo G, Lewis DA, Krimer LS (2006) Properties of excitatory synaptic responses in fast-spiking

interneurons and pyramidal cells from monkey and rat prefrontal cortex. Cereb Cortex 16:541-552.

Rosanova M, Timofeev I (2005) Neuronal mechanisms mediating the variability of somatosensory evoked potentials during sleep oscillations in cats. J Physiol 562.2:569-582.

Sanchez-Vives MV, McCormick DA (2000) Cellular and network mechanisms of rhythmic recurrent activity in neocortex. Nat Neurosci 3:1027-1034.

Shu Y, Hasenstaub A, McCormick DA (2003) Turning on and off recurrent balanced cortical activity. Nature 423:288-293.

Steriade M (2004) Neocortical cell classes are flexible entities. Nat Rev Neurosci 5:121-134.

Steriade M, Nuñez A, Amzica F (1993a) A novel slow (<1 Hz) oscillation of neocortical neurons in vivo : depolarizing and hyperpolarizing components. J Neurosci 13:3252-3265.

Steriade M, Nuñez A, Amzica F (1993b) Intracellular analysis of relations between the slow (<1 Hz) neocortical oscillations and other sleep rhythms of electroencephalogram. J Neurosci 13:3266-3283.

Steriade M, Timofeev I, Grenier F (2001) Natural waking and sleep states: a view from inside neocortical neurons. J Neurophysiol 85:1969-1985.

Steriade M, Timofeev I, Dürmüller N, Grenier F (1998) Dynamic properties of corticothalamic neurons and local cortical interneurons generating fast rhythmic (30-40 Hz) spike bursts. J Neurophysiol 79:483-490.

Thimm J, Mechler A, Lin H, Rhee S, Lal R (2005) Calcium-dependent open/closed conformations and interfacial energy maps of reconstituted hemichannels. J Biol Chem 280:10646-10654.

Thomson AM, Deuchars J (1994) Temporal and spatial properties of local circuits in neocortex. Trends Neurosci 17:119-126.

Timofeev I, Steriade M (1996) Low-frequency rhythms in the thalamus of intact-cortex and decorticated cats. J Neurophysiol 76:4152-4168.

Timofeev I, Contreras D, Steriade M (1996) Synaptic responsiveness of cortical and thalamic neurones during various phases of slow sleep oscillation in cat. J Physiol 494:265-278.

Timofeev I, Grenier F, Steriade M (2001) Disfacilitation and active inhibition in the neocortex during the natural sleep-wake cycle: An intracellular study. Proc Natl Acad Sci U S A 98:1924-1929.

Timofeev I, Grenier F, Bazhenov M, Sejnowski TJ, Steriade M (2000) Origin of slow cortical oscillations in deafferented cortical slabs. Cereb Cortex 10:1185-1199.

Wilson CJ, Kawaguchi Y (1996) The origins of two-state spontaneous membrane potential fluctuations of neostriatal spiny neurons. J Neurosci 16:2397-2410.

2.9 Figures

Figure II- 1 Active and silent states in 4 simultaneously recorded neurons and in the EEG.

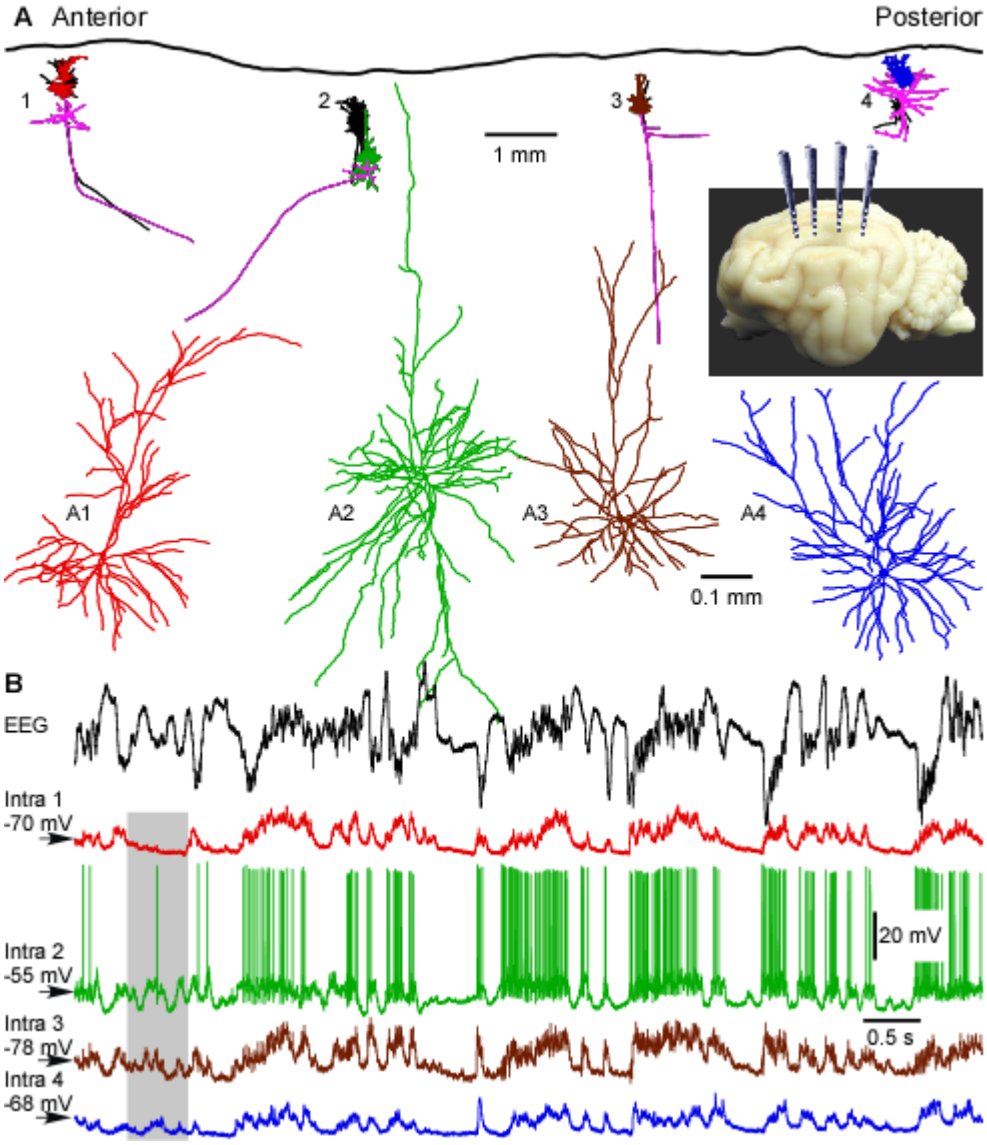

A, Location and morphology of cells recorded in one experiment. Four electrodes for intracellular recordings were positioned at 4 mm intervals along the suprasylvian gyrus, in areas 5, 7 and 21 (inset). With each intracellular electrode, several cells were sequentially recorded and stained. An overview shows reconstructions of all cells from this experiment. An overview shows reconstructions of all cells from this experiment. Colored are 4 simultaneously recorded neurons. Color code is the same for their dendritic trees in **A** and the intracellular traces in **B**. In the overview, pink lines show axons of these 4 neurons.

Other neurons, recorded in this experiment are drawn in black in the overview. In **A1-A4** the 4 simultaneously recorded neurons are shown at expanded view. Cells **A1** and **A3** were pyramids. Cells **A2** and **A4** had non-pyramidal morphology, but were also excitatory, as judged by their spiny dendrites (not shown). **B**, Simultaneously recorded EEG and membrane potential of 4 cells, shown in **A1-A4**. The EEG electrode was positioned between the intracellular recording sites 2 and 3. Membrane potential traces are color coded as in **A1-A4**. The shadowed area shows a period of silence in cell 1, while the other cells were active.

Figure II- 2 Two methods of state detection.

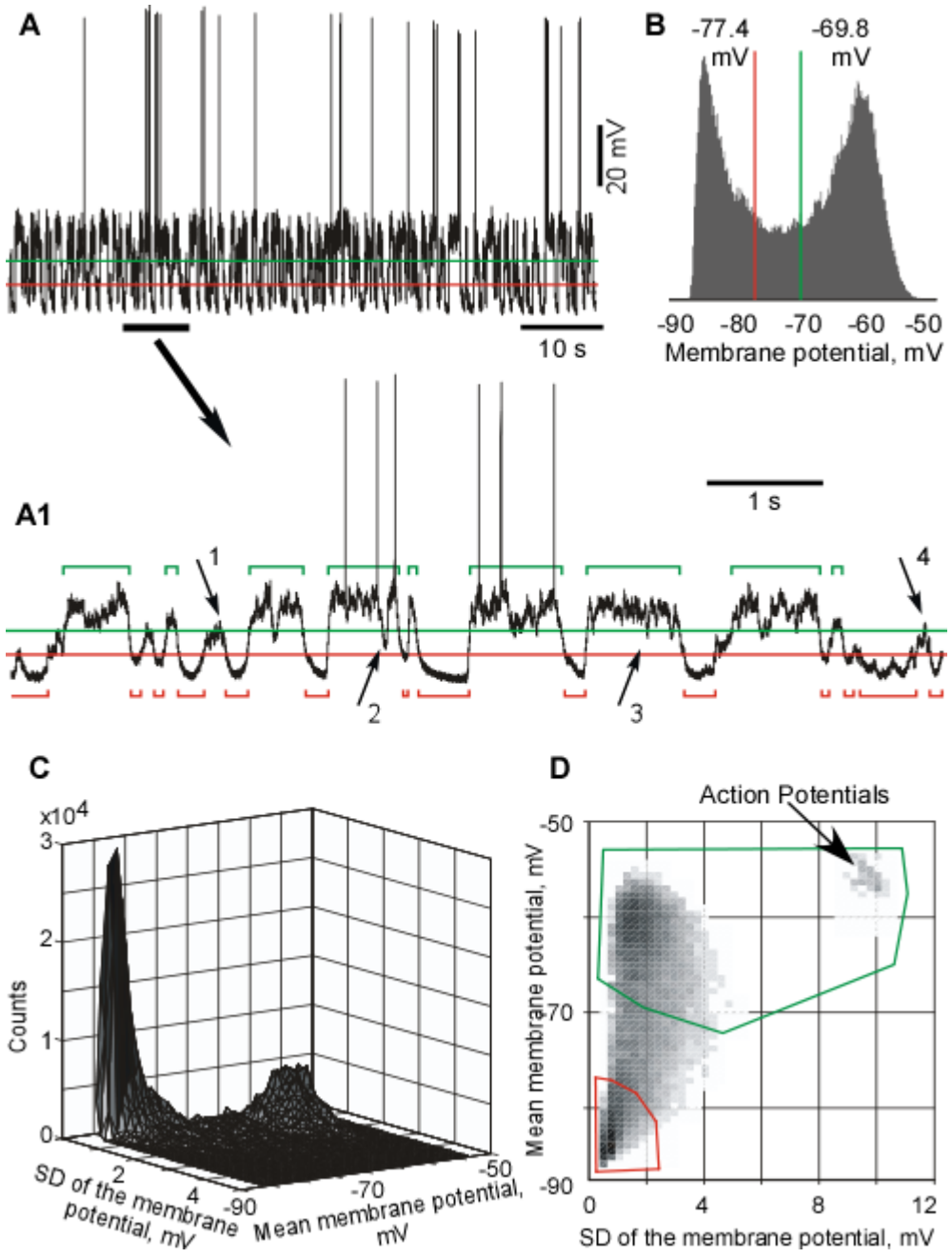

The first method **(A,B)** uses membrane potential levels, while the second method **(C,D)** exploits, in addition to the levels, also the variability of the membrane potential to discriminate between active and silent states. **A**, Membrane potential trace of a neocortical cell, and expanded view of its part **(A1)**, with threshold levels for state detection and detected states (active: green, silent: red). "States" were defined as periods during which the membrane potential remained above the threshold for active states, or below the

threshold for silent states, for >40 ms. To avoid disturbances by transient membrane potential peaks, shorter level crossings were not considered as states (arrows 1, 4), and two active or two silent states separated by <40 ms were extended to fill the gap and pasted together (arrows 2, 3). The levels for state detection were set at equal distances between the peaks of bimodal distribution of the membrane potential values **(B)**. **C**, 3D density distribution of the data from **A**. The mean membrane potential and its standard deviation (SD) were calculated in a running window of 25 ms. These values were used as X and Y coordinates; the Z axis is the frequency of their occurrence. **D**, Top view of the plot from **C**, with the regions used for detection of active (green) and silent (red) states outlined. The X-axis is extended compared with **C**, to include the points with very high SD, which correspond to the windows containing action potentials. Z axis is grey level-coded.

Figure II- 3 Clusters of active and silent states in simultaneously recorded cells.

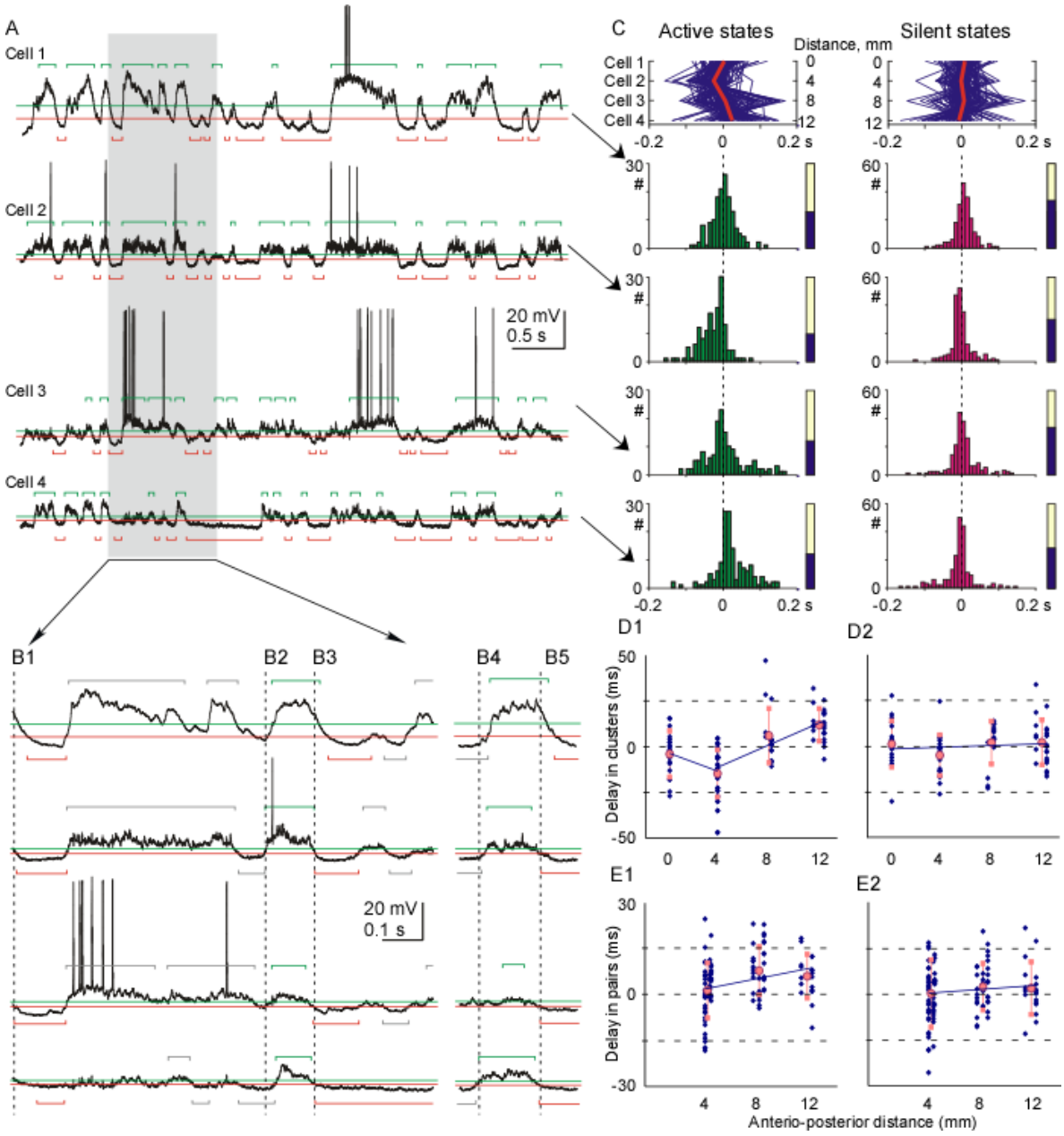

A, Membrane potential traces of 4 simultaneously recorded cells and expanded view of its part **(B)**, with state detection levels and detected states (silent: red, active: green). States formed a cluster, if they occurred in all recorded cells with the onsets separated by <200 ms. **B1-B5** show examples of "clusters", with clustered states (silent: **B1**, **B3**, **B5**; active: **B2**, **B4**) colored, non-clustered states are grey. Vertical interrupted lines: onset of the first state in each cluster. **C1, C2**, In top panels, each cluster is represented by a blue line, connecting state onsets in all cells. Red line: averaged delays of clustered states in 4 cells.

Distance between recorded cells in antero-posterior direction is indicated relative to the most anterior cell. For each cell, distributions of the onsets of clustered states and the portion of clustered states (filled part of the bars) are shown. **D1, D2**, Mean delay of clustered states plotted against the antero-posterior position of recorded cells. Data for 89 cells (blue symbols) and averages for 4 recording positions (pink: mean and SD). In **D1** two trend-lines are shown since the delays of active states in the cells recorded at 4 mm position were significantly different from both, more anterior and more posterior positions. **E1, E2**, Mean delay of state onsets in simultaneously recorded cell pairs (n=104) plotted against the antero-posterior distance between the cells. Mean delay of state onsets in a more posteriorly located cell was calculated relative to the state onsets in more anteriorly located cell. Other conventions as in **(D)**.

Figure II- 4 Population analysis of the onsets of active and silent states in simultaneously recorded neurons.

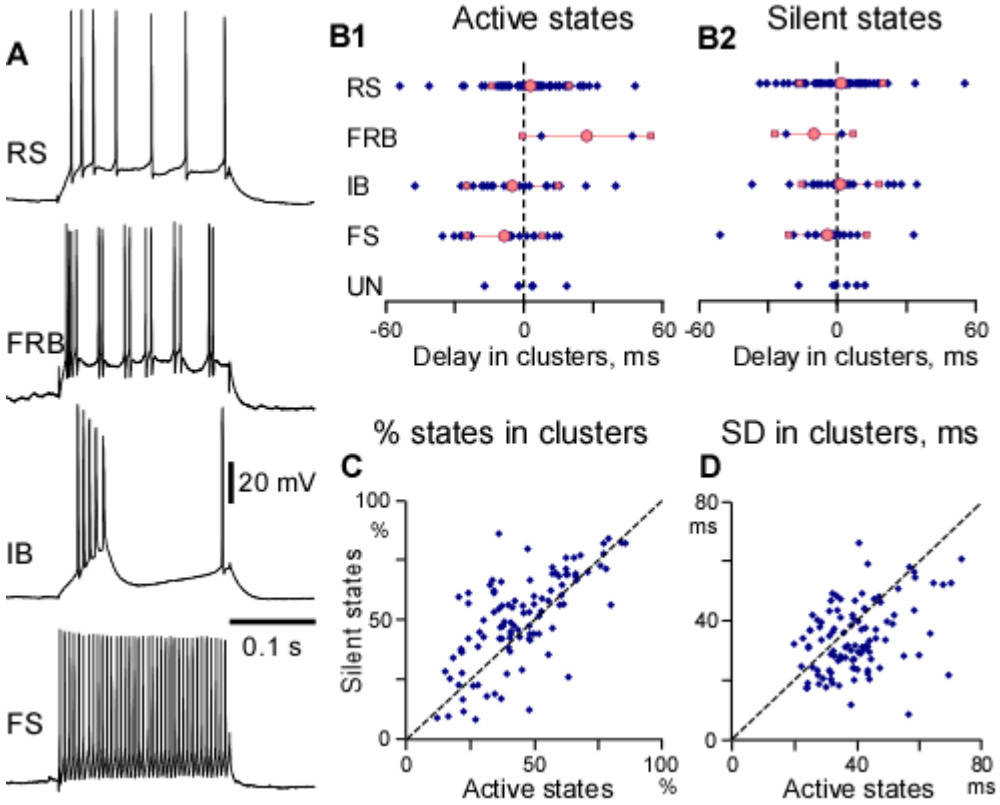

A, Electrophysiological identification of neurons. Responses of regular-spiking (RS), fast-rhythmic-bursting (FRB), intrinsically-bursting (IB) and fast-spiking (FS) cells to depolarizing current pulses. **B**, Relative delays of involvement of cells with different intrinsic membrane properties in clusters of active **(B1)** and silent **(B2)** states. Each diamond symbol represents data for one cell; pink symbols are averages for cells of each class (circles: mean, squares: SD). **C-D**, Comparison of the statistics of clustered active and silent states. Each point represents data for one cell, with the value for the silent states (ordinate) plotted against the respective value for active states (abscissa). **C**, Number of states involved in clusters, in percent of the total number of states in a cell. **D**, SD of the onsets of clustered states in a cell.

Chapter III

3.0 Origin of active states in local neocortical networks during slow sleep oscillation.

Sylvain Chauvette[1], Maxim Volgushev[2,3,4], Igor Timofeev[1]

[1]The Centre de recherche Université Laval Robert-Giffard (CRULRG), Laval University, Québec, G1J 2G3, Canada

[2]Department of Neurophysiology, Ruhr-University Bochum, D-44780, Germany

[3]Institute of Higher Nervous Activity and Neurophysiology, Moscow, 117485, Russia

[4]University of Connecticut Storrs, Department of Psychology, CT 06269-1020, USA

Published in Cerebral Cortex, 2010

Complete citation: Chauvette S, Volgushev M, Timofeev I (2010) Origin of Active States in Local Neocortical Networks during Slow Sleep Oscillation. Cerebral Cortex 20:2660-2674.

Titre en français:

3.0 Origine des états actifs dans les réseaux néocorticaux locaux pendant l'onde lente du sommeil.

3.1 Résumé en français

Le sommeil à ondes lentes est caractérisé par des alternances spontanées d'activité et de silence dans le réseau cortico-thalamique, mais la cause de ces transitions du silence vers l'activité demeure inconnue. Nous avons investigué les mécanismes locaux qui sous-tendent la genèse de l'activité en utilisant des enregistrements simultanés de potentiels de champ multi-sites, des enregistrements multi-unitaires, ainsi que des enregistrements intracellulaires simultanés de 2 à 4 neurones voisins chez des chats, soit pendant un sommeil naturel ou sous anesthésie. Nous démontrons que l'activité peut débuter dans n'importe quel neurone ou à n'importe quelle profondeur, avec des délais de dizaines de millisecondes dans les autres cellules ou sites d'enregistrements. Typiquement cependant, l'activité débutait dans les couches profondes, puis impliquait les couches superficielles, mais apparaissait plus tard au milieu du cortex. Nous avons aussi trouvé que les décharges neuronales débutaient, après le déclenchement des états actifs, à des profondeurs qui correspondent à la couche V du cortex. Ces résultats supportent l'hypothèse que la transition du silence vers l'activité est générée par des évènements synaptiques spontanés où n'importe quel neurone peut devenir actif en premier. À cause de la nature probabiliste du déclenchement de l'état actif, les larges neurones pyramidaux des couches profondes qui sont équipées du plus grand nombre de contacts synaptiques et d'un grand champ de projections, sont les mieux placés pour induire et propager l'état actif dans tout le réseau.

3.2 Abstract

Slow-wave sleep is characterized by spontaneous alternations of activity and silence in cortico-thalamic networks, but the causes of transition from silence to activity remain unknown. We investigated local mechanisms underlying initiation of activity, using simultaneous multisite field potential, multiunit recordings and intracellular recordings from 2-4 nearby neurons in naturally sleeping or anesthetised cats. We demonstrate that activity may start in any neuron or recording location, with tens of milliseconds delay in other cells and sites. Typically however, activity originated at deep locations, then involved some superficial cells, but appeared later in the middle of the cortex. Neuronal firing was also found to begin, after the onset of active states, at depths that correspond to cortical layer V. These results support the hypothesis, that switch from silence to activity is mediated by spontaneous synaptic events, whereby any neuron may become active first. Due to probabilistic nature of activity onset, the large pyramidal cells from deep cortical layers, which are equipped with the most numerous synaptic inputs and large projection fields, are best suited for switching the whole network into active state.

3.3 Introduction

Slow-wave sleep is characterized by the presence of slow oscillation in the electroencephalogram (EEG) (Blake and Gerard, 1937). This slow oscillation consists of alternating periods of silence and activity in the cortico-thalamic networks (Contreras and Steriade, 1995; Steriade et al., 2001; Timofeev et al., 2001). The active states are associated with depolarized membrane potential, vigorous synaptic activity, and cell firing, while during silent states, membrane potential is hyperpolarized and cells do not discharge. The high-density EEG-recording in humans revealed that the slow oscillation spread over the cortex as traveling waves that may originate at different sites, but typically in prefrontal-orbitofrontal regions (Massimini et al., 2004). In agreement with these human EEG data, our simultaneous multisite intracellular recordings in cat neocortex revealed that activity originated typically, but not exclusively, at a certain location (area 5/7 border), and spread from there in both anterior and posterior directions (Volgushev et al., 2006). All neurons in the neocortex, and most neurons in their target structures, are involved in the slow rhythm and oscillate in-phase, being simultaneously silent or simultaneously active (Contreras and Steriade, 1995; Mahon et al., 2006; Steriade et al., 1993; Steriade et al., 2001; Timofeev and Steriade, 1996; Volgushev et al., 2006). How does activity originate during silent state, when no action potentials are generated by neocortical neurons? Three hypotheses on the origin of activity have been proposed. The first hypothesis suggests that spontaneous transmitter release in large neuronal populations occasionally depolarizes some cells to the firing threshold, thus initiating an active state in the network (Timofeev et al., 2000). The spontaneous release hypothesis predicts that activity may start in any neuron, although cells receiving largest excitatory convergence will have higher probability of being activated before the others. The second hypothesis suggests that transition from silence to activity is mediated by intrinsic oscillations of layer V pyramidal neurons, which remain more depolarized because of their intrinsic or synaptic properties, and generate some spikes between the active states when other cortical neurons are silent (Sanchez-Vives and McCormick, 2000). Once initiated by layer V neurons, activity then propagates to other cortical layers. The layer V neurons hypothesis predicts, that activity always originates in these neurons, while appears later in other cells. The third hypothesis attributes transitions

from silent to active states to the selective synchronization of spatially structured neuronal ensembles involving a small number of cells (Cossart et al., 2003). The selective synchronization hypothesis predicts that even during the silent states, some neurons of the network still generate irregular spontaneous firing. More recent studies provided controversial results. Intracortical recordings from epileptic patients demonstrated that active states originate in superficial layers (Cash et al., 2009). However, optical and patch-clamp recordings from layer II-III neurons from visual and somatosensory cortex of healthy rats demonstrated very low firing rates of these neurons, making them unlikely candidates for active state initiation (Greenberg et al., 2008; Waters and Helmchen, 2006). Extracellular unit recordings from layer V neurons revealed that each neuron has its unique spiking pattern (Luczak et al., 2007) that contradicts the idea of stochastic origin of active states (Cossart et al., 2003; Timofeev et al., 2000), but supports the hypothesis that particular set of neurons lead active state origin (Sakata and Harris, 2009; Sanchez-Vives et al., 2008; Sanchez-Vives and McCormick, 2000).

To test the above hypotheses and to understand the origin of active states, we investigated in which layer and in cells of which type subthreshold activity starts first and how is it transformed into neuronal firing. We performed multisite local field potential (LFP), extracellular multiunit, and intracellular recordings from closely located neurons in cat neocortex during natural slow-wave sleep and anesthesia-induced slow oscillation. We show that in local neocortical networks subthreshold activity could originate first in any neuron and at any depth, but activation of large pyramidal cells from deep layers is more likely to occur first, probably due to the large excitatory convergence on these cells.

3.4 Material and methods

Experiments were carried out in accordance with the guidelines published in the NIH Guide for the Care and Use of Laboratory Animals (NIH publication no. 86-23, revised 1987) and were approved by the Committee for Animal Care of Laval University.

Preparation. *Experiments in anesthetized animals*. Acute experiments were carried out on 16 adult cats of both sexes that had been anesthetized with ketamine and xylazine (10-15 and 2-3 mg/kg i.m., respectively). All pressure points and the tissues to be incised were infiltrated with lidocaine (0.5%). The animals were paralyzed with gallamine triethiodide and artificially ventilated, maintaining the end-tidal CO2 concentration at 3.5-3.8%. A permanent sleep-like state, as ascertained by continuous recording of the EEG, was maintained throughout the experiments by administering additional doses of ketamine (5 mg/kg). The body temperature was monitored by a rectal probe and maintained at 37^{o}C via a feedback-controlled heating pad. The heart rate was continuously monitored (90-110 beats/min). The stability of intracellular recordings was ensured by cisternal drainage, bilateral pneumothorax, hip suspension, and by filling the hole made for recordings with a solution of 4% agar.

Experiments in non-anesthetized animals. Experiments on non-anesthetized animals were conducted on 2 adult cats, chronically implanted as previously described (Steriade et al., 2001; Timofeev et al., 2001). Briefly, surgical procedures for chronic implantation of recording and stimulating electrodes were carried out under deep barbiturate anesthesia (Somnotol, 35 mg/kg, i.p.), followed by two to three administrations, every 12 h, of analgesic (buprenorphine, 0.03 mg/kg, i.m.) to prevent pain. Penicillin (500,000 units i.m.) was injected during three consecutive days. During surgery, the cats were implanted with electrodes for electro-oculogram (EOG), electromyogram (EMG) from neck muscles, and intracortical EEG recordings. In addition, a chamber allowing the intracellular penetrations of micropipettes was placed over neocortical areas 5 and 7. Acrylic dental cement was used to fix on the skull the electrodes and recording chamber.

Recording. LFP were recorded in the vicinity of impaled neurons and also from more distant sites, using either tungsten electrodes (10-12 MΩ) or 16-channel silicon probe (NeuroNexus Technologies, Inc. Ann Arbor, MI, USA) with 100 μm separation between recorded sites, inserted perpendicularly to the surface in neocortical areas 5, 7, or 21. Dual,

triple, or quadruple intracellular recordings from suprasylvian association areas 5 and 7 were performed using glass micropipettes filled with a solution of 2.5 M potassium-acetate (KAc). A high-impedance amplifier with active bridge circuitry was used to record the membrane potential and to inject current into the neurons. Neurons were recorded throughout the cortical thickness, whereby lateral distance between simultaneously recorded cells was usually about 100 μm but never exceeded 300 μm. The recorded cells were electrophysiologically identified as previously described (Connors and Gutnick, 1990; Gray and McCormick, 1996; Steriade, 2004; Steriade et al., 1998). All electrical signals were sampled at 20 kHz and digitally stored on Vision (Nicolet, Wisconsin, USA). Offline computer analysis of electrographic recordings was done with IgorPro software (Lake Oswego, Oregon, USA) and with custom written MATLAB (The MathWorks, Inc.) programs. At the end of experiments, the cats were given a lethal dose of pentobarbital (50 mg/kg i.v.).

Analysis. To quantify the timing of the active state onset, we used two methods. With the first method, we fitted portions of the membrane potential traces (or of LFP recordings), which included the transitions from silent to active states with a sigmoid function and defined the onset time of active state at 10% of the fit amplitude (see Figs. III.1, III.4, III.5, and III.7). A reference channel was chosen arbitrarily and the onset time of active state detected in recordings from each other electrode was then compared to this reference. These values were calculated for every cycle to produce delay histograms (see Figs. III.1, III.5, and III.7). Varying the intervals used for sigmoid fitting did not significantly affect results on estimation of timing of active state onset (Fig. III.S1). In the second method, for detection of active and silent states in intracellular recordings we used a combination of the level of membrane potential and the strength of its fluctuations (Volgushev et al., 2006). The mean membrane potential and its standard deviation (SD) were calculated in a running window of 25 ms, and occurrence of pairs of mean and SD values were plotted as 3D distribution (Fig. III.S2). Silent states form a sharp peak at hyperpolarized potentials and low SD values while active states are represented by a broader hill at more depolarized potentials and higher SD values. Since the location of the peaks corresponding to active and silent states differs along both axes, the use of a combination of these two parameters improves detection and separation of the states. For detection of states in the LFP, we used

the method based on different spectral composition of active and silent states, and the increased contribution of high frequency fluctuations to the LFP during active states (Mukovski et al., 2007).

For current-source density (CSD) analysis (see Fig. III.2), the LFP recordings were filtered between 0.5 and 6 Hz to eliminate the influence of other rhythm. According to original description (Mitzdorf, 1985; Mitzdorf and Singer, 1978; Nicholson and Freeman, 1975), we used the following formula to calculate the CSD:

$-Im = (1/R) * ((\Phi i+2 - 2 \Phi i + \Phi i-2) / (Z2))$

where

Φi = field potential in mV at a given electrode "i"

R = in MOhms

Z = distance between electrodes in mm

Im = CSD in mV/mm2

For:

Im > 0 Source => outward current

Im < 0 Sink => inward current

For population analysis of activity onsets in groups of two to four simultaneously recorded neurons (see Fig. III.6d), we calculated the delay of activity onset in a particular cell relative to the mean onset time of the recorded group of cells for every transition from silent to active state. These delays were compiled for many cycles (more than 50) and a mean delay for each cell was calculated and plotted in relation to the recording depth (blue points in Fig. III.6 d) and electrophysiological type of the cell (see Fig. III.11 b).

3.5 Results

We studied the origin of active states in local neocortical networks during slow-wave sleep and anesthesia-induced slow oscillation using multisite LFP, multiunit activities, and simultaneous intracellular recordings from 2-4 neurons. To obtain the depth profile of the field potentials and distribution of current sinks and sources, we made recordings with a 16-channel silicon probe inserted perpendicularly to the cortical surface. The same recordings were also used to estimate the depth profile of multiunit activities during slow-wave sleep. To further investigate the underlying neuronal processes, simultaneous recordings of LFP from deep layers and intracellular activity of 2-4 closely located neurons were used.

3.5.1 Depth profile of field potentials, current sinks and sources during natural slow-wave sleep

During natural slow-wave sleep, the LFP displays characteristic picture of slow oscillation (Fig. III.1), which reflect alternation of active and silent states in the neocortical network (Rudolph et al., 2007; Steriade et al., 2001; Timofeev et al., 2001). Slow waves are evident throughout the cortex, but their amplitude and polarity change gradually with recording depth.

To study the depth profile of activity onset and to see whether it originates in a particular cortical layer, we detected the onsets of activity in LFP recorded simultaneously at different depth. LFP waves, corresponding to the transitions from silence to activity were fitted with a sigmoid curve, and the time point at 10% of the fit amplitude was taken as the onset of active state (Fig. III.1 a). The activity onset time detected with this method changed only marginally when the length of the intervals containing the silent-active transition, which were used for fitting was changed, thus showing that detection of onset time was robust (Fig. III.S1). For each channel, a distribution of activity onsets relative to the deepest recorded channel (LFP-16, Fig. III.1 b, c) was calculated. This analysis revealed clearly different patterns of activity onsets in superficial and deep layers. In deep layers, activity started typically at 1400-1600 μm, (Figure III.1c, channels 14-16), and propagated from there towards the middle of the cortex (Figure III.1c, channel 7). Both the peak shift and width of the onset delay distributions increased systematically in channels 14 through

7, indicating the increase of delays of active state onsets and their variability (Figure III.1 b, c). In the superficial layers, the LFP signal was inversed as compared to deep recordings, the distributions of activity onset delays were broader indicating that activity in the superficial layers appeared with highly variable timing relative to deep recordings (Fig. III.1 c). All but one distribution of activity onset delays covered zero, demonstrating that activity may appear first at any depth (Fig. III.1c). Similar results were obtained, when the onsets of active states were detected with a method exploiting differential spectral composition of the LFP during active and silent states (Mukovski et al., 2007) (data not shown). Similar results were obtained in ketamine-xylazine anesthetized cats (Chauvette et al., 2007).

To investigate further the depth distribution of possible sources of activity during slow sleep oscillation, we performed current-source density analysis (Mitzdorf, 1985; Mitzdorf and Singer, 1978; Nicholson and Freeman, 1975). In the current-source density map (Fig. III.2c), extracellular current sinks correspond to intracellular inward (depolarizing) current, while current sources correspond to intracellular outward (hyperpolarizing) current (Mitzdorf, 1985; Mitzdorf and Singer, 1978). The map reveals a strikingly clear relation between alternating pattern of current sinks and sources and alternating periods of active and silent states (Fig. III.2 a-c). During silent states, we observed strong sinks in the upper layers (positions 3-6 in Fig. III.2 c) and sources in deeper layers (positions 8-12). Upon the transition to active states, the picture reverses to the opposite: sinks in the deeper layers and sources in the upper layers. During active states, the sources and sinks are generally weaker and much more variable both in space and in time than during silent states, indicating that during activity in neocortical networks, the flow of currents through the cortical depth is less regular and subject to stronger variability. Activity-onset triggered average shows that the reversal of the depth profile of sinks and sources is typical for the transition from silence to activity: a sharp transition from a strong superficial sink and deeper source to weaker deep sinks and superficial sources stands out very clear in Figure III.2e (n=101 episodes averaged for each channel). Examination at higher temporal resolution reveals that during the transition to activity, a switch from sources to sinks occurs earlier around channel 12 (Fig. III.2 e, right panel, see arrow) and then “spreads” upwards, towards

channel 8. This observation is consistent with the depth profile of activity onset, described above.

3.5.2 Depth distribution of firing at the onset of active state in simultaneously recorded multiunit activity during slow-wave sleep

To study depth profile of firing of neocortical neurons during transition from silent to active state, we performed multiunit recordings during slow-wave sleep (Fig. III.3). The onset of active state was detected using sigmoid fits of the field potential from deepest electrode, at 10% of the amplitude of transition from silent to active state (see Fig. III.1 for detail). Distinct from in vitro results (Sanchez-Vives et al., 2008; Sanchez-Vives and McCormick, 2000), in vivo multi-unit recordings during natural slow-wave sleep did not show any firing during silent state at any cortical depth (Fig. III.3). Absence of firing during the silent state stands out clearly both in individual recordings (Fig. III.3 a, b) and in the averaged data for 290 silence-activity cycles recorded at 5 different locations in suprasylvian gyrus during 5 sleep episodes (Fig. III.3 c, d). The earliest firing was detected just after the onset of active state in electrodes 8-12, which corresponds to the depth of 800 to 1200 μm and thus to the layer V of the suprasylvian gyrus (Hassler and Muhs-Clement, 1964). Activities recorded from that depth have also showed the highest firing probability (Fig. III.3 c, d). Neurons start to discharge only when depolarized to their firing threshold. In these experiments first spikes occur after field potential recordings already started a transition toward active states, indicating that at least some neurons started to depolarize at this time.

To investigate the relation between the onset of neuronal depolarization and the onset of firing we performed intracellular recordings from the same cortical area from cats under ketamine-xylazine anesthesia (Fig. III.4), which closely reproduces sleep slow-oscillation (Contreras and Steriade, 1995). During slow oscillation, the membrane potential of neocortical neurons switched between two states: active state, associated with depolarized membrane potential, vigorous synaptic activity and firing, and silent state, during which membrane potential was hyperpolarized and the cells did not generate action potentials (Fig. III.4, see also figs. III.5, III.7-10, and III.S2). Active state onsets were determined using sigmoid fits of the membrane potential traces after removal of spikes (Fig III.4a). Active state onset was used then as a trigger to build histograms of all spikes (Fig

III.4b) and of the first spikes (one from each active state, Fig. III.4c). Using these data, for each cell we determined the minimum delay of the first spike among all active states ("earliest spike") and calculated the average delay of the first spikes in that cell. This analysis showed that cells from deep layers have a clear tendency to fire before other cells. Both the earliest spike delay and averaged first spike delay were shorter in deep layer cells (Fig. III.4d, e). In agreement with modeling studies (Diesmann et al., 1999; Marsalek et al., 1997) we found that the earliest spike delays were shortest for neurons that exhibited highest firing rates (Fig. III.4 f). In agreement with our extracellular unit recordings during slow-wave sleep (Fig. III.3), we found that highest firing rates were observed in cells recorded deeper than 800 μm (Fig. III.4 g).

3.5.3 Activity onset in simultaneously recorded nearby neurons during slow oscillation and slow-wave sleep

To study cellular mechanisms of the active state onsets, which underlay the slow waves, we made simultaneous LFP and quadruple, triple, or dual intracellular recordings from nearby neurons (< 200 μm lateral distance, Fig. III.5). Most of recordings were made under ketamine/xylazine anesthesia. The recorded cells were electrophysiologically identified (Fig. III.5 c), and some of them (n=12) were intracellularly labeled and reconstructed using a Neurolucida system (Fig. III.5 a, b). On a coarse time scale, periods of activity and silence occurred at about the same time in all simultaneously recorded nearby neurons, independent of their depth (Fig. III.5 d, see also Figs. III.7, III.10 and III.S2). We never observed inversed phase relation between slow waves in membrane potential traces of simultaneously recorded neurons.

To quantify the timing of the active states in simultaneously recorded neurons we have used two approaches, similar to those used in analysis of LFP. The first method used the time at 10% amplitude of a sigmoid fitting of the transition from silent to active state to identify **the onset of active state** (Fig. III.5 e, see Fig. III.1 and III.S1 for onsets in LFP). The second method exploited the level of membrane potential and the strength of its fluctuations (Volgushev et al., 2006) to separate states (Fig. III.S2) and thus detected **the beginning of developed active states.** The results obtained with both state detection methods are described together.

On the fine time scale, the sequence of involvement of simultaneously recorded neurons in activity was not uniform, but varied from one cycle to the other, whereby any neuron could be leading in some particular cycles (Figs. III.5 e and III.S2 b). Distributions of activity onset delays in any cell relative to the other always covered zero, indicating the high variability in the sequence of activation of neurons (Fig. III.5 f).

Population analysis of activity onset estimated with both methods revealed that neurons recorded in deep layers were leading, as indicated by high occurrence of negative delays in these cells as compared to superficial layer neurons (Fig. III.6 a, d). In neurons recorded at intermediate depths, activity usually started after the other cells, as indicated by the high occurrence of positive delays. Finally, in cells from superficial layers, positive and negative delays were nearly equally frequent, and the spread of delays was high. This depth profile stands out very clearly in the plot of running average of activity onset delays (red symbols in Fig. III.6 d). For further quantification of the dependence of activity onset on recording depth, we segregated the cells by the recording depth in three nearly-equally populated groups. Group averages confirmed the above conclusions. For the ***onsets*** of active states (method of sigmoid fitting), the averaged delay was negative for the group of deep cells (-1.1±7.4 ms, mean ±SD, n=27, mean depth 1373 μm, all cells located deeper than 1050 μm), but positive, close to zero for the middle group (0.5±4.4 ms, n=27, mean depth 763 μm, ranging from 575 to 1050 μm), and the group of superficial cells (0.6±4.7 ms, n=27, mean depth 442 μm, all cells located superficially to 575 μm) (Fig. III.6 d1). The averaged delay of ***developed*** active states was negative, –3.38±13.2 ms (n=36) in the group of deep layer cells (mean recorded depth 1476 μm, all cells located deeper than 1100 μm), positive in the middle group (2.9±10.6 ms, mean depth 920 μm, depth ranging from 670 to 1100 μm, n=35), and close to zero in the group of superficially located cells (0.56±12.46 ms, mean depth 485 μm, all cells located superficially to 670 μm, n=36) (Fig. III.6 d2). Slight difference in timing estimated with the two methods could be due to the different steepness of activity onset in different neurons. Figure III.S3 illustrates such an example, with large time difference in the onsets of active states in two neurons, but a much less difference in the timing of the beginning of the developed state. Opposite examples, with smaller time difference of the onsets and larger time difference between developed states were also observed (not shown). The reason for the different steepness of activity onset

could be a combination of the strength of synaptic drive, properties of individual synaptic responses, and intrinsic membrane properties of a cell (Cruikshank et al., 2007; Llinás, 1988; Wang et al., 2006). Conclusion on the earlier onset of activity in deep-layer cells is further substantiated by the pair-wise analysis. For each pair of simultaneously recorded cells, we have calculated activity onset delay in the more superficially recorded cell relative to the deeper neuron in the pair. The pairs in which the deeper cell was leading were encountered by far more frequently than the pairs with the upper cell leading (25 pairs, blue vs. 10 pairs, green, in Fig. III.6 a1, b1; and 54 pairs, blue, vs. 23 pairs, green, in Fig. III.6 a2, b2). P-values for deeper vs. upper leading of a bilateral binomial test approximated by normal law were 0.011 for ***onsets of active states*** (Fig. III.6 a1) and 0.0004 for ***developed active states*** method (Fig. III.6 a2) indicating highly significant differences. Interestingly, this difference was clearly expressed also in the pairs composed of cells with only minor depth difference (<100 μm, n=23 pairs, gray in Fig. III.6 a2, c2 and n=18 pairs, gray in Fig. III.6 a1, c1).

To verify whether the conclusions drawn from intracellular recordings made under ketamine/xylazine anesthesia hold true for natural slow-wave sleep, we performed intracellular recordings from single cells and simultaneous intracellular from pairs of cells in non-anesthetized and non-paralyzed cats (Figs. III.7, III.8). Similar to previous studies (Rudolph et al., 2007; Steriade et al., 2001; Timofeev et al., 2001), during quiet waking and rapid-eye-movement (REM) sleep, the LFP displayed typical activated pattern and neurons remained in active state (not shown). During slow-wave sleep, the large amplitude slow waves in the LFP were associated with transitions between silent and active states in the membrane potential of cortical neurons (Figs. III.7 a, and III.8 a). Analysis of simultaneous recordings from 5 pairs of RS neurons confirmed that the main characteristics of slow oscillations seen in the multisite intracellular recordings under ketamine/xylazine anesthesia are also evident during natural slow-wave sleep. Specifically, in recordings made during natural slow wave sleep we found evidence for (i) clear correspondence between slow waves in the LFP and alternations of active and silent states in the membrane potential, with common periods of activity and silence in simultaneously recorded cells (Fig. III.7 a). (ii) Variable sequential order of involvement of recorded cells in activity, whereby the order of cell involvement may reverse even in the nearby cycles separated by

less than 1s (Fig. III.7 b). (iii) Variable delays between activity onsets in simultaneously recorded neurons relative one to the other and the LFP waves, the delays occasionally reaching tens of milliseconds (Fig. III.7 c). Taken together, these results show that inferences from the data obtained during anesthesia-induced slow oscillation provide useful clues on cellular mechanisms of natural slow-wave sleep.

3.5.4 Synaptic buildup at the onset of active states

The onset of active states is dominated by excitatory conductances (Haider et al., 2006; Rudolph et al., 2007). They may be produced by either spike-independent spontaneous transmitter release (minis) or synaptic release triggered by action potentials generated by neurons which are already engaged in activity. Because minis have small amplitude and are not synchronized, a minis-driven onset of active state in a neuron should manifest itself by a slow buildup of depolarization before the spiking threshold is eventually reached. If active states of the network originate by this mechanism, the slow buildup of depolarization prior/at the beginning of active state should be most often encountered in leading neurons. In contrast to spontaneous origin of activity, active states in neurons driven by already activated network should exhibit faster depolarization at the transition from the silent to active state. We have looked for these characteristic signatures in transitions in intracellular recordings during natural sleep (Fig. III.8), and anesthetized cats (Fig. III.9). In all these experimental conditions, we have observed transitions toward active states of both types, with slow or rapid buildup of depolarization. Figure 8 illustrates transitions of both slow and fast types in the neighboring activity cycles, recorded in the same cell during natural slow-wave sleep. Figure III.8 b, (1) shows a rapid transition with a smooth front and no clearly discernible individual synaptic potentials. In the next cycle, transition in that cell was slow, with uneven front on which many individual synaptic events that summate and buildup the depolarization towards the active state are apparent (Fig. III.8 b, 2). Both types of transitions were also observed under ketamine/xylazine anesthesia (Fig. III.9). A signature of spontaneous release-driven onset of active states would be an increase of the membrane potential variability towards the end of silent states due to the increased spontaneous release. Indeed, the standard deviation of the membrane potential clearly increased in presumably leading neurons in the majority of cycles of slow oscillation just prior to the onset of active state (Fig. III.9 b). If a slow build up of

depolarization due to spontaneous release indeed plays role in initiation of active states, it should be most pronounced in neurons which engage in activity earlier than other cells. To test this conjecture, we used multisite intracellular recordings and computed for each neuron and oscillation cycle the relation between the maximal slope of transition to an active state and delay of the onset of active state in that neuron relative to other simultaneously recorded neurons (Fig. III.10). Results of this analysis are consistent with the above conjecture: in a vast majority of neurons (17 out of 18) transition was slower when the cell was involved earlier in the active state (Fig. III.10 b, d). However, one neuron recorded at depth of 900 μm [which corresponds to upper layer 5 according to (Hassler and Muhs-Clement, 1964)] exhibited atypical behavior. It had fastest slope of transition to active state in those cycles when it was leading other cells, but slightly slower transition when activated later than other cells (Fig. III.10 d, black line). Typical for this neuron was a clear presence of synaptic events prior to the onset of active state (Fig. III.10 c, 1) and bursts of action potentials during spontaneous activity and current injection (Fig. III.10 c, 2). This and other neurons with such properties are best suited to lead onsets of network active states.

Next, we investigated if active states originated earlier in neurons of a particular electrophysiological class. In agreement with our previous observations (Timofeev et al., 2000) all electrophysiological types of neurons could be recorded at any depth (Fig. III.11 a). The group analysis revealed a clear tendency for intrinsically-bursting (IB) neurons to lead in activity onsets (averaged delay –9.0+18.4 ms, n=7 cells, Fig. III.11 b). Two kinds of pair-wise analysis corroborate this result. The IB neurons were leading in all 5 pairs consisting of an IB and a regular-spiking (RS) cell, and in 3 out of 4 pairs consisting of an IB and a fast-rhythmic-bursting (FRB) cell (Fig. III.11 c). Furthermore, in these pairs, the IB cells were leading in the majority of individual cycles (Fig. III.11 d, 76.4% of cycles in IB-RS pairs, $p<0.001$ and 57.1% of cycles in IB/FRB pairs, $p=0.054$). These results show that despite stochastic nature of active state onset, the IB cells engage in active states before other neurons, and thus are in the position to either initiate or to spread the onset of active state.

3.6 Discussion

Our study of local mechanisms of origin of slow oscillation with multisite LFP, multiunit recordings, and simultaneous intracellular recordings from 2-4 neurons revealed a clear depth profile of activity onsets. In both, extracellular and intracellular recordings, activity started most frequently at deep locations, but appeared later in the middle of the cortex. This general tendency was apparent despite a high cycle-to-cycle variability of onsets at any depth. Our data emphasize that the LFP waves and the distribution of current sinks and sources were mirror-like in the deep as compared to the superficial layers. In contrast to the LFP and CSD, the slow waves in the membrane potential of simultaneously recorded neurons were always in-phase, independent of their depth. We never observed firing during hyperpolarizing silent state in multiunit recordings or intracellular recordings obtained during both natural slow-wave sleep and ketamine/xylazine-induced slow oscillations. This result is in a striking contrast to some previous studies performed in vitro (Compte et al., 2003; Sanchez-Vives et al., 2008; Sanchez-Vives and McCormick, 2000) or with in vivo multiunit recordings from sensory cortices of anesthetized rats (Hasenstaub et al., 2007; Sakata and Harris, 2009), which observed firing of some neurons during silent state of the network. Our multiunit recordings during natural sleep and intracellular recordings under ketamine/xylazine anesthesia show that deep layer (presumably layer V) neurons have a clear tendency to depolarize and fire action potentials at the onset of active state earlier than other neurons and thus lead the onset of activity in the network. The leading neurons revealed a prominent synaptic buildup prior to the onset of active states, when no firing was observed in nearby neurons, and the firing of the first action potential in these neurons had the shortest latency from the onset of active states. This conclusion on the leading role of large deep layer pyramids in the onset of active states is in agreement with previous studies (Sakata and Harris, 2009; Sanchez-Vives and McCormick, 2000), but stands in a marked contrast to results of intracortical recordings from human cortex surrounding epileptic foci, in which active states originated in superficial layers (Cash et al., 2009). One possible reason for this peculiar finding could be alterations of cell properties in the cortical tissue surrounding epileptic foci.

3.6.1 Cortical origin of active states during slow sleep oscillation.

Several lines of evidence show that alternation of active and silent states (Steriade et al., 1993), which underlies slow oscillation, is of cortical origin. The slow oscillation was observed in athalamic animals (Steriade et al., 1993) and other isolated cortical preparations (Sanchez-Vives and McCormick, 2000; Timofeev et al., 2000), but not in the thalamus of decorticated animals (Timofeev and Steriade, 1996). Our results provide further evidence corroborating this assumption. In case of initiation of cortical activity by thalamic input, a characteristic picture of current sinks originating in the granular layer and spreading to other cortical layers would be expected (Mitzdorf, 1985; Mitzdorf and Singer, 1978). Moreover, if thalamocortical neurons would contribute significantly to initiation of active states (Hughes et al., 2002; Zhu et al., 2006), multiunit recordings would reveal the earliest firing at the onset of active states in layer IV cells, which receive strongest thalamic input. Since such patterns of CSD and multiunit firing were never observed during transitions to active states, thalamic initiation of active states could be excluded.

3.6.2 Origin of activity: What drives the first neuron to generate the first spike?

Three hypothetic mechanisms have been proposed so far to explain the intracortical origin of activity during slow oscillation: spontaneous release (Timofeev et al., 2000), intrinsic properties of layer V neurons (Sanchez-Vives and McCormick, 2000), and selective synchronization of small neuronal ensembles (Cossart et al., 2003) (see Introduction).

The latter mechanism requires that at least some neurons are active and generate spikes during the silent states of the cortical network. In this and previous studies (Contreras and Steriade, 1995; Steriade et al., 2001; Timofeev et al., 2001; Timofeev and Steriade, 1996; Volgushev et al., 2006), not a single neuron was systematically active while other cells were in silent states. Thus, firing of a particular set of neurons during network silence was not observed, contradicting the notion that specific set of neurons is responsible for initiating network active states (Cossart et al., 2003; Sanchez-Vives and McCormick, 2000).

Several arguments make also the mechanism relying exclusively on intrinsic oscillations in layer V neurons (Sanchez-Vives and McCormick, 2000), or other cortical neurons, an unlikely explanation of the origin of active states in vivo. Most of the known intrinsic currents, that are capable of maintaining prolonged depolarization and firing, require a strong initial signal for their activation (Fleidervish and Gutnick, 1996; Pedroarena and Llinás, 1997). The source for such a signal is lacking during the silent state, when no action potentials are generated in the network. The only current that is activated close to the resting membrane potential and that can lead to a cell discharge is hyperpolarization-activated depolarizing current (McCormick and Pape, 1990). However, this current is weak in cortical neurons, and cannot lead to their discharges as it does in the thalamic neurons. Direct proof that intrinsic properties of cortical neurons cannot alone support initiation of active states comes from in vitro studies showing that active states are abolished by blocking postsynaptic glutamate receptors (Sanchez-Vives and McCormick, 2000; Shu et al., 2003). It is worth noting, that the exclusive role of layer 5 neurons in the generation of active states was demonstrated only in slices maintained in "modified" artificial cerebrospinal fluid. In these conditions all (Sanchez-Vives and McCormick, 2000), or about a half (Shu et al., 2003) of layer V neurons continuously fire during silent states. Such a pattern was never observed in vivo in anesthetized or naturally sleeping cats (see above).

The mechanism of initiation of activity, which relies on spontaneous release (Timofeev et al., 2000), appears more realistic. Active states originate from silent state, when all cortical neurons are silent and do not fire spikes, and thus only spike-independent, spontaneous release takes place (Paré et al., 1997; Salin and Prince, 1996; Timofeev et al., 2000). Its total postsynaptic effect on a neuron depends on the number of synapses at the neuron, and the frequency of spontaneous events. In the neocortex, silent states are associated with an increase of extracellular Ca2+ concentration (Crochet et al., 2005; Massimini and Amzica, 2001) which mediates an increase in evoked release probability towards the end of silent state (Crochet et al., 2005). The frequency of miniatures is positively correlated with both of these factors (Prange and Murphy, 1999), therefore it should increase towards the end of a silent state (Timofeev et al., 2000). Because excitatory synapses are much more numerous than inhibitory, increasing frequency of spontaneous

release at all synapses is likely to shift its net balance towards excitation (Haider et al., 2006; Rudolph et al., 2007). This scenario is supported by the fact that some transitions from silence to activity during natural sleep (Fig. III.8) or anesthesia (Figs. III.9-10) indeed exhibited a slow buildup of depolarization with a large number of individual synaptic events discernible on its slope. The first spike occurs in deeply lying neurons when depth-positive field potential already started transition in depth negative direction, but before sharp transition (Fig. III.3). Therefore, it is possible that only a few neurons from deep layers started to depolarize at this time. According to cortical dipole generation theory (Niedermeyer and Lopes da Silva, 2005), only a few neurons from layer V might be necessary to influence the generation of EEG events. Eventually, the depolarization induced by spontaneous release would reach the threshold, leading to generation of action potentials. In this scenario, any neuron could generate the first spike. This conclusion is supported by our results, showing that activity may originate first in any neuron (Figs. III.5, III.7, and III.S2), and by the results of in vitro imaging study, demonstrating that activity could start from any neuronal group (Cossart et al., 2003). However, for statistical reasons, cells with the largest number of inputs, such as large layer 5 pyramids (DeFelipe and Farinas, 1992), would have advantages in sensing and summating both spontaneous synaptic events and EPSPs from other, just activated, cells. Once large layer V pyramids are activated, their broad projections and the ability to generate bursts of action potentials, which increase their postsynaptic impact (Lisman, 1997; Timofeev et al., 2000), make them best suited for activation of other neurons (Sanchez-Vives and McCormick, 2000; Timofeev et al., 2000). These properties of large layer V pyramids might be especially important for integration of spontaneous and evoked synaptic potentials and activation of other cells in slices, where connectivity is severely reduced. This could be a likely reason why Sanchez-Vives and McCormick in their pioneer work (Sanchez-Vives and McCormick, 2000) on oscillations in slices found that large layer V pyramidal neurons were responsible for active state initiation.

A major role for large layer V pyramids and IB cells in the initiation and spread of active states in the network in vivo is supported by the tendency of these cells to show earlier onset of activity as compared to cells of other types and from other layers. This tendency was apparent in both multiunit recordings during natural sleep (Fig. III.3) and in

intracellular recordings under ketamine/xylaxine anesthesia (Fig. III.4, III.11). However, our results also show that this leading role is due not to the intrinsic oscillations of layer V pyramids, but rather to their ability to integrate spontaneous events effectively because of the large dendritic tree and huge excitatory convergence onto these cells.

3.6.3 Origin of current sinks and sources during slow oscillation.

In the superficial and the deep layers, the LFP signal and the distribution of current sinks and sources are clearly different. At 600-700 μm from the surface, the polarity of the waves in the LFP is inversed (Niedermeyer and Lopes da Silva, 2005), and also the picture of current sinks and sources is mirror-like: strong superficial sinks and deep sources during silent states alternate with deep sinks and superficial sources during active states. In a marked contrast to the LFP, the intracellular recordings showed no phase reversal with the recording depth. In the neurons recorded simultaneously above and below 600 μm, slow membrane potential oscillations are always in-phase, but never in contra-phase one to the other (Fig. III.5, III.10, III.12a). Interestingly, despite the difference in the depth profile of polarity of slow waves in the LFP and in membrane potential of neurons, the delays in the onset of developed active states as determined using LFPs or intracellular recordings have similar depth profiles (Fig. III.12b).

Thus, not all cells contributed equally to the macroscopic picture of slow waves. Contribution of a cell to the LFP signal depends on its electric asymmetry and on its ability to maintain differential charges of its compartments along axo-somato-dendritic axis (Niedermeyer and Lopes da Silva, 2005). Large pyramidal neurons from deep layers, with their apical dendrites reaching the cortical surface, are well suited to produce electrical signals sensed by LFP electrodes (Niedermeyer and Lopes da Silva, 2005). Due to the large electrotonic distance, the membrane potential at two compartments may differ by several millivolts (Schiller et al., 1997; Stuart et al., 1997) and thus cause significant current flow along the apical dendrites. Reversal of slow wave polarity in the LFP depth profile comes then as natural consequence of differential location of recording electrode relative to the dipoles of large pyramids from deep layers.

Intracellular recordings showed that during silent states, somata of all cortical cells in all layers are hyperpolarized, and no action potentials are generated. However, spike-

independent spontaneous transmitter release might still take place (Paré et al., 1997; Salin and Prince, 1996; Timofeev et al., 2000). Since at the dendrites, the number of excitatory synapses is several-fold higher than of inhibitory, but at/close to soma inhibitory synapses prevail, the spontaneous input might lead to a depolarization of dendrites relative to the soma. High density of potassium channels may contribute further to the outward current at axo-somatic compartment (Guan et al., 2006; Hu et al., 2007; Pruss et al., 2005; Saganich et al., 2001). Combination of these factors would produce net inward current at dendrites (extracellular current sink in upper layers), but net outward current at somatic region (extracellular current source in deep layers), as observed during silent states.

During active states, synaptic activity increases dramatically. Experimental data from cortical slices and computer simulations suggest that excitatory and inhibitory inputs to cortical cells are balanced (Destexhe et al., 2003; Shu et al., 2003), and in behaving animals inhibition even dominates (Shu et al., 2003). The relative contribution of inhibition may be enhanced because inhibitory interneurons integrate the excitatory inputs more effectively (Cruikshank et al., 2007; Markram et al., 2004; Povysheva et al., 2006), and are capable of generating high frequency non-adapting trains of action potentials, thus compensating for the smaller number of inhibitory synapses. As a result, strong excitatory and inhibitory inputs with inhibition dominating will produce in the dendrites high amplitude fluctuations, while changing little the mean level of dendritic membrane potential. In contrast, somatic membrane potential in layer V large pyramids during active states is depolarized by up to 15-20 mV relative to silent states, and cells generate axo-somatic action potentials. Due to these factors, polarity of the somato-dendritic dipole changes to the opposite: during active states, net inward current flows in the soma (extracellular sinks in deep layers) but net outward current through the dendrites (extracellular sources in superficial layers).

3.6.4 Conclusion: a scenario for active state onset.

Results of our study suggest that large pyramidal cells from deep layers play a central role in initiation and spread of active states during slow oscillation in vivo. Both LFP and intracellular recordings point to an earlier activation in deep layers, and both multiunit and intracellular recordings point to an earlier firing of cells located in layer V.

This activation starts from the silent state, when no cells are firing. Because slow oscillation has a cortical origin, absence of cell firing during silent states restricts possible mechanisms of active state origin to spike-independent processes. The spike-independent process causes buildup of depolarization that occasionally reaches spike threshold in some cells. Firing of these cells initiates the activity in the rest of network. Spontaneous release necessary for active state initiation may occur not only from nerve terminals, but also from glial cells surrounding synapses (Fellin et al., 2009). In contrast to earlier hypotheses, we suggest that activity does not necessarily originate in layer V cells. Due to the stochastic nature of spontaneous transmitter release, the first transition from silence to activity may occur in any neuron. However, because of the large number of synaptic inputs and the broad divergence of the outputs, large layer V pyramidal neurons are best suited for integration of spontaneous inputs and initiation of activity in the whole neocortical network.

3.7 Funding and acknowledgments

Canadian Institutes of Health Research (MOP-37862, MOP-67175), National science and engineering research council of Canada (grant 298475) and National Institute of Neurological Disorders and Stroke (1R01NS060870-01) to IT; Bundesministerium für Bildung und Forschung (01GQ07112) and startups from University of Connecticut to M.V. S.C. is a Canadian Institutes of Health Research fellow. I.T. is Fonds de la recherche en santé du Québec Research Scholar.

Acknowledgements

We are grateful to Michael Mukovski for the help with data processing, to Anton Sirota for advices on the current-source density analysis, and to Marina Chistiakova for comments on early versions of the manuscript.

3.8 References

Blake H, Gerard RW. 1937. Brain potentials during sleep. Am J Physiol 119:692-703.

Cash SS, Halgren E, Dehghani N, Rossetti AO, Thesen T, Wang C, Devinsky O, Kuzniecky R, Doyle W, Madsen JR, Bromfield E, Eross L, Halasz P, Karmos G, Csercsa R, Wittner L, Ulbert I. 2009. The human K-complex represents an isolated cortical down-state. Science 324:1084-1087.

Chauvette S, Volgushev M, Mukovski M, Timofeev I. 2007. Local origin and long-range synchrony of active state in neocortex during slow oscillation. In: Timofeev I, editor. Mechanisms of spontaneous active states in the neocortex. Kerala, India: Research Signpost. p 73-92

Compte A, Sanchez-Vives MV, McCormick DA, Wang X-J. 2003. Cellular and network mechanisms of slow oscillatory activity (<1 Hz) and wave propagations in a cortical network model. J Neurophysiol 89:2707-2725.

Connors BW, Gutnick MJ. 1990. Intrinsic firing patterns of divers neocortical neurons. Trends Neurosci 13:99-104.

Contreras D, Steriade M. 1995. Cellular basis of EEG slow rhythms: a study of dynamic corticothalamic relationships. J Neurosci 15:604-622.

Cossart R, Aronov D, Yuste R. 2003. Attractor dynamics of network UP states in the neocortex. Nature 423:283-288.

Crochet S, Chauvette S, Boucetta S, Timofeev I. 2005. Modulation of synaptic transmission in neocortex by network activities. Eur J Neurosci 21:1030-1044.

Cruikshank SJ, Lewis TJ, Connors BW. 2007. Synaptic basis for intense thalamocortical activation of feedforward inhibitory cells in neocortex. Nat Neurosci 10:462-468.

DeFelipe J, Farinas I. 1992. The pyramidal neuron of the cerebral cortex: morphological and chemical characteristics of the synaptic inputs. Prog Neurobiol 39:563-607.

Destexhe A, Rudolph M, Pare D. 2003. The high-conductance state of neocortical neurons in vivo. Nat Rev Neurosci 4:739-751.

Diesmann M, Gewaltig MO, Aertsen A. 1999. Stable propagation of synchronous spiking in cortical neural networks. Nature 402:529-533.

Fellin T, Halassa MM, Terunuma M, Succol F, Takano H, Frank M, Moss SJ, Haydon PG. 2009. Endogenous nonneuronal modulators of synaptic transmission control cortical slow oscillations in vivo. Proc Natl Acad Sci U S A 106:15037-15042.

Fleidervish IA, Gutnick MJ. 1996. Kinetics of slow inactivation of persistent sodium current in layer V neurons of mouse neocortical slices. J Neurophysiol 76:2125-2130.

Gray CM, McCormick DA. 1996. Chattering cells: superficial pyramidal neurons contributing to the generation of synchronous oscillations in the visual cortex. Science 274:109-113.

Greenberg DS, Houweling AR, Kerr JND. 2008. Population imaging of ongoing neuronal activity in the visual cortex of awake rats. Nat Neurosci 11:749-751.

Guan D, Lee JCF, Tkatch T, Surmeier DJ, Armstrong WE, Foehring RC. 2006. Expression and biophysical properties of Kv1 channels in supragranular neocortical pyramidal neurones. J Physiol (Lond) 571:371-389.

Haider B, Duque A, Hasenstaub AR, McCormick DA. 2006. Neocortical network activity in vivo is generated through a dynamic balance of excitation and inhibition. J Neurosci 26:4535-4545.

Hasenstaub A, Sachdev RNS, McCormick DA. 2007. State changes rapidly modulate cortical neuronal responsiveness. J Neurosci 27:9607-9622.

Hassler R, Muhs-Clement K. 1964. Architektonischer Aufbau des sensomotorischen und parietalen Cortex der Katze. J Hirnforschung 6:377-422.

Hu H, Vervaeke K, Storm JF. 2007. M-channels (Kv7/KCNQ channels) that regulate synaptic integration, excitability, and spike pattern of CA1 pyramidal cells are located in the perisomatic region. J Neurosci 27:1853-1867.

Hughes SW, Cope DW, Blethyn KL, Crunelli V. 2002. Cellular mechanisms of the slow (<1 Hz) oscillation in thalamocortical neurons in vitro. Neuron 33:947-958.

Lisman JE. 1997. Bursts as a unit of neural information: making unreliable synapses reliable. Trends Neurosci 20:38-43.

Llinás RR. 1988. The intrinsic electrophysiological properties of mammalian neurons: insights into central nervous system function. Science 242:1654-1664.

Luczak A, Bartho P, Marguet SL, Buzsaki G, Harris KD. 2007. Sequential structure of neocortical spontaneous activity in vivo. PNAS 104:347-352.

Mahon S, Vautrelle N, Pezard L, Slaght SJ, Deniau J-M, Chouvet G, Charpier S. 2006. Distinct patterns of striatal medium spiny neuron activity during the natural sleep-wake cycle. J Neurosci 26:12587-12595.

Markram H, Toledo-Rodriguez M, Wang Y, Gupta A, Silberberg G, Wu C. 2004. Interneurons of the neocortical inhibitory system. Nat Rev Neurosci 5:793-807.

Marsalek P, Koch C, Maunsell J. 1997. On the relationship between synaptic input and spike output jitter in individual neurons. Proc Natl Acad Sci U S A 94:735-740.

Massimini M, Amzica F. 2001. Extracellular calcium fluctuations and intracellular potentials in the cortex during the slow sleep oscillation. J Neurophysiol 85:1346-1350.

Massimini M, Huber R, Ferrarelli F, Hill S, Tononi G. 2004. The sleep slow oscillation as a traveling wave. J Neurosci 24:6862-6870.

McCormick DA, Pape HC. 1990. Properties of a hyperpolarization-activated cation current and its role in rhythmic oscillation in thalamic relay neurons. J Physiol 431:291-318.

Mitzdorf U. 1985. Current source-density method and application in cat cerebral cortex: investigation of evoked potentials and EEG phenomena. Physiol Rev 65:37-100.

Mitzdorf U, Singer W. 1978. Prominent excitatory pathways in the cat visual cortex (A 17 and A 18): a current source density analysis of electrically evoked potentials. Exp Brain Res 33:371-394.

Mukovski M, Chauvette S, Timofeev I, Volgushev M. 2007. Detection of active and silent states in neocortical neurons from the field potential signal during slow-wave sleep. Cereb Cortex 17:400-414.

Nicholson C, Freeman JA. 1975. Theory of current source-density analysis and determination of conductivity tensor for anuran cerebellum. J Neurophysiol 38:356-368.

Niedermeyer E, Lopes da Silva F. 2005. Electroencephalography: Basic principles, clinical applications and related fields. Philadelphia: Lippincott Williams & Wilkins. 1309

Paré D, Lebel E, Lang EJ. 1997. Differential impact of miniature synaptic potentials on the soma and dendrites of pyramidal neurons in vivo. J Neurophysiol 78:1735-1739.

Pedroarena C, Llinás R. 1997. Dendritic calcium conductances generate high-frequency oscillation in thalamocortical neurons. Proc Natl Acad Sci U S A 94:724-728.

Povysheva NV, Gonzalez-Burgos G, Zaitsev AV, Kroner S, Barrionuevo G, Lewis DA, Krimer LS. 2006. Properties of excitatory synaptic responses in fast-spiking interneurons and pyramidal cells from monkey and rat prefrontal cortex. Cereb Cortex 16:541-552.

Prange O, Murphy TH. 1999. Correlation of miniature synaptic activity and evoked release probability in cultures of cortical neurons. J Neurosci 19:6427-6438.

Pruss H, Derst C, Lommel R, Veh RW. 2005. Differential distribution of individual subunits of strongly inwardly rectifying potassium channels (Kir2 family) in rat brain. Molecular Brain Research 139:63-79.

Rudolph M, Pospischil M, Timofeev I, Destexhe A. 2007. Inhibition determines membrane potential dynamics and controls action potential generation in awake and sleeping cat cortex. J Neurosci 27:5280-5290.

Saganich MJ, Machado E, Rudy B. 2001. Differential expression of genes encoding subthreshold-operating voltage-gated K+ channels in brain. J Neurosci 21:4609-4624.

Sakata S, Harris KD. 2009. Laminar Structure of Spontaneous and Sensory-Evoked Population Activity in Auditory Cortex. Neuron 64:404-418.

Salin PA, Prince DA. 1996. Spontaneous GABAA receptor-mediated inhibitory currents in adult rat somatosensory cortex. J Neurophysiol 75:1573-1588.

Sanchez-Vives MV, Descalzo VF, Reig R, Figueroa NA, Compte A, Gallego R. 2008. Rhythmic spontaneous activity in the piriform cortex. Cereb Cortex 18:1179-1192.

Sanchez-Vives MV, McCormick DA. 2000. Cellular and network mechanisms of rhythmic recurrent activity in neocortex. Nat Neurosci 3:1027-1034.

Schiller J, Schiller Y, Stuart G, Sakmann B. 1997. Calcium action potentials restricted to distal apical dendrites of rat neocortical pyramidal neurons. J Physiol 505 (Pt 3):605-616.

Shu Y, Hasenstaub A, McCormick DA. 2003. Turning on and off recurrent balanced cortical activity. Nature 423:288-293.

Steriade M. 2004. Neocortical cell classes are flexible entities. Nat Rev Neurosci 5:121-134.

Steriade M, Contreras D, Dossi RC, Nuñez A. 1993. The slow (<1 Hz) oscillation in reticular thalamic and thalamo-cortical neurons: scenario of sleep rhythm generation in interacting thalamic and neocortical networks. J Neurosci 13:3284-3299.

Steriade M, Nuñez A, Amzica F. 1993. Intracellular analysis of relations between the slow (<1 Hz) neocortical oscillations and other sleep rhythms of electroencephalogram. J Neurosci 13:3266-3283.

Steriade M, Nuñez A, Amzica F. 1993. A novel slow (<1 Hz) oscillation of neocortical neurons in vivo : depolarizing and hyperpolarizing components. J Neurosci 13:3252-3265.

Steriade M, Timofeev I, Durmuller N, Grenier F. 1998. Dynamic properties of corticothalamic neurons and local cortical interneurons generating fast rhythmic (30-40 Hz) spike bursts. J Neurophysiol 79:483-490.

Steriade M, Timofeev I, Grenier F. 2001. Natural waking and sleep states: a view from inside neocortical neurons. J Neurophysiol 85:1969-1985.

Stuart G, Schiller J, Sakmann B. 1997. Action potential initiation and propagation in rat neocortical pyramidal neurons. J Physiol 505 (Pt 3):617-632.

Timofeev I, Grenier F, Bazhenov M, Sejnowski TJ, Steriade M. 2000. Origin of slow cortical oscillations in deafferented cortical slabs. Cereb Cortex 10:1185-1199.

Timofeev I, Grenier F, Steriade M. 2000. Impact of intrinsic properties and synaptic factors on the activity of neocortical networks in vivo. J Physiol (Paris) 94:343-355.

Timofeev I, Grenier F, Steriade M. 2001. Disfacilitation and active inhibition in the neocortex during the natural sleep-wake cycle: An intracellular study. Proc Natl Acad Sci U S A 98:1924-1929.

Timofeev I, Steriade M. 1996. Low-frequency rhythms in the thalamus of intact-cortex and decorticated cats. J Neurophysiol 76:4152-4168.

Volgushev M, Chauvette S, Mukovski M, Timofeev I. 2006. Precise long-range synchronization of activity and silence in neocortical neurons during slow-wave sleep. J Neurosci 26:5665-5672.

Wang Y, Markram H, Goodman PH, Berger TK, Ma J, Goldman-Rakic PS. 2006. Heterogeneity in the pyramidal network of the medial prefrontal cortex. Nat Neurosci 9:534-542.

Waters J, Helmchen F. 2006. Background synaptic activity is sparse in neocortex. J Neurosci 26:8267-8277.

Zhu L, Blethyn KL, Cope DW, Tsomaia V, Crunelli V, Hughes SW. 2006. Nucleus- and species-specific properties of the slow (<1 Hz) sleep oscillation in thalamocortical neurons. Neuroscience 141:621-636.

3.9 Figures

Figure III- 1 Depth profile of the LFP during natural slow-wave sleep.

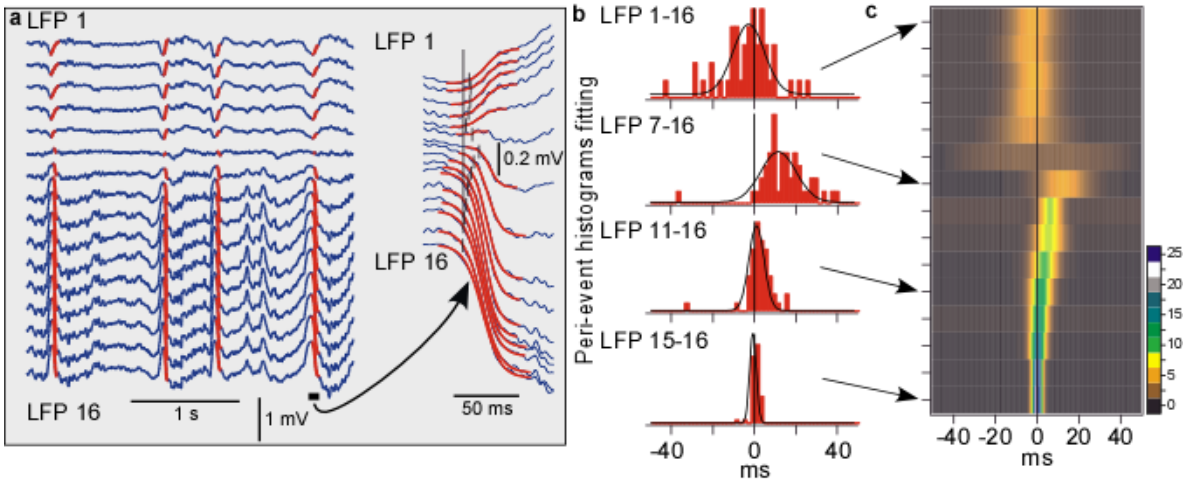

(a) Local field potentials recorded with a 16-channel Michigan probe, inserted perpendicularly to the cortical surface. Red lines show sigmoidal fits of the transitions from silent state to active states. The point at which a fit reached 10% of its amplitude was taken as the onset time of an active state. One cycle is shown at expanded scale. **(b)** Histograms of delays of the active state onsets in indicated channels relative to the activity onset in channel 16, taken as the reference. 50 cycles were used. Black lines show Gaussian fits. **(c)** Depth profile of active state onsets. For each channel, Gaussian fit of the distribution of activity onset delays relative to channel 16 is shown, color-coded for n cycles as indicated by the scale bar.

Figure III- 2 Alternating pattern of current sinks and sources during natural slow-wave sleep revealed with current-source density analysis.

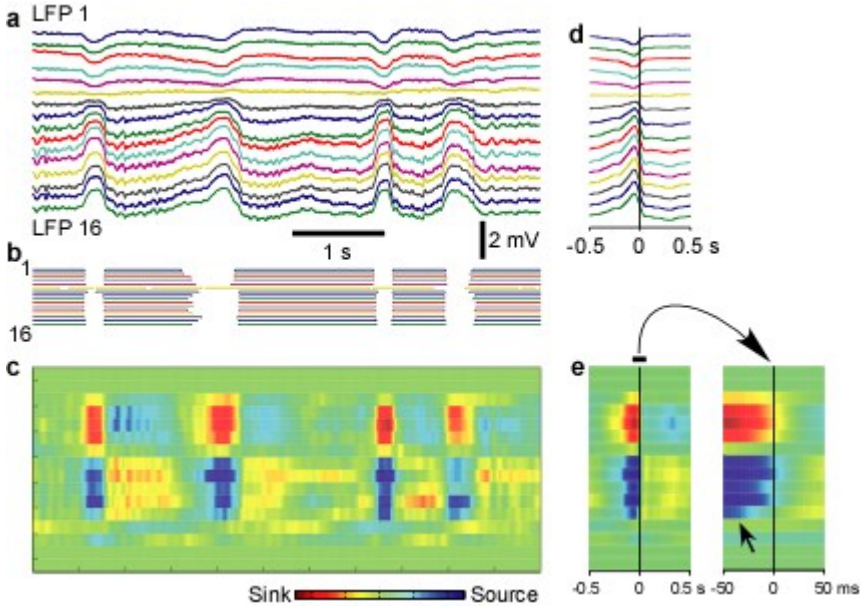

(a) Depth profile of local field potentials recorded with a 16-channel Michigan probe inserted perpendicularly to the cortical surface. **(b)** active states detected in LFP traces from **a**. **(c)** Current-source density analysis of the traces from **a**. Note alternating pattern of sinks and sources corresponding to the slow waves in the LFP. **(d)** Depth profile of averaged LFPs during the transition from silent to active states. Mid amplitude in the transition from silent to active states in channel 16 in a 150 s recording segment were taken as reference (zero point in timescale in **d**) for calculating averages (n=101) in all channels. **(e)** Averaged current-source density during the transition from silent to active state, and its central portion at tenfold higher temporal resolution (right panel).

Note that during active states, the flow of current is less pronounced and more variable in terms of spatio-temporal organization of sources and sinks than during silent states.

Figure III- 3 Depth distribution of neuronal firing during slow-wave sleep.

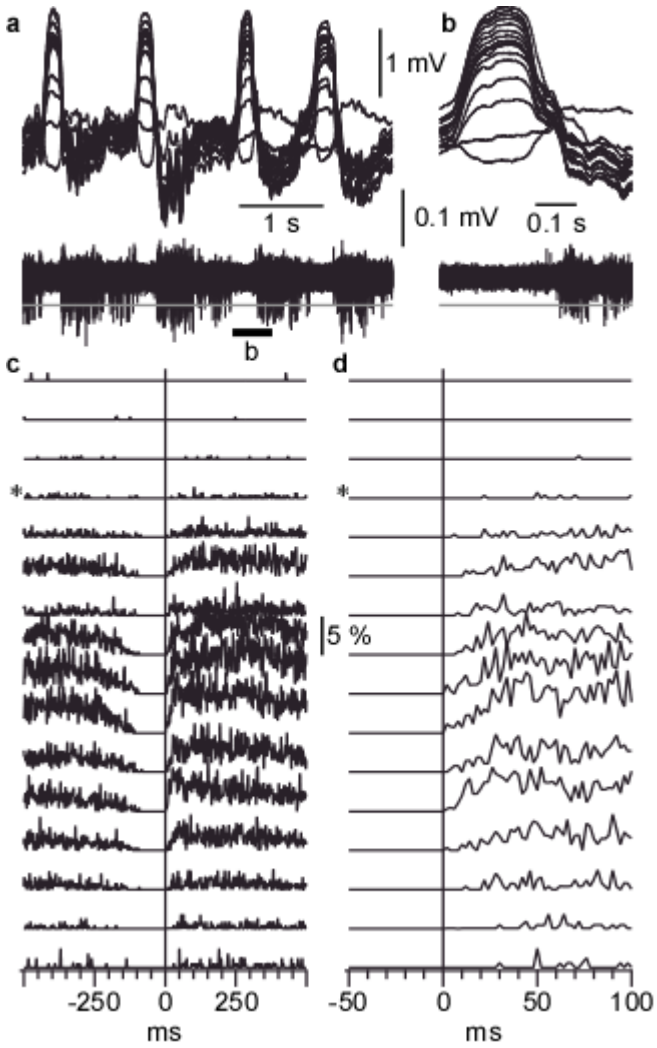

(a) Local field potential (top traces) and multiunit activity (bottom trace) recordings at the border of cortical areas 5 and 7 (associative cortex) during short episode of slow-wave sleep. Recordings were performed with a 16-channel silicon probe inserted perpendicularly to the cortical surface. The recording sites were separated by 100 µm, the upper recording site was just below cortical surface. Local field potential and multiunit activity traces were obtained from the same electrodes, by band-pass filtering 0.1 Hz to 10 kHz and 0.5 kHz to 10 kHz, respectively. **(b)** A segment from a as indicated by the bar, at higher temporal resolution. **(c)** Probability distributions of multiunit firing during a cycle of slow oscillation. Pooled data from 290 cycles from 5 different sleep episodes. Spikes were detected as all peaks that exceeded a threshold (grey lines in **a** and **b**), set at 5x standard

deviation of the noise fluctuations during silent state. * indicates the electrode at which the polarity of slow-waves were reversed. Vertical line shows onset of active state determined in the LFP recorded from the deepest electrode. **(d)** Zoom in on the silent to active state transition from **c**. Note that the first firing occurs in neurons located between 800 and 1200 μm from cortical surface.

Figure III- 4 Cells from deep layers fire earlier than other cells at the onset of active state.

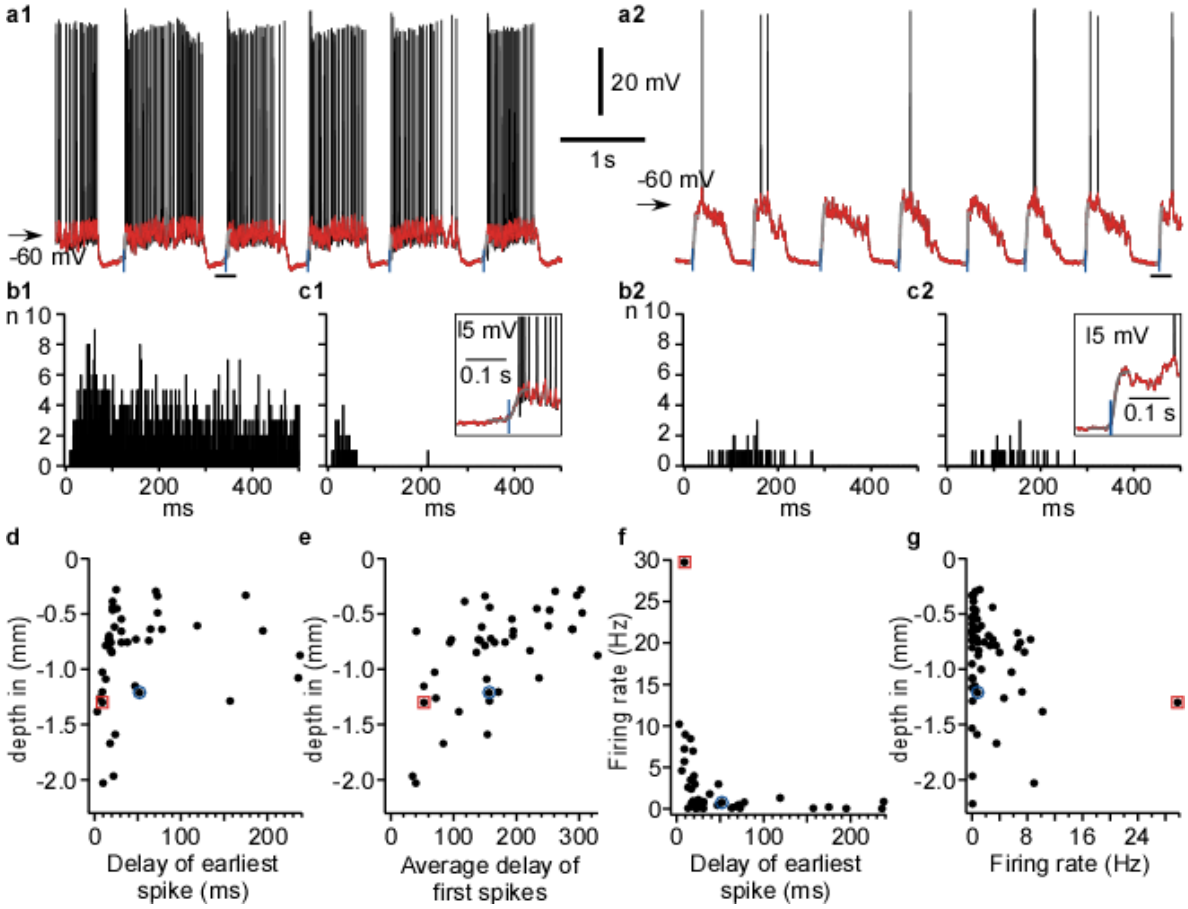

(a) Intracellular recording from 2 cells in area 7 of cat neocortex, with an exceptionally high firing rate **(a1)** and low firing rate **(a2)**. Black traces show original recordings, superimposed red traces show the same segment of recordings after removing action potentials. The onset of active states (blue vertical lines) was determined with sigmoid fit (grey line) of the transition from silent to active state, at 10% of the fit amplitude. Insets show enlarged cycles indicated by the horizontal bars in **a**. **(b)** Histograms of ***all*** spikes in cells shown in **a1** and **a2** relative to the active state onset (**b1**, 49 cycles, **b2**, 65 cycles). Bin width is 1 ms. **(c)** Histograms of the ***first*** spike delay at onsets of active states. Note that even in the cell with a very high firing rate, the first spike occurred several milliseconds after the onset of cell depolarization. No spikes occurred before the active state (depolarization) started. **(d)** Cell depth plotted against the delay of the ***earliest*** spike from

all active states. Note that earliest spike delays in cells located between -1.0 and -1.4 mm were shorter than in other cells. **(e)** Cell depth plotted against the first spike delay ***averaged*** over all active states. Note again that cells from deep layers have a tendency to fire earlier than others. **(f)** Firing rate of cells plotted against the delay to the ***earliest*** spike at the onset of an active state. Note that cells with higher firing rate had shorter earliest spike delays. **(g)** Cell depth plotted against their firing rate. In (**d-g**), red square symbols mark data from the cell shown in **a1**, and blue circle symbols show data from the cell presented in **a2**.

Figure III- 5 Onsets of active states in local neuronal constellations.

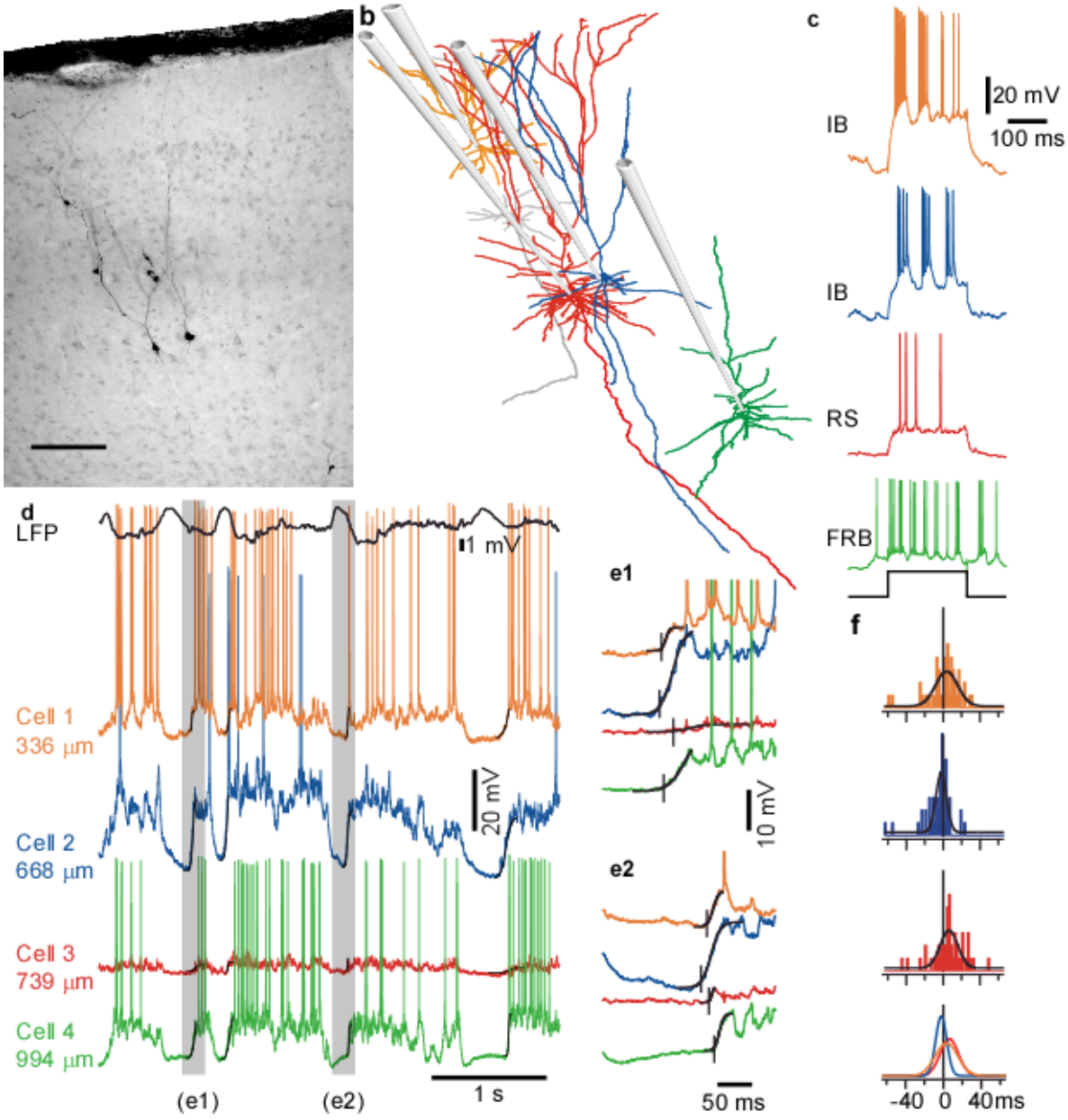

Data from four simultaneously recorded neurons are color-coded; each neuron is represented by its own color in **b-f**. **(a)** Microphotograph and **(b)** Neurolucida reconstructions of four simultaneously recorded pyramidal cells. The grey neuron was recorded prior to the cell-3 (red) with the same electrode. Position of recording electrodes is shown schematically. **(c)** Responses of the neurons from **b** to depolarizing current pulses and their electrophysiological identification as intrinsically-bursting (IB), regular spiking

(RS) and fast-rhythmic-bursting (FRB) cells. **(d)** LFP and intracellular activities of four simultaneously recorded neurons. Black lines superimposed on membrane potential traces show sigmoid fits of active state onsets. **(e)** Two periods from **d** shown at expanded scale. Vertical bars indicate active state onsets. Note the different order of activity onset in neurons in the two episodes. **(f)** Distributions of delays of active state onsets in cells 1-3 relative to the activity onset in cell 4 taken as reference. The lowermost panel shows an overlay of the three distributions. Note the negative shift of the cell 2, blue delay distribution, indicating that this IB cell had tendency to lead in the majority of cycles, and the positive shift of histogram for cell 3 (red) indicating that this RS cell was often the last involved in activity.

Figure III- 6 Depth profile of activity onset in simultaneously recorded neurons: Population analysis.

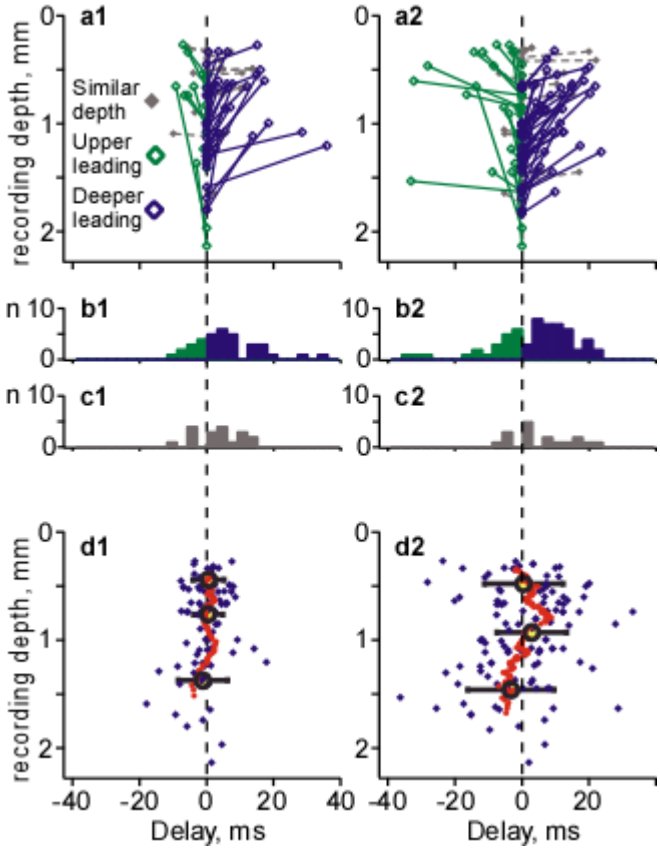

(a) Dependence of activity onset on the recording depth in cell pairs. Each pair of simultaneously recorded neurons is represented by two symbols connected with a line. Y-coordinates show the depth at which the cell was recorded. Delays of activity onsets in the upper cell in a pair were calculated relative to the activity onsets in the deeper cell, taken as reference. Positive delays (blue) indicate pairs with deeper cell leading; negative delays (green) indicate pairs with upper cell leading. Grey indicate recordings with similar depth (vertical difference <100 μm). Left column, analysis of the onsets of active states obtained with the method of sigmoid fits; right column, detection of the beginning of developed active states using the method based on values of membrane potential and its SD. **(b, c)** Distributions of the delays in cell pairs, colour coded as in **a**. **(d)** Dependence of the delay of activity onset in state clusters on recording depth. Each blue diamond symbol represents data for one cell. Running averages (red symbols) were calculated for sets of 17 neurons. For gross averages (cycles, ±SD) cells were segregated in three nearly equally populated

groups, **(d1)** above 575 µm (n=27), between 575 and 1050 µm (n=27), and deeper than 1050 µm (n=27). **(d2)** above 670 µm (n=36), between 670 and 1100 µm (n=35), and deeper than 1100 µm (n=36). Note that most often activity started earlier in the deeper neurons.

Figure III- 7 The high variability of active state onsets in cells during natural sleep.

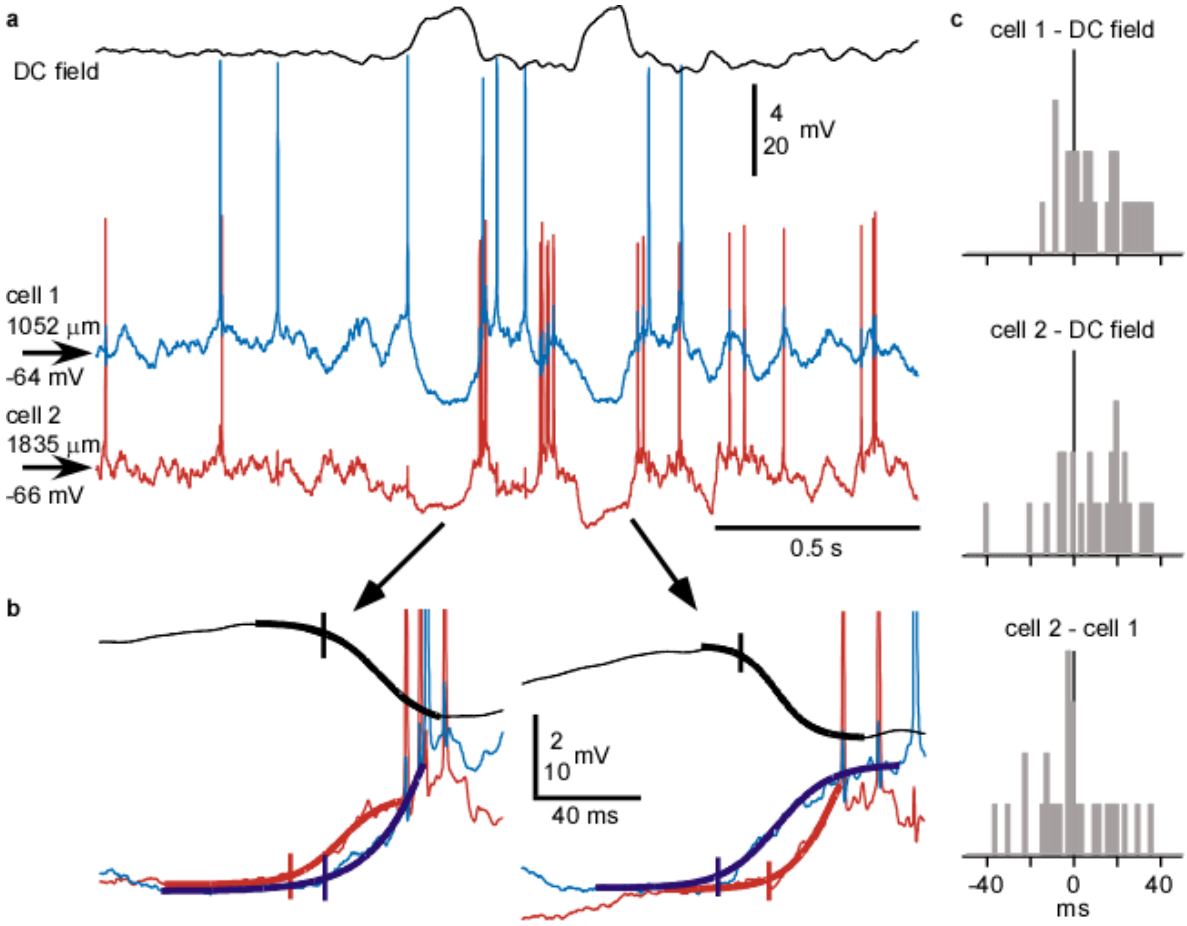

(a) Simultaneously recorded DC field potential and intracellular activity of two closely located (<100 µm in lateral distance) neurons. **(b)** Two cycles from a shown at expanded scale. Action potentials are truncated. Thick line show sigmoid fits of transitions to active states. Note the opposite order of activity onset in the two cells in two consecutive cycles. **(c)**. Distributions of the activity onset delays in the two cells relative to the onset of active state in DC field potential and in the simultaneously recorded cell. Note that all distributions cover zero, and thus in any pair the opposite orders of activation were encountered, with delays up to 40 ms.

Figure III- 8 Progressive build up *vs.* sharp transitions from silent to active states.

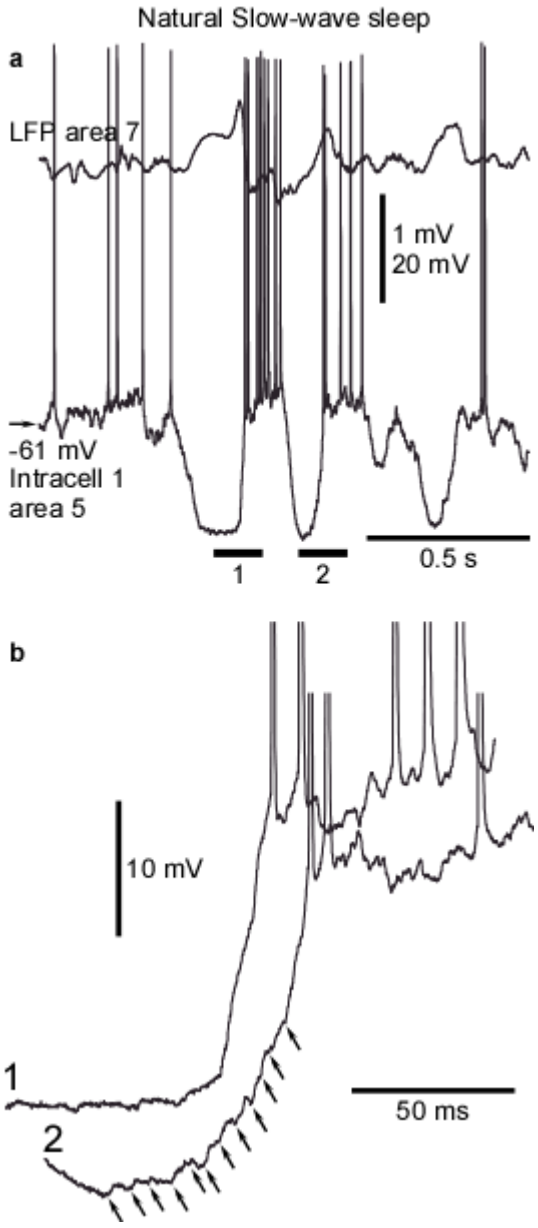

(a) Intracellular and local field potential recordings during natural slow-wave sleep. **(b)** Zoom in on active state onsets from two consecutive cycles. Note the presence of many individual events (oblique arrows) in the onset with slow development of depolarization (2), and a smooth slope of a rapid transition (1).

Figure III- 9 Membrane potential fluctuations increase just before the onset of active state.

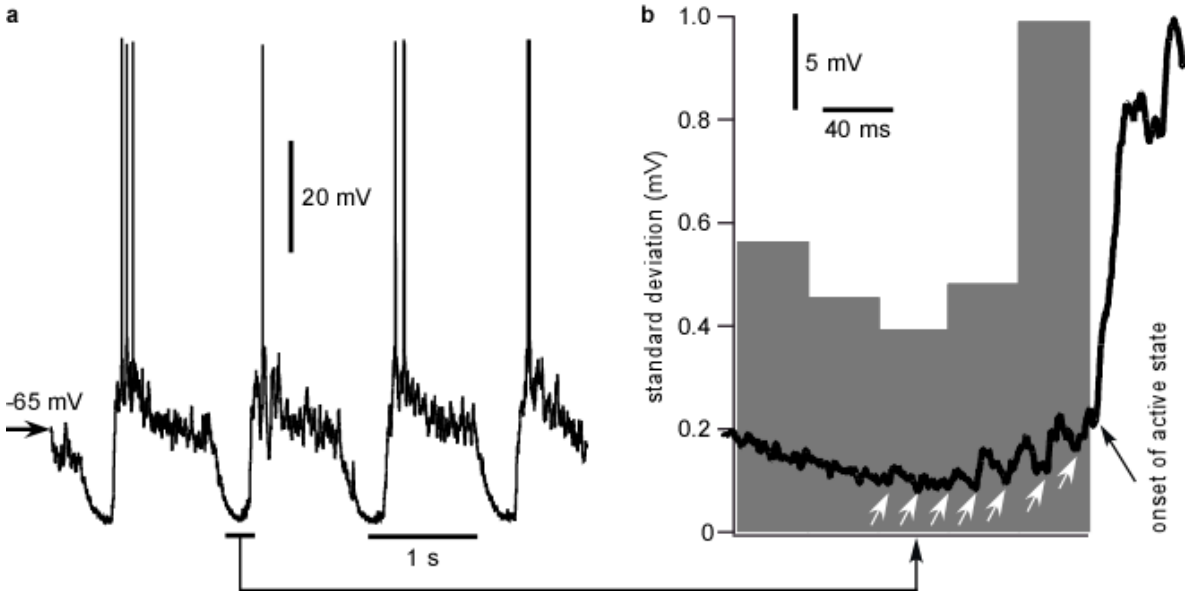

(a) Intracellular recording in suprasylvian gyrus (area 7) of cat anesthetized with a mixture of ketamine and xylazine. **(b)** A segment from **a** is enlarged and superposed on a histogram showing the averaged membrane potential standard deviation (n= 50 cycles, 0 time is active state onset defined with sigmoid fit). Bin width is 40 ms. Note the large increase in the standard deviation of the membrane potential just prior to the active state onset.

Figure III- 10 Earlier involvement in activity is associated with slower transitions to active states.

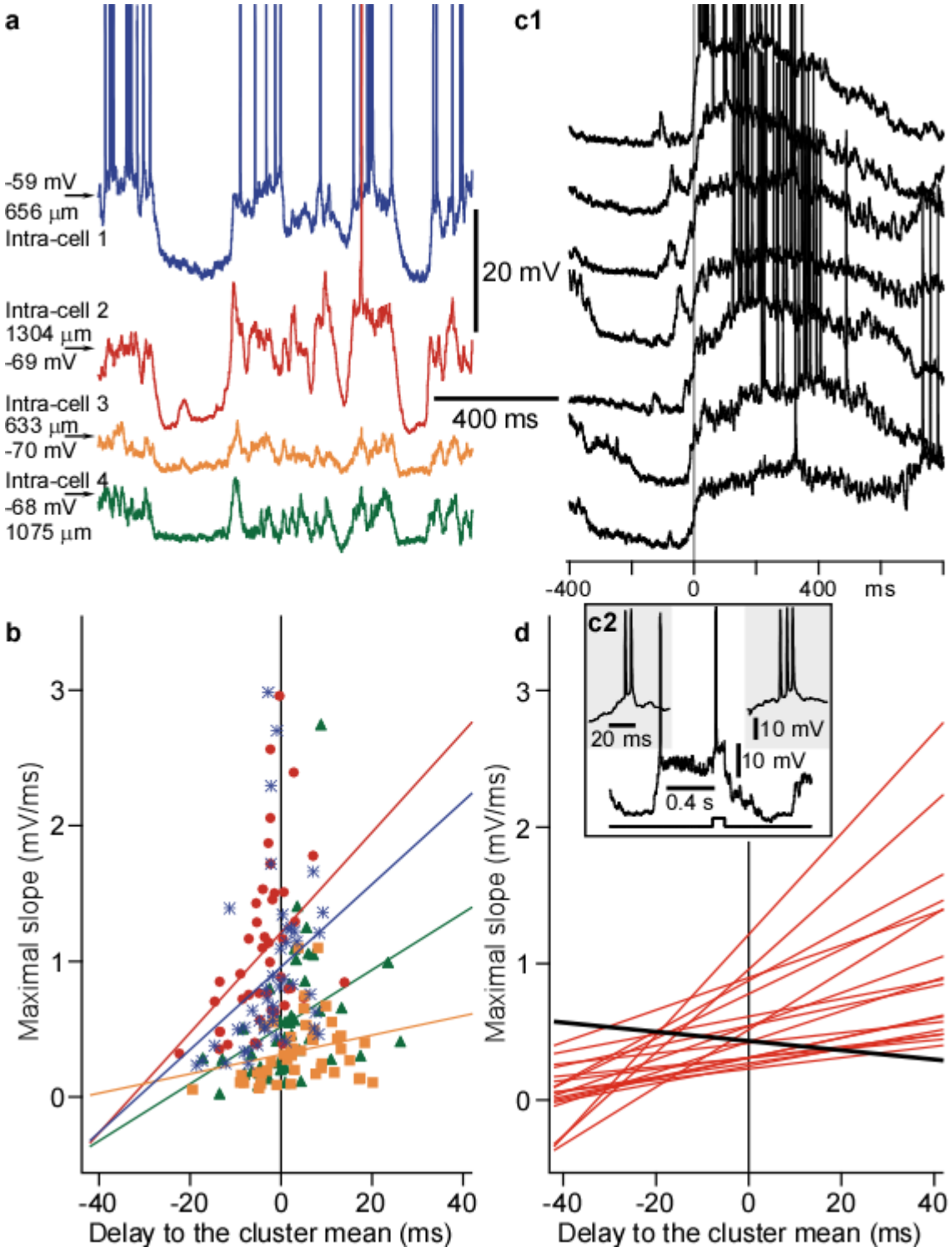

(a) A segment of simultaneous quadruple intracellular recording from closely located neurons in area 7, performed under ketamine/xylazine anesthesia. **(b)** Maximal slope of a transition from silent to active state, estimated from sigmoid fitting, plotted against the delay of the cell relative to the mean onset of activity in the cluster. Each point shows data for one cycle. For each cell a regression line is shown. Color code corresponds to the four cells in **a**. Note that in cycles in which activity onset in a cell was earlier than in other cells (negative delays), the slope of transition was smaller, typical for a progressive synaptic buildup. **c1**. Examples of transitions from silent to active state in a cell that often showed a strong buildup of depolarization prior to the transition. Zero time is half amplitude of depolarization. The cell was intrinsically-bursting, as identified by bursts during both spontaneous activity (left inset in **c2**) and in responses to depolarizing current pulses (right inset in **c2**). **d**. Relation between maximal slope of transition from silent to active states and the delay of activity onset in the cell relative to the mean onset in the cluster. Regression lines (as in **b**) for 18 cells. Note that in 17 out of 18 neurons, earlier onsets of active state were associated with smaller slopes of transition. The only one cell showing an inverse relation (black line) is illustrated in **c**.

Figure III- 11 Intrinsically-bursting cells are leading the onset of active states.

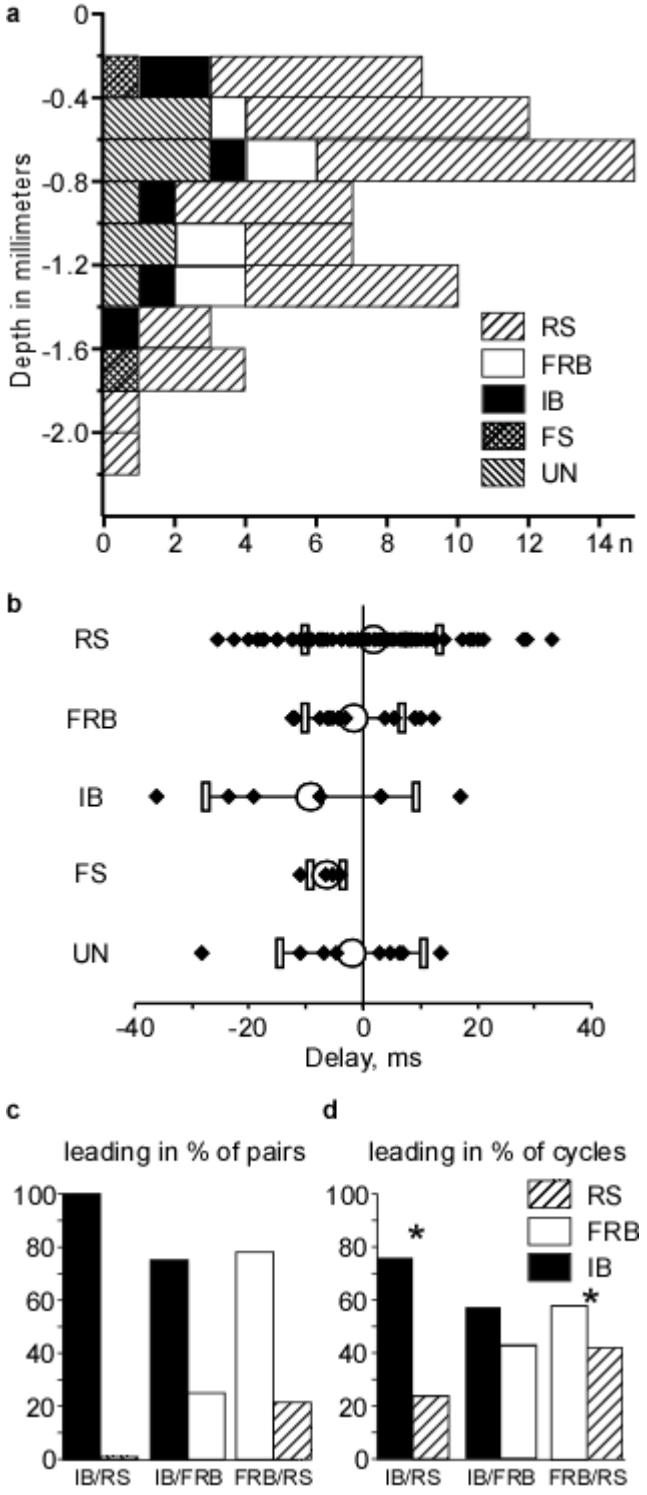

(a) Depth-distribution of different types of neocortical neurons, as indicated by symbols: regular-spiking (RS), fast-rhythmic-bursting (FRB), intrinsically-bursting (IB) and fast spiking (FS). UN - unidentified neurons. Note that neurons of all electrophysiological types

were found at any depth. **(b)** Delay of onsets of clustered active states in cells of different electrophysiological types. **(c, d)** Activity onset in pairs composed of different cell types. IB cells were leading in all pairs consisting of IB/RS cells (n=5 pairs), and in 3 out of 4 IB/FRB pairs. In these pairs, the IB cells were also leading in most of individual activity cycles (IB/RS: n= 210 cycles; IB/FRB, n=182 cycles). In FRB/RS pairs, FRB cells were leading in 7 out of 9 pairs, and in majority of cycles (n=544 cycles). * in **(d)** indicates significant difference, $p<0.05$ to a bilateral binomial test approximated by normal law. For IB/FRB pairs, $p=0.054$.

Figure III- 12 Comparison of the depth profiles of field potential and intracellular events during slow oscillation.

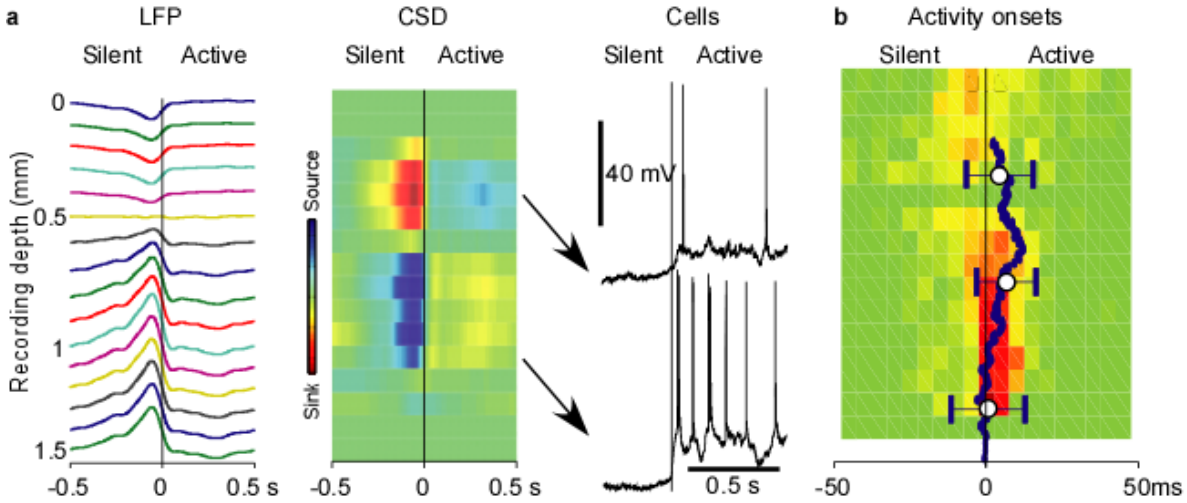

(a) Depth profile of the LFP, CSD and intracellular activity during transition from silent to active state during natural slow-wave sleep. Arrows show approximate depth of the two neurons relative to the CSD profile (LFP and CSD plots are from Fig. III.2). **(b)** Depth profile of the onsets of active states in the LFP (data from Fig. III.1) and the running average of active state onsets in intracellularly recorded neurons (data from Fig. III.6 d2).

3.10 Supplemental information

Figure III- S1 Sigmoid-fitting method for active state onset is robust and reliable.

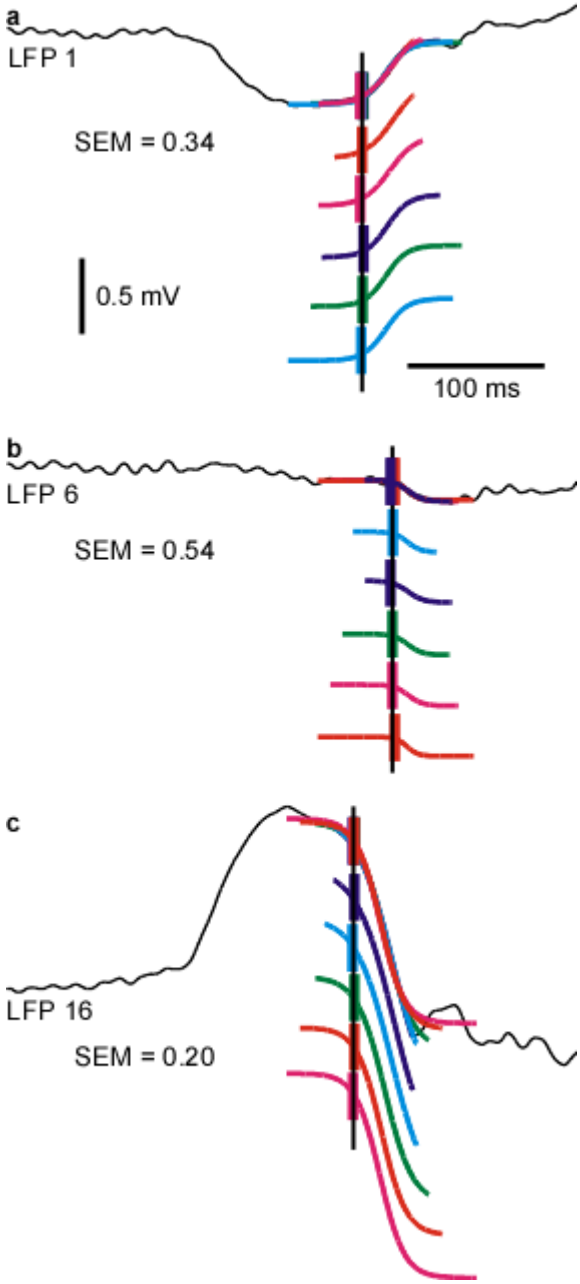

a, b, c – LFP, recorded in the supreficial layers (**a**, LFP 1), mid layer in which the polarity of slow oscillations reverse (**b**, LFP 6) and deep layer (**c**, LFP 16) during one cycle of a slow oscillation. In each recording, 5 increasingly long intervals which included the transition from silent to active state were fitted with a sigmoid function. These fits are

superimposed on the trace and are also shown separately below the traces. Thick colored vertical lines show the detected timing of onset of active state, which was defined as the time at 10% of the transition amplitude. Vertical thin black lines illustrate the mean of active state onset detected by the 5 different fits. Standard errors to the mean (SEM) values for the time of active state onset are given for each channel. Note that although intervals of very different length were used for the fittings, detected time of active state onset was similar and its SEM small.

Figure III- S2 Diverse sequential order of involvement of neighboring cells in active states.

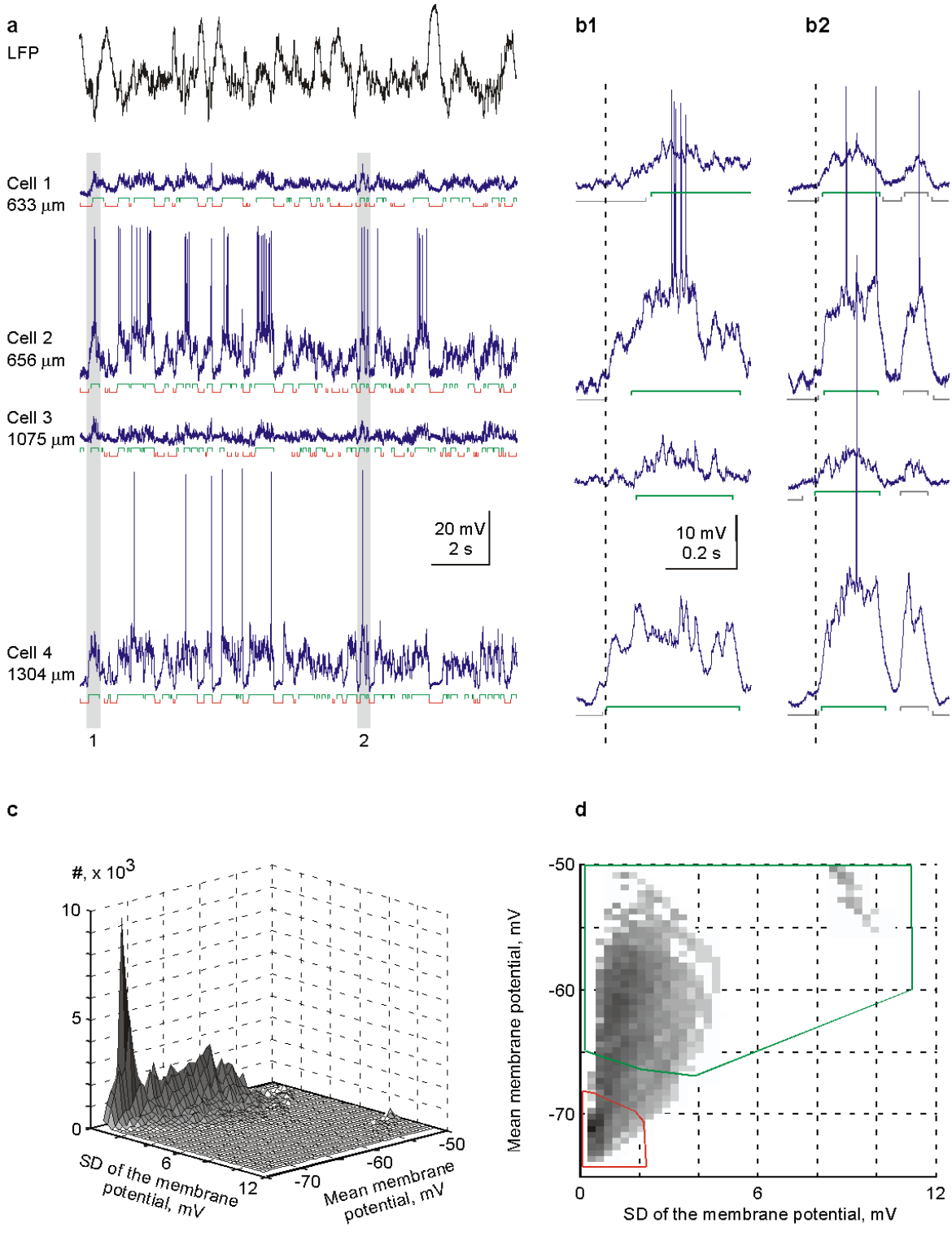

(a) Simultaneously recorded LFP and intracellular activity of four cells in the neocortex. Green lines below each trace indicate periods of active states, red lines indicate silent states. **(b1, b2)** Expanded fragments of the periods indicated by grey bars 1 and 2 in **a**. Active states forming state cluster are shown with green lines. Vertical dotted line marks the onset of the active state in the leading cell. Note that in the two clusters of states, the sequence of involvement of cells in activity is different. **(c, d)** Detection of active and silent states. 3D density distribution of the data from cell 4 in **(a)**, side view **(c)**, and top view **(d)**. The mean membrane potential and its standard deviation (SD) were calculated in a running window of 25 ms. These values were used as X and Y coordinates; the Z axis is the frequency of their occurrence. Silent states are represented by the peak at low membrane potential and low SD values. Active states are represented by a broader hill at more depolarized membrane potentials and higher SD values. The rightmost cloud of points represents windows with action potentials. The regions used for detection of active (green) and silent (red) states are outlined in the top view **(d)**.

Figure III- S3 Difference in delays of active state onset and developed active states.

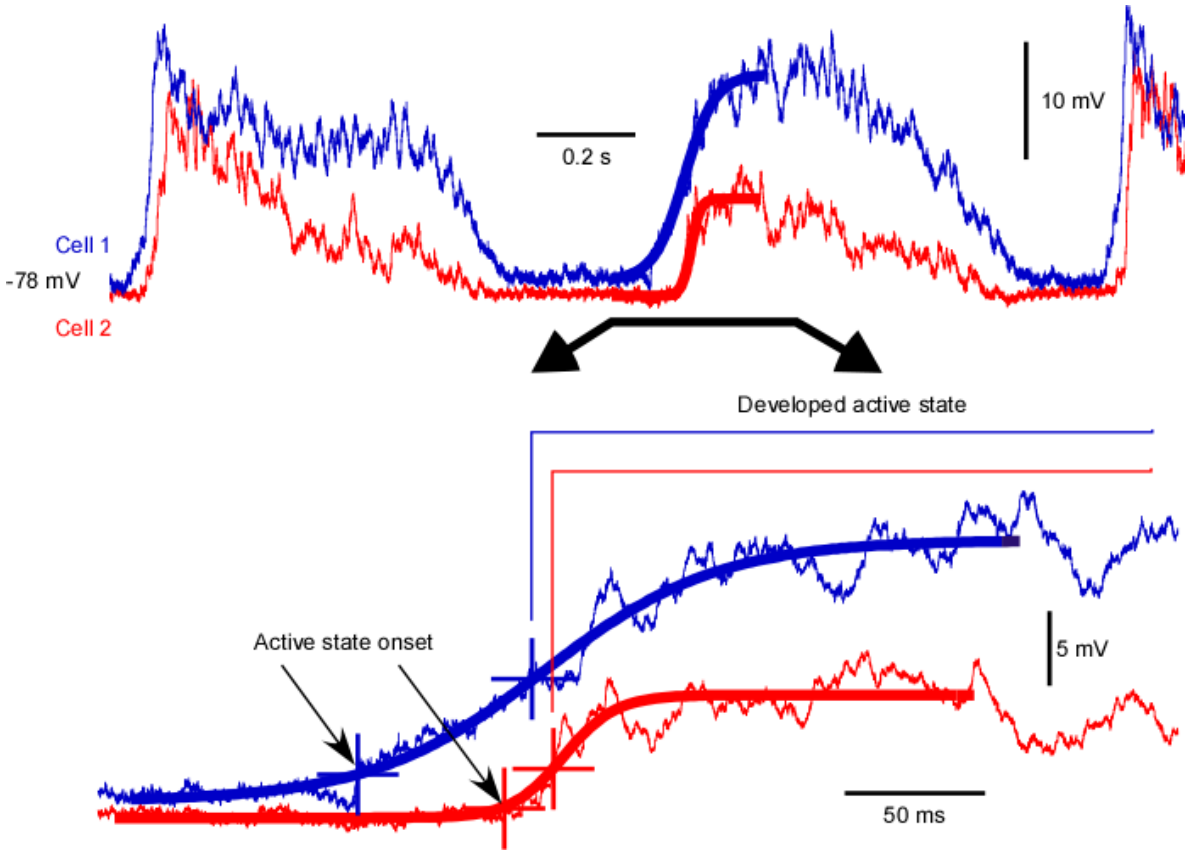

Intracellular activities of two simultaneously recorded neurons. Thick lines show sigmoid fits of active state onsets. Active state onsets are indicated in the bottom panel by arrows. Developed active states are detected when the membrane potential is depolarized and standard deviation of its fluctuations is high (see Fig. III.S2). In the shown example the delay between onsets of active state in two neurons was 52 ms, but the delay in the time of occurrence of the developed states was only 6 ms.

Chapter IV

4.0 Properties of slow oscillation during slow-wave sleep and anesthesia in cats.

Authors: Sylvain Chauvette[1], Sylvain Crochet[1,2,3], Maxim Volgushev[4], and Igor Timofeev[1]
Authors affiliations:
1 Département de psychiatrie et de neurosciences, The Centre de recherche Université Laval Robert-Giffard (CRULRG), Laval University, Québec, (QC), G1J 2G3, Canada
2 INSERM U1028; CNRS UMR5292; Lyon Neuroscience Research Center, Integrative Physiology of Brain Arousal System Team, Lyon, F-69000, France
3 University Lyon 1, Lyon, F-69000, France
4 University of Connecticut Storrs, Department of Psychology, CT 06269-1020, USA

Published in the Journal of neuroscience, 2011

Complete citation: Chauvette S, Crochet S, Volgushev M, Timofeev I (2011) Properties of Slow Oscillation during Slow-Wave Sleep and Anesthesia in Cats. The Journal of Neuroscience 31:14998-15008.

Titre en français:

4.0 Propriétés de l'oscillation lente pendant le sommeil à ondes lentes et sous anesthésie chez le chat.

4.1 Résumé en français:

L'anesthésie profonde est couramment utilisée comme modèle du sommeil à ondes lentes. L'anesthésie à la kétamine-xylazine reproduit les principales caractéristiques de l'onde lente du sommeil : des ondes lentes de large amplitude dans le potentiel de champ et celles-ci sont générées par une alternance d'états hyperpolarisés et dépolarisés dans les neurones corticaux. Toutefois, une comparaison quantitative directe du potentiel de champ et des fluctuations de potentiel de membrane pendant le sommeil naturel et l'anesthésie est manquante. Il demeure donc inconnu dans quelles mesures les propriétés de l'oscillation lente du sommeil sont bien reproduites par le modèle d'anesthésie à la kétamine-xylazine. Ici, nous avons utilisé des enregistrements de potentiels de champ et des enregistrements intracellulaires dans différentes aires corticales chez le chat afin de comparer directement les propriétés de l'oscillation lente pendant le sommeil naturel et lors d'une anesthésie à la kétamine-xylazine. Pendant le sommeil à ondes lentes, l'activité corticale montrait une plus grande puissance dans la gamme des fréquences lentes/delta (0.1-4 Hz) et dans la gamme des fréquences de type fuseau (8-14 Hz), alors que sous anesthésie, la puissance dans la gamme des ondes gamma (30-100 Hz) était supérieure. Sous anesthésie, les ondes lentes étaient plus rythmiques et plus synchronisées à travers le cortex. Les enregistrements intracellulaires ont révélé que les états silencieux étaient plus longs et l'amplitude de la transition entre les états actifs et silencieux dans le potentiel de membrane était plus grande sous anesthésie. Les ondes lentes étaient largement uniformes à travers les différentes aires corticales pendant l'anesthésie, mais pendant le sommeil à ondes lentes, elles étaient plus amples dans les aires associatives et visuelles, alors qu'elles étaient plus petites et moins régulières dans les aires corticales somatosensorielles et motrices. Nous concluons que, bien que les principales caractéristiques de l'oscillation lente dans le sommeil et l'anesthésie semblent similaires, de multiples caractéristiques cellulaires et de réseau sont différemment exprimées lors du sommeil naturel par rapport l'anesthésie à la kétamine-xylazine.

4.2 Abstract

Deep anesthesia is commonly used as a model of slow-wave sleep (SWS). Ketamine–xylazine anesthesia reproduces the main features of sleep slow oscillation: slow, large-amplitude waves in field potential, which are generated by the alternation of hyperpolarized and depolarized states of cortical neurons. However, direct quantitative comparison of field potential and membrane potential fluctuations during natural sleep and anesthesia is lacking, so it remains unclear how well the properties of sleep slow oscillation are reproduced by the ketamine–xylazine anesthesia model. Here, we used field potential and intracellular recordings in different cortical areas in the cat to directly compare properties of slow oscillation during natural sleep and ketamine–xylazine anesthesia. During SWS cortical activity showed higher power in the slow/delta (0.1– 4 Hz) and spindle (8 –14 Hz) frequency range, whereas under anesthesia the power in the gamma band (30 –100 Hz) was higher. During anesthesia, slow waves were more rhythmic and more synchronous across the cortex. Intracellular recordings revealed that silent states were longer and the amplitude of membrane potential around transition between active and silent states was bigger under anesthesia. Slow waves were mostly uniform across cortical areas under anesthesia, but in SWS, they were most pronounced in associative and visual areas but smaller and less regular in somatosensory and motor cortices. We conclude that, although the main features of the slow oscillation in sleep and anesthesia appear similar, multiple cellular and network features are differently expressed during natural SWS compared with ketamine–xylazine anesthesia.

4.3 Introduction

Slow-wave sleep (SWS) is characterized by large amplitude slow waves in the electroencephalogram (Blake and Gerard, 1937). Their repetitive and more or less regular appearance during slow-wave sleep and under anesthesia is commonly referred to as slow oscillation, which consists of an alternation of active (Up) and silent (Down) states in the cortico-thalamic network (Steriade et al., 1993c; Steriade et al., 1993b, a; Cowan and Wilson, 1994). During active states, neocortical neurons are depolarized, reveal vigorous synaptic activities, and may fire action potentials, while during silent states, they are hyperpolarized, display few synaptic events and do not fire spikes (Contreras and Steriade, 1995; Steriade et al., 2001; Timofeev et al., 2001; Chauvette et al., 2010). Intracellular recordings from non-anesthetized cats (Steriade et al., 2001; Timofeev et al., 2001; Rudolph et al., 2007; Chauvette et al., 2010), and rats (Mahon et al., 2006; Okun et al., 2010) demonstrated that when local field potential (LFP) displays slow waves, cortical and striatal neurons alternate between active and silent states. In contrast, when LFP displays activated patterns, normally associated with wakefulness and REM sleep, the membrane potential of cortical neurons doesn't express silent states and no large amplitude LFP waves occur (Matsumura, 1979; Steriade et al., 2001; Timofeev et al., 2001; Rudolph et al., 2007; Okun et al., 2010; Constantinople and Bruno, 2011). Similar activities were found during active, but not quiet wakefulness in mice (Crochet and Petersen, 2006; Poulet and Petersen, 2008; Gentet et al., 2010). After prolonged periods of wakefulness, local slow waves can occur in otherwise awake animals (Vyazovskiy et al., 2011).

Experiments on cats and rats anesthetized with ketamine/xylazine or urethane revealed a slow cortical activity similar to that observed during natural SWS (Steriade et al., 1993c; Steriade et al., 1993b, a; Contreras and Steriade, 1995; Haider et al., 2006; Volgushev et al., 2006; Haider et al., 2007; Hasenstaub et al., 2007; Luczak et al., 2007; Chauvette et al., 2010; Sharma et al., 2010). Anesthesia-induced slow oscillation appears more regular than SWS (Steriade et al., 1993b; Wolansky et al., 2006; Clement et al., 2008), and its frequency was higher with ketamine/xylazine than urethane anesthesia (Steriade et al., 1993b; Sharma et al., 2010) indicating that properties of the slow oscillation are not fixed, but depend upon experimental conditions. Recordings from different cortical

areas show a preferential origin of slow waves at specific locations (Massimini et al., 2004; Volgushev et al., 2006; Kurth et al., 2010; Nir et al., 2011), suggesting regional specificity.

Ketamine-xylazine anesthesia is extensively used as a model of sleep slow oscillation; however no direct comparison of the properties of slow oscillation during anesthesia and SWS had been done so far. To address this issue we performed LFP and intracellular recordings across different cortical areas in both naturally sleeping and ketamine-xylazine anesthetized cats. We found that despite apparent similarities major differences exist between SWS and anesthesia.

4.4 Material and methods

Experiments were carried out in accordance with the guideline of the Canadian Council on Animal Care and approved by the Laval University Committee on Ethics and Animal Research. The cats were purchased from an established animal breeding supplier. Good health conditions of all animals were certified by the supplier and determined upon arrival to animal house by physical examination, which was performed by animal facilities technicians and a veterinarian in accordance with requirements of Canadian Council on Animal Care. The animals were used for experiments in 5-20 days from arrival to the local animal house.

General description and database. We recorded field potentials, extracellular unit, and intracellular activities of cortical neurons in various cortical areas of cats during natural sleep or in cats anesthetized with ketamine-xylazine. We used recordings from database acquired over the last ten years for neurons recorded from suprasylvian gyrus (associative cortex, 36 cats in acute experiments and 4 cats in chronic experiments), postcruciate gyrus (somatosensory cortex, 5 cats in acute experiments and 1 cat in chronic experiments), precruciate gyrus (motor cortex, 1 cat in acute experiments and 1 cat in chronic experiments), and posterior marginal gyrus (primary visual cortex, 2 cats in chronic experiments). In order to complement our database with multisite local field potential (LFP) recordings and to collect additional intracellular data, we performed additional experiments in motor (1 acute and 1 chronic), somatosensory (4 chronic), and visual (3 acute and 1 chronic) cortices. Because in the same experiment we were able to record from several cortical areas, altogether we used 43 cats for acute experiments and 8 cats for chronic experiments.

Preparation. Experiments on anesthetized animals. For acute experiments the cats of both sexes were anesthetized with ketamine and xylazine (10-15 and 2-3 mg/kg i.m., respectively). All pressure points and tissues to be incised were infiltrated with lidocaine (0.5%). The animals were paralyzed with gallamine triethiodide (20 mg/kg) and artificially ventilated, maintaining the end-tidal CO_2 concentration at 3.5-3.8%. A permanent sleep-like state, as ascertained by continuous recording of the LFP, was maintained throughout the experiments by administering additional doses of ketamine and xylazine (5 and 1 mg/kg, respectively) or just ketamine (5 mg/kg). The additional anesthesia was

administrated when LFP slow waves were absent for 20-30 sec. The body temperature was monitored by a rectal probe and maintained at 37°C via a feedback-controlled heating blanket. The heart rate was continuously monitored (90-110 bpm). The stability of intracellular recordings was reinforced by cisternal drainage, bilateral pneumothorax, and by filling the hole made for recordings with a solution of 4% agar.

Experiments on non-anesthetized animals. Chronic experiments were conducted using an approach similar to that previously described (Steriade et al., 2001; Timofeev et al., 2001). For implantation of recording chamber and electrodes, 4 cats (data from the old database) were anesthetized with sodium pentobarbital (30 mg/kg), and 4 cats were anesthetized with isoflurane (0.75-2%), in accordance with the current recommendation of the Committee for Animal Care of Laval University. All other procedures were very similar. Briefly, prior to surgery, the animal was given a dose of pre-anesthetic, which was composed of ketamine (15 mg/kg), buprenorphine (0.01 mg/kg), and acepromazine (0.3 mg/kg). After site shaving and cat intubation for gaseous anesthesia, the site of incision was washed with at least three alternating passages of proviodine solution and alcohol. Lidocaine (0.5%) was injected at the site of incision and applied at all pressure points. During surgery, electrodes for LFP recordings, electromyogram (EMG) from neck muscle, and electro-oculogram (EOG) were implanted and fixed with acrylic dental cement. Custom-made recording chambers were fixed for future intracellular recordings. Eight to ten screws were fixed to the cranium. Four bolts were covered in the dental cement that also covered bone-fixed screws, permanently implanted electrodes and fixed recording chamber to allow future head-restrained recordings without any pressure point. Throughout the surgery, the body temperature was maintained at 37°C using a water circulating thermo-regulated blanket. Hearth beat and oxygen saturation were continuously monitored using a pulse oximeter (Rad-8, MatVet, Montreal, Canada) and the level of anesthesia was adjusted to maintain a hearth beat at 110-120 per minute. A lactate ringer solution (10 ml/kg/h, i.v.) was given during the surgery. Following the surgery, cats were given buprenorphine (0.01 mg/kg) or anafen (2 mg/kg) twice a day for three days, and baytril (5 mg/kg) once a day for seven days. About a week was allowed to animals to recover from the surgery before the first recording session. Usually, 2-3 days of training were sufficient for cats to remain in head-restrain position for 2-4 hours and display 1-3 full sleep-wake cycles including

periods of quiet wakefulness, SWS, and REM sleep. The recordings were performed up to 40 days after the surgery.

Recordings. All recordings were done in a Faraday chamber. Using AM 3000 amplifiers (A-M systems, Sequim, WA, USA) with custom modifications, LFPs were recorded in marginal gyrus (visual cortex [areas 17 and 18]), suprasylvian gyrus (associative cortex [areas 5, 7, and 21]), ectosylvian gyrus (auditory cortex [areas 22 and 50]), postcruciate gyrus (somatosensory cortex [area 3]), precruciate gyrus (motor cortex [areas 4 and 6]), and frontal gyrus (medial prefrontal cortex [area 32]) using tungsten electrodes (2 MΩ, bandpass filter 0.1 Hz to 10 kHz). We aimed to implant electrodes at 1 mm below the cortical surface. Intracellular recordings were performed using glass micropipettes filled with 2.5 M of potassium acetate (KAc) and having a resistance of 30-70 MΩ. A high-impedance amplifier with active bridge circuitry (Neurodata IR-283 amplifiers, Cygnus Technology, PA, USA, lowpass filter 10 kHz), was used to record the membrane potential and to inject current into the neurons. Intracellular recordings were performed from areas 3, 4, 7, and 17 according to the atlas (Reinoso-Suarez, 1961). In acute experiments, a chloridized silver wire, placed between the skull and the temporal muscle, was used as a reference electrode. In chronic experiments, a silver wire was fixed either in the frontal bone over the sinus cavity or over the cerebellum. All electrical signals were sampled at 20 kHz and digitally stored on Vision (Nicolet, Wisconsin, USA). At the end of experiments, the cats were anesthetized with ketamine-xylazine to record LFP activities with the same electrodes as during natural states of vigilance. After collecting 1 hour or more of recordings, the cats were euthanized with a lethal dose of pentobarbital (50 mg/kg i.v.).

Data analysis. Electrographic recordings were analyzed offline using custom-written routines in IgorPro (Lake Oswego, Oregon, USA) and MATLAB (MathWorks, Natick, MA) environment. To measure the amplitude of slow oscillation we used intracellular recordings. The amplitude of field potential recordings depends on the activity of cellular elements in the region but also on the electrode location relative to electrical dipole(s). Because the cortical thickness is different in different areas the amplitude of LFP at 1 mm from surface of pia can give erroneous estimation of slow oscillation amplitude. It is generally assumed that during slow wave activity, the membrane potential of neurons has

a bimodal distribution (Metherate and Ashe, 1993) and this was the case in the majority of our recordings (Fig. IV-1, a1-b1 and a3-b3). However, when transitions between active and silent states were slow and their duration was comparable to the time a neuron spent in those states, the membrane potential distribution was not bimodal, although silent states could be clearly identified (Fig. IV-1, a2-b2, a4-b4). In order to resolve this problem we analyzed periods around transitions from silent to active states. We first selected time at half-amplitude of transitions from silent to active state from 1 min segment of a recording. We then selected segments of ±100 ms from that point (Fig. IV-1c) and compiled a histogram using all these segments (Fig. IV-1d, gray histograms). On all occasions the distribution of the membrane potential was bimodal, however, due to natural fluctuation of the membrane potential the two maxima were broad. Therefore, from selected segments we computed averages (Fig. IV-1c, black traces) and calculated the histogram of membrane potential distribution from these averaged traces (Fig. IV-1d, black histogram). The results gave clear bimodal distribution of membrane potential (Fig. IV-1). This method allowed unbiased analysis of all recorded neurons.

The frequency composition of electric signals was calculated using Fast Fourier Transformation of multiple 20 sec segments of LFP traces. From power spectrum of each data segment we calculated the integral power in the frequency ranges between 0.1 Hz and 4 Hz for slow and delta activities, 8 Hz and 14 Hz for spindles, and 30 Hz and 100 Hz for gamma-band fluctuations. We also calculated autocorrelation of field potential and membrane potential recordings and coherence between pairs of simultaneously recorded LFPs. Coherence was calculated using MatLab (R2011b) function *mscohere*, which utilizes Welch's averaged modified periodogram method to calculate the magnitude squared coherence estimate. Periodic Hamming windows with 50% overlap were used to obtain 8 equal-length sections of each signal. Coherence function was calculated with a step of 0.1526 Hz. Then, coherence in three frequency ranges: slow and delta (0.2-4 Hz), spindle (8-14 Hz), and gamma (30-100 Hz), was calculated by averaging the values within the respective range. Unless specified, all numerical values are given as mean ± standard deviation. Specific statistical tests are indicated in the text.

4.5 Results

We employed two different strategies to compare properties of LFP, extracellular unit activity, and intracellular membrane potential traces during natural SWS and ketamine-xylazine anesthesia. Field potentials were recorded with chronically implanted electrodes during natural sleep-wake cycle and thereafter under ketamine-xylazine anesthesia. This allowed to compare LFP signals pair-wise, each pair consisting of recordings made from the same electrode in the same animal during natural sleep and anesthesia. Intracellular recordings from neurons in different cortical areas were made sequentially during natural sleep or anesthesia, therefore intracellular data were analyzed as groups.

On one occasion (Fig. IV-2), we were able to record LFP and extracellular unit activities of the same neuron in the somatosensory cortex (postcruciate gyrus, area 3) during waking state, SWS and ketamine-xylazine anesthesia (Fig. IV-2b, insets). During waking state characterized by high-frequency low amplitude activity in the LFP, the neuronal firing was continuous and did not reveal periodic patterns (Fig. IV-2). Only central peak, but no additional peaks were present in the autocorrelogram of neurons' firing (Fig. IV-2b, left panel). Upon transition to SWS, evidenced by characteristic large amplitude slow waves in the LFP and EEG, the neuronal firing became grouped and occurred during depth-negative phases of the LFP (Fig. IV-2a). Several minutes after injection of ketamine-xylazine anesthesia, the rhythmicity and the frequency of slow waves increased, the firing rate increased and became highly rhythmic (Fig. IV-2). Similar to SWS the neuronal firing occurred during depth-negative phases of the LFP (Fig. IV-2a). The rhythmicity of neuronal firing increased as evidenced by multiple alternating peaks and troughs in the auto-correlogram (Fig. IV-2b, right panel).

To examine whether these changes in activity could be generalized to other cortical areas, we have studied cortical electrographic activities in cat neocortex during natural SWS and during ketamine-xylazine anesthesia in precruciate gyrus, postcruciate gyrus, frontal gyrus, marginal gyrus, suprasylvian gyrus, and ectosylvian gyrus (Fig. IV-3a). Figure IV-3b shows results of a typical experiment in which field potentials were recorded simultaneously from multiple cortical locations using chronically implanted electrodes, first during an episode of natural SWS, and then during ketamine-xylazine anesthesia. Slow oscillation is clearly present in each individual trace in this example: all recordings in Fig.

IV-3b express slow, large amplitude waves, and fulfill a formal criterion of a low (< 4 Hz) over high (> 4 Hz) frequencies power ratio greater than 3 (Mukovski et al., 2007). An averaged ratio for all 11 locations was 6.11±5.8 during anesthesia and 8.18±6.9 (mean ± SEM) during SWS. However, the whole picture of the slow oscillation recorded simultaneously from multiple locations was clearly different during SWS as compared to anesthesia. During SWS, slow waves were always more prominent in suprasylvian gyrus (Fig. IV-3b, locations 8, 9, 10). In other cortical areas, slow waves were of smaller amplitude and even not evident in some cycles (Fig. IV-3b, left panel). In all cortical regions, the intervals between slow waves were highly irregular. Upon injection of ketamine-xylazine anesthesia, the pattern of slow oscillation changed (Fig. IV-3b, right panel). The slow waves became more regular, rhythm-like. They also were more generalized across different cortical regions, so that every wave was evident in all simultaneously recorded channels.

The differences between patterns of slow waves in field potential observed during SWS and anesthesia were corroborated by results of intracellular recordings. Figure IV-3c-f shows examples of membrane potential traces of neurons recorded in different areas of the neocortex during SWS or anesthesia. All neurons recorded during SWS or under ketamine-xylazine anesthesia exhibited alternating active (depolarized) and silent (hyperpolarized) states. However, during anesthesia the slow oscillation appears to be more rhythmic. Furthermore, during anesthesia the slow oscillation was of overall higher amplitude and the silent states were of longer duration than in SWS (Fig. IV-3c-f).

To validate and quantify these differences, we have compared, for SWS and anesthesia, and for different cortical regions, the following parameters: spectral composition, rhythmicity and coherence of the slow oscillation, its amplitude and the duration of silent states.

4.5.1 Less power in the slow and spindle range, but more in the high frequency range during ketamine-xylazine anesthesia than in natural sleep.

Although LFPs recorded in a same animal in both SWS and ketamine-xylazine anesthesia expressed clear slow activities, spectral analysis revealed substantial differences in their frequency composition. Figure IV-4 shows an example of LFP recorded in one experiment in somatosensory cortex (area 3) of the right hemisphere during a SWS episode

and then under ketamine-xylazine anesthesia. A higher rhythmicity of slow oscillation and an increase in fast activities (see filtered traces in Fig. IV-4a) can be clearly seen in the recording obtained under anesthesia. Power spectra of 20-second epochs around the illustrated segments of recordings revealed marked differences in three characteristic frequency ranges (Fig. IV-4b). Power in the slow and delta frequency range (0.1 – 4 Hz) and at spindle frequencies (8-14 Hz) in suprasylvian gyrus was significantly higher during SWS (Fig. IV-4c). A similar pattern was found in different regions, but the difference did not reach significance level. When data from all investigated areas were pooled together the power was significantly decreased for slow/delta ($p=0.003$, two-tailed one-sample t-test), and for spindle frequency range ($p<0.0001$), but the gamma range activities were dramatically increased under anesthesia (Fig. IV-4c, $p<0.0001$).

4.5.2 Stronger rhythmicity of neuronal activity during anesthesia than in natural sleep.

LFP, extracellular unit, and membrane potential of cortical neurons showed a stronger rhythmicity of slow oscillation under anesthesia (Figs. IV-2, IV-3). To quantify the rhythmicity, we computed autocorrelations of 20 s segments of LFP and intracellular recordings (40 neurons) during SWS and under anesthesia (Fig. IV-5). During SWS, the slow waves appeared with only weak, if at all, rhythmicity. This is evidenced by the low amplitude or the absence of secondary peaks with a period of 1-2 s in the autocorrelograms (Fig. IV-5, left column). Under anesthesia, autocorrelograms of both LFP and intracellular recordings from all 4 investigated areas expressed several clear secondary peaks. These recurrent peaks occurring at regular intervals are indicative of a strong rhythmicity of the slow oscillation (Fig. IV-5a,b right columns). The amplitude of the secondary peak, usually occurring between 0.5 and 1.5 sec, was significantly higher during anesthesia than in SWS for all studied areas (Fig. IV-5c) indicating a strong increase in the rhythmicity of the slow oscillation under ketamine-xylazine anesthesia.

4.5.3 Higher coherence of slow oscillation between different regions during ketamine-xylazine anesthesia than during SWS.

Simultaneous LFP recordings made from multiple cortical regions during SWS and subsequent anesthesia (Fig. IV-3b) suggest that slow waves occur more synchronously in

different cortical regions during anesthesia than in SWS. To assess this relation quantitatively, we have calculated pair-wise coherence of the LFPs recorded at different locations during SWS and compared it to the coherence of LFPs recorded during anesthesia from the same pairs of chronically implanted electrodes (Fig. IV-6). The coherence was calculated for three frequency ranges (Fig. IV-6): slow and delta (0.2-4 Hz), spindle (8-14 Hz), and gamma (30-100 Hz). The coherence between different cortical regions during anesthesia was high for all investigated ranges of frequencies (Fig. IV-6c, green-yellow-brown plots). It was systematically higher during the anesthesia than during natural SWS for signal components in the slow and delta range (0.2-4 Hz, 0.594±0.102 vs. 0.507±0.149, $p<0.001$, N=45 pairs of recordings from the same electrodes during anesthesia and SWS, Wilcoxon paired Test) and in the gamma frequency range (30-100Hz, 0.43±0.031 vs. 0.399±0.024, $p<0.003$). In this example, for the spindle range, the difference did not reach significance level (0.435±0.094 vs. 0.425±0.031, $p=0.147$). In the scatter plots in which coherence during anesthesia is plotted against coherence during the SWS for each pair of recorded electrodes, most points are located above the diagonal for slow/delta and gamma frequencies (Fig. IV-6a, b). Higher coherence during anesthesia is particularly evident in coherence difference (anesthesia minus SWS) color (red-white-blue) plots by a strong domination of blue colors indicating a higher coherence during anesthesia (Fig. IV-6c). To validate these results, we performed the same analysis on n=165 pairs (4 cats) of SWS and anesthesia recordings. In each pair of electrodes, the coherence was calculated in epochs of 15s (10-12 epochs for each recording) and then averaged for that pair of electrodes. For the whole sample, the coherence in all three frequency ranges was significantly higher during the anesthesia than during SWS: 0.524±0.109 vs. 0.487±0.127, $p<0.001$, Wilcoxon paired Test, for slow and delta range (0.2-4 Hz), 0.442±0.1 vs. 0.429±0.088, $p=0.008$ for the spindle range (8-14 Hz), and 0.4±0.051 vs. 0.386±0.029, $p<0.001$ for the gamma range (30-100 Hz). Thus, slow waves as well as activity in the spindle and gamma frequency ranges were more synchronized during anesthesia as compared to natural SWS.

4.5.4 Silent states are more prominent during anesthesia than in SWS.

Intracellular recordings suggested that for a given cortical area, the slow oscillation was usually of smaller amplitude and silent states of a shorter duration during SWS as compared to anesthesia (e.g. examples in Fig. IV-3c-f). To assess these differences

quantitatively, we measured the duration of silent states at half amplitude of transition to and from silent states. Comparison of silent states in all recordings performed under anesthesia to all recordings made during SWS revealed that the duration of silent states was significantly shorter during SWS in each investigated area and for all areas pooled together (Fig. IV-7a1). The proportion of time spent in silent state, calculated as the ratio of time a cell spent in silent state to the total time analyzed was also higher under anesthesia than in SWS. This difference was significant both when recordings from all cortical regions were pooled together and when data were segregated by cortical area (Fig. IV-7b1).

The amplitude of slow oscillation recorded intracellularly was calculated as described in the method section (Fig. IV-1). For the whole sample, when recordings made from different cortical areas were pooled together, the amplitude of slow oscillation was significantly larger under ketamine-xylazine anesthesia than in natural SWS (Fig. IV-7c1). When the comparison was made separately for recordings obtained in each area, the amplitude of silent states during anesthesia was significantly higher than in SWS in area 3, but not in other areas (Fig. IV-7c1).

Next, we compared the duration and amplitude of silent states in membrane potential of neurons recorded during slow oscillation between different areas in the same experimental condition of either SWS or anesthesia. This comparison revealed area specific differences in silent state duration in both SWS and anesthesia (Fig. IV-7a2, b2). A striking difference between SWS and anesthesia was observed for the amplitude of slow oscillation, which showed area-specific differences during SWS that were not present under anesthesia (Fig. IV-7c2).

4.6 Discussion

In this study we demonstrated that despite a generally similar appearance of slow oscillation during deep SWS and anesthesia, their quantitative comparison revealed multiple features that are distinct in these two brain states. (1) During anesthesia the rhythmicity of slow oscillation in the LFP and intracellular recordings was higher than in SWS. (2) During anesthesia the LFP power in slow and delta (0.1-4 Hz) and in spindle (8-14 Hz) frequency ranges was decreased, but the power of gamma activity was doubled. (3) During anesthesia the coherence of LFP in different areas and for all investigated frequency ranges was higher than during SWS. (4) Intracellular recordings revealed area-specific differences of slow oscillation amplitude during SWS with larger amplitudes in visual and associative areas and smaller amplitudes in somatosensory area. Anesthesia increased the amplitude of slow oscillation in most areas and abolished differences between areas. (5) The duration of silent states was also area specific, both during SWS and under anesthesia, however in every area, anesthesia increased the duration of silent states to 148-240% compared to its value during SWS.

4.6.1 Effects of anesthesia on cortical neurons

Slow oscillation is composed of two different phases: an active phase when cortical neurons are depolarized and may fire action potentials and a silent phase when cortical neurons are hyperpolarized and silent (Steriade et al., 1993b). This general pattern of slow oscillation was seen in both SWS and ketamine-xylazine anesthesia. Silent state is a period of disfacilitation (absence of synaptic activity) during which the membrane potential of cortical neurons is primarily dominated by potassium leak conductance (Wilson et al., 1983; Metherate and Ashe, 1993; Contreras et al., 1996; Timofeev et al., 1996; Wilson and Kawaguchi, 1996; Timofeev et al., 2001). Active states are associated with high levels of excitatory and inhibitory conductances of both synaptic and intrinsic origin (Wilson and Kawaguchi, 1996). Excitation and inhibition can be roughly balanced (Haider et al., 2006) or dominated by inhibition (Rudolph et al., 2007) depending upon experimental condition. Ketamine is a non-competitive, use- and voltage-dependent antagonist of N-methyl-D-aspartate (NMDA) receptors leading to a partial blockade of glutamatergic neurotransmission (Liu et al., 2006; MacDonald et al., 1991). Therefore, the use of

ketamine should decrease excitatory conductance. Indeed, in all investigated cortical regions, we observed under ketamine-xylazine anesthesia an increase of both the duration of silent states and the proportion of time spent in silent states (Fig. IV-7a, b). This implies a decrease in the duration of active states. This observation is congruent to a recent finding demonstrating that a hypofunction of NMDA-receptor due to genetic modulation or antagonist application increases the length of silent states (Fellin et al., 2009). A recent study demonstrated that a decrease in inhibition had similar effects: it shortened active states and prolonged silent states (Sanchez-Vives et al., 2010). This suggests that a fine tuning of excitation and inhibition in each cortical area is responsible for the generation of a particular frequency of slow oscillation and that manipulations leading to a decrease of the efficiency of either excitation or inhibition will shorten active states and lengthen silent states. Several further effects of ketamine on cortical neurons had been reported. Ketamine application hyperpolarizes cortical neurons via a block of HCN1 channels, enhances synaptic responses (Chen et al., 2009), and enhances Ca^{2+} spikes and dendritic excitability in pyramidal cells in vitro, but not in vivo because synaptic activity reduces dendritic spiking in cortical neurons (Potez and Larkum, 2008). Ketamine also inhibits nicotinic cholinoreceptors (Rudolph and Antkowiak, 2004), however, since the firing of cholinergic neurons is strongly reduced during both SWS and anesthesia (Steriade and McCarley, 2005; Boucetta and Jones, 2009) it is unlikely that ketamine induces slow oscillations via this mechanism. Ketamine may also potentiate GABA responses (Rudolph and Antkowiak, 2004; Alkire et al., 2008), however at anesthetic doses, it acts exclusively on $\alpha6\beta2\delta$ and $\alpha6\beta3\delta$ receptors (Hevers et al., 2008) which, in mammalian brain, were found only in the granular layer of cerebellum (Pirker et al., 2000). GABAergic action of ketamine unlikely contributes to the generation of active and silent states in the thalamocortical system.

We observed a significant increase in the amplitude of intracellularly recorded slow oscillation (Fig. IV-7c) that was likely due to a more pronounced hyperpolarization during silent states induced by ketamine-xylazine anesthesia. In all recorded areas, we observed a more pronounced hyperpolarization during silent states in anesthetized cats as compared to SWS. However, in chronic experiments, the reference electrode remained implanted for weeks or months, and thus could develop some DC polarization. Therefore we are not confident in comparing absolute values of the membrane potential, but we compare the

difference between active and silent states (Fig. IV-7). Xylazine is an agonist for alpha-2 adrenergic receptors, which are abundant in the neocortex (Hedler et al., 1981; Nicholas et al., 1993). Alpha-2 adrenoreceptor agonist clonidine activates a potassium current in rat spinal cord neurons (Sonohata et al., 2004). Noradrenaline also increases potassium conductance in mouse entorhinal cortex (Pralong and Magistretti, 1995). In the locus coeruleus, noradrenaline and alpha-2 adrenoreceptor agonists activate potassium current, while alpha-2 antagonist blocks them (Arima et al., 1998). Activation of alpha-2 adrenoreceptor increases cortical activity via closure of h-channels (Wang et al., 2007). Therefore, the action of xylazine could contribute to both the longer duration and the bigger difference in amplitude between active and silent states observed in our experiments in anesthetized animals.

4.6.2 Anesthesia, sleep, consciousness

Higher brain functions occurring during conscious states require coordinated spatio-temporal firing in large neuronal constellations with hierarchal organization (Konorski, 1967; Buzsaki, 2010) involving internally and externally generated signals (Edelman, 2003). A minimal time of 0.5-1 sec is required to be conscious (Libet et al., 1967; Edelman, 2003). Continuous neuronal firing of cortical, thalamic, and striatal neurons occurs during persistent active (depolarized) network states in awake animals (Steriade et al., 2001; Timofeev et al., 2001; Mahon et al., 2006; Vyazovskiy et al., 2009) as well as during REM sleep (Hirsch et al., 1983; Steriade et al., 2001; Timofeev et al., 2001). This fulfills the requirement for uninterrupted coordinated activity; therefore some forms of consciousness could occur during both waking state and REM sleep. On the contrary, during SWS cortical, thalamocortical, and striatal neurons oscillate between active and silent states (Hirsch et al., 1983; Steriade et al., 2001; Timofeev et al., 2001; Mahon et al., 2006). Active states are depolarized states in cortical and striatal neurons, but in thalamocortical neurons they are associated with multiple IPSPs originating from burst firing of reticular thalamic neurons (Contreras and Steriade, 1995; Timofeev and Steriade, 1996). During SWS, dominated by slow oscillation with a period of around 1 sec, the duration of silent states is about 150-200 ms and neurons spend 5-10% of time in silent states (Fig. IV-7). Therefore, in deep SWS the continuous neuronal firing lasts less than 1 sec thus impairing the emergence of conscious experience. Slow-wave activity is highest and more global at

the onset of sleep period and then progressively decreases toward the end of sleep (Achermann and Borbely, 2003; Vyazovskiy et al., 2009; Nir et al., 2011). It is well accepted that the expression of slow oscillation in cortical areas is correlated with activities in those areas during wake (Huber et al., 2004). Like in human, most of sensory information in cat arrives via visual system. Therefore, we expected, and it was indeed the case to obtain larger amplitude of slow oscillation in area 17 (Fig. IV-7). The neurons in area 7 also showed larger amplitude of slow oscillation, because this is a poly-sensory area with visual dominance (Bignall, 1967). It is likely that in rodent cortex the biggest amplitude of slow waves would be recorded in somatosensory areas, as this is the leading sensory system in these animals. During slow waves, neurons in large cortical territories reveal almost simultaneous alternations of activity and silence (Volgushev et al., 2006). Because of the decreased slow-wave activity toward the end of sleep period, the duration of active states, estimated from extracellular unit recordings, increases and often lasts longer than 1 sec (Vyazovskiy et al., 2009). Therefore, some form of conscious processes are possible during late SWS and the majority of dreams reported outside REM episodes was found during these late periods of sleep, when cortical neurons display longer uninterrupted firing stretches (Payne and Nadel, 2004).

Recent reviews discuss whether general anesthesia-induced amnesia, rather than loss of consciousness, plays a more important role in the overall effects of anesthesia (Rudolph and Antkowiak, 2004; Alkire et al., 2008; Tononi and Koch, 2008). All agreed that deep SWS might be considered as an unconscious state. When ketamine-xylazine anesthesia is used the duration of silent states approximately doubles and the cortical network spends almost 20% of time in silent states (Fig. IV-7), preventing an essential condition of conscious states, i.e. persistent neuronal firing. The synchrony of slow waves under ketamine-xylazine anesthesia is higher than during SWS (Figs. IV-3, IV-6). Therefore, the active states occur more synchronously across cortical areas, virtually all cortical neurons become silent simultaneously making logical processing of information and conscious states during ketamine-xylazine anesthesia impossible. Overall, we suggest that the enhanced presence of slow waves under anesthesia as compared to SWS may be used as a safe criterion to estimate annihilation of conscious state.

4.7 Acknowledgment

We are grateful to Sergiu Ftomov for excellent technical support, Josée Seigneur for logistic support and Monty Escabi and Stanislav Volgushev for advice on data processing. This study was supported by Canadian Institutes of Health Research (MOP-37862, MOP-67175), National Science and Engineering Research Council of Canada (grant 298475) and National Institute of Neurological Disorders and Stroke (1R01-NS060870 and 1R01-NS059740) to I.T. Start-up funds from University of Connecticut to M.V. S.Ch. is a Canadian Institutes of Health Research fellow. S.Cr is funded by Agence Nationale de la Recherche, France. I.T. is Fonds de la Recherche en Santé du Québec Research Scholar.

4.8 References

Achermann P, Borbely AA (2003) Mathematical models of sleep regulation. Front Biosci 8:s683-693.

Alkire MT, Hudetz AG, Tononi G (2008) Consciousness and anesthesia. Science 322:876-880.

Arima J, Kubo C, Ishibashi H, Akaike N (1998) Alpha2-adrenoceptor-mediated potassium currents in acutely dissociated rat locus coeruleus neurones. J Physiol 508 (Pt 1):57-66.

Bignall KE (1967) Comparison of optic afferents to primary visual and polysensory areas of cat neocortex. Experimental Neurology 17:327-343.

Blake H, Gerard RW (1937) Brain potentials during sleep. Am J Physiol 119:692-703.

Boucetta S, Jones BE (2009) Activity profiles of cholinergic and intermingled gabaergic and putative glutamatergic neurons in the pontomesencephalic tegmentum of urethane-anesthetized rats. J Neurosci 29:4664-4674.

Buzsaki G (2010) Neural syntax: Cell assemblies, synapsembles, and readers. Neuron 68:362-385.

Chauvette S, Volgushev M, Timofeev I (2010) Origin of active states in local neocortical networks during slow sleep oscillation. Cereb Cortex 20:2660-2674.

Chen X, Shu S, Bayliss DA (2009) Hcn1 channel subunits are a molecular substrate for hypnotic actions of ketamine. J Neurosci 29:600-609.

Clement EA, Richard A, Thwaites M, Ailon J, Peters S, Dickson CT (2008) Cyclic and sleep-like spontaneous alternations of brain state under urethane anaesthesia. PLoS ONE 3:e2004.

Constantinople Christine M, Bruno Randy M (2011) Effects and mechanisms of wakefulness on local cortical networks. Neuron 69:1061-1068.

Contreras D, Steriade M (1995) Cellular basis of eeg slow rhythms: A study of dynamic corticothalamic relationships. J Neurosci 15:604-622.

Contreras D, Timofeev I, Steriade M (1996) Mechanisms of long-lasting hyperpolarizations underlying slow sleep oscillations in cat corticothalamic networks. J Physiol 494:251-264.

Cowan RL, Wilson CJ (1994) Spontaneous firing pattern and axonal projections of single corticostriatal neurons in the rat medial agranular cortex. J Neurophysiol 71:17-32.

Crochet S, Petersen CC (2006) Correlating whisker behavior with membrane potential in barrel cortex of awake mice. Nat Neurosci 9:608-610.

Edelman GM (2003) Naturalizing consciousness: A theoretical framework. Proc Natl Acad Sci U S A 100:5520-5524.

Fellin T, Halassa MM, Terunuma M, Succol F, Takano H, Frank M, Moss SJ, Haydon PG (2009) Endogenous nonneuronal modulators of synaptic transmission control cortical slow oscillations in vivo. Proc Natl Acad Sci U S A 106:15037-15042.

Gentet LJ, Avermann M, Matyas F, Staiger JF, Petersen CCH (2010) Membrane potential dynamics of gabaergic neurons in the barrel cortex of behaving mice. Neuron 65:422-435.

Haider B, Duque A, Hasenstaub AR, McCormick DA (2006) Neocortical network activity in vivo is generated through a dynamic balance of excitation and inhibition. J Neurosci 26:4535-4545.

Haider B, Duque A, Hasenstaub AR, Yu Y, McCormick DA (2007) Enhancement of visual responsiveness by spontaneous local network activity in vivo. J Neurophysiol 97:4186-4202.

Hasenstaub A, Sachdev RNS, McCormick DA (2007) State changes rapidly modulate cortical neuronal responsiveness. J Neurosci 27:9607-9622.

Hedler L, Stamm G, Weitzell R, Starke K (1981) Functional characterization of central alpha-adrenoceptors by yohimbine diastereomers. Eur J Pharmacol 70:43-52.

Hevers W, Hadley SH, Luddens H, Amin J (2008) Ketamine, but not phencyclidine, selectively modulates cerebellar gaba(a) receptors containing alpha6 and delta subunits. J Neurosci 28:5383-5393.

Hirsch JC, Fourment A, Marc ME (1983) Sleep-related variations of membrane potential in the lateral geniculate body relay neurons of the cat. Brain Res 259:308-312.

Huber R, Ghilardi MF, Massimini M, Tononi G (2004) Local sleep and learning. Nature 430:78-81.

Konorski J (1967) Integrative activity of the brain: An interdisciplinary approach. Chicago and London: The University of Chicago Press.

Kurth S, Ringli M, Geiger A, LeBourgeois M, Jenni OG, Huber R (2010) Mapping of cortical activity in the first two decades of life: A high-density sleep electroencephalogram study. J Neurosci 30:13211-13219.

Libet B, Alberts WW, Wright EW, Jr., Feinstein B (1967) Responses of human somatosensory cortex to stimuli below threshold for conscious sensation. Science 158:1597-1600.

Luczak A, Bartho P, Marguet SL, Buzsaki G, Harris KD (2007) Sequential structure of neocortical spontaneous activity in vivo. Proc Natl Acad Sci U S A 104:347-352.

Mahon S, Vautrelle N, Pezard L, Slaght SJ, Deniau J-M, Chouvet G, Charpier S (2006) Distinct patterns of striatal medium spiny neuron activity during the natural sleep-wake cycle. J Neurosci 26:12587-12595.

Massimini M, Huber R, Ferrarelli F, Hill S, Tononi G (2004) The sleep slow oscillation as a traveling wave. J Neurosci 24:6862-6870.

Matsumura M (1979) Intracellular synaptic potentials of primate motor cortex neurons during voluntary movement. Brain Res 163:33-48.

Metherate R, Ashe JH (1993) Ionic flux contributions to neocortical slow waves and nucleus basalis-mediated activation: Whole-cell recordings *in vivo*. J Neurosci 13:5312-5323.

Mukovski M, Chauvette S, Timofeev I, Volgushev M (2007) Detection of active and silent states in neocortical neurons from the field potential signal during slow-wave sleep. Cereb Cortex 17:400-414.

Nicholas AP, Pieribone V, Hokfelt T (1993) Distributions of mrnas for alpha-2 adrenergic receptor subtypes in rat brain: An in situ hybridization study. J Comp Neurol 328:575-594.

Nir Y, Staba Richard J, Andrillon T, Vyazovskiy Vladyslav V, Cirelli C, Fried I, Tononi G (2011) Regional slow waves and spindles in human sleep. Neuron 70:153-169.

Okun M, Naim A, Lampl I (2010) The subthreshold relation between cortical local field potential and neuronal firing unveiled by intracellular recordings in awake rats. J Neurosci 30:4440-4448.

Payne JD, Nadel L (2004) Sleep, dreams, and memory consolidation: The role of the stress hormone cortisol. Learning & Memory 11:671-678.

Pirker S, Schwarzer C, Wieselthaler A, Sieghart W, Sperk G (2000) Gabaa receptors: Immunocytochemical distribution of 13 subunits in the adult rat brain. Neuroscience 101:815-850.

Potez S, Larkum ME (2008) Effect of common anesthetics on dendritic properties in layer 5 neocortical pyramidal neurons. J Neurophysiol 99:1394-1407.

Poulet JFA, Petersen CCH (2008) Internal brain state regulates membrane potential synchrony in barrel cortex of behaving mice. Nature 454:881-885.

Pralong E, Magistretti PJ (1995) Noradrenaline increases k-conductance and reduces glutamatergic transmission in the mouse entorhinal cortex by activation of alpha 2-adrenoreceptors. Eur J Neurosci 7:2370-2378.

Reinoso-Suarez F (1961) Topographischer hirnatlas der katze, fur experimental-physiologische untersuchungen. Darmstadt: E. Merck.

Rudolph M, Pospischil M, Timofeev I, Destexhe A (2007) Inhibition determines membrane potential dynamics and controls action potential generation in awake and sleeping cat cortex. J Neurosci 27:5280-5290.

Rudolph U, Antkowiak B (2004) Molecular and neuronal substrates for general anesthetics. Nat Rev Neurosci 5:709-720.

Sanchez-Vives MV, Mattia M, Compte A, Perez-Zabalza M, Winograd M, Descalzo VF, Reig R (2010) Inhibitory modulation of cortical up states. J Neurophysiol 104:1314-1324.

Sharma AV, Wolansky T, Dickson CT (2010) A comparison of sleeplike slow oscillations in the hippocampus under ketamine and urethane anesthesia. J Neurophysiol 104:932-939.

Sonohata M, Furue H, Katafuchi T, Yasaka T, Doi A, Kumamoto E, Yoshimura M (2004) Actions of noradrenaline on substantia gelatinosa neurones in the rat spinal cord revealed by in vivo patch recording. J Physiol 555:515-526.

Steriade M, McCarley RW (2005) Brainstem control of wakefulness and sleep. New York: Plenum.

Steriade M, Nuñez A, Amzica F (1993a) Intracellular analysis of relations between the slow (<1 hz) neocortical oscillations and other sleep rhythms of electroencephalogram. J Neurosci 13:3266-3283.

Steriade M, Nuñez A, Amzica F (1993b) A novel slow (<1 hz) oscillation of neocortical neurons *in vivo* : Depolarizing and hyperpolarizing components. J Neurosci 13:3252-3265.

Steriade M, Contreras D, Dossi RC, Nuñez A (1993c) The slow (<1 hz) oscillation in reticular thalamic and thalamo-cortical neurons: Scenario of sleep rhythm generation in interacting thalamic and neocortical networks. J Neurosci 13:3284-3299.

Steriade M, Timofeev I, Grenier F (2001) Natural waking and sleep states: A view from inside neocortical neurons. J Neurophysiol 85:1969-1985.

Timofeev I, Steriade M (1996) Low-frequency rhythms in the thalamus of intact-cortex and decorticated cats. J Neurophysiol 76:4152-4168.

Timofeev I, Contreras D, Steriade M (1996) Synaptic responsiveness of cortical and thalamic neurones during various phases of slow sleep oscillation in cat. J Physiol 494:265-278.

Timofeev I, Grenier F, Steriade M (2001) Disfacilitation and active inhibition in the neocortex during the natural sleep-wake cycle: An intracellular study. Proc Natl Acad Sci U S A 98:1924-1929.

Tononi G, Koch C (2008) The neural correlates of consciousness. An update. Annals of the New York Academy of Sciences 1124:239-261.

Volgushev M, Chauvette S, Mukovski M, Timofeev I (2006) Precise long-range synchronization of activity and silence in neocortical neurons during slow-wave sleep. J Neurosci 26:5665-5672.

Vyazovskiy VV, Olcese U, Hanlon EC, Nir Y, Cirelli C, Tononi G (2011) Local sleep in awake rats. Nature 472:443-447.

Vyazovskiy VV, Olcese U, Lazimy YM, Faraguna U, Esser SK, Williams JC, Cirelli C, Tononi G (2009) Cortical firing and sleep homeostasis. Neuron 63:865-878.

Wang M, Ramos BP, Paspalas CD, Shu Y, Simen A, Duque A, Vijayraghavan S, Brennan A, Dudley A, Nou E, Mazer JA, McCormick DA, Arnsten AF (2007) Alpha2a-adrenoceptors strengthen working memory networks by inhibiting camp-hcn channel signaling in prefrontal cortex. Cell 129:397-410.

Wilson C, Chang HT, Kitai ST (1983) Disfacilitation and long-lasting inhibition of neostriatal neurons in the rat. Exp Brain Res 51:227-235.

Wilson CJ, Kawaguchi Y (1996) The origins of two-state spontaneous membrane potential fluctuations of neostriatal spiny neurons. J Neurosci 16:2397-2410.

Wolansky T, Clement EA, Peters SR, Palczak MA, Dickson CT (2006) Hippocampal slow oscillation: A novel eeg state and its coordination with ongoing neocortical activity. J Neurosci 26:6213-6229.

4.9 Figures

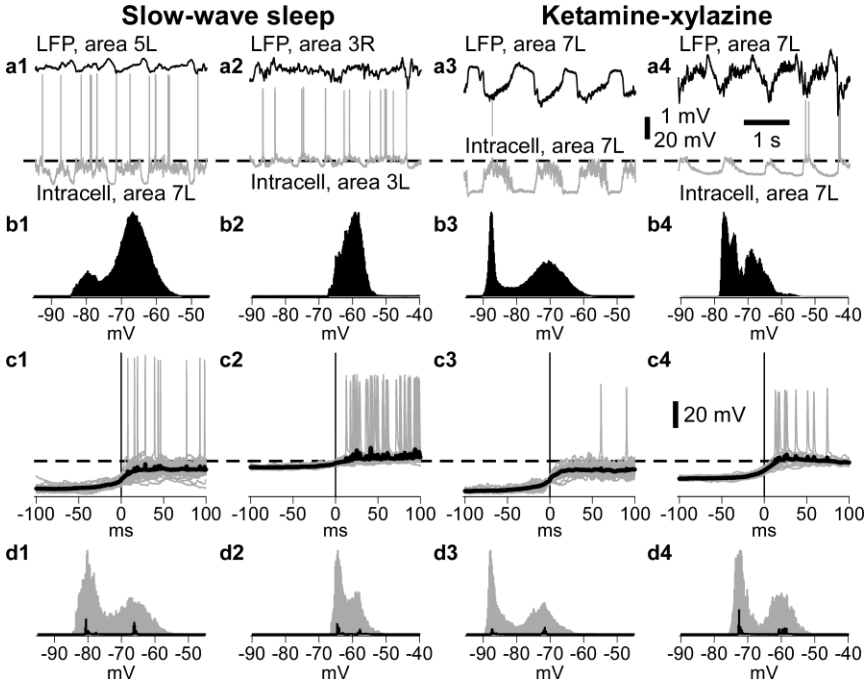

Figure IV-1 Calculation of the amplitude of slow oscillation in the membrane potential during transitions from silent to active states.

Columns 1 and 3 show recordings during slow-wave sleep and ketamine-xylazine anesthesia with clearly bimodal distribution of membrane potential, while columns 2 and 4 show recordings with clear silent and active states, but no clear bimodality of the membrane potential distribution. **b** Histograms of membrane potential distribution from a 60s segments from cells shown in **a**. **c** Transitions from silent to active states (time zero corresponding to the time at half amplitude) and event-triggered average (thick black traces). All transitions of a 60s segment are displayed in gray. **d** Histograms of all gray segments shown in **c** (gray histogram). Histograms of event-triggered average are shown in black. Note the bimodal distribution for all recordings with this method.

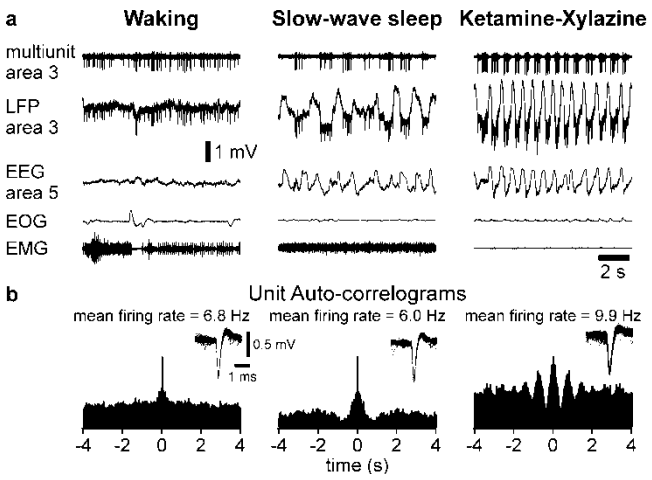

Figure IV-2 Fragments of continuous electrographic recordings during waking, slow-wave sleep and ketamine-xylazine anesthesia.

a Traces of multiunit activity and local field potential in cortical area 3, EEG from area 5, EOG, and EMG recorded in one cat during indicated conditions. Corresponding recordings were obtained with the same electrodes. **b** Autocorrelograms of the unit recording from the neuron shown in **a**. Insets: Fifty spikes and their average (grey line) of the unit shown in a for the three recorded states. Note a dramatic increase in rhythmicity of cortical activities under ketamine-xylazine anesthesia.

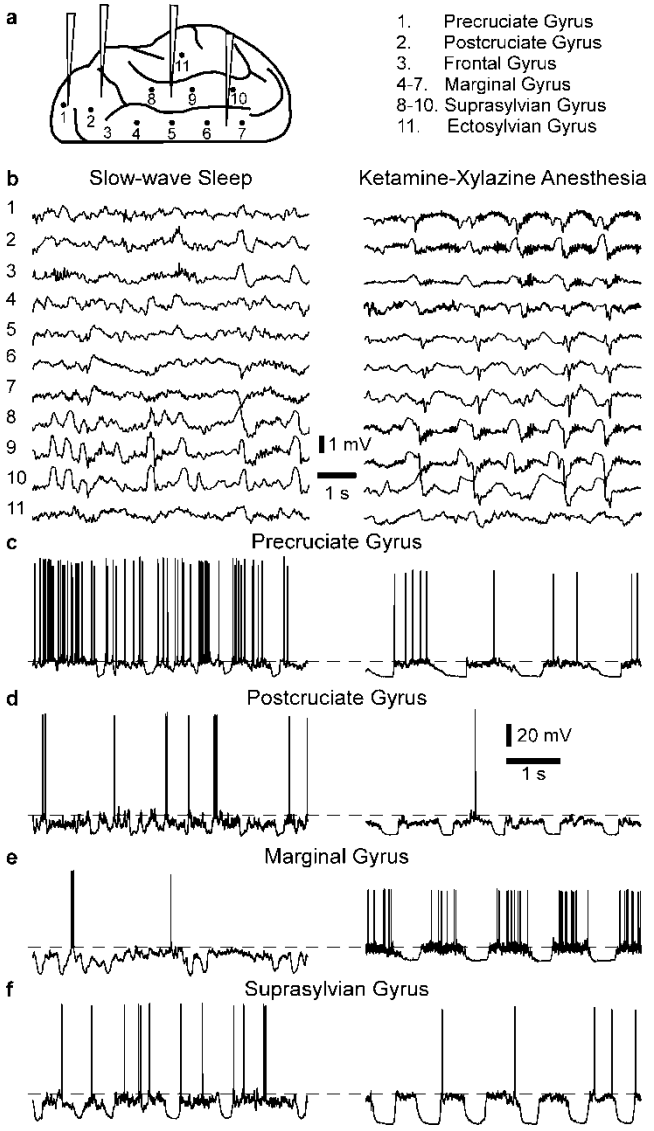

Figure IV-3 Typical field potential and intracellular recordings from different cortical areas during natural slow-wave sleep and ketamine-xylazine anesthesia.

a Schematic representation of the location of electrodes for local field potential (black dots with numbers indicate recording sites for traces in **b**) and for intracellular recordings (pipette drawing, for traces in **c-f**). **b** Field potentials recorded simultaneously in different cortical areas in one cat using the same set of chronically implanted electrodes, either during slow-wave sleep (left column) or under ketamine-xylazine anesthesia (right column). In slow-wave sleep recordings, note the most prominent slow oscillation in suprasylvian gyrus (electrode locations 8-10). In anesthesia recordings, note the high synchrony of slow waves at all locations. **c-f** Typical segments of intracellular recordings

during slow-wave sleep (left column) or ketamine-xylazine anesthesia (right column). Intracellular recordings from: **c** precruciate gyrus, **d** postcruciate gyrus, **e** marginal gyrus, and **f** suprasylvian gyrus. The scale is the same for all intracellular traces. Grey dotted lines indicate -60 mV.

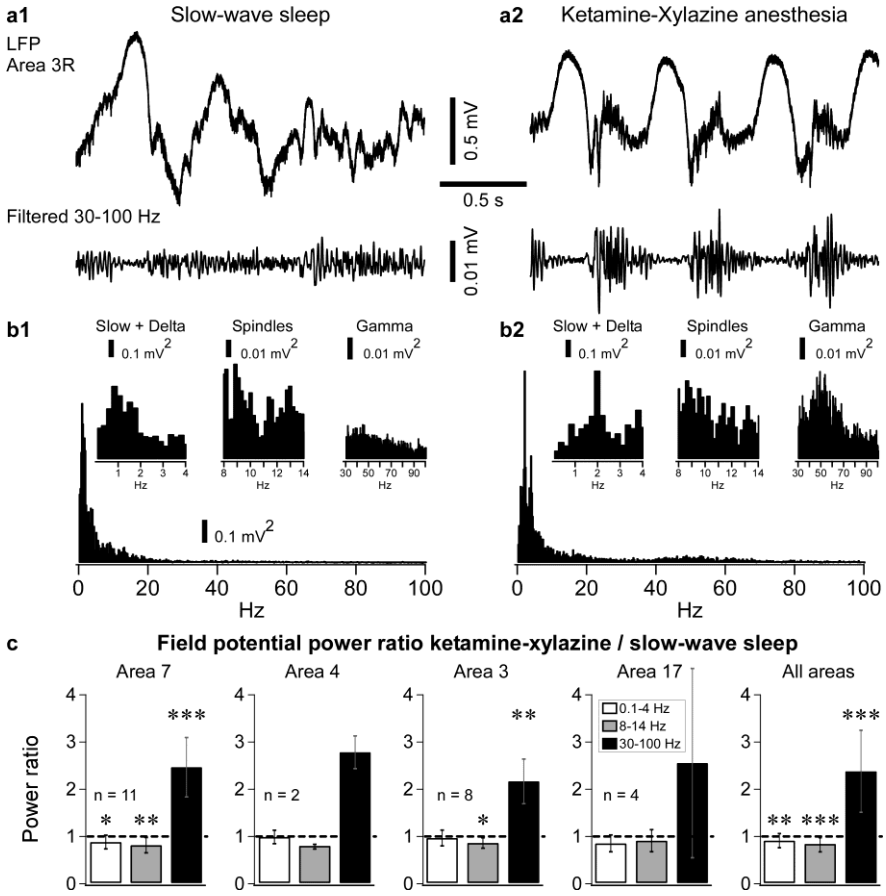

Figure IV-4 Spectral composition of local field potentials is different during slow-wave sleep and anesthesia.

a Segment of LFP recorded in the right somatosensory cortex (area 3, upper trace) and its high frequency component (30-100 Hz, lower trace) during SWS (**a1**) and under ketamine-xylazine anesthesia (**a2**). Recordings in **a1** and **a2** are from the same chronically implanted electrode in the same animal. **b** Power spectra (0-100 Hz) of a 20s epoch of the same recording as in a. Insets show a zoom-in of slow and delta (0.1-4 Hz), spindle (8-14 Hz), and gamma (30-100 Hz) frequency ranges. **c** Mean ratio (ketamine-xylazine anesthesia / SWS) of the integral power in the three frequency ranges (0.1-4 Hz, 8-14 Hz, and 30-100 Hz). The mean power ratio was calculated from ten pairs of 20s epochs of LFP recorded

from the same electrodes during anesthesia and SWS in different cortical locations. Note the higher power during SWS in 0.1-4 Hz and 8-14 Hz, but the large increase in gamma power under ketamine-xylazine anesthesia. * p<0.05, ** p<0.01, ***p<0.001, Wilcoxon signed rank test for area specific comparisons, one-sample t-test for pooled data.

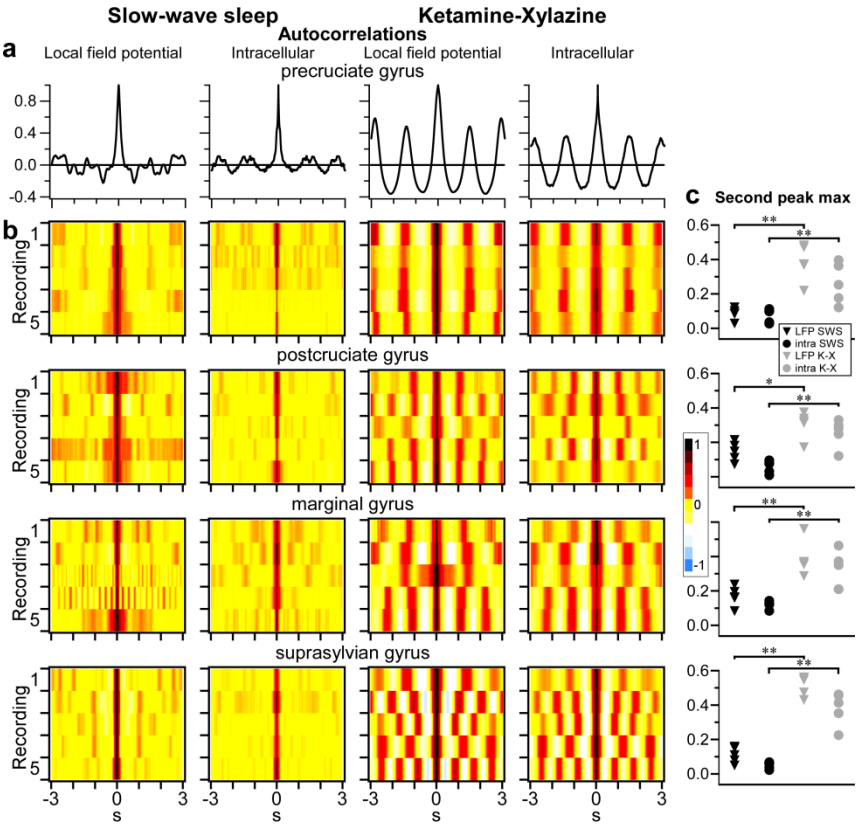

Figure IV-5 Rhythmicity of slow waves in local field potential and membrane potential is higher during ketamine-xylazine anesthesia than in SWS.

a, b Autocorrelograms of local field potential (columns 1 and 3) or membrane potential (columns 2 and 4) recorded either during slow-wave sleep (left columns) or during ketamine-xylazine anesthesia (right columns) in the precruciate gyrus. Examples in **a** and recording #1 of precruciate gyrus in color-coded panels in **b** show the same data. **b** Each panel shows 5 typical examples of color-coded autocorrelations in four different cortical areas as indicated. Note the strong rhythmicity of both field potential and intracellular activities under ketamine-xylazine anesthesia as evidenced by periodically alternating peaks (red) and troughs (yellow) in the autocorrelograms. **c** The magnitude of the second peak in autocorrelation of LFP and membrane potential during SWS and anesthesia in the

four cortical areas. In all cases, the magnitude of the second peak was significantly higher under anesthesia (Two-tailed Mann Whitney test, * $p < 0.05$, ** $p < 0.01$).

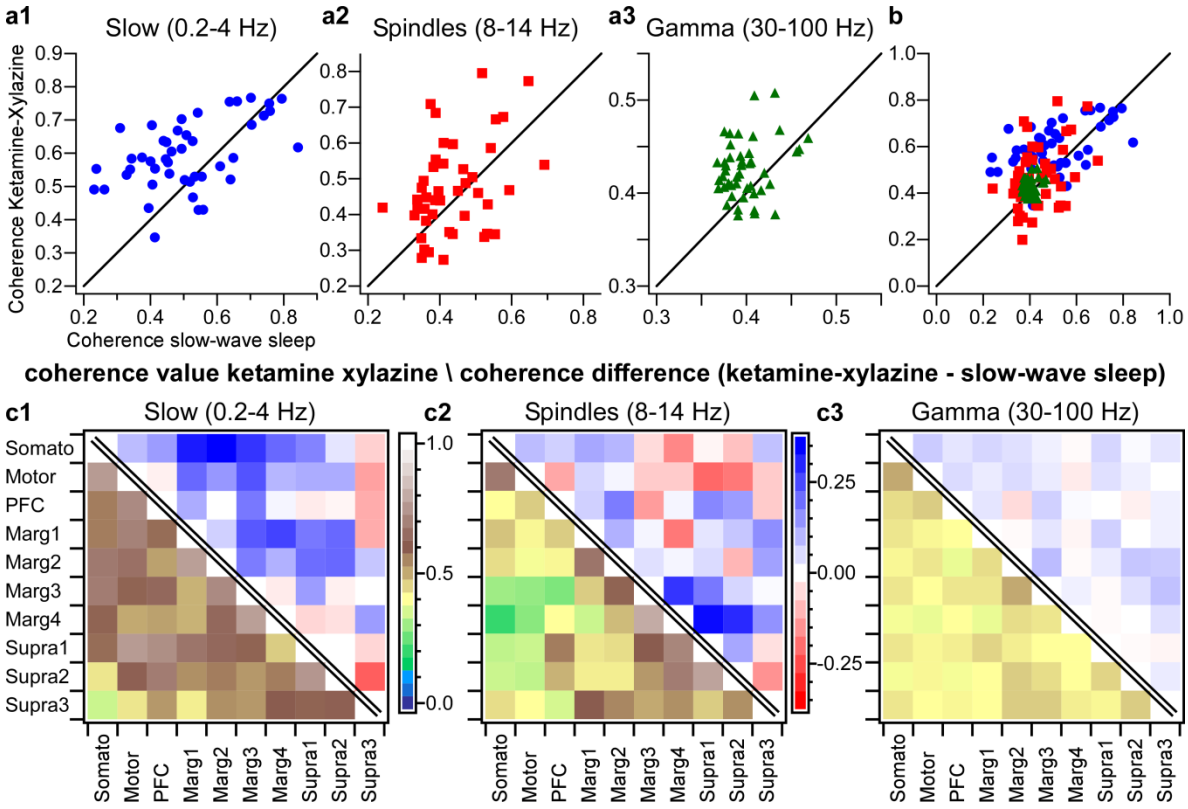

Figure IV-6 Higher coherence of slow oscillation during ketamine-xylazine anesthesia than in slow-wave sleep.

Coherence in the slow/delta frequency range (0.2-4 Hz, **a1**), in the spindle frequency range (8-14 Hz, **a2**), and in the gamma frequency range (30-100 Hz, **a3**) of LFPs recorded during ketamine-xylazine anesthesia plotted against coherence calculated from recordings made with the same electrodes, but during slow-wave sleep (LFP recordings shown in figure IV-3**b**). **b** Data from **a1**, **a2**, and **a3**, but plotted on the same scale. **c** (panels above the diagonal, red-white-blue color code) The difference (anesthesia - slow-wave sleep) in coherence for each pair of recording sites for slow/delta frequencies (**c1**), spindle frequencies (**c2**), and gamma frequencies (**c3**). Blue colors indicate higher coherence during anesthesia; red colors indicate higher coherence during sleep. Note that most pairs show a stronger coherence during ketamine-xylazine anesthesia than during sleep (seen as a positive difference, blue). Recording sites indicated as following (see Fig. IV-3**a**). **c** (panels

below the diagonal, green-yellow-brown) Coherence values for each pair of recording sites under ketamine-xylazine anesthesia. Somato: postcruciate gyrus; Motor: precruciate gyrus; PFC: frontal gyrus; Marg: marginal gyrus, and Supra: suprasylvian gyrus. 1 is the most anterior and 4 is the most posterior site.

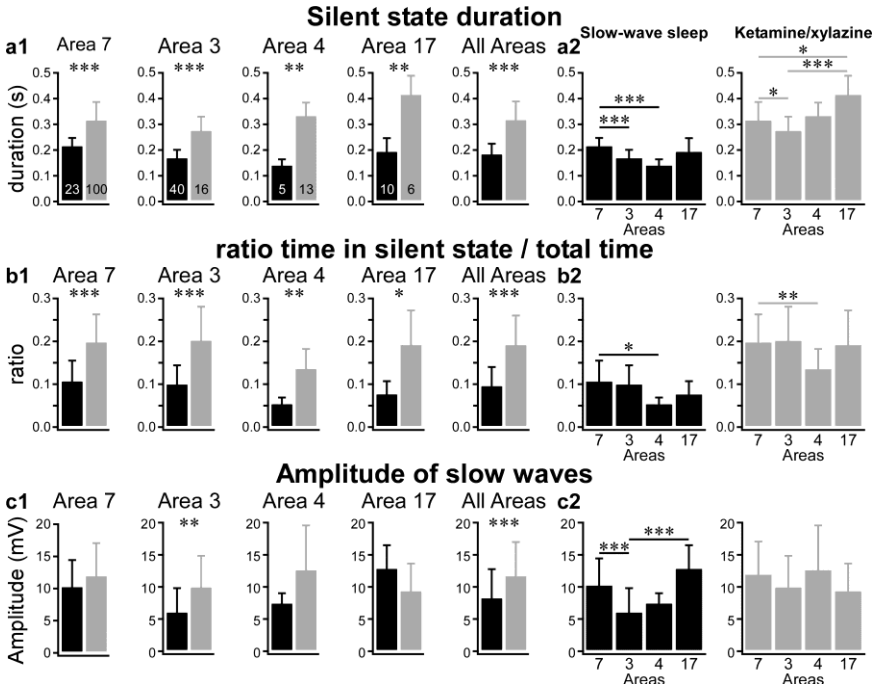

Figure IV-7 Silent states are more prominent during anesthesia than in slow-wave sleep (SWS).

a1, **a2** Mean duration of silent states measured at half-amplitude transitions from active to silent and from silent to active states in intracellular recordings during sleep (black) or anesthesia (grey). **a1** Comparison of the mean silent state duration during SWS and under anesthesia for each cortical area and pooled data from all areas. **a2** Comparison between different areas during SWS and anesthesia. Note that duration of silent states is significantly longer under anesthesia than during SWS. **b1**, **b2** Mean ratio of time spent in silent state over total time. Comparison scheme as in a. Note the longer time spent in silent states during anesthesia than during SWS. **c1**, **c2** Mean amplitude of membrane potential shift between silent and active state during slow oscillation measured from intracellular recordings. Comparison scheme as in **a**. Note that pooled data show significantly larger membrane potential transition amplitude under anesthesia as compared to SWS. Note that amplitude of membrane potential transition between silent and active states is significantly

different between cortical areas during SWS, but not during anesthesia. The number of cells recorded in each condition is indicated within each bar in **a1**. *p<0.05, **p<0.01, ***p<0.001. **a1**, **b1**, **c1** - Mann-Whitney test for n<15, unpaired t-test with Welch correction's for larger samples. **a2**, **b2**, **c2** - Kruskal-Wallis test with Dunn's correction.

Chapter V

5.0 Sleep oscillations in the thalamocortical system induce long-term neuronal plasticity

Sylvain Chauvette[1†], Josée Seigneur[1†], Igor Timofeev[1,2,*]

Affiliations:

[1]The Centre de Recherche Institut Universitaire en Santé Mentale de Québec (CRIUSMQ), Laval University, Québec, G1J 2G3, Canada.

[2]Department of Psychiatry and Neuroscience, Laval University, Québec G1V 0A6 Canada.

* Corresponding Author

† These authors contributed equally to this work and share co-first authorship.

Published in Neuron, 2012

Complete citation: **Chauvette**, S., J. Seigneur, et al. (2012) Sleep Oscillations in the Thalamocortical System Induce Long-Term Neuronal Plasticity. Neuron 75(6): 1105-1113.

Titre en français:

5.0 Les oscillations du sommeil dans le système thalamocortical induisent de la plasticité neuronale à long terme.

5.1 Résumé en Français

La plasticité à long terme contribue à la formation de la mémoire et le sommeil joue un rôle critique dans la consolidation de la mémoire. Cependant, ce n'est pas clair si l'oscillation lente du sommeil peut induire par elle-même une plasticité à long terme qui contribue à la rétention de la mémoire. En utilisant des stimulations pré-thalamiques *in vivo*, nous avons investigué la réponse corticale évoquée dans différents états de vigilance. Nous avons trouvé que les potentiels évoqués pendant l'éveil étaient amplifiés après un épisode de sommeil à ondes lentes (avec ou sans stimulation pendant le sommeil) en comparaison à l'épisode d'éveil précédent. *In vitro*, nous avons déterminé que cette amplification avait un mécanisme post-synaptique qui est dépendant du calcium et qui requiert des périodes d'hyperpolarisation (ondes lentes) et une co-activation des récepteurs AMPA et NMDA. Nos résultats suggèrent que la potentiation à long terme se produit pendant le sommeil à ondes lentes ce qui supporte une contribution de cette potentiation à la mémoire.

5.2 Abstract

Long-term plasticity contributes to memory formation and sleep plays a critical role in memory consolidation. However, it is unclear whether sleep slow oscillation by itself induces long-term plasticity that contributes to memory retention. Using pre-thalamic stimuli *in vivo*, we investigated the cortical evoked response in different states of vigilance. We found that somatosensory evoked potentials during wake were enhanced after a slow-wave sleep episode (with or without stimulation during sleep) as compared to a previous wake episode. *In vitro*, we determined that this enhancement has a postsynaptic mechanism that is calcium-dependent, requires hyperpolarization periods (slow waves), and requires a co-activation of both AMPA and NMDA receptors. Our results suggest that long-term potentiation occurs during slow-wave sleep supporting its contribution to memory.

5.3 Introduction

An early study demonstrated that the rate of forgetting is lower during sleep as compared to wakefulness (Jenkins and Dallenbach, 1924). Recent advances propose that a major role of sleep is memory consolidation (Diekelmann and Born, 2010; Maquet, 2001; Siegel, 2005). Both slow-wave sleep (SWS) and rapid eye movement (REM) sleep can contribute to the memory consolidation, but early stages of sleep (mainly SWS) increased procedural memory (Gais et al., 2000), pharmacological blockage of REM sleep did not impair procedural memory (Rasch et al., 2009). Boosting slow oscillation with extracranial fields (Marshall et al., 2006) or training-related increase in slow-wave activity (Huber et al., 2004) correlated with an increased memory retention suggesting that SWS is critical for memory formation. A plausible physiological mechanism of memory is synaptic plasticity (Bear, 1996; Hebb, 1949; Steriade and Timofeev, 2003). Ocular dominance experiments on young cats demonstrated that sleep plays crucial role in brain development (Frank et al., 2001). If indeed SWS induces synaptic plasticity, the signal processing before and after the SWS period should be different, however physiological data on SWS-dependent modulation of signal processing during waking that follows sleep are missing.

Intracellular activities of cortical neurons during wake and REM sleep are characterized by steady depolarization and firing, while during SWS the depolarization and firing alternates with hyperpolarization and silence (Chauvette et al., 2010; Steriade et al., 2001; Timofeev et al., 2001). Mimicking neuronal firing during SWS, continuous rhythmic stimulation or repeated trains of cortical stimuli in brain slices were shown to induce steady-state synaptic depression, but synaptic responses were enhanced after the trains of stimuli (Galarreta and Hestrin, 1998, 2000). The repeated grouped firing during SWS resembles the classical long-term potentiation (LTP) protocol (Bliss and Lomo, 1973). Both AMPA and NMDA receptors are subject to long-term plasticity (Kirkwood et al., 1993; Zamanillo et al., 1999) and these receptors are also responsible for the sleep-dependent memory formation (Gais et al., 2008). A classical neocortical mechanism of postsynaptic LTP depends on NMDA receptor activation, which leads to calcium entry and an activation of kinase cascade including CaMKII that phosphorylate AMPA receptor and leads to the insertion of GluR1-containing AMPA receptor into synapses (Lisman et al., 2012; Malinow and Malenka, 2002). Increased or reduced activity during wake affected the physiological

responses during subsequent sleep (Huber et al., 2006; Huber et al., 2008). Here we used a reversed approach observing if sleep will affect responses in the subsequent wake period. We tested the hypothesis that SWS enhances synaptic efficacy via its unique pattern of activities, namely neuronal depolarization and firing (active or UP states) intermingled with hyperpolarizing periods (silent or down states), will induce long-term changes in synaptic efficacy.

5.4 Results

5.4.1 Evoked responses are potentiated after slow-wave sleep

We recorded multiple electrographic signals from non-anesthetized head-restrained cats, including electro-oculogram (EOG), electromyogram (EMG), and local field potential (LFP) from different cortical areas (Figure V-1A-C). States of vigilance were characterized as in our previous studies (Steriade et al., 2001; Timofeev et al., 2001). To study the effect of SWS on synaptic (network) plasticity, we used medial lemniscus stimulation (1Hz) and recorded the evoked potential responses in the somatosensory cortex during wake/sleep transitions (see Experimental procedures). In the example shown in figure V-1, the mean amplitude of the N1 response was 0.213 ± 0.030 mV during the first wake episode (Figure V-1D-F). As the first slow waves appeared in the LFPs, we stopped the stimulation for the whole first episode of SWS and restarted it as soon as the animal woke up (W2); the N1 response was transiently increased and then it was reduced, but it remained enhanced as compared to wake 1; the mean amplitude of N1 response was 0.241 ± 0.037 mV during the second wake episode (Figure V-1D-F). Stimulations were applied in the following sleep episode, which was composed of SWS and REM sleep periods. The responses were highly variable during SWS (SWS2, 0.234 ± 0.073 mV) and showed the largest amplitude during REM sleep (0.330 ± 0.035 mV). The mean amplitude during the third wake episode was further increased (W3, 0.274 ± 0.039 mV) as compared to the first two wake episodes (Figure V-1D-F). The amplitude of responses was significantly different in all waking periods ($p<0.001$ for all comparison, one way ANOVA Kruskal-Wallis with Dunn's multiple comparison test). The SWS-dependent increase in evoked potential did not depend on whether stimulations occurred during SWS (Figure V-S1) or not (Figures V-1, V-2).

5.4.2 REM sleep does not play a significant role in the enhancement of response

On an experimental day, the increase always occurred between the first and the second period of wake and often between the second and the third period of wake. When the increased amplitude of evoked potential saturated after few SWS/wake transitions, the presence of REM sleep did not lead to further enhancement (Figure V-2) as it appears in the

figure V-1D-F. In that example, responses were significantly enhanced after the first sleep episode (0.615 ± 0.144 mV in wake 1 vs. 0.666 ± 0.112 mV in wake 2, $p<0.001$, unpaired t-test with Welch's correction) but responses were not further enhanced after the following sleep episodes (no statistical differences in consecutive waking state from wake 2 to wake 8, Figure V-2C, $p>0.05$, one way ANOVA Kruskal-Wallis with Dunn's multiple comparison test). However, the response during all waking periods remained significantly different from wake 1 ($p<0.01$, one-way ANOVA, Dunnett's multiple comparison test). The overall mean amplitude for a first wake episode (n=13, from 3 different cats) was 0.297 ± 0.176 mV and it was 0.328 ± 0.177 mV during wake2; this difference was highly significant (Figure V-1G, $p<0.001$, Wilcoxon matched-pairs signed rank test). Even relatively short periods of SWS were sufficient to enhance responses in the second wake episode (Figure V-1H).

5.4.3 Intracellular responses during wake – slow-wave sleep – wake transitions

We obtained six intracellular recordings from somatosensory cortical neurons in which we recorded evoked responses to medial lemniscus stimuli during two consecutives wake episodes separated by a period of SWS, although it was not always the first and second wake episodes (Figure V-3). As expected, membrane potential recordings showed the presence of prolonged silent states during SWS, which were absent during wake (Figure V-3A). Responses were highly variable during SWS (not shown), while they were stable during wake (Figure V-3B,D). In five out of the six intracellular recordings in which we were able to obtain stable recording throughout wake-SWS-wake transitions (85 recording sessions, near 200 wake-SWS-wake transitions, 2 animals), the response amplitude was increased in the second wake episode (post-SWS) as compared to the first episode (pre-SWS), however due to the small number of recordings, the difference was not significant (Figure V-3C, $p=0.2$, Wilcoxon matched-pairs signed rank test).

5.4.4 *In vitro*, only the *full sleep-like* pattern of stimulation replicates the *in vivo* results

To characterize the mechanisms implicated in the potentiation of evoked responses, we performed whole-cell recordings from layer 2-3 pyramidal regular-spiking neurons *in vitro*. From *in vivo* LFP recordings, we extracted the timing of a single unit firing recorded during SWS (Figure V-4A) and during wake (Figure V-5A) and used that timing to build *sleep-like* (Figure V-4B) and *wake-like* (Figure V-5B) pattern of synaptic stimulation; the timing of slow waves was also detected to build the intracellular hyperpolarizing current pulses stimulation pattern replicating hyperpolarizing (silent) states of SWS (Figure V-4B, see Experimental procedures). The stimulation protocols are detailed in (Figure V-S2). The mean membrane potential of neurons recorded *in vitro* was maintained to about -65 mV to mimic the membrane potential of cortical neurons during wake or active phases of SWS. Minimal intensity stimuli were applied in the vicinity of recorded neurons. The *sleep-like* pattern of synaptic stimulation induced a transient facilitation only ((Figure V-4C) 0.640 ± 0.245 mV in control vs. 0.817 ± 144 mV in the first minute after conditioning, $p<0.05$, Mann-Whitney test). A long-lasting facilitation of responses was induced using a combination of *sleep-like* synaptic stimulation and intracellular hyperpolarizing current pulses with the timing of slow waves (*full sleep-like pattern*, (Figure V-4D), 0.994 ± 0.527 mV in control vs. 1.184 ± 0.833 mV after conditioning, $p<0.001$, Mann-Whitney test). The pattern of facilitation was identical to the one observed after a period of SWS (compare Figure V-4D with Figure V-1D, wake2).

The *wake-like* synaptic stimulation pattern did not show any facilitation of evoked responses (Figure V-5C). To model the neuromodulation activities present during waking state, we added the cholinergic agonist carbachol in the bath (200 μM), which in agreement with previous observations (Gil et al., 1997) significantly decreased the amplitude of responses in control conditions ((Figure V-5D), 0.596 ± 0.361 mV vs. 0.454 ± 0.123 mV, $p<0.001$, Mann-Whitney test). After the *wake-like* synaptic stimulation pattern on the background of carbachol action, we observed only a transient enhancement of responses (0.679 ± 0.179 mV, $p<0.05$, Mann-Whitney test). These results demonstrated that a synaptic activation with the *sleep-like* pattern of spiking, accompanied with postsynaptic

hyperpolarizations (*full sleep-like* protocol) corresponding to silent states of SWS was the only tested condition that induced LTP of evoked responses.

5.4.5 Mechanisms of the enhancement of responses during the *full sleep-like* stimulation

Shuffling the timing of synaptic stimulations from the *sleep-like* pattern, application of intracellular hyperpolarizing current pulses alone, or rhythmic (2.5 Hz) synaptic stimulations did not reveal any long-term plasticity (Figure V-6A-C). The paired-pulse (ISI 50 ms) test showed (a) an enhancement of responses to stimuli after the *full sleep-like* protocol of stimulation (not shown), but (b) the paired-pulse ratio did not change (Fig. V-6D). This combined with the fact that intracellular hyperpolarizing potentials were needed to induce LTP of evoked responses suggests that the enhancement was postsynaptic. Using the *full sleep-like* protocol of stimulation with BAPTA (25 mM) added to the patch solution to block calcium postsynaptic mechanisms abolished the enhancement of the response (Figure V-6E). Adding the NMDA receptor antagonist AP5 (100 μM) or the AMPA receptor antagonist CNQX (10 μM) to the bath solution blocked the enhancement of response by either drugs suggesting that the investigated form of LTP requires a co-activation of both receptor types (Figure V-6F,G). These results indicate that the mechanism of enhancement of responses during the *full sleep-like* stimulation is compatible with the classical LTP.

5.5 Discussion

Our *in vivo* results showed that cortical evoked response to medial lemniscal stimuli during wake was enhanced in a subsequent wake episode whether stimuli were applied or not during SWS supporting the hypothesis of memory consolidation during SWS. Our *in vitro* results showed that only the *full sleep-like* pattern of stimulation (synaptic + hyperpolarization) mimicking SWS was able to induce the initial transient and the longer-lasting enhancement of responses. Importantly, *in vitro* results showed that this enhancement was postsynaptic, calcium-dependent, and required an activation of both NMDA and AMPA receptors matching the classical neocortical postsynaptic LTP.

The cortical slow oscillation has a frequency of about 1 Hz (Steriade et al., 1993). One Hz stimulation usually induces long-term depression in neocortex, but irregular pattern of low-frequency stimulation does not (Perrett et al., 2001). During the silent phase, neurons are hyperpolarized and no firing occurs. During the active phase, neurons are depolarized and multiple presynaptic spikes occur early after the onset of depolarization (Chauvette et al., 2010; Luczak et al., 2007). The network activities during sleep and the experimental protocol of the *full sleep-like* stimulation used in this study are compatible with protocols of induction of spike-timing dependent synaptic facilitation (Sjöström et al., 2008). The transition from hyperpolarized to depolarized states coupled with synaptic activities during active states is a natural pattern for spike-timing dependent plasticity. Therefore the presence of hyperpolarizing (silent) states appears to be a key component for the induction of LTP during sleep.

According to the sleep synaptic homeostasis hypothesis (Tononi and Cirelli, 2003, 2006), SWS results in a general synaptic downscaling because of a strong reduction in gene expression contributing to LTP (Cirelli et al., 2004; Cirelli and Tononi, 2000a, b). However, the total cortical level of kinase (CaMKII) does not change between sleep and waking state (Guzman-Marin et al., 2006; Vyazovskiy et al., 2008). Other studies have demonstrated that sleep-dependent memory consolidation requires the co-activation of both AMPA and NMDA receptors (Gais et al., 2008) and that sleep promotes LTP using a parallel involvement of protein kinase A, CaMKII, and ERK (Aton et al., 2009). Sleep also promotes the translation of mRNAs related to plasticity (Seibt et al., 2012). Classical LTP

consists in a calcium entry via NMDA receptors that will activate different kinase cascades among which CaMKII would play a critical role by phosphorylating AMPA receptor. Once phosphorylated, GluR1-containing AMPA receptors are translocated to the synapse leading to LTP. Also, the translocation of AMPA receptors to the synapse (Lisman et al., 2012; Malinow and Malenka, 2002) that likely occurs during SWS does not require new gene expression. This indicates that synaptic potentiation leading to memory formation can occur during SWS despite a reduction in the expression of genes responsible for LTP.

Are there inconsistencies of our results with previous studies? (a) After prolonged waking periods the slope of callosal evoked responses increases (Vyazovskiy et al., 2008). The earliest phases of evoked potential responses induced by callosal stimulation is composed of antidromic spikes followed by orthodromic spikes (Chang, 1953). This indicates that waking period can increase the excitability of callosal axons. (b) The frequency and amplitude of mEPSCs is higher in slices collected from animals after prolonged waking as compared to sleep (Liu et al., 2010). This is likely due to a rebound over excitability in the absence of acetylcholine. Indeed, waking state is characterized by activities of cholinergic system and acetylcholine reduces the amplitude of EPSPs [(Gil et al., 1997) and Figure V-5D]. (c) In somatosensory cortical slices of juvenile rats, calcium-permeable AMPA receptors were shown to be present at the synapse when animals were sacrificed after the wake period and it was absent after the sleep period, (Lante et al., 2011). Obviously, not all type of AMPA receptors are removed from synapses during sleep, thus it does not preclude the insertion of other AMPA receptors types at synapses during sleep. A recent study in cats showed that intracortical inhibition of m-TOR signaling abolished sleep-dependent plasticity, while no effects were observed in the plasticity induced during wake (Seibt et al., 2012). Therefore, it is very likely that plasticity induced during wake or during sleep have different mechanisms.

The stimulation of medial lemniscal fibers is not a learning task per se, thus it is difficult to affirm whether this experiment simulates a declarative or a non-declarative learning task. However, most of procedural learning tasks implicate the somatosensory system and procedural memory was shown to benefit from SWS (Huber et al., 2004; Rasch et al., 2009), which is also in agreement with our results. The enhancement of responses was always present after the first SWS episode and often also after the second SWS

episode, but then the response was saturated. Our results suggest that once potentiated the response cannot be further potentiated for a certain time window. This is in agreement with studies on humans showing that mainly early sleep and naps, rich in slow waves, are important for memory improvement (Gais et al., 2000; Mednick et al., 2003; Nishida and Walker, 2007). Our results show a potentiation of cortical responsiveness after a period of SWS and that an imitation of sleep slow oscillation *in vitro* was sufficient to strengthen the cortical synapses providing a physiological mechanism for sleep-dependent memory formation.

5.6 Experimental Procedures

Experiments were carried out in accordance with the guideline of the Canadian Council on Animal Care and approved by the Laval University Committee on Ethics and Animal Research.

In vivo experiments. Experiments were conducted on 4 adult non-anesthetized cats. The cats were purchased from an established animal breeding supplier. Good health conditions of all animals were certified by the supplier and determined upon arrival to animal house by physical examination, which was performed by animal facilities technicians and a veterinarian in accordance with requirements of the Canadian Council on Animal Care. The surgery was performed on animals in 5-20 days from their arrival to the local animal house. We recorded field potentials and intracellular activities of cortical neurons from somatosensory cortex of cats during natural sleep/wake transitions. We also recorded field potentials from other cortical areas.

Preparation. Chronic experiments were conducted using an approach similar to that previously described (Steriade et al., 2001; Timofeev et al., 2001). For implantation of recording chamber and electrodes, cats were anesthetized with isoflurane (0.75-2%). Prior to surgery, the animal was given a dose of pre-anesthetic, which was composed of ketamine (15 mg/kg), buprenorphine (0.01 mg/kg), and acepromazine (0.3 mg/kg). After site shaving and cat intubation for gaseous anesthesia, the site of incision was washed with at least three alternating passages of a 4% chlorexidine solution and 70% alcohol. Lidocaine (0.5 %) and/or marcaïne (0.5 %) was injected at the site of incision and at all pressure points. During surgery, electrodes for LFP recordings, electromyogram (EMG) from neck muscle, and electro-oculogram (EOG) were implanted and fixed with acrylic dental cement. Custom-made recording chambers were fixed over somatosensory cortex for future intracellular recordings. Eight to ten screws were fixed to the cranium. To allow future head-restrained recordings without any pressure point, four bolts were covered in the dental cement that also covered bone-fixed screws, permanently implanted electrodes, and fixed recording chamber. Throughout the surgery, the body temperature was maintained at 37^{o}C using a water circulating thermo-regulated blanket. Hearth beat and oxygen saturation were continuously monitored using a pulse oximeter (Rad-8, MatVet, Montreal, Canada) and the

level of anesthesia was adjusted to maintain a hearth beat at 110-120 per minute. A lactate ringer solution (10 ml/kg/h, i.v.) was given during the surgery. Following the surgery, cats were given buprenorphine (0.01 mg/kg) or anafen (2 mg/kg) twice a day for three days, and baytril (5 mg/kg) once a day for seven days. About a week was allowed to animals to recover from the surgery before the first recording session occurred. Usually, 2-3 days of training were sufficient for cats to remain in head-restrained position for 2-4 hours and display several periods of quiet wakefulness, SWS, and REM sleep. The recordings were performed up to 40 days after the surgery. In this study the LFP data were analyzed from the first recording session of the day only. Animals were kept awake for at least one hour prior to recording session.

Recordings and in vivo stimulation. All *in vivo* recordings were done in a Faraday chamber. LFPs were recorded using tungsten electrodes (2 MΩ, bandpass filter 0.1 Hz to 10 kHz) and amplified with AM 3000 amplifiers (A-M systems, Sequim, WA, USA) with custom modifications. We aimed to implant electrodes at 1 mm below the cortical surface. A coaxial electrode (FHC, Bowdoin, ME, USA) was implanted in the medial lemniscus fibers for stimulation. Electric stimuli were delivered at 1 Hz in all states of vigilance (wake, SWS, REM). Given the high spontaneous (≈5 Hz) and evoked firing rates (up to 125 Hz) in cuneatothalamic pathway (medial lemniscus) and the high efficacy of synaptic transmission in this pathway (Alloway et al., 1994), 1 Hz stimulation could not induce synaptic plasticity per se. Intracellular recordings were performed using glass micropipettes filled with 2.5 M of potassium acetate and having a resistance of 30-70 MΩ. A high-impedance amplifier with active bridge circuitry (Neurodata IR-283 amplifiers, Cygnus Technology, PA, USA, lowpass filter 10 kHz), was used to record the membrane potential and to inject current into neurons. Intracellular recordings were performed from somatosensory cortex according to the atlas (Reinoso-Suarez, 1961). A silver wire was fixed either in the frontal bone over the sinus cavity or in the occipital bone over the cerebellum and was used as a reference electrode. All electrical signals were digitally sampled at 20 kHz on Vision (Nicolet, Wisconsin, USA) and stored for off-line analysis. At the end of experiments, the cats were euthanized with a lethal dose of pentobarbital (100 mg/kg i.v.).

In vitro experiments. Experiments were conducted on 30 Sprague Dawley rats (P21-P30, Charles River Laboratories International, Inc.).

Slice preparation. Rats were first anesthetized with ketamine-xylazine (40 and 10 mg/kg). The brain was then quickly dissected and maintained in ice-cold artificial cerebrospinal fluid (ACSF) containing (in mM): NaCl 124, KCl 2.8, $CaCl_2$ 1.2, $MgSO_4$ 2, NaH_2PO_4 1.25, $NaHCO_3$ 26, and D-glucose 10 (Sigma-Aldrich Canada, Canada), pH 7.4, aerated with 95% O_2 and 5% CO_2. Osmolarity was 300 ± 5 mOsm. Coronal slices (350-400 μm) from one hemisphere were cut with a vibratome to obtain complete sections containing the somatosensory cortex. Slices were transferred to a holding chamber where they were kept at room temperature for at least 1h in the same ACSF and aerated with 95% O_2, 5% CO_2. The brain slices were transferred into a submerged recording chamber maintained at 34°C, containing the perfusion ACSF at a rate of 3 ml/min. The perfusion solution was identical to the cutting solution.

Recordings. Pyramidal neurons in layers II/III were preselected using an infrared differential interference contrast camera microscopy on an upright microscope based on their triangular shape and on their morphology after Lucifer Yellow 0.2% staining (LY, Sigma Aldrich Canada, Canada). We obtained somatic whole-cell current-clamp recordings (10-20 MΩ access resistances) with patch pipettes (resistance between 3-5 MOhm) containing (mM): Potassium D-gluconate 130, 4-(2-hydroxyethyl)-1-piperazineethanesulfonic acid (HEPES), 10, KCl 10, $MgCl_2$ 2, ATP 2, and GTP 2 (Sigma-Aldrich Canada, Canada) at pH 7.2 and 280 mOsm. In separate experiments, BAPTA 25mM (Sigma-Aldrich Canada, Canada) was added to the patch solution to block calcium. AP5 (100 μM) or CNQX (10 μM) (both from Sigma-Aldrich Canada, Canada) were also added to the bath solution to block AMPA and NMDA receptors respectively, and carbachol (200 μM) (Sigma-Aldrich Canada, Canada) was also added to model cholinergic activities during wake. To model wake-like membrane potential values, a steady depolarizing current was injected to maintain the membrane potential near -65 mV.

Cortical slices stimulation. Two tungsten electrodes (1-2 MΩ) were placed in layers II/III for extracellular electrical stimulation. Pulses of 0.01-0.02 ms duration and of 0.01-0.15 mA intensity were delivered at a minimal intensity in order to obtain EPSPs and some

failures. This intensity of stimulation reproduces the basic properties of single-axon EPSPs *in vivo* (Crochet et al., 2005). Minimal intensity stimuli were delivered every 5 sec in control and after conditioning, because that frequency of microstimulation does not induce synaptic plasticity in cortical slices (Seigneur and Timofeev, 2010).

LFP recordings during natural sleep and waking states were used to extract the timing of a unit firing during wake and during SWS (about 10 minutes for each state); the timing of onset of slow waves was also extracted from LFP recordings as described previously (Mukovski et al., 2007). To model silent states in patch-clamp recordings *in vitro* we applied hyperpolarizing current pulses of 200 ms [mean silent states during SWS (Chauvette et al., 2011)] starting at the exact timing estimated from *in vivo* LFP recordings. To isolate extracellular spikes the LFP was band-pass filtered (60 Hz - 10 kHz). We used only spikes from single unit recordings. As the unit was well isolated and that the spike amplitude was well above the noise level, a threshold was manually set to detect the timing of spikes. An example of such detection can be found in our previous publication (Chauvette et al., 2011). We used the exact timing of spikes detected *in vivo* to microstimulate electrically cortical slices. Binary files used for stimulation were generated and run in Clampex software (Axon pClamp 9, Molecular Devices, USA) to trigger the stimulators for *wake-like*, *sleep-like* and *full sleep-like* stimulation pattern applied *in vitro* (Figure S2). Obviously, no stimuli were delivered during hyperpolarizing states. The *sleep-like*, *full sleep-like,* or *wake-like* stimulation sessions lasted for about 10 min.

To test whether a specific pattern of *sleep-like* stimuli was needed to induce LTP we either shuffled the timing of interstimuli intervals using "Randbetween" function from Microsoft Office Excel (Shuffled test [Fig. 6A]) or we stimulated at 2.5 Hz continuously for 10 minutes to deliver the same number of stimuli as in the *sleep-like* protocol (Rhythmic test [Fig. 6C]). To test alterations in presynaptic release probability, the paired-pulse protocol (50 ms interstimuli interval) was used prior and after the *full sleep-like* stimulation (Fig. 6D).

Data analysis. Electrographic recordings were analyzed offline using custom-written routines in IgorPro (Lake Oswego, Oregon, USA). The delta power was calculated from 1

sec sliding time window as the integral power between 0.2 and 4 Hz of full spectrogram; the EMG power was calculated as the integral power between 5 and 500 Hz.

Statistical analysis. All numerical values are given as mean ± standard deviation. Specific statistical tests are indicated in the text and in figures legend and were performed in Prism5 (Graphpad software Inc., La Jolla, CA, USA). Briefly, data was first tested for normal distribution and if data had a normal distribution, parametric tests were used otherwise; the equivalent non-parametric test was used. If only two groups of data were compared, two-tailed unpaired t-test with Welch's correction (parametric) or two-tailed Mann-Whitney test (non-parametric) was used. When the data was paired, then two-tailed Wilcoxon matched-pairs signed rank test (non-parametric) was applied. When more than two groups of data were compared, one way ANOVA Kruskal-Wallis (non-parametric) with Dunn's multiple comparison test was applied.

5.7 References

Alloway, K.D., Wallace, M.B., and Johnson, M.J. (1994). Cross-correlation analysis of cuneothalamic interactions in the rat somatosensory system: influence of receptive field topography and comparisons with thalamocortical interactions. J Neurophysiol *72*, 1949-1972.

Aton, S.J., Seibt, J., Dumoulin, M., Jha, S.K., Steinmetz, N., Coleman, T., Naidoo, N., and Frank, M.G. (2009). Mechanisms of Sleep-Dependent Consolidation of Cortical Plasticity. Neuron *61*, 454-466.

Bear, M.F. (1996). A synaptic basis for memory storage in the cerebral cortex. Proc Natl Acad Sci *93*, 13453-13459.

Bliss, T.V., and Lomo, T. (1973). Long-lasting potentiation of synaptic transmission in the dentate area of the anaesthetized rabbit following stimulation of the perforant path. J Physiol *232*, 331-356.

Chang, H.T. (1953). Cortical response to activity of callosal neurons. J Neurophysiol *16*, 117-131.

Chauvette, S., Crochet, S., Volgushev, M., and Timofeev, I. (2011). Properties of Slow Oscillation during Slow-Wave Sleep and Anesthesia in Cats. J Neurosci *31*, 14998-15008.

Chauvette, S., Volgushev, M., and Timofeev, I. (2010). Origin of active states in local neocortical networks during slow sleep oscillation. Cereb Cortex *20*, 2660-2674.

Cirelli, C., Gutierrez, C.M., and Tononi, G. (2004). Extensive and divergent effects of sleep and wakefulness on brain gene expression. Neuron *41*, 35-43.

Cirelli, C., and Tononi, G. (2000a). Differential expression of plasticity-related genes in waking and sleep and their regulation by the noradrenergic system. J Neurosci *20*, 9187-9194.

Cirelli, C., and Tononi, G. (2000b). Gene expression in the brain across the sleep-waking cycle. Brain Res *885*, 303-321.

Crochet, S., Chauvette, S., Boucetta, S., and Timofeev, I. (2005). Modulation of synaptic transmission in neocortex by network activities. Eur J Neurosci *21*, 1030-1044.

Diekelmann, S., and Born, J. (2010). The memory function of sleep. Nat Rev Neurosci *11*, 114-126.

Frank, M.G., Issa, N.P., and Stryker, M.P. (2001). Sleep enhances plasticity in the developing visual cortex. Neuron *30*, 275-287.

Gais, S., Plihal, W., Wagner, U., and Born, J. (2000). Early sleep triggers memory for early visual discrimination skills. Nat Neurosci *3*, 1335-1339.

Gais, S., Rasch, B., Wagner, U., and Born, J. (2008). Visual-procedural memory consolidation during sleep blocked by glutamatergic receptor antagonists. J Neurosci *28*, 5513-5518.

Galarreta, M., and Hestrin, S. (1998). Frequency-dependent synaptic depression and the balance of excitation and inhibition in the neocortex. Nat Neurosci *1*, 587-594.

Galarreta, M., and Hestrin, S. (2000). Burst firing induces a rebound of synaptic strength at unitary neocortical synapses. J Neurophysiol *83*, 621-624.

Gil, Z., Connors, B.W., and Amitai, Y. (1997). Differential regulation of neocortical synapses by neuromodulators and activity. Neuron *19*, 679-686.

Guzman-Marin, R., Ying, Z., Suntsova, N., Methippara, M., Bashir, T., Szymusiak, R., Gomez-Pinilla, F., and McGinty, D. (2006). Suppression of hippocampal plasticity-related gene expression by sleep deprivation in rats. J Physiol (Lond) *575*, 807-819.

Hebb, D.O. (1949). Organization of behavior (New York: Wiley).

Huber, R., Ghilardi, M.F., Massimini, M., Ferrarelli, F., Riedner, B.A., Peterson, M.J., and Tononi, G. (2006). Arm immobilization causes cortical plastic changes and locally decreases sleep slow wave activity. Nat Neurosci *9*, 1169-1176.

Huber, R., Ghilardi, M.F., Massimini, M., and Tononi, G. (2004). Local sleep and learning. Nature *430*, 78-81.

Huber, R., Maatta, S., Esser, S.K., Sarasso, S., Ferrarelli, F., Watson, A., Ferreri, F., Peterson, M.J., and Tononi, G. (2008). Measures of Cortical Plasticity after Transcranial Paired Associative Stimulation Predict Changes in Electroencephalogram Slow-Wave Activity during Subsequent Sleep. J Neurosci *28*, 7911-7918.

Jenkins, J.G., and Dallenbach, K.M. (1924). Obliviscence during Sleep and Waking. Am J Psychol *35*, 605-612.

Kirkwood, A., Dudek, S.M., Gold, J.T., Aizenman, C.D., and Bear, M.F. (1993). Common forms of synaptic plasticity in the hippocampus and neocortex in vitro. Science *260*, 1518-1521.

Lante, F., Toledo-Salas, J.C., Ondrejcak, T., Rowan, M.J., and Ulrich, D. (2011). Removal of synaptic Ca(2)+-permeable AMPA receptors during sleep. J Neurosci *31*, 3953-3961.

Lisman, J., Yasuda, R., and Raghavachari, S. (2012). Mechanisms of CaMKII action in long-term potentiation. Nat Rev Neurosci *13*, 169-182.

Liu, Z.-W., Faraguna, U., Cirelli, C., Tononi, G., and Gao, X.-B. (2010). Direct evidence for wake-related increases and sleep-related decreases in synaptic strength in rodent cortex. J Neurosci *30*, 8671-8675.

Luczak, A., Bartho, P., Marguet, S.L., Buzsaki, G., and Harris, K.D. (2007). Sequential structure of neocortical spontaneous activity in vivo. Proc Natl Acad Sci U S A *104*, 347-352.

Malinow, R., and Malenka, R.C. (2002). AMPA receptor trafficking and synaptic plasticity. Annu Rev Neurosci *25*, 103-126.

Maquet, P. (2001). The role of sleep in learning and memory. Science *294*, 1048-1052.

Marshall, L., Helgadottir, H., Molle, M., and Born, J. (2006). Boosting slow oscillations during sleep potentiates memory. Nature *444*, 610-613.

Mednick, S., Nakayama, K., and Stickgold, R. (2003). Sleep-dependent learning: a nap is as good as a night. Nat Neurosci *6*, 697-698.

Mukovski, M., Chauvette, S., Timofeev, I., and Volgushev, M. (2007). Detection of active and silent states in neocortical neurons from the field potential signal during slow-wave sleep. Cereb Cortex *17*, 400-414.

Nishida, M., and Walker, M.P. (2007). Daytime naps, motor memory consolidation and regionally specific sleep spindles. PloS one *2*, e341.

Perrett, S.P., Dudek, S.M., Eagleman, D., Montague, P.R., and Friedlander, M.J. (2001). LTD induction in adult visual cortex: role of stimulus timing and inhibition. J Neurosci *21*, 2308-2319.

Rasch, B., Pommer, J., Diekelmann, S., and Born, J. (2009). Pharmacological REM sleep suppression paradoxically improves rather than impairs skill memory. Nat Neurosci *12*, 396-397.

Reinoso-Suarez, F. (1961). Topographischer Hirnatlas der Katze, fur Experimental-Physiologische Untersuchungen (Darmstadt: E. Merck).

Seibt, J., Dumoulin, M.C., Aton, S.J., Coleman, T., Watson, A., Naidoo, N., and Frank, M.G. (2012). Protein synthesis during sleep consolidates cortical plasticity in vivo. Curr Biol *22*, 676-682.

Seigneur, J., and Timofeev, I. (2010). Synaptic impairment induced by paroxysmal ionic conditions in neocortex. Epilepsia *52*, 132-139.

Siegel, J.M. (2005). Clues to the functions of mammalian sleep. Nature *437*, 1264-1271.

Sjöström, P.J., Rancz, E.A., Roth, A., and Häusser, M. (2008). Dendritic Excitability and Synaptic Plasticity. Physiol Rev *88*, 769-840.

Steriade, M., Nuñez, A., and Amzica, F. (1993). A novel slow (<1 Hz) oscillation of neocortical neurons *in vivo* : depolarizing and hyperpolarizing components. J Neurosci *13*, 3252-3265.

Steriade, M., and Timofeev, I. (2003). Neuronal plasticity in thalamocortical networks during sleep and waking oscillations. Neuron *37*, 563-576.

Steriade, M., Timofeev, I., and Grenier, F. (2001). Natural waking and sleep states: a view from inside neocortical neurons. J Neurophysiol *85*, 1969-1985.

Timofeev, I., Grenier, F., and Steriade, M. (2001). Disfacilitation and active inhibition in the neocortex during the natural sleep-wake cycle: An intracellular study. Proc Natl Acad Sci U S A *98*, 1924-1929.

Tononi, G., and Cirelli, C. (2003). Sleep and synaptic homeostasis: a hypothesis. Brain Res Bull *62*, 143-150.

Tononi, G., and Cirelli, C. (2006). Sleep function and synaptic homeostasis. Sleep Med Rev *10*, 49-62.

Vyazovskiy, V.V., Cirelli, C., Pfister-Genskow, M., Faraguna, U., and Tononi, G. (2008). Molecular and electrophysiological evidence for net synaptic potentiation in wake and depression in sleep. Nat Neurosci *11*, 200-208.

Zamanillo, D., Sprengel, R., Hvalby, O., Jensen, V., Burnashev, N., Rozov, A., Kaiser, K.M., Koster, H.J., Borchardt, T., Worley, P.*, et al.* (1999). Importance of AMPA receptors for hippocampal synaptic plasticity but not for spatial learning. Science *284*, 1805-1811.

5.8 Acknowledgements

We thank Sergiu Ftomov for his excellent technical support. This study was supported by CHIR, NIH, NSERC, and FRSQ.

Author contributions

S.C. and I.T. performed *in vivo* experiments and the related analysis; J.S. performed *in vitro* experiments and the related analysis. S.C. and J.S. share co-first authorship. S.C., J.S., and I.T. designed the experiments and contributed to writing the manuscript.

Competing financial interest

The authors declare no competing financial interests.

5.9 Figures

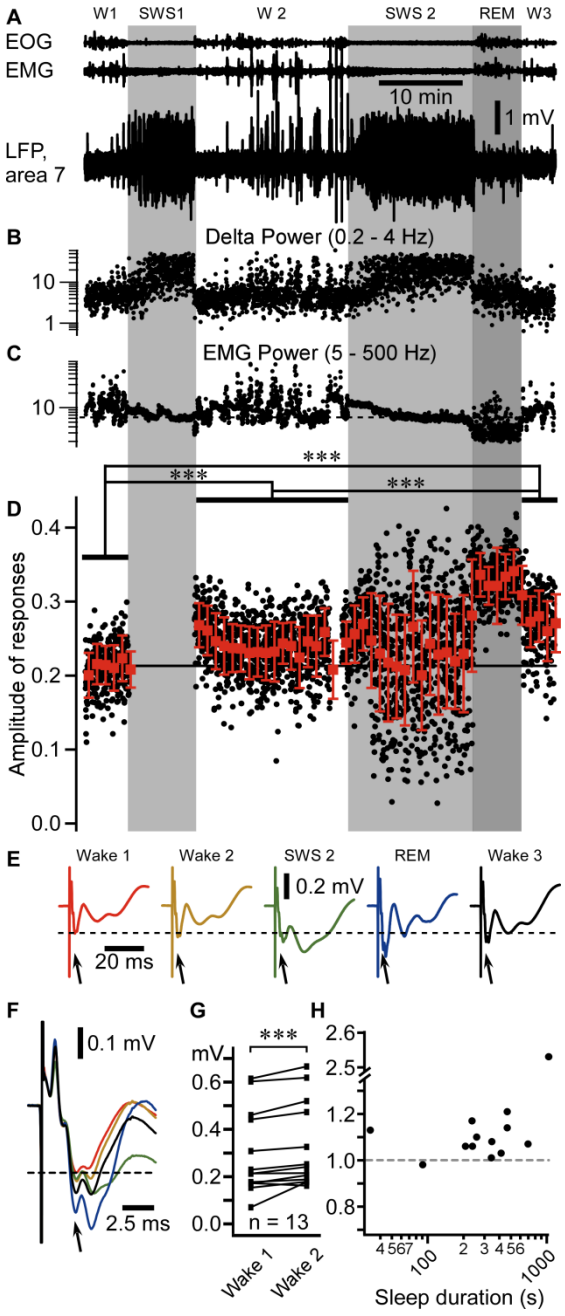

Figure V- 1 Amplitude of evoked potential responses (N1) to medial lemniscus stimuli throughout sleep-wake periods.

(A) Fragment of electro-oculogram (EOG), electromyogram (EMG), and local field potential (LFP) recorded in area 7 of a cat during sleep/wake transitions (W1-3 – Wake; SWS – Slow-wave sleep; REM – Rapid eye movement sleep. Light gray area depicts SWS episodes, darker gray area depicts a REM episode.

(B) Dots represent the delta power (area between 0.2 and 4 Hz in the Fast Fourier transform) of 1 second bins from the LFP segment shown in A.

(C) Dots represent the EMG power.

(D) Black dots represent individual evoked responses (N1) amplitude recorded in the LFP of somatosensory cortex (area 3) to the medial lemniscus stimuli (1Hz). Red squares are the running averages and the standard deviation for 60 responses (1 min). ***$p<0.001$, one way ANOVA Kruskal-Wallis with Dunn's multiple comparison test.

(E) Averaged area 3 evoked responses for each states of vigilance. The dotted line here and in panel F indicates the voltage of the mean response amplitude in wake 1, and the arrows point to the component of the response that was studied.

(F) Zoom-in and superimposition of averages presented in E (same color code).

(G) Group data from 13 "wake1-SWS-wake2" sequences, from 4 cats. Paired comparison of the mean response amplitude during wake1 and wake2 (pre-SWS and post-SWS) episodes. ***$p<0.001$, Wilcoxon matched-pairs signed rank test.

(H) Normalized (to wake 1 mean amplitude of evoked response) change in amplitude of response plotted against sleep duration.

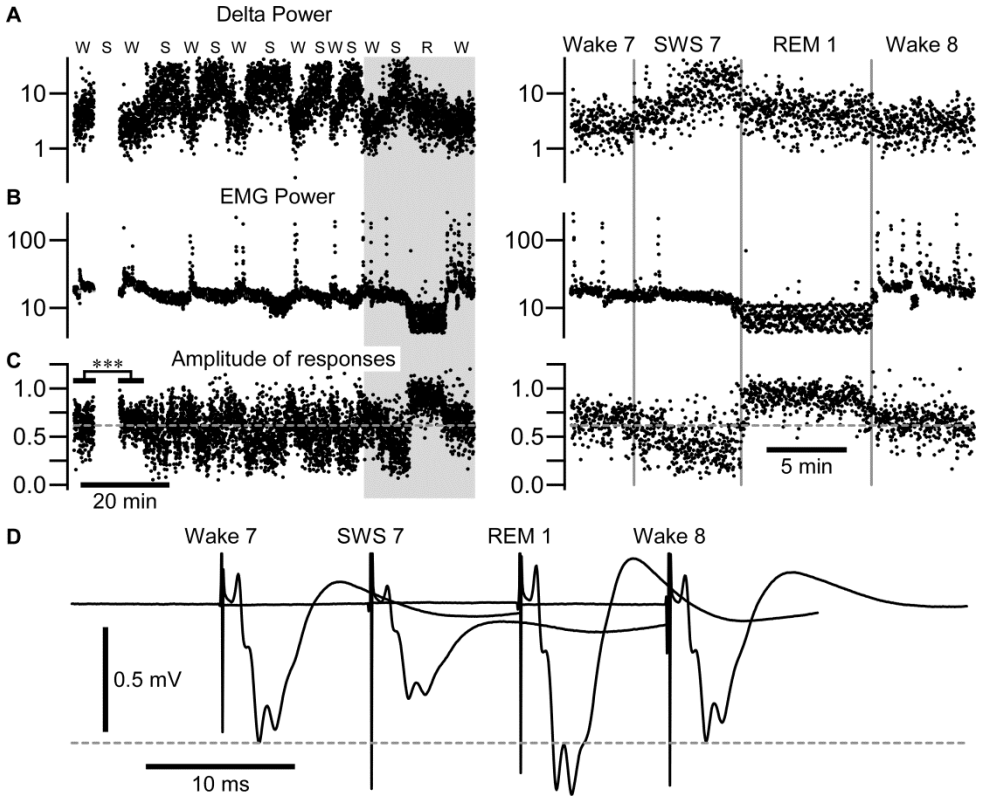

Figure V- 2 Late REM sleep does not potentiate somatosensory evoked potential in a following wake episode.

The delta power calculated from an area 7 local field potential (A) and EMG power (B) calculated around each medial lemniscal stimulus (±500 ms).

(C) The amplitude of somatosensory evoked potential. W – Wake, S – SWS, R – REM sleep. Note that no stimulation was delivered during the first slow-wave sleep episode and that responses were very significantly enhanced in the second wake episode as compared to the first wake episode; ***$p<0.001$, unpaired t-test with Welch's correction. The right panel corresponds to the shaded area in (A, B, C) expanded. The amplitude of response was not enhanced after late REM sleep; $p=0.7$, unpaired t-test with Welch's correction.

(D) Averaged response in each state of vigilance from wake 7 to wake 8 as indicated.

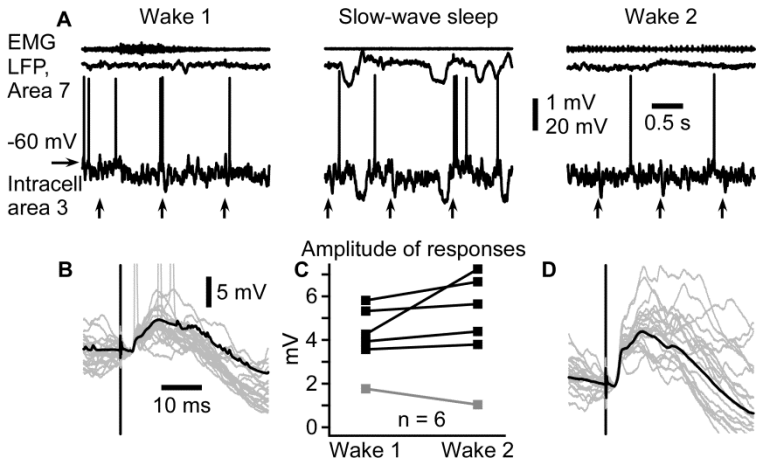

Figure V- 3 Intracellularly recorded evoked responses are enhanced after a period of slow-wave sleep.

(A) Electromyogram (EMG) from neck muscle, surface local field potential (LFP) from area 7, and intracellular recording from somatosensory cortex in consecutive states of vigilance as indicated. Vertical arrows indicate the time of medial lemniscus stimulation.

(B, D) Superimposition of 20 individual responses (gray traces) and the averaged response (black trace) during the first (B) and the second (D) episode of wake. Note that responses are ampler in the second episode of wake.

(C) Paired comparison of intracellular response amplitude of 6 neurons during two consecutive wake episodes separated by a slow-wave sleep episode. Each symbol represents the averaged response amplitude of one neuron during either wake 1 (left) or wake 2 (right). Lines indicate responses of the same neuron in two conditions.

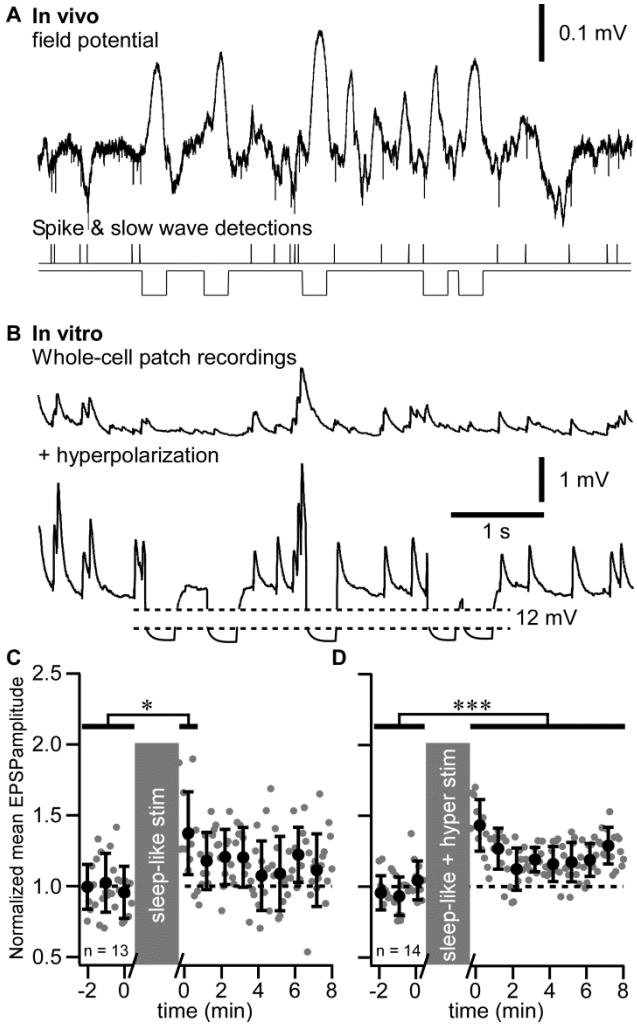

Figure V-4: Slow-wave sleep pattern of synaptic stimulation combined to intracellular hyperpolarization pulses induces long-term potentiation *in vitro*.

(A) *In vivo* field potential recording during a slow-wave sleep period of a cat. Extracellular spikes were detected and their timing was used for the synaptic stimulation pattern. Slow waves were also detected during the same time period and their timing was used for intracellular membrane potential hyperpolarization.

(B) *In vitro* recordings during *sleep-like* synaptic stimulation pattern (upper trace) and during the full *sleep-like* pattern of stimulation (synaptic + hyperpolarizing pulses, lower trace).

(C) Group data of normalized EPSP amplitude of *in vitro* whole-cell recordings in control and after *sleep-like* synaptic pattern of stimulation.

(D) Group data of normalized EPSP amplitude in control and after the *full sleep-like* pattern of stimulation. Gray dots are individual responses amplitude and black circles are the running averages and standard deviation for 12 consecutive responses (1 min). *$p<0.05$, ***$p<0.001$, Mann-Whitney test. Grey boxes indicate the 10 minutes stimulation protocol that was used.

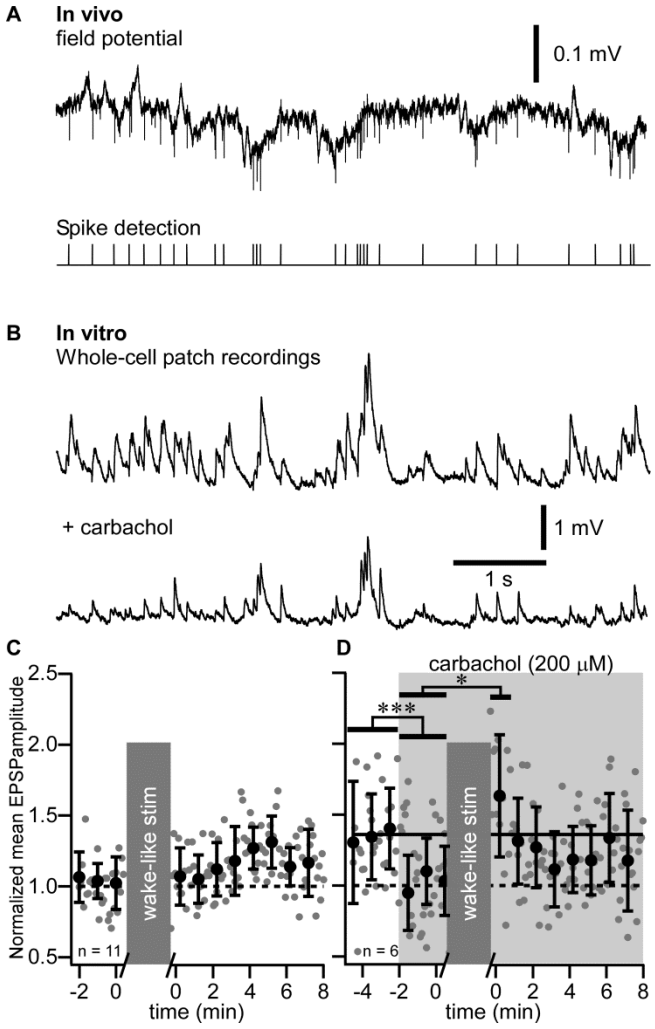

Figure V-5: Absence of long-term potentiation after wake pattern of stimulation *in vitro*.

(A) *In vivo* field potential recording during waking period of a cat. Extracellular spikes were detected and their timing was used as synaptic stimulation pattern.

(B) *In vitro* recordings during *wake-like* pattern of synaptic stimulation in control (Upper trace) and after adding 200 μM of carbachol (Lower trace).

(C) Group data of normalized EPSP amplitude of *in vitro* whole-cell recordings in control and after *wake-like* pattern of synaptic stimulation.

(D) Group data of normalized EPSP amplitude of *in vitro* whole-cell recordings in control and after *wake-like* pattern of synaptic stimulation in presence of carbachol (shaded area). Gray dots are individual responses amplitude and black circles are the running averages and

standard deviation for 12 consecutive responses (1 min). *$p<0.05$, ***$p<0.001$, Mann-Whitney test. Grey boxes indicate the 10 minutes stimulation protocol that was used.

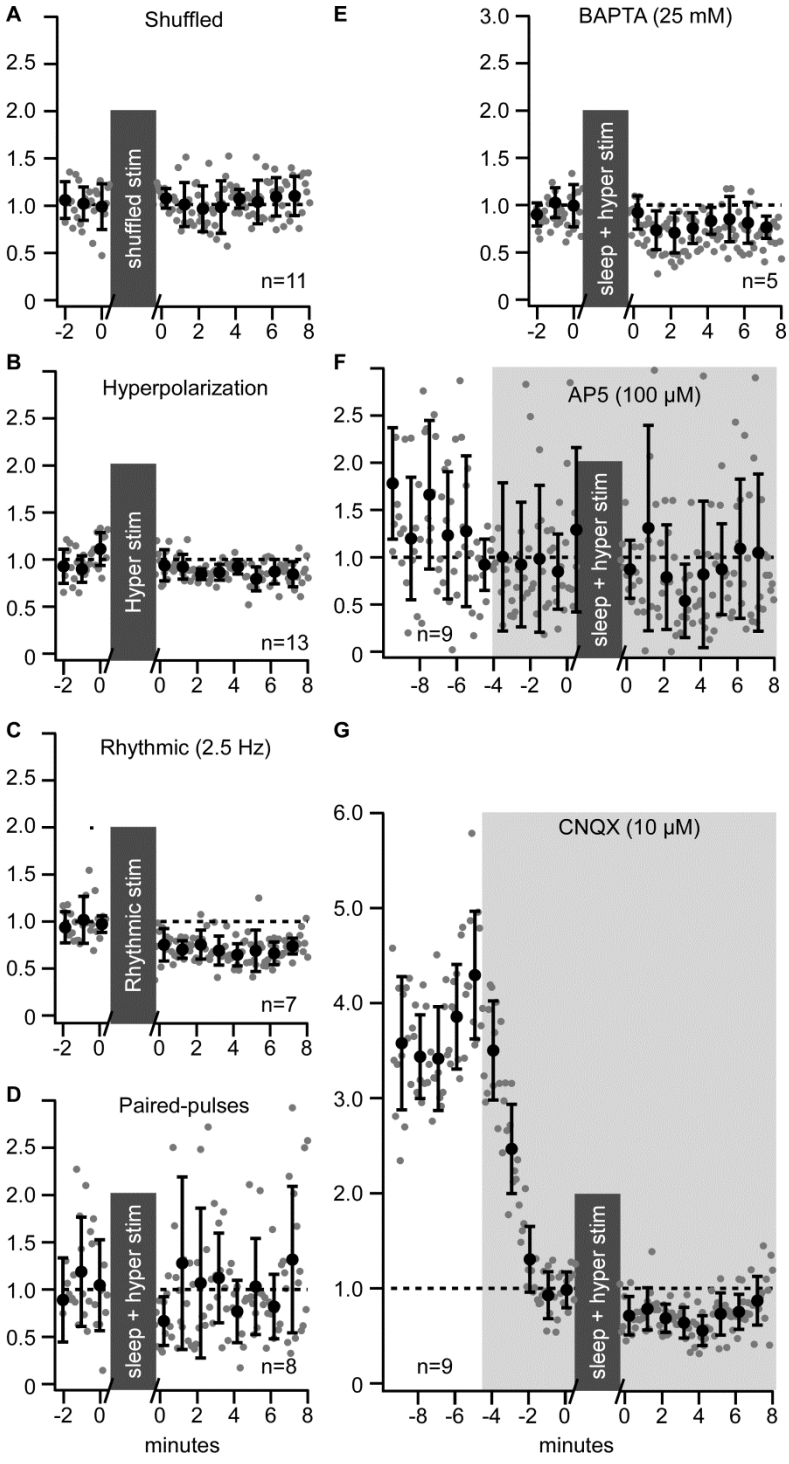

Figure V- 6 Properties of long-term plasticity induced by sleep pattern of stimulation.

(A) Group data of normalized EPSP amplitude of *in vitro* whole-cell recordings in control and after shuffled timing of sleep pattern of synaptic stimulation.

(B) Group data of normalized EPSP amplitude in control and after a period with the hyperpolarization pattern of stimulation only (no synaptic stimulation).

(C) Group data of normalized EPSP amplitude in control and after rhythmic pattern of synaptic stimulation (2.5 Hz).

(D) Paired-pulse (ISI 50 ms) test applied before and after the full sleep stimulation pattern (synaptic + hyperpolarization). Group data of normalized EPSP amplitude in control and after period with the full sleep stimulation pattern in presence of the calcium chelator BAPTA (25 mM) (E), the NMDA antagonist AP5 (100 μM) (F), or the AMPA antagonist CNQX (10 μM) (G). For all panels, gray dots are individual responses amplitude and black circles are the running averages and standard deviation for 12 consecutive responses (1 min). **$p<0.01$, ***$p<0.001$ Mann-Whitney test. Grey boxes indicate the 10 minutes stimulation protocol that was used.

5.10 Supplemental Information

5.10.1 Supplemental figures

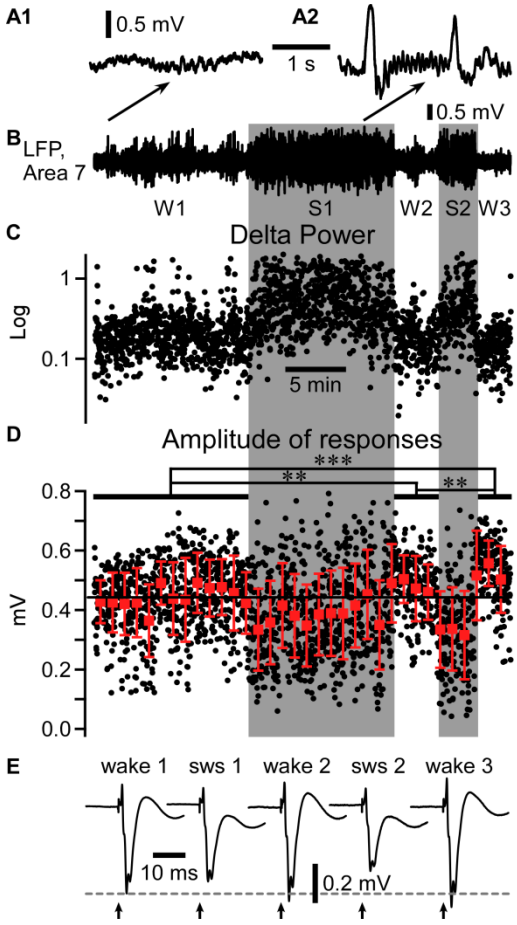

Figure V-S1: Field potential evoked responses are enhanced after a period of slow-wave sleep.

(A1, A2) Short expanded fragment from the local field potential (LFP) segment shown in B during wake (W) and slow-wave sleep (S), respectively. Shaded areas depict episodes of slow-wave sleep.

(B) Fragment of LFP recorded in cat's suprasylvian gyrus (area 7) during wake/sleep transitions as indicated.

(C) Black dots represent the delta power calculated as the area between 0.2 and 4 Hz in the FFT of 1 second bins from the LFP segment shown in B.

(D) Black dots represent individual evoked responses (N1) amplitude recorded in the LFP of somatosensory cortex of cats (area 3) to stimuli delivered in the medial lemniscus fibers

(1Hz). Note the large variability in response amplitude during periods of slow-wave sleep and note also that responses in a wake episode are of larger amplitude than in the previous wake episode. **$p<0.01$, ***$p<0.001$, one way ANOVA Kruskal-Wallis with Dunn's multiple comparison test. Red squares are the running averages and the standard deviation for 60 consecutive responses (1 min).

(E) Averaged area 3 evoked responses for each state of vigilance. Note that responses during wake are facilitated after a slow-wave sleep episode as compared to a previous period of wake and that averaged responses are of smaller amplitude during slow-wave sleep as compared to wake.

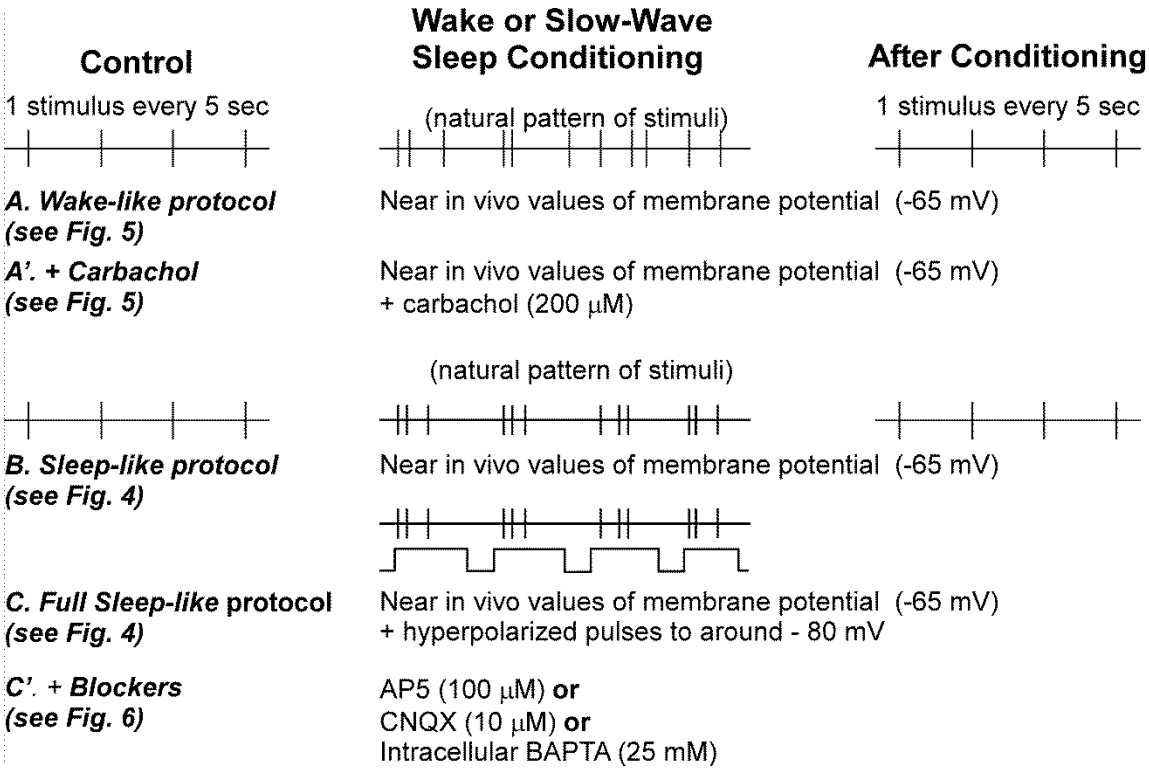

Figure V-S2: Stimulating protocol to investigate effects of steady-state synaptic plasticity.

Protocol will consist of single stimuli (30-60) applied every 5 sec followed by train of stimuli replicating wake sleep patterns (A-A') or slow-wave sleep patterns (B, C, C'), followed by single stimuli (one every 5 sec) lasting for at least 20 min. Experiments were done at membrane potential replicating wake (A), with the use of cholinergic agonists (A') that models cholinergic activities during waking state, with sleep pattern of synaptic stimulation (*Sleep-like protocol,* B), or with sleep pattern of synaptic stimulation combined with intracellular hyperpolarization pulses (*Full sleep-like protocol,* C). The *full sleep-like* protocol was also tested in the presence of different blockers (C').

Chapter VI

6.0 Low-threshold calcium spike dependent gating in thalamus.

Authors: AS Ferecskó [1, 3], J Seigneur [1, 2], S Chauvette [1, 2], K Kovács [1, 4], F Lajeunesse [1, 2], A Sík [1, 4], and I Timofeev [1, 2] *

[1] Department of Psychiatry and Neuroscience, Université Laval, Quebec, Canada.

Present address:

[2] Centre de Recherche Institut Universitaire en Santé Mentale de Québec (CRIUSMQ), Laval University, Québec, G1J 2G3, Canada

[3] UCB Pharma, Slough, U.K. 216 Bath Road, Slough, SL1 4EN, UK

[4] Neuropharmacology and Neurobiology Section, Neuronal Networks Group, College of Medical and Dental Sciences, School of Clinical and Experimental Medicine, University of Birmingham, Vincent Drive, Edgbaston, Birmingham, B15 2TT, UK

To be submitted.

Titre en français:

6.0 Blocage thalamique dépendant de potentiels d'actions calciques à bas seuil.

6.1 Résumé en français

Le thalamus est la principale porte d'entrée vers le cortex cérébral, cependant les mécanismes cellulaires exacts de blocage thalamique sont encore inexplorés. Le calcium est connu pour être essentiel à la transmission synaptique et les ondes fuseaux (spindles) sont accompagnées de potentiels d'action calciques à bas seuil (LTS) dans le thalamus. Nous avons émit l'hypothèse que les LTSs générés par les neurones thalamo-corticaux au cours des ondes fuseaux du sommeil induisent une diminution locale de Ca^{2+} extracellulaire, ce qui est suffisant pour affecter la transmission synaptique. Nous montrons ici que les potentiels évoqués induits lors des ondes fuseaux du sommeil ont une amplitude réduite par rapport aux potentiels évoqués enregistrés hors des ondes fuseaux. Nous démontrons également que, durant et immédiatement après des potentiels d'action calciques spontanés ou évoqués, le taux d'échec synaptique suite à des stimuli pré-thalamiques a augmenté de façon spectaculaire. Les LTSs ont été associés à une diminution locale majeure de Ca^{2+} extracellulaire et cette diminution de la concentration calcique affecte grandement la transmission synaptique parce que les canaux responsables des LTSs sont co-localisés avec les synapses.

6.2 Abstract

The thalamus has been considered as the main gateway to the cerebral cortex although the exact cellular mechanisms of thalamic gating are still unexplored. Calcium is known to be essential for synaptic transmission and spindles are accompanied with low-threshold Ca^{2+} spikes (LTSs) in the thalamus. We hypothesized that LTSs generated by thalamocortical neurons during sleep spindles induce a local extracellular Ca^{2+} depletion, which is sufficient to impair synaptic transmission. Here we show that evoked potentials induced during sleep spindles were reduced in amplitude as compared to evoked potentials recorded outside spindles. We also demonstrate that during and immediately after spontaneous or elicited Ca^{2+} spikes, the rate of synaptic failures to prethalamic stimuli was dramatically increased. LTSs were associated with a major local depletion of extracellular Ca^{2+} concentration and this depletion was efficient to affect the synaptic transmission because the channels mediating low-threshold Ca^{2+} current are co-localized with synapses.

6.3 Introduction

During sleep the threshold for sensory stimuli is much higher as compared to waking state [1]. It was already proposed that the leading structure in the gating of peripheral information to cerebral cortex is the thalamus [2]. The thalamocortical (TC) neurons are relatively hyperpolarized during slow-wave sleep (SWS), they are relatively depolarized during REM sleep [3], and probably also during waking state [4]. When sufficient depolarizing volleys reach the already depolarized TC neurons, they generate action potentials in a tonic mode, while an excitatory drive at hyperpolarized voltages triggers Ca^{2+}-mediated low-threshold spikes (LTSs) with bursts of action potentials [5-7]. Therefore evoked responses in neocortex can be obtained and even enhanced during SWS [8-10].

The transmission of auditory information is substantially reduced during spindle activities [11]. The question we asked was how the spindle-related gating occurs if TC neurons fire at both de- and hyperpolarized states? Normal [12-14] or pathological [15] brain activities induce a transient decrease in the extracellular Ca^{2+} concentration ($[Ca^{2+}]_o$) that affects synaptic transmission. Local changes in $[Ca^{2+}]_o$ affect synaptic efficacy and modulate short-term plasticity [12,16,17]. LTSs in thalamic neurons result in a dramatic increase of intracellular Ca^{2+} concentration [18,19]. We hypothesized that the generation of LTSs in a TC neuron results in a temporal local depletion of extracellular Ca^{2+}, which affects Ca^{2+}-dependent neurotransmitter release. Therefore, after a Ca^{2+} spike, for a given time, the presynaptic neurotransmitter release is hindered with an outcome of a decrease in cortical responsiveness.

6.4 Results

The first set of experiments was performed in non-anesthetized animals [20]. We tested whether within the somatosensory system the cortical responses are impaired during sleep spindles, an oscillation dominated by Ca^{2+} spikes in the thalamus. To avoid any possible gating in ascending prethalamic structures (i.e. dorsal column nuclei), we stimulated medial lemniscus (ML) fibers, the main ascending somatosensory pathway, and we recorded evoked potentials in the primary somatosensory cortical area (S1) during natural sleep in cats (Fig. VI-1a-d). In the example shown in Figure VI-1a the stimulus intensity was of 0.9 mA and the mean maximal depth-negative amplitude of evoked potential (N1) in this experiment was 131.4±72.1 μV (n=506). These data include consecutive responses occurring during both spindles and other network states. However, the amplitude of responses evoked during spindles was significantly smaller (77.1±39.4 μV, $p<0.001$, Kruskal-Wallis test with Dunn's correction) than the amplitude of responses occurring just prior to spindles (182.9±60.4 μV) or immediately after spindles (168.8±58.0 μV). A significant reduction in the amplitude of responses during spindles was found in all recording sessions (n=10, two animals). To compare responses to stimuli preceding spindles in all experimental sessions with different intensities of stimulation, we used normalized responses (Fig. VI-1e). The overall data show a highly significant ($p=0.0059$) reduction in N1 response during spindles.

Does this reduction have a cortical or a thalamic origin? It was demonstrated that the earliest response detected reliably in the neocortex upon stimulation of ascending prethalamic pathways is generated by axon terminals of TC cells [21]. In our experiments this initial response was a short-lasting (<1 ms) depth-positive deflection (Fig. VI-1d, P1). The P1 component of the response was reduced during spindles (Fig. VI-1d, inset) suggesting a reduction in the firing of TC neurons elicited upon stimulation of ML. In all recording sessions there was a highly significant ($p<0.001$) linear correlation between P1 and N1 components of the response (Fig. VI-1f), and the mean Spearman correlation coefficient was 0.50 ± 0.18 (n = 10). This indicates that the modulation of amplitude of early cortical synaptic responses (N1) directly depends on the firing of TC neurons.

The next set of experiments was performed in cats anesthetized with barbiturates, a type of anesthesia that induces spindles activities alternating with interspindle lull periods [22]. We investigated how spontaneous or evoked LTSs in TC neurons influence their responses to presynaptic volleys (Fig. VI-2). Intracellular recordings were obtained from the ventral posterolateral (VPL) thalamic nucleus. In these conditions, TC neurons displayed spindles appearing as rhythmic IPSP sequences occasionally accompanied with LTSs (Fig. VI-2a). Electrical ML stimuli were applied at 1 Hz, that is well below spontaneous or evoked firing in this pathway [23]. Therefore, some stimuli occurred during spindles while others occurred during interspindle lulls (Fig. VI-2a). Similar to previous observations in the ventral lateral (VL) nucleus [24], the all-or-none EPSPs (2-7 mV) were characterized with a sharp rising phase and a slow decaying phase during interspindle lulls (Fig. VI-2b, left panel). Some reduction in the response amplitude as well as a faster decaying phase was recorded during spindles (Fig. VI-2b, right panel). The decrease in EPSP duration during spindles was likely due to IPSP-mediated shunting, and some stimuli failed to elicit a response. The failure rate during spindles was higher than during interspindle lulls. In the example shown in the Figure VI-2a, the failure rate during interspindle lull was 25 % and it increased to 37% during spindles (Fig. VI-2c). A majority of the 45 investigated neurons showed an increase in failure rate during spindles (Fig. VI-2d, $p=0.0039$, Wilcoxon matched-pairs signed rank test). At this point, we hypothesized that the generation of LTSs during spindles results in a temporal depletion of extracellular Ca^{2+} that is entering postsynaptic neurons via low-threshold Ca^{2+} channels and therefore Ca^{2+} spikes generated by the postsynaptic neuron cause a reduction in the presynaptic neurotransmitter release. In order to demonstrate that indeed LTSs are responsible for this phenomenon and not other processes occurring during spindles that could cause an increase in the synaptic failure rate, we artificially triggered LTSs as a rebound after hyperpolarizing current pulses. We applied ML stimuli at different delays from the onset of the LTS (Fig. VI-3a). In all tested neurons (n=15), the maximal failure rate occurred at the peak of the LTS or at the onset of its decaying phase as shown in Figure VI-3b in which the observed phenomenon was systematically tested over a wide range of stimuli intervals (n=6). To test whether the occurrence of Ca^{2+} spikes is associated with an increase in the failure rate in other neuronal types, we recorded intracellular activities of two reticular thalamic neurons

from the peri-VPL sector. In these neurons, the increase in failure rate associated with spindle activities was even more dramatic than in VPL TC neurons (Supplementary Figure VI-S1).

To exclude all possible effects of organized network activities on the LTS-dependent failure rate increase, we performed in vitro whole-cell recordings from the rat VPL nucleus in physiological ($[Ca^{2+}]_o$ 1.2 mM) conditions. The stimulating protocol was similar to the one shown in Figure VI-3a. In current-clamp experiments the LTS (Fig. VI-4a) and in voltage-clamp experiments the T-current (Fig. VI-4b) were associated with an increase in failure rates (Fig. VI-4d).

To verify whether a significant local extracellular Ca^{2+} depletion indeed took place during the LTS, we measured the change in $[Ca^{2+}]_o$ with Ca^{2+}-sensitive electrodes positioned ≈10 μm from the edge of the soma of the recorded neuron in which an LTS was evoked. We found that the LTS was associated with a small decrease in the $[Ca^{2+}]_o$ (Fig. VI-4c). The recorded decrease in $[Ca^{2+}]_o$ was 23.09±5.77 μM. To control whether indeed synaptic failure rates were modulated by an LTS, we performed two control experiments. (a) We recorded a neuron in which identical hyperpolarizing current pulses either generated or not an LTS (Fig. VI-5a). During LTSs there was a decrease in $[Ca^{2+}]_o$ and an associated increase in failure rates of responses to ML stimuli ($p=0.0078$, Mann-Whitney test), while if an LTS was not elicited, there was no change in $[Ca^{2+}]_o$ and no change in failure rates. (b) We used dual intracellular recordings from two closely located TC neurons that responded to ML stimulation and in which an LTS was elicited in one neuron. The failure rate in this neuron was 100% during LTSs (significantly higher than in control [$p=0.002$, Mann-Whitney test]) and it had a tendency to an increase in the neighboring neuron (Fig. VI-5b).

The recorded decrease in $[Ca^{2+}]_o$ (Figs. VI-4c and VI-5a) unlikely provided sufficient influence on synaptic release. However, it should be noted that Ca^{2+} depletion takes place in the peri-membranal space and the Ca^{2+}-sensitive electrode recorded the averaged change in extracellular space at some distance from the membrane occupied by several cellular elements. In order to better evaluate the possible changes in the $[Ca^{2+}]_o$ in

the immediate surroundings of the recorded neuron, we investigated the extent of Ca^{2+} diffusion in extracellular space using a three-dimensional finite element method (FEM) model. This computational approach allowed to estimate the magnitude of $[Ca^{2+}]_o$ fluctuations in the vicinity of the neuronal membrane, when an LTS occurs in this neuron, as well as at some distance from the neuron. A TC neuron was modeled with 4 cylindrical sections (1 soma, 2 proximal, and one distal dendritic segments; Fig. VI-6a). Typically, the extracellular space occupies ~20% of the brain [25]. Therefore the TC neuron was inserted in a large environment filled at about 80% of its total volume with boxes representing other neuronal and non-neuronal elements (Fig. VI-6b). The $[Ca^{2+}]_o$ was set to 1.2 mM prior to the LTS. It was modeled with time-varying boundary conditions to mimic physiological Ca^{2+} influx at the TC neuron membrane (Fig. VI-6c-d; see Methods for a complete description). Pump mechanism was similarly added to the model to provide the extrusion of Ca^{2+} from the intracellular domain (Fig. VI-6d). Overall, the same amount of Ca^{2+} entering the cell through T-channels was extruded by pumps and the estimated intracellular Ca^{2+} concentration returned to baseline after some time. The model reproduced the magnitude of $[Ca^{2+}]_o$ recorded in vitro at the estimated distance of 10 μm from the cell body (Fig. VI-6e). The $[Ca^{2+}]_o$ dynamics were slightly faster in the model than in experimental recordings likely due to relatively slow kinetics of Ca^{2+}-sensitive electrodes. The estimated $[Ca^{2+}]_o$ dynamics at various lateral distances from the cell body showed the very local character of the extracellular Ca^{2+} depletion (Fig. VI-6f-g), suggesting that these changes in $[Ca^{2+}]_o$ would primarily affect synaptic boutons formed on the neuron that generated the LTS. In the vicinity of dendrites, the depletion was larger near proximal dendrites than at distal dendrite (Fig. VI-6g). Near the junction between the soma and the dendrite, the depletion could reach a magnitude of 100 μM. After an LTS both the experimental trace and the simulation outcome showed an "overshoot" in $[Ca^{2+}]_o$ (Fig. VI-6e), resulting in a $[Ca^{2+}]_o$ temporally higher than the initial value of 1.2 mM.

Overshoots in $[Ca^{2+}]_o$ were observed near the soma and near dendrites (Fig. VI-6e-f). After removing Ca^{2+} pump mechanisms from the model, the $[Ca^{2+}]_o$ still returned to the baseline (not shown), however with much longer delay (Fig. VI-6h-i). These results indicate that the overshoot in $[Ca^{2+}]_o$ produced during an LTS is induced by the combined

action of Ca^{2+} pumps and the Ca^{2+} diffusion in the extracellular space. Both mechanisms contribute to return $[Ca^{2+}]_o$ to a normal value in the vicinity of the TC neuron.

Postsynaptic Ca^{2+} microdomains and vesicle release depend critically upon $[Ca^{2+}]_o$ and on the co-localization of Ca^{2+} channels with docked vesicles [26,27], with effects spanning up to 300 nm [26], while the synaptic cleft is only in the order of 20 nm [28]. Because changes in $[Ca^{2+}]_o$ induced by the LTS of a single neuron are local, their effects should be stronger if postsynaptic T-channels are located close to synapses. We used silver enhanced preembedding immunogold staining and electron microscopy to investigate the co-localization of T-channels with a variety of synapses formed on TC neurons. We identified ten large presynaptic boutons with multiple release sites, a characteristic of lemniscal synapses [29]. In all of them a $Ca_v3.1$ subunit of T-channels was found on the postsynaptic membrane either near synapses or between release sites of a presynaptic bouton (Fig. VI-7a). Similar results were found for small boutons with asymmetric synapses [presumably formed by corticothalamic terminals [29]]. From 150 investigated synapses, 22% of T-channels ($Ca_v3.1$ subunit) on postsynaptic dendrite were found within the first 50 nm from the edge of the postsynaptic density and 90% of them were found within the first 500 nm (Fig. VI-7b). In reticular thalamic neurons, 28% of T-channels ($Ca_v3.3$ subunit) were located within the first 50 nm from the edge of the synaptic density (Fig. VI-7c). These results indicate that in the thalamus of cats, T-channels on postsynaptic dendrites tend to be located in the proximity of synapses. This enables them to exert an efficient synaptic feedback control of neurotransmitter release via a reduction of the $[Ca^{2+}]_o$ during or after a postsynaptic Ca^{2+} spike.

6.5 Discussion

We demonstrated, using a combination of various technical approaches that the generation of LTSs in the thalamus results in a temporal local depletion of $[Ca^{2+}]_o$ that strongly increased the synaptic failure rate. We showed that (1) evoked response amplitude was strongly reduced during sleep spindles which are accompanied with LTSs in the thalamus, (2) the synaptic failure rate in TC neurons was increased both during spindles or during induced LTSs, (3) an LTS in a single TC neuron increased the synaptic failure of incoming inputs, (4) in the peri-somatic region, the LTS generation decreased the $[Ca^{2+}]_o$ by several tens of μM, and (5) the high density of postsynaptic T-channels in peri-synaptic region positions them for an efficient control of $[Ca^{2+}]_o$ and therefore presynaptic release.

Synaptic release highly depends on changes in $[Ca^{2+}]_o$ [30-32]. In different synapses the peak intracellular concentration of Ca^{2+} during action potential in presynaptic boutons varies from less than one to several hundred micromoles [33-35]. In a given synaptic bouton the rise in Ca^{2+} concentration is stable [34,35] and small changes (<100 nM) of Ca^{2+} concentration are sufficient to change the probability of release by a factor 2 [36]. $[Ca^{2+}]_o$ undergoes global dynamic changes during physiological and pathological brain activities, being higher during silent network states and lower during active network states [13,15]. The changes in $[Ca^{2+}]_o$ within these physiological/pathological parameters could dramatically affect the efficacy of synaptic transmission [14,37]. Previous experimental and computational studies demonstrated also that synaptic activities, in particular the activation of NMDA receptors, induces a local depletion of $[Ca^{2+}]_o$, which reduces the synaptic release and enhances short-term synaptic depression [12,16,17]. These studies demonstrated that synaptic activity controls synaptic efficacy of the same synapses in an activity-dependent manner. Here we show that the activity of a postsynaptic neuron via the generation of an LTS can efficiently control synaptic transmission. We revealed that in the thalamus, T-channels are located predominantly in the peri-synaptic region (Fig. VI-7), thus the Ca^{2+}-dependent synaptic feedback mechanism could be very efficient in this structure. Indeed, similar to our study (Fig. VI-7c), a high density of $Ca_v3.3$ subunit close to postsynaptic density was found in the reticular nucleus of thalamus [38]. In neocortex most the $Ca_v2.3$ subunits were located within 500 nm from postsynaptic density on spines [39]. Activation of spines on

pyramidal cells, in particular spines with thin necks induces a major Ca^{2+} influx [40] that likely affects $[Ca^{2+}]_o$ around these spines. Our results demonstrate that during Ca^{2+} spikes the postsynaptic Ca^{2+} channels co-localized with synapses, provide efficient local control of $[Ca^{2+}]_o$, therefore controlling mediator release. We suggest that Ca^{2+} spikes for which the Ca^{2+} channels are co-localized with synapses in any neuron can control synaptic efficiency and short-term synaptic dynamics.

As we mentioned in the introduction, during SWS the threshold for sensory stimuli increases dramatically. This implies that sleep impairs the coordinated firing of large neuronal constellations. During SWS the membrane potential of TC neurons is more hyperpolarized as compared to REM sleep [3] and likely waking state [4]. Cortical neurons synchronously oscillate between depolarizing active (UP) and hyperpolarizing silent (DOWN) states [41,42]. This might be sufficient to obliterate the coordinated firing. However, neuronal firing in ascending systems persists. We showed here that thalamic burst firing reduces presynaptic release (Figs. VI-3-5). Cortical neurons also display an increased burst firing during SWS [43] suggesting that they may also control presynaptic release via Ca^{2+}-spike-dependent mechanism. This may have two purposes: (a) Reduced ability of TC neurons to respond to synaptic volleys after Ca^{2+} spikes disturbs spatio-temporal pattern of firing in thalamus, thus preventing transfer of meaningful information via thalamus, but preserving some ability of the TC system to respond to incoming volleys. (b) Because neurotransmitter reuptake, synthesis, and replenishment of synaptic vesicles is a very energy demanding process [44], the reduction of neurotransmitter release aims to save energy.

Altogether, these results provide a new insight into the physiological mechanism of Ca^{2+} spike-dependent synaptic feedback and contribute to the thalamic gating occurring during SWS.

6.6 Acknowledgments

We thank Pierre Giguère and Sergiu Ftomov for their excellent technical support. This study was supported by CHIR, NIH, NSERC, MRC, and FRSQ.

Author contributions

S.C. performed in vivo experiments in non-anesthetized animals and the related analysis; A.F., S.C., and I.T. performed in vivo experiments in anesthetized animals and the related analysis; J.S. performed in vitro experiments and the related analysis. F.L. built the FEM model and performed simulations and the related analysis. K.K. performed electron microscopy experiments and the related analysis. All authors contributed to design the experiments and to writing the manuscript.

Competing financial interest

The authors declare no competing financial interests.

6.7 References

1. Mullin, F.J. & Kleitman, N. Variations in the threshold of auditory stimuli necessary to awaken the sleeper. Am J Physiol 123, 477-481 (1938).
2. Steriade, M. & Pare, D. Gating in Cerebral Networks, (Cambridge University Press, New York, 2007).
3. Hirsch, J.C., Fourment, A. & Marc, M.E. Sleep-related variations of membrane potential in the lateral geniculate body relay neurons of the cat. *Brain Res* 259, 308-312 (1983).
4. Steriade, M., McCormick, D.A. & Sejnowski, T.J. Thalamocortical oscillations in the sleeping and aroused brain. *Science* 262, 679-685 (1993).
5. Jahnsen, H. & Llinás, R. Electrophysiological properties of guinea-pig thalamic neurones: an in vitro study. *J Physiol* 349, 205-226 (1984).
6. Jahnsen, H. & Llinás, R. Ionic basis for electroresponsiveness and oscillatory properties of guinea-pig thalamic neurones in vitro. *J Physiol* 349, 227-247 (1984).
7. Rosanova, M. & Timofeev, I. Neuronal mechanisms mediating the variability of somatosensory evoked potentials during sleep oscillations in cats. *J Physiol* 562.2, 569-582 (2005).
8. Massimini, M., Rosanova, M. & Mariotti, M. EEG slow (approximately 1 Hz) waves are associated with nonstationarity of thalamo-cortical sensory processing in the sleeping human. *J Neurophysiol* 89, 1205-1213 (2003).
9. Rector, D.M., Schei, J.L. & Rojas, M.J. Mechanisms underlying state dependent surface-evoked response patterns. *Neuroscience* 159, 115-126 (2009).
10. Shaw, F.Z., Lee, S.Y. & Chiu, T.H. Modulation of somatosensory evoked potentials during wake-sleep states and spike-wave discharges in the rat. *Sleep* 29, 285-293 (2006).
11. Dang-Vu, T.T., et al. Interplay between spontaneous and induced brain activity during human non-rapid eye movement sleep. *Proc Natl Acad Sci USA* 108, 15438-15443 (2011).
12. Rusakov, D.A. & Fine, A. Extracellular Ca^{2+} depletion contributes to fast activity-dependent modulation of synaptic transmission in the brain. *Neuron* 37, 287-297 (2003).

13. Massimini, M. & Amzica, F. Extracellular calcium fluctuations and intracellular potentials in the cortex during the slow sleep oscillation. *J Neurophysiol* 85, 1346-1350. (2001).

14. Crochet, S., Chauvette, S., Boucetta, S. & Timofeev, I. Modulation of synaptic transmission in neocortex by network activities. *Eur J Neurosci* 21, 1030-1044 (2005).

15. Pumain, R., Kurcewicz, I. & Louvel, J. Fast extracellular calcium transients: involvement in epileptic processes. *Science* 222, 177-179 (1983).

16. Egelman, D.M. & Montague, P.R. Computational properties of peri-dendritic calcium fluctuations. *J Neurosci* 18, 8580-8589 (1998).

17. King, R.D., Wiest, M.C. & Montague, P.R. Extracellular calcium depletion as a mechanism of short-term synaptic depression. *J Neurophysiol* 85, 1952-1959 (2001).

18. Cueni, L., et al. T-type Ca^{2+} channels, SK2 channels and SERCAs gate sleep-related oscillations in thalamic dendrites. *Nat Neurosci* 11, 683-692 (2008).

19. Errington, A.C., Renger, J.J., Uebele, V.N. & Crunelli, V. State-dependent firing determines intrinsic dendritic Ca^{2+} signaling in thalamocortical neurons. *J Neurosci* 30, 14843-14853 (2010).

20. Information on materials and methods is available on Nature Neuroscience Online.

21. Mitzdorf, U. & Singer, W. Prominent excitatory pathways in the cat visual cortex (A 17 and A 18): a current source density analysis of electrically evoked potentials. *Exp Brain Res* 33, 371-394 (1978).

22. Dempsey, E.W. & Morison, R.S. The reproduction of rhythmically recurrent cortical potentials after localized thalamic stimulation. *Am J Physiol* 135, 293-300 (1942).

23. Alloway, K.D., Wallace, M.B. & Johnson, M.J. Cross-correlation analysis of cuneothalamic interactions in the rat somatosensory system: influence of receptive field topography and comparisons with thalamocortical interactions. *J Neurophysiol* 72, 1949-1972 (1994).

24. Timofeev, I. & Steriade, M. Fast (mainly 30—100 Hz) oscillations in the cat cerebellothalamic pathway and their synchronization with cortical potentials. *J Physiol* 504, 153-168 (1997).

25. Syková, E. & Nicholson, C. Diffusion in brain extracellular space. *Physiol. Rev*. 88, 1277-1340 (2008).

26. Becherer, U., Moser, T., Stuhmer, W. & Oheim, M. Calcium regulates exocytosis at the level of single vesicles. *Nat Neurosci* 6, 846-853 (2003).

27. Parekh, A.B. Ca^{2+} microdomains near plasma membrane Ca^{2+} channels: impact on cell function. *J Physiol* 586, 3043-3054 (2008).

28. Peters, A., Palay, S. & Webster, H. *The Fine Structure of the Nervous System*, (Oxford Univ Press, New York, 1991).

29. Liu, X.B., Honda, C.N. & Jones, E.G. Distribution of four types of synapse on physiologically identified relay neurons in the ventral posterior thalamic nucleus of the cat. *J Comp Neurol* 352, 69-91 (1995).

30. Dodge, F.A. & Rahamimoff, R. Co-operative action of calcium ions in transmitter release at the neuromuscular junction. *J Physiol* 193, 419-432 (1967).

31. Goda, Y. & Stevens, C.F. Two components of transmitter release at a central synapse. *Proc Natl Acad Sci USA* 91, 12942-12946 (1994).

32. Silver, R.A., Lubke, J., Sakmann, B. & Feldmeyer, D. High-probability uniquantal transmission at excitatory synapses in barrel cortex. *Science* 302, 1981-1984 (2003).

33. Augustine, G.J. How does calcium trigger neurotransmitter release? *Curr Opin Neurobiol* 11, 320-326 (2001).

34. Koester, H.J. & Sakmann, B. Calcium dynamics associated with action potentials in single nerve terminals of pyramidal cells in layer 2/3 of the young rat neocortex. *J Physiol* 529, 625-646 (2000).

35. Brenowitz, S.D. & Regehr, W.G. Reliability and heterogeneity of calcium signaling at single presynaptic boutons of cerebellar granule cells. *J Neurosci* 27, 7888-7898 (2007).

36. Awatramani, G.B., Price, G.D. & Trussell, L.O. Modulation of transmitter release by presynaptic resting potential and background calcium levels. *Neuron* 48, 109-121 (2005).

37. Seigneur, J. & Timofeev, I. Synaptic impairment induced by paroxysmal ionic conditions in neocortex. *Epilepsia* 52, 132-139 (2010).

38. Liu, X.-B., Murray, K.D. & Jones, E.G. Low-threshold calcium channel subunit $Ca_v3.3$ is specifically localized in GABAergic neurons of rodent thalamus and cerebral cortex. *J Comp Neurol* 519, 1181-1195 (2011).

39. Parajuli, L.K., et al. Quantitative regional and ultrastructural localization of the $Ca_v2.3$ subunit of R-type calcium channel in mouse brain. *J Neurosci* 32, 13555-13567 (2012).

40. Harnett, M.T., Makara, J.K., Spruston, N., Kath, W.L. & Magee, J.C. Synaptic amplification by dendritic spines enhances input cooperativity. *Nature* 491, 599-602 (2012).

41. Chauvette, S., Volgushev, M. & Timofeev, I. Origin of active states in local neocortical networks during slow sleep oscillation. *Cereb Cortex* 20, 2660-2674 (2010).

42. Timofeev, I., Grenier, F. & Steriade, M. Disfacilitation and active inhibition in the neocortex during the natural sleep-wake cycle: An intracellular study. *Proc Natl Acad Sci USA* 98, 1924-1929 (2001).

43. Steriade, M., Timofeev, I. & Grenier, F. Natural waking and sleep states: a view from inside neocortical neurons. *J Neurophysiol* 85, 1969-1985 (2001).

44. Fykse, E. & Fonnum, F. Amino acid neurotransmission: Dynamics of vesicular uptake. *Neurochem Res* 21, 1053-1060 (1996).

45. Castro-Alamancos, M.A. Properties of primary sensory (lemniscal) synapses in the ventrobasal thalamus and the relay of high-frequency sensory inputs. *J Neurophysiol* 87, 946-953 (2002).

46. Fedirko, N., Svichar, N. & Chesler, M. Fabrication and use of high-speed, concentric H^+- and Ca^{2+}-selective microelectrodes suitable for in vitro extracellular recording. *J Neurophysiol* 96, 919-924 (2006).

47. Zomorrodi, R., Ferecskó, A.S., Kovács, K., Kröger, H. & Timofeev, I. Analysis of morphological features of thalamocortical neurons from the ventroposterolateral nucleus of the cat. *J Comp Neurol* 518, 3541-3556 (2010).

48. Blaustein, M.P. & Hodgkin, A.L. The effect of cyanide on the efflux of calcium from squid axons. *J Physiol* 200, 497-527 (1969).

49. Kovács, K., Sík, A., Ricketts, C. & Timofeev, I. Subcellular distribution of low-voltage activated T-type Ca^{2+} channel subunits ($Ca_v3.1$ and $Ca_v3.3$) in reticular thalamic neurons of the cat. *J Neurosci Res* 88, 448-460 (2010).

6.8 Figures

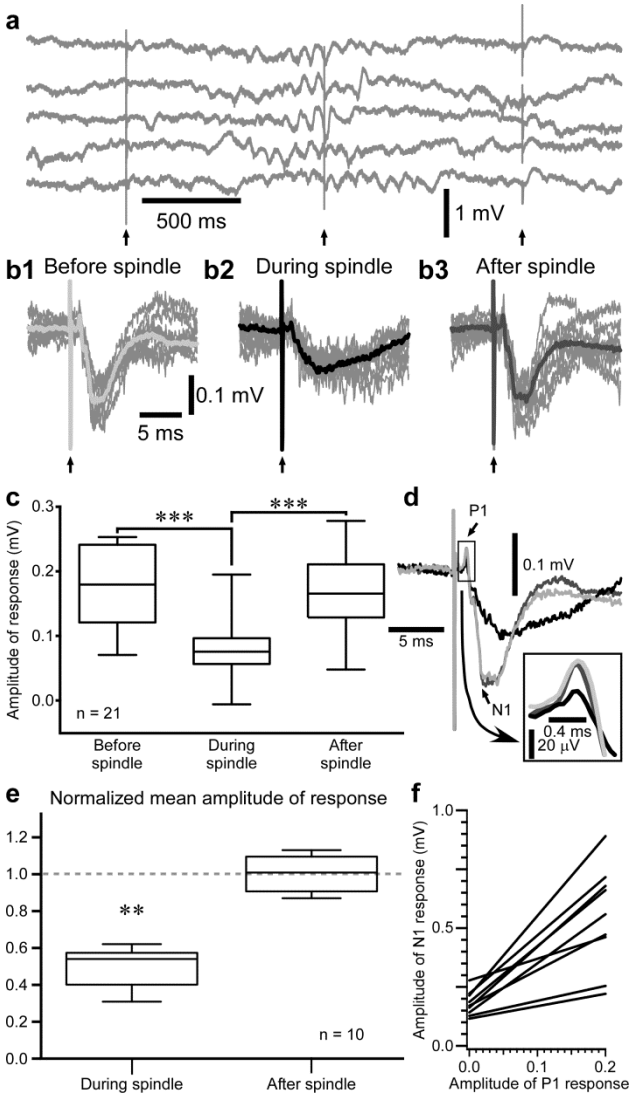

Figure VI-1 Strong reduction in cortical response amplitude to pre-thalamic stimuli during spindles.

(**a**) Five examples of local field potential recorded in the somatosensory cortex following medial lemniscus stimuli (indicated by vertical arrows) delivered at 1 Hz. Each example is composed of a stimulus occurring before, during, and after spindles. (**b**) Ten examples (thin gray traces) and the averaged response (thick trace, average from 21 stimuli) to stimuli occurring before (**b1**), during (**b2**), and after (**b3**) spindles. (**c**) Box plot of amplitude of responses (n = 21, all from a single sleep episode) to stimuli delivered before, during, and after spindles. ***$p<0.001$ (Kruskal-Wallis test with Dunn's correction). (**d**)

Superimposition of averaged traces shown in (**b**) with the same color code. Note the strong reduction in P1 (inset) and N1 responses to stimuli delivered during spindles. (**e**) Mean amplitude of response normalized to the response of stimulation occurring before spindle. n= 10 sleep episodes, **p<0.01, Wilcoxon signed rank test. (**f**) Linear fitting of amplitude of N1 response plotted against the amplitude of P1 response plotted for the 10 sleep episodes.

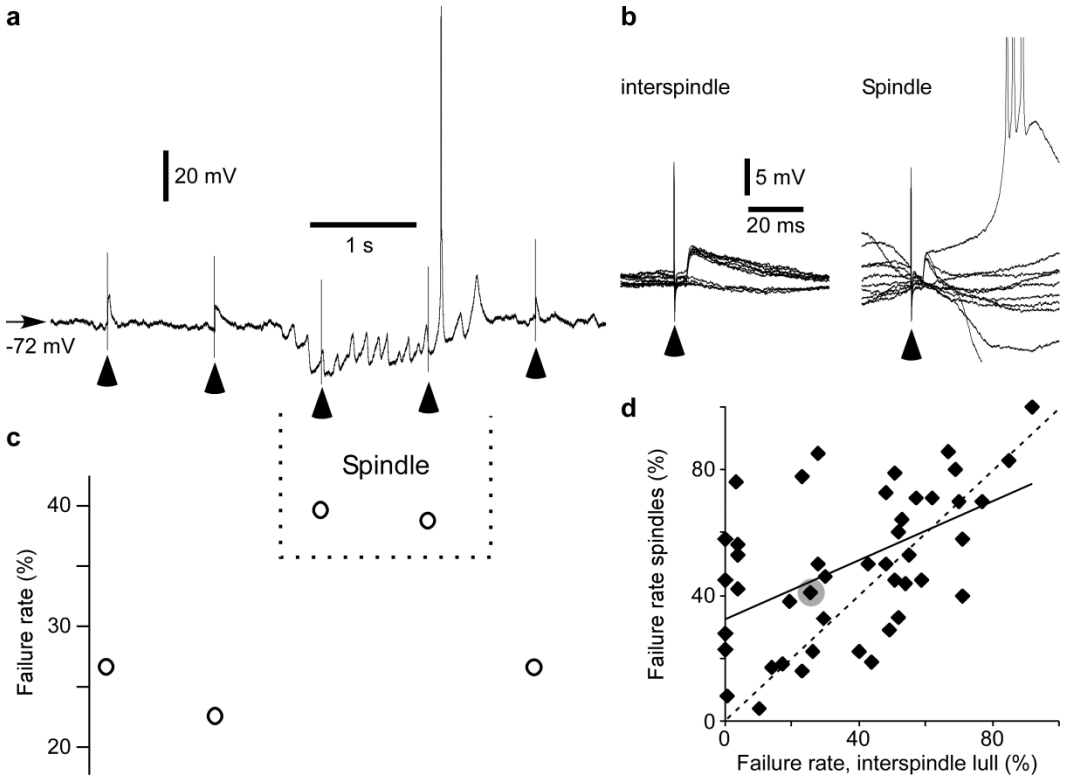

Figure VI-2 Responses and failure rates in the VPL thalamic nucleus to electrical stimulation of the medial lemniscus during spindles and interspindle lulls.

(**a**) Intracellular recording of a TC neuron from the VPL nucleus during lemniscal stimulation. During spindles the TC neuron reveals rhythmic IPSPs accompanied with rebound low-threshold calcium spikes. Low intensity stimulation of prethalamic afferents elicited EPSPs and some synaptic failures. Electrical stimuli are indicated by arrow heads. (**b**) Examples of superimposed responses and failures during spindles and interspindle lulls, separately. (**c**) Failure rate of lemniscal EPSPs during spindles and interspindle lulls for the neuron shown in **a**. (**d**) Scatter plot indicates the failure rate during spindles and interspindle lulls for all investigated neurons. The neuron represented by the grey symbol is shown in **a-c**.

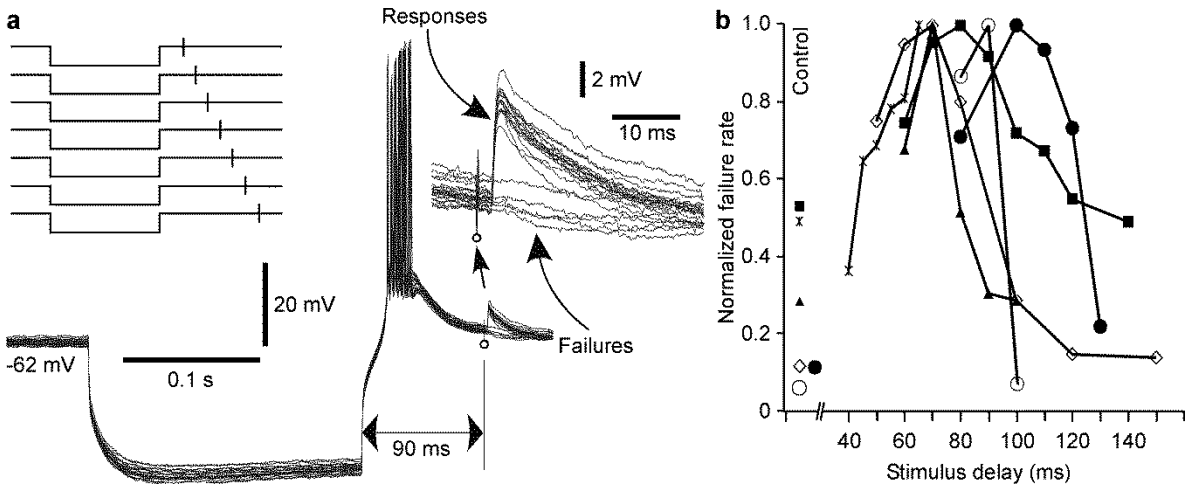

Figure VI-3 Increased failure rate following an LTS in thalamocortical (TC) neurons of the VPL nucleus in vivo.

(**a**) Superimposition of intracellular recording segments (n=20) including responses and failures to prethalamic stimuli (see inset for enlarged view) after rebound LTS spike (stimuli are indicated by empty circles) and a schematic diagram of the experimental paradigm representing injected current followed by prethalamic stimuli (vertical bars) with different delays. (**b**) Variation of failure rates of six TC neurons. Normalized rate of failures are plotted against the delay of prethalamic stimulus measured from the offset of the hyperpolarizing current. Each symbol represents an individual neuron recorded from the VPL nucleus. Controls indicate the failure rate of each neuron measured during interspindle lulls without LTS.

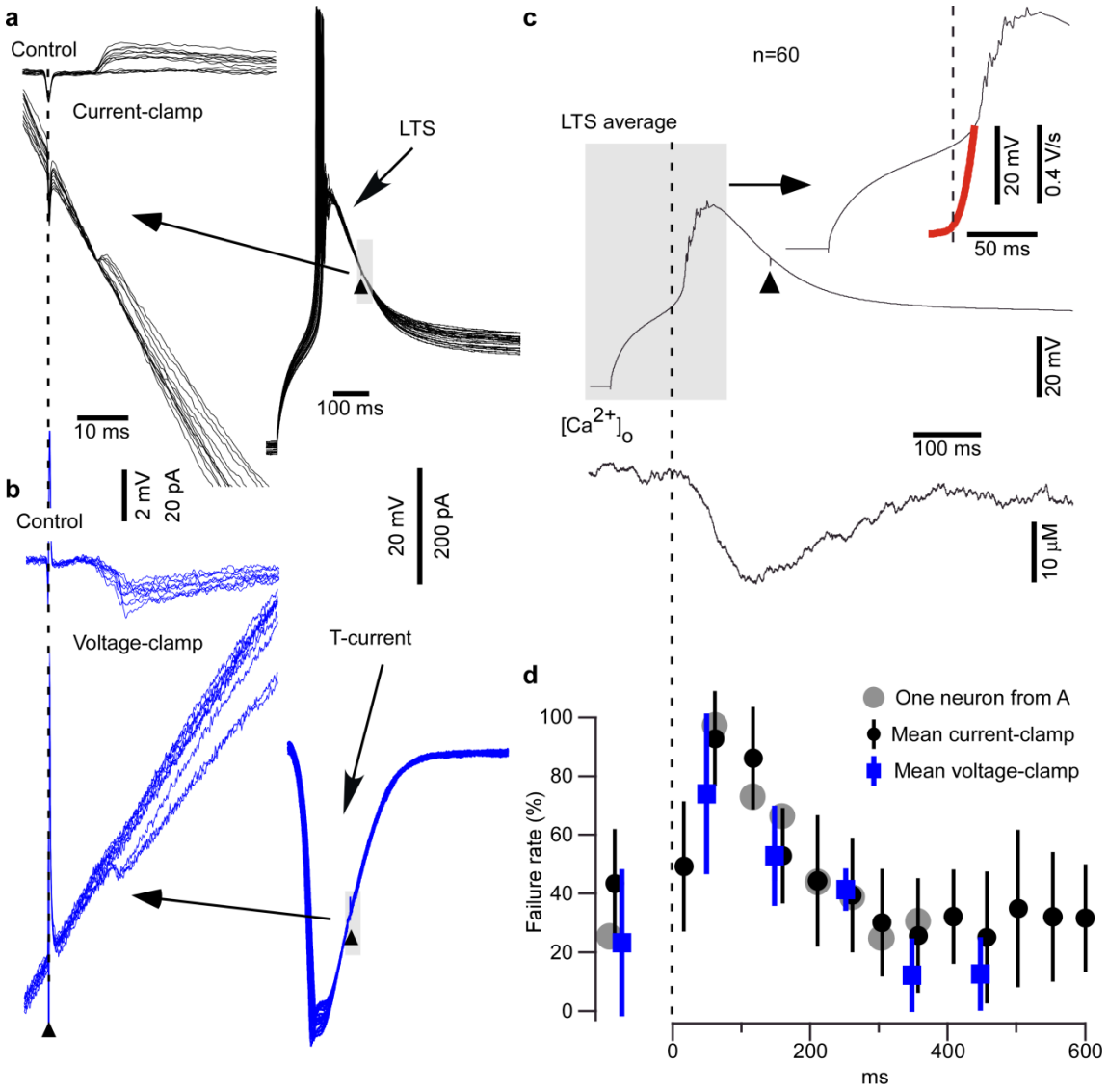

Figure VI-4 Evoked LTS induces an increase of synaptic failures from lemniscal stimulations and Ca^{2+} depletion in the vicinity of neuron.

Lemniscal stimulations were delivered in control conditions and 150 ms after the onset of an LTS and responses were recorded in current-clamp (**a**) or voltage-clamp (**b**) mode. (**c**) LTS onset is estimated at 0.1 V/s of the LTS average (n=60) (red line). The extracellular Ca^{2+} depletion measured with Ca^{2+} sensitive pipettes at ≈10 µm from the recorded site is delayed by 20 ms from the onset of LTS. (**d**) Failure rate for 8 recorded VPL neurons in current-clamp and voltage-clamp, * $p<0.05$, ** $p<0.01$, Mann-Whitney test.

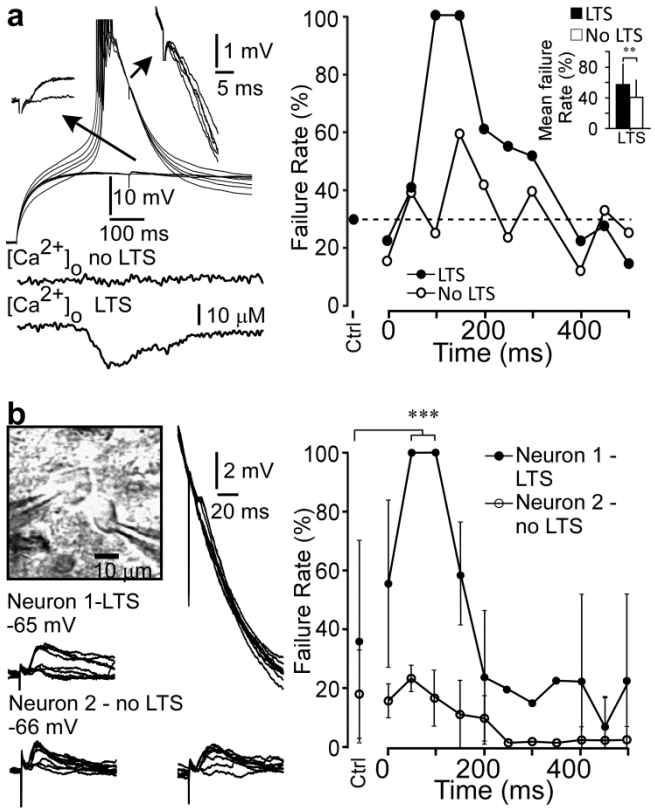

Figure VI-5 Specificity of LTS dependent increase in synaptic failure rates.

(**a**) In response to the same hyperpolarizing pulse the TC neuron did or did not generate rebound LTS. The significant increase in failure rate occurred only when the neuron generated an LTS (p=0.0078, Mann-Whitney test, first 400 ms were compared). (**b**) Lemniscal responses in two neighboring VPL neurons recorded simultaneously when an LTS occurred in only one neuron. The image shows spatial location of the two neurons. Examples show neuronal responses to medial lemniscus stimulation in control and 150 ms after the end of the hyperpolarization are shown, when the LTS was present in just one neuron. Mean failure rate for four paired recordings when one neuron of the pair generated an LTS.

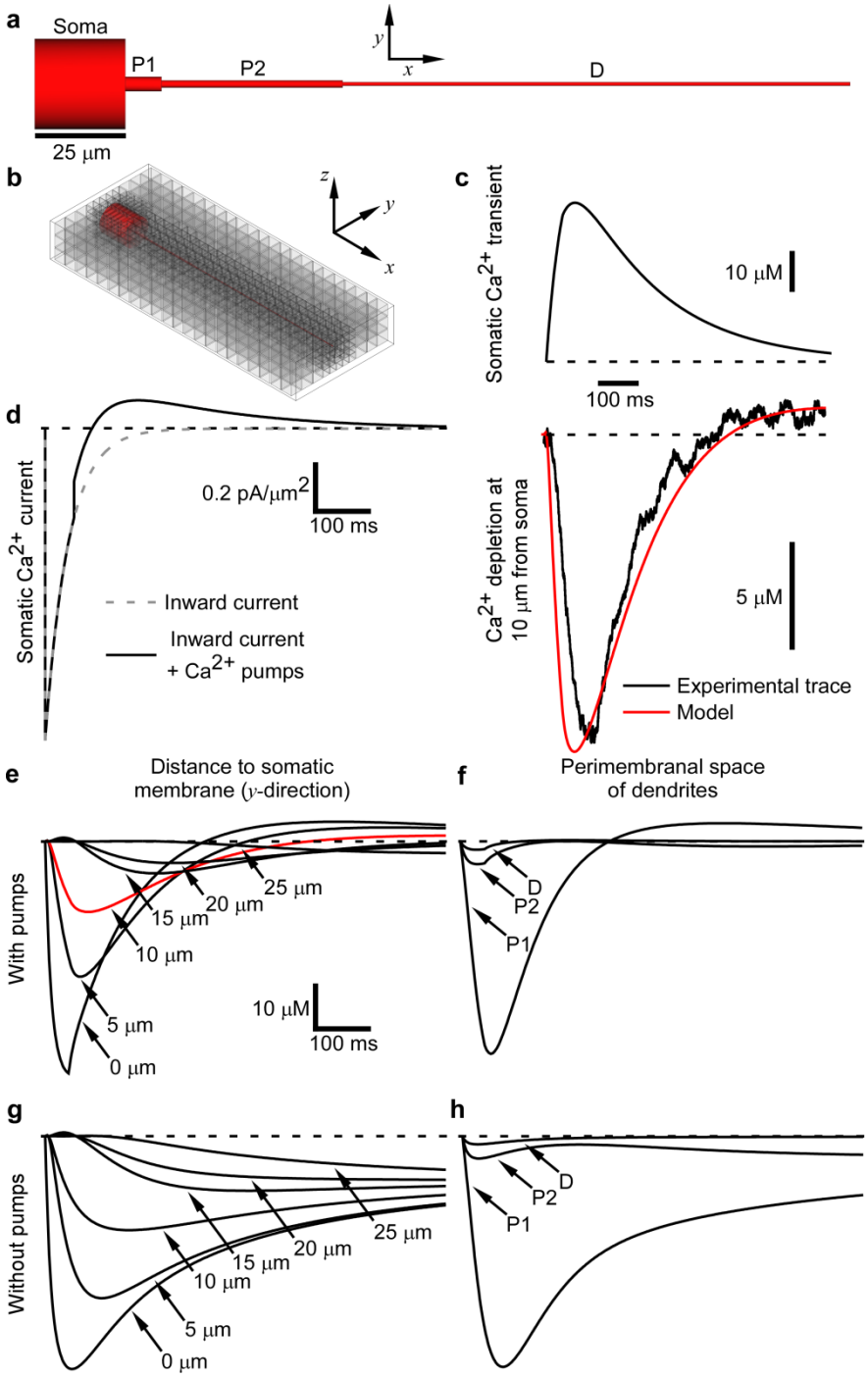

Figure VI-6 $[Ca^{2+}]_o$ dynamics probed in a FEM model.

(**a**) Four sections model of a TC neuron: one somatic section, two proximal (P1 and P2), and one distal (D) dendritic sections. (**b**) 3D environment to the modeled TC neuron. Boxes of different sizes were built to represent cellular objects surrounding the investigated neuron. The environment was bounded by a 250 µm × 100 µm × 34 µm box. (**c**) Change of

Ca^{2+} concentration in the soma. (**d**) Modeled Ca^{2+} currents. (**e**) Dynamics of $[Ca^{2+}]_o$ at 10 μm from the soma. The simulation trace (red) is compared to the experimental trace (black) obtained approximately at the same distance. (**f**) $[Ca^{2+}]_o$ dynamics at various distances from the soma (in the y-direction). The red trace is the same as in (**e**). (**g**) $[Ca^{2+}]_o$ dynamics in the peri-membranal space of dendrites. Traces were obtained at the middle of each dendritic section (in x-direction). (**h** and **i**) Same as **f** and **g**, but with blocked Ca^{2+} pumps mechanism. Baseline levels (dotted lines) are 1.2 mM for $[Ca^{2+}]_o$.

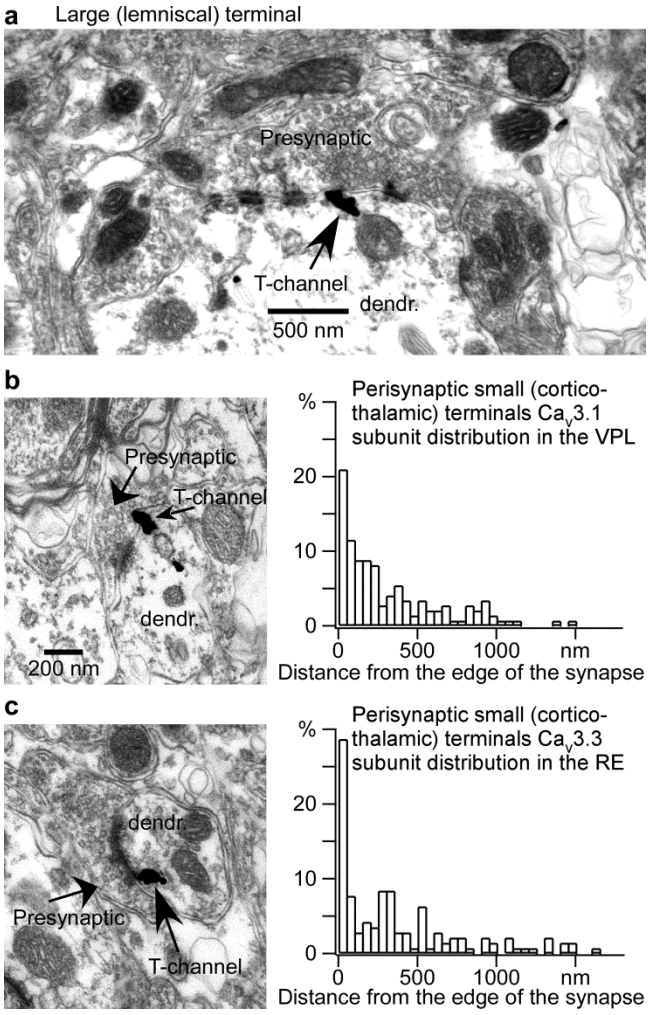

Figure VI-7 Electron microphotographs showing co-localization of $Ca_v3.1$ subunit in dendrites of TC neurons and $Ca_v3.3$ subunit in dendrites of a reticular (RE) neuron with synapses.

Immunogold particles were found on the dendritic plasma membranes of postsynaptic cells (arrows). (**a**) Immunolabelling for $Ca_v3.1$ subunit was localized within the synaptic knob between release sites of presumably lemniscal terminals. (**b**) Small (corticothalamic) synapse with round vesicles on thin dendrites in VPL labeled with $Ca_v3.1$. (**c**) $Ca_v3.3$ subunit localized perisynaptically in dendrites of RE neurons receiving small (corticothalamic) synapse with round vesicles. Histograms in **b** and **c** indicate the distribution of immunogold particles measured from the edge of the postsynaptic density along the dendritic membrane. Calibration bar for **b** applies also to **c**.

6.9 Online Methods and Supplementary Materials:

6.9.1 Material and methods:

Experiments were carried out in accordance with the guideline of the Canadian Council on Animal Care and approved by the Laval University Committee on Ethics and Animal Research.

In vivo experiments in non-anesthetized animals. These experiments were conducted on 2 adult non-anesthetized cats. We recorded field potentials from different cortical areas including from the somatosensory cortex during natural sleep/wake transitions.

Preparation. Chronic experiments were conducted using an approach similar to that previously described (for more details see [41-43]). Briefly, for the implantation of electrodes, cats were anesthetized with isoflurane (0.75-2%). During surgery, electrodes for LFP recordings, electromyogram (EMG) from neck muscle, electro-oculogram (EOG), and a system for head-restrained recordings without any pressure point were implanted and fixed with acrylic dental cement. About a week was allowed to animals to recover from the surgery before the first recording session occurred. Usually, 2-3 days of training were sufficient for cats to remain in head-restrained position for 2-4 hours and display several periods of quiet wakefulness, SWS, and REM sleep. The recordings were performed up to 40 days after the surgery.

In vivo experiments in anesthetized animals. These experiments were conducted on 12 adult cats. Cats were anesthetized with sodium pentobarbital (25-30 mg/kg, i.p.). All pressure points and tissues to be incised were infiltrated with lidocaine (0.5%). The animals were paralyzed with gallamine triethiodide (20 mg/kg) and artificially ventilated, maintaining the end-tidal CO_2 concentration at 3.5-3.8%. The body temperature was monitored by a rectal probe and maintained at 37^{o}C via a feedback-controlled heating blanket. The heart rate was continuously monitored (90-110 bpm). The stability of intracellular recordings was reinforced by cisternal drainage, bilateral pneumothorax, and by filling the hole made for recordings with a solution of 4% agar.

Recordings. All *in vivo* recordings were done in a Faraday chamber. LFPs were recorded using tungsten electrodes (2 MΩ, bandpass filter 0.1 Hz to 10 kHz) and amplified with AM 3000 amplifiers (A-M systems, Sequim, WA, USA). We aimed to implant electrodes at 1 mm below the cortical surface. A coaxial electrode was implanted in the medial lemniscus (ML) fibers for stimulation. Intracellular recordings were performed using glass micropipettes filled with 3 M of potassium acetate (resistance of 30-70 MΩ). A high-impedance amplifier with active bridge circuitry (Neurodata IR-283 amplifiers, Cygnus Technology, PA, USA, lowpass filter 10 kHz) was used to record the membrane potential and to inject current into neurons. All electrical signals were sampled at 20 kHz on Vision (Nicolet, Wisconsin, USA) for off-line analysis. At the end of experiments, the cats were euthanized with sodium pentobarbital (100 mg/kg i.v.).

In vitro experiments. Experiments were conducted on 21 Sprague Dawley rats (P21-P30, Charles River Laboratories International, Inc.).

Slice preparation. Rats were first anesthetized with ketamine-xylazine (40 and 10 mg/kg). The brain was then quickly dissected and maintained in ice-cold artificial cerebrospinal fluid (ACSF) containing (in mM): NaCl 124, KCl 2.8, $CaCl_2$ 1.2, $MgSO_4$ 2, NaH_2PO_4 1.25, $NaHCO_3$ 26, and D-glucose 10 (Sigma-Aldrich Canada, Canada), pH 7.4, aerated with 95% O_2 and 5% CO_2. Osmolarity was 300 ± 5 mOsm. The same ACSF was used for the recordings. Sagittal slices (350-400 μm) from one hemisphere were cut with a vibratome to obtain complete sections containing the VPL nucleus and nearby ML fibers. The recordings were made in submerged recording chamber maintained at 34◦C, containing the perfusion ACSF aerated with 95% O_2, 5% CO_2 at a rate of 3 ml/min.

Recordings. VPL thalamocortical neurons were preselected using an infrared differential interference contrast camera-microscopy. We obtained somatic whole-cell recordings (10-20 MΩ access resistances) with patch pipettes (resistance 3-5 MOhm) containing (mM): Potassium D-gluconate 130, 4-(2-hydroxyethyl)-1-piperazineethanesulfonic acid (HEPES) 10, KCl 10, $MgCl_2$ 2, ATP 2, and GTP 2 (Sigma-Aldrich Canada, Canada) at pH 7.2 and 280 mOsm.

Stimulation protocol. A stimulating tungsten electrode was inserted into the ML to obtain evoked EPSP in the VPL neurons. Lemniscal EPSPs were characterized according to the established criteria [45]. Evoked LTS were obtained by hyperpolarizing membrane potential of TC neurons with a 750 ms pulse every 5 sec.

*Calcium-sensitive electrodes***.** Concentric Ca^{2+}-sensitive electrodes were custom made as described in [46]. Concentric ion-selective microelectrodes were fabricated from two thin-walled borosilicate glass capillaries of different diameters. All capillaries are first clean with 95% ethanol and dry at 100 ºC for 30 min. The wider capillary [(OD) of 2.0 mm and (ID) of 1.6 mm (A-M Systems 6180)] was pulled on a Brown–Flaming P-87 puller to obtain a tip diameter of 2-4 µm. The resulting micropipette was exposed to N,N-dimethyltrimethylsilylamine (Fluka 41716) for 1 min. The silanization was stopped by exposing the pipette to ethanol 95% for 2 min followed by a heating to 120 ºC for 2h. A Ca^{2+}-selective ion exchanger cocktail (Fluka 21048) was then incorporated into the tip to form ≈100 µm column. The remaining volume was filled with a solution of 100 mM $CaCl_2$ for membrane stabilization. The inner pipette was pulled using thin-walled glass with an OD of 1.2 mm and an ID of 0.9 mm (A-M System 6165) to produce a tip diameter of 1 µm. The pipette was backfilled with a solution containing 3 M KCl and 150 mM $CaCl_2$. The smaller diameter pipette was threaded within the larger barrel and through the column of ion exchanger, until its end was 4–6 µm from the tip of the outer pipette. The inner pipette was then secured around the opening of the outer pipette using UV reactive dental composite (Tetric Flow, Ivoclar Vivadent). Electrical contact to the inner pipette was made with a silver chloride electrode. Ca^{2+} sensitive electrode was calibrated using standard solutions with [Ca^{2+}] of 0.5, 1, 1.5, 2, 4, 6 mM.

***Data analysis*.** All electrographic recordings (both *in vivo* and *in vitro*) were analyzed offline using custom-written routines in IgorPro (Lake Oswego, Oregon, USA).

Statistical analysis. Unless specified, all numerical values are given as mean ± standard deviation. Specific statistical tests are indicated in the text or in figures legend.

Computational model.

To model the $[Ca^{2+}]_o$ dynamics, we used the finite element method (FEM). A three-dimensional structure representing a TC neuron and its environment was built in the computer-aided design (CAD) software FreeCAD (GNU General Public License, http://sourceforge.net/apps/mediawiki/free-cad/index.php?title=Main_Page). The TC neuron was modeled as a 4 cylindrical sections neuron following average VPL neuron geometries [47]. The somatic surface area was about 3000 μm2 (diameter = 25 μm, length = 25 μm), the two proximal sections had respective diameters of 4 μm and 2 μm and lengths of 10 μm and 50 μm. The distal section was 140 μm long with constant diameter (1 μm). Other cellular objects of the environment were modeled by boxes of various sizes. To increase resolution in the peri-membranal space, boxes were made smaller in the vicinity of the neuron (Fig. VI-6b). The environment was bounded by a 250 μm × 100 μm × 34 μm box. This environment was sufficiently large to ensure that the boundary conditions did not alter numerical solutions in peri-neuronal space. All the objects filled about 80% of the structure volume.

The CAD structure was directly imported in Elmer (GNU General Public License, CSD-IT Center for Science) to solve finite element partial differential equations (PDEs). The Netgen (GNU Lesser General Public License, http://www.hpfem.jku.at/netgen/) plug-in of Elmer was used to generate a triangular surface mesh and a tetrahedral volume mesh. 62752 triangles, 161346 tetrahedra, and 36425 vertices were generated. The size of surface/volume elements was not uniform throughout the structure and was adapted to precisely fill the extracellular space and to ensure proper numerical solutions.

The governing PDE to solve for $[Ca^{2+}]_o$ dynamics was the diffusion equation:

$$\frac{\partial \left[Ca^{2+}\right]_o}{\partial t} = D\nabla^2 \left[Ca^{2+}\right]_o + \text{sources} - \text{sinks}\,, \qquad \text{Equation (1)}$$

where D = 0.6 $\mu m^2/ms$ [48] is the diffusion coefficient. Sinks and sources in the right-hand side of equation (1) represent Ca^{2+} influx through T-channels (inward current) and its extrusion via Ca^{2+} pumps (outward current), respectively. The initial condition for $[Ca^{2+}]_o$ was set to 1.2 mM [15]. Reflective boundary conditions ($\partial [Ca^{2+}]_o/\partial t = 0$) were applied to the walls of the 3D environment and to passive objects to represent non-permeable membranes.

Ca^{2+} influx through T-channels and its extrusion via Ca^{2+} pumps were modeled as time-varying boundary conditions at the TC cell membrane. We matched the amplitude of the extracellular Ca^{2+} depletion recorded in the experiments and in the model (Fig. VI-6e). Kinetics was based on Ca^{2+} imaging experiments [19]. The time constant of the inward current was the same for somatic, proximal and distal sections (τ_{in} = 0.04 s). The time constant for the outward current changed along the somatodendritic axis according to [19]: τ_{in} = 0.2 s for the somatic section and for the first proximal section, τ_{in} = 0.15 s for the second proximal section and τ_{in} = 0.1 s for the distal section. Because $[Ca^{2+}]_i$ amplitude varies throughout the dendritic arbor [19], we scaled dendritic inward currents. The strength of the Ca^{2+} pumps was adjusted so that the total amount of Ca^{2+} entering the cell for an infinite time was equal to the amount leaving the cell. The time-varying boundary conditions for the TC neuron membrane were

$$\Phi(t < 0.05) = \begin{cases} -1.162e^{-t/0.04} & \text{at soma} \\ -0.375e^{-t/0.04} & \text{at proximal dendrite 1} \\ -0.187e^{-t/0.04} & \text{at proximal dendrite 2} \\ -0.112e^{-t/0.04} & \text{at distal dendrite} \end{cases} \qquad \text{Equation (2)}$$

$$\Phi(t \geq 0.05) = \begin{cases} -1.162e^{-t/0.04} + 0.230e^{-t/0.2} & \text{at soma} \\ -0.375e^{-t/0.04} + 0.075e^{-t/0.2} & \text{at proximal dendrite 1} \\ -0.187e^{-t/0.04} + 0.048e^{-t/0.15} & \text{at proximal dendrite 2} \\ -0.112e^{-t/0.04} + 0.044e^{-t/0.1} & \text{at distal dendrite,} \end{cases} \qquad \text{Equation (3)}$$

in pA/μm^2. Times are in seconds. By integrating equations (2) and (3), one can obtain the evolution of $\Delta [Ca^{2+}]_i$ in time in each TC neuron section:

$$\Delta\left[Ca^{2+}\right]_i = \frac{1}{V}\int A\Phi \, dt, \qquad \text{Equation (4)}$$

where V and A are respectively the volume and the membrane area of the section.

The solution to equation (1) was evaluated at each vertex and interpolated in the remaining extracellular space. We simulated 700 ms epochs divided in 400 time steps (1.75 ms time steps).

Electron microscopy. The electron microscopy study was done as described in [49]. A region of interest containing the VPL or the reticular thalamic nucleus from cat's brain was removed and 50 μm-thick coronal sections were cut with a VT-1000S Vibratome (Leica, Wetzlar, Germany). The sections were washed several times in 0.1 M PB, cryoprotected by immersion in 30% w/v sucrose overnight, then permeabilized over liquid nitrogen.

Preembedding Immunogold Reactions. To reveal the subcellular distribution of T-type Ca^{2+} channels, sections were washed in Tris-buffered saline (TBS) and blocked with first blocking solution (2% w/v bovine serum albumin (BSA; Sigma-Aldrich), 5% w/v milk powder, 5% v/v normal goat serum (NGS; Vector Laboratories, Burlingame, CA), 0.1 g/ml glycine (Sigma-Aldrich), and 0.1 g/ml L-lysine (Sigma-Aldrich) in TBS) for 60 min, washed once in TBS, and incubated overnight at 4°C either with rabbit anti-$Ca_v3.1$ (α1G) or rabbit anti-$Ca_v3.3$ (α1I) primary antibody (1:50; Alomone Labs, Israel) containing 5% v/v NGS and 1% w/v BSA in TBS.

The sections were washed and blocked with second blocking solution [0.8% w/v BSA, 0.1% v/v cold-water fish skin gelatin (Aurion Immunoresearch, Wageningen, The Netherlands), 2% v/v NGS, 0.1 g/ml glycine, 0.1 g/ml L-lysine, 0.05% v/v sodium azide (Sigma-Aldrich) in TBS for 30 min. The ultrasmall (0.8 nm) gold particles were coupled to goat anti-rabbit IgG (Aurion Immunoresearch) diluted 1:100 in the second blocking solution overnight at 4°C. The tissues were fixed for 10 min in 1% v/v glutaraldehyde solution (made up in TBS). The sections were washed three times for 10 min each in enhancement conditioning solution (Aurion Immunoresearch), and the gold particles were intensified with IntenSE Silver Enhancement Reagents (Amersham, Arlington Heights, IL). At the end of the immunogold reactions, sections were incubated in 1% v/v OsO_4 for 40 min and dehydrated in graded ethanol (70% v/v ethanol containing 1% w/v uranyl acetate) and in propyleneoxide. After incubation overnight in epoxy resin (Durcupan, Fluka, Buchs, Switzerland), the sections were mounted onto slides, and polymerized at 58°C for 48 hr. Regions of interest were reembedded and sectioned serially in 50-nm sections, then counterstained in lead citrate for 5 min for electron microscopy [49]. Ultrathin serial sections were collected on Formvar-coated single slot grids. To confirm the specificity of the voltage-dependent calcium channel antibodies, antisera were incubated overnight at 4°C

with 1 μg of the peptide against which the antibody was produced. Sections were treated with these complexes, followed by the same protocol described above. Specific immunoreactivity could not be detected when either the primary or the secondary antibody or both antibodies were omitted.

6.9.2 Supplemental Figure

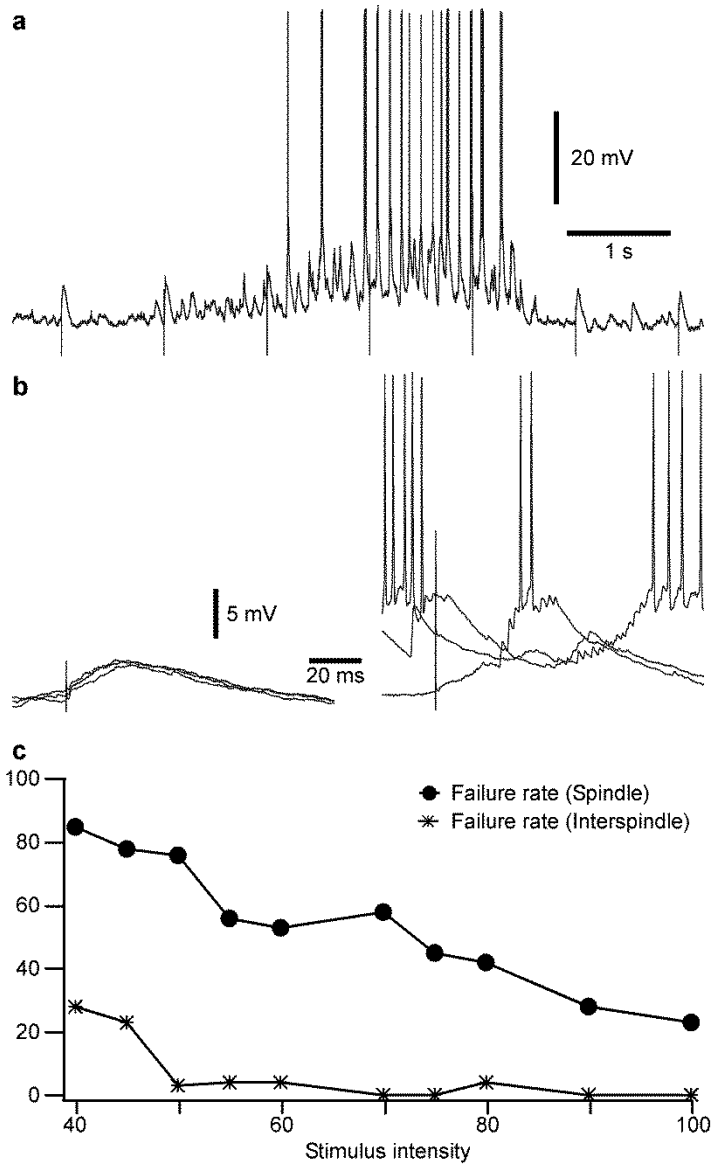

Figure VI-S1 Responses and failures of a reticular neuron to lemniscal stimuli in vivo.

(**a**) Intracellular recording of a reticular neuron during lemniscal stimulation. (**b**) Superimposed examples of responses during interspindle lulls (left panel) and failures during spindles (right panel). (**c**) The graph indicates the failure rate of this reticular neuron with respect to the stimulation intensity in spindles and interspindle lulls.

Chapter VII

7.0 General conclusion

The first three studies presented in this thesis were dedicated at understanding the mechanism of generation and propagation of the slow oscillation, a hallmark rhythm of SWS. We then studied how this rhythm could contribute to long-term synaptic plasticity, a plausible mechanism implicated in memory. In the last study presented in this manuscript, we investigated the role of another important sleep rhythm, namely spindles, in the gating of sensory information that occurs during sleep. We are currently working the mechanism of generation of different spindle types (slow vs. fast spindles) and their potential role in plasticity.

7.1 Summary of the results

The main results of these studies could be summarized as follow:

1) The first study (Chapter II) was conducted on ketamine-xylazine anesthetized cats, a type of anesthesia that induces rhythms similar to SWS, to study the propagation of slow waves in the neocortex. We showed that virtually all cortical neurons are involved in the slow rhythm and that both activity and silence occur almost synchronously in cells that are located up to 12 mm apart. We found that active states were generated in a spot and then propagated to surroundings regions, which was similar to studies in humans (Massimini et al., 2004; Kurth et al., 2010). The intriguing finding of this study was that the termination of activity (or onset of silent states) was even more synchronized than the onset of activity and did not seem to propagate. In another study, we showed that the synaptic inhibition was crucial for the synchronous termination of active states (Chen et al., 2012).

2) In the following study (Chapter III), we investigated the mechanism of origin of active states and the vertical propagation of activity. The study was conducted using two preparations: one using ketamine-xylazine anesthetized cats and the other using head-restrained non-anesthetized cats. Using LFP, intracellular, and multi-unit recordings, we found that the activity could be initiated in any cortical layer for a given cycle of the slow oscillation; however most of them were initiated in cortical layer V. The figure I like the

most in this study is the one using a 16-channel silicon probe to record LFP and multi-unit activities during SWS (Fig. III-3). This figure shows that there is no firing during silent states in naturally sleeping animals which is different from studies using multi-unit recordings in slice preparations (Sanchez-Vives and McCormick, 2000; Sanchez-Vives et al., 2008) or in anesthetized animals (Sakata and Harris, 2009; Vyazovskiy et al., 2011b; Eschenko et al., 2012). However, none of the above-mentioned studies actually showed extracellular spikes, instead mainly raster plots showing the timing of presumed spikes or firing rated were reported, it thus remains unclear whether the spike detection also included noise or not. At least, in our conditions of non-anesthetized animals, we showed that no firing occurs during silent states although some EPSPs can be recorded. This and the fact that extracellular calcium concentration increases during silent states (Massimini and Amzica, 2001; Crochet et al., 2005) strongly suggest that EPSPs recorded at the onset of membrane potential depolarization are from spike-independent releases. We then concluded that activity was more often generated in layer V due to the probabilistic nature of active state onsets; these pyramidal cells having the largest dendritic tree and receiving the most numerous synapses among cortical neurons. Another recent study in slices also showed that layer V cortico-cortical connections were essential for efficient horizontal propagation (Wester and Contreras, 2012). These results are different from intracortical LFP recordings from epileptic human patients (Cash et al., 2009; Csercsa et al., 2010) in which activity was found to begin more often in upper cortical layers. However, it remains unclear whether this difference is due to the epileptic conditions of the patient or if it is actually a species difference. At least, one model of epilepsy showed a strong neuronal loss in deep cortical layers few weeks after a white matter trauma was performed (Avramescu et al., 2009).

3) While the first study was conducted in anesthetized animals only, the second study was performed using both anesthetized and non-anesthetized cats and we found many similarities between natural SWS and ketamine-xylazine anesthesia. In the third study (Chapter IV), we wanted to characterize and quantify the differences between these two preparations. Using LFP, multi-units, and intracellular recordings, we showed that the slow oscillation was more rhythmic, more coherent between distant sites, and more ample in anesthetized preparation as compared to SWS. Also, silent states were of longer duration.

Area-specific differences in slow wave amplitude were present during SWS but under ketamine-xylazine anesthesia no differences could be observed between the same cortical areas. Gamma frequency-band was strongly enhanced under anesthesia while spindles and surprisingly, slow/delta frequency bands were diminished as compared to SWS.

4) Having characterized the origin of active states of the slow oscillation and its propagation we wanted to characterize the modulation of synaptic transmission by the different states of vigilance, but more specifically by SWS rhythms. In the fourth study (Chapter V), using *in vivo* and *in vitro* techniques, we found that SWS can induce LTP in the neocortex. *In vivo* using stimulation of the medial lemniscus fibers (somatosensory ascending pathway), we measured the amplitude of evoked potential in the somatosensory cortex in different consecutive states of vigilances. We found that responses during wake were enhanced after a period of SWS as compared to the previous wake episode, and this enhancement was present whether stimuli were applied or not during SWS. Responses were the most enhanced and the less variable during REM sleep, however REM sleep did not lead to further enhancement in a following wake episode. Using *in vitro* whole-cell recordings, we showed that the LTP observed *in vivo* could be reproduced only using a pattern of stimulation mimicking SWS activities (synaptic stimulation with the timing of a unit firing recorded during SWS and hyperpolarizing current pulses with the timing of slow waves extracted from the same recording). We also characterized the mechanism of this LTP which was compatible with the classic LTP observed in neocortex, because it required the activation of both NMDA and AMPA receptors and was calcium-dependent. Most the studies on LTP are from purely non-physiological stimulation patterns that is high frequency stimulations or even tetanic stimulations. In this study, we used only low frequency stimulation (1 Hz), which is usually associated with LTD, and we were able to observe LTP that was induced by SWS. Thus this study provided a potential physiological mechanism of memory.

5) In the last study included in this thesis (Chapter VI), we studied the role of spindles and of the related LTSs occurring during this sleep oscillation in a mechanism of thalamic gating. This last study was performed using several techniques; among them are LFP

recordings in non-anesthetized animals, intracellular recordings in anesthetized animals, whole-cell recordings in thalamocortical slices, three-dimensional computational model, and electron microscopy. We showed that T-channels were located in the synapses and that during LTSs, there was a local depletion in calcium that led to an increased synaptic failure rate. Spindles are known to be accompanied with LTSs in thalamocortical neurons, thus spindles might play a leading role in the thalamic sensory gating of information that occurs during sleep.

We conclude that slow oscillation originates in a focal point from which it propagates to neighboring cortical areas. Onsets of silent states occur more synchronously than onsets of active states and active inhibition would play a critical role in the synchronisation of silent state onsets. Active states are generated by a summation of spike-independent mediator releases and are initiated more often in layer V only due to probabilistic reasons. Ketamine-xylazine anesthesia, a model of SWS, share many similarities to SWS, but also shows quantitative differences such as the rhythmicity of slow waves and their coherence between distant sites, being both stronger under anesthesia. Silent periods were of longer duration and slow waves of larger amplitude as compared to SWS. Slow-wave sleep induces LTP of evoked potential for wake period as compared to a wake episode that occurred before SWS. Slow waves play also a critical role in the formation of LTP, because hyperpolarisations of postsynaptic neurons corresponding to slow waves were essential for the induction of LTP *in vitro*. This LTP followed the classical LTP mechanism that requires an activation of NMDA receptors which allows calcium entry that activate different kinases cascade which then lead to the insertion of GluR1-containing AMPA receptor to the membrane. Finally, spindles contribute to the thalamic gating of sensory information occurring during sleep because of LTSs generated in TC neurons. These LTSs significantly reduce the local extracellular calcium concentration and prevent synaptic transmissions a short time window. We are now developing a project to evaluate the role of different type of spindles in the memory formation and their potential role in plasticity in the TC network.

7.2 Technical considerations

It is worth to note that most of the results presented in this thesis come from *in vivo* studies, and as much as it was possible, studies were performed in non-anesthetized animals. In such conditions, the connectivity of the brain is preserved intact and also very importantly, the ionic milieu is unaffected in such preparations. As described in the introduction, extracellular calcium naturally fluctuates during slow oscillation and the highest concentration is usually of about 1.2 mM (Massimini and Amzica, 2001; Crochet et al., 2005). Most of *in vitro* studies are using 2 mM or even higher calcium concentration in the artificial cerebrospinal fluid which can have a huge impact in cell properties and synaptic release probability. For example, we showed in figures I-2 and I-3 that bursting cells lost their ability to burst in presence of higher calcium concentration. Extracellular calcium concentration also strongly affects the spike after hyperpolarizing potential (Boucetta et al., (in press)). In addition to the calcium concentration, the presence of network activity is also critical for short-term plasticity (Crochet et al., 2006; Reig et al., 2006; Reig and Sanchez-Vives, 2007; Sanchez-Vives et al., 2007). These are only two example of how techniques used might strongly influence the results of a study. However, *in vivo* techniques also have weaknesses and among them is the limitation to study specific channel mechanism or the low spatial resolution. In our studies, we used *in vitro* techniques or computational models only to characterize mechanisms that could not be characterized *in vivo*, thus we are confident that our results are highly valuable.

7.3 Final Remarks

In this thesis, we studied many features of sleep including the mechanism of generation and propagation of slow waves and the role of SWS in long-term plasticity. We obtained several intracellular and local field potential recordings from non-anesthetized animals. In agreement with previous studies, we found that SWS is composed of alternating periods of intense activity (active states; cortical neurons are depolarized and reveal vigorous synaptic activities that might lead to action potentials) and periods of silence (silent states; cortical neurons are hyperpolarized and reveal very few synaptic activities), while waking state is characterized by a depolarized membrane potential and vigorous

synaptic activities (Fig. VII-1A). During SWS, we found that within the suprasylvian gyrus of cats, active states originated at the border between area 5 and 7, and from this point, they propagated in both anterior and posterior directions, while a study in humans showed that most of cycles originated in the frontal cortex and propagated from that point to the rest of the brain (Fig. VII-1B). Knowing the principal site for the origin of active state in cats, we then studied the vertical propagation of active state in this particular area. We found that active states are mainly generated within cortical layer 5 in both naturally sleeping animals and ketamine-xylazine anesthetized animals (Fig. VII-1C). However any neurons could be leading in a particular cycle, which raised the question of why neurons from layer 5 are leading most of the cycles. Layer 5 pyramidal neurons are equipped with the most numerous synaptic contacts among cortical neurons having the largest dendritic tree (Fig. VII-1D, red cell from layer 3, orange cell from layer 5). Active states emerge as a consequence of a summation of spike-independent mediator releases and some transitions from silent to active state show a smooth and rapid slope of transition while others show the presence of many individual synaptic events at the onset of the transition with a slower development of the depolarization (Fig. VII-1D). Thus, layer 5 pyramidal cells are likely leading most of the cycles due to the probabilistic nature of active states onset. Several factors influence the occurrence of miniature EPSPs such as an increase in extracellular calcium and long period of inactivity (150-200 ms), and it occurs preferentially in stronger synapses. Slow waves modulate extracellular calcium concentration, release probability, and affect short-term synaptic plasticity (Fig. VII-1E), while during wake these parameters are thought to be relatively stable (Fig. VII-1F). Slow waves are known to group spindles and spindles are accompanied with LTSs in thalamocortical neurons. Comparing somatosensory evoked potentials elicited during or outside spindles revealed that pre-thalamic synaptic transmission is strongly reduced during spindles (Fig. VII-1G), and this was shown to be caused by a strong depletion in the extracellular calcium. This would be a physiological mechanism of thalamic gating during sleep. Why would it be important? First, obviously to allow for a much less disturbed sleep, but maybe also this would be important for memory consolidation. One of the hypotheses for memory consolidation is that during slow-wave sleep, an active reactivation of circuits implicated in the learning process occurs. During the reactivation, it might be important for the brain to be isolated

from external stimuli. We then studied the importance of slow-wave sleep in the formation of long-term potentiation. We showed that early slow-wave sleep episodes were very efficient in enhancing responses to medial lemniscus stimuli during a post-SWS wake episode as compared to a pre-SWS wake episode (Fig. VII-1H). Slow waves play a major role in this form of long-term potentiation, likely by pairing presynaptic excitation with postsynaptic depolarisations and long-term potentiation is believed to play a key role in memory formation and consolidation.

Several factors influences the occurrence of miniature EPSPs such as an increase in extracellular calcium, which occurs during silent states, such as long period of inactivity (150-200 ms), and it occurs preferentially in stronger synapses. It was also shown by different labs that long-term potentiation and learning tasks increase slow waves density in a following sleep episode. It is then likely that more miniatures EPSPs will occur in potentiated synapses making these neurons more likely to starts activity in the network. This might serve as a mechanism of reactivation during sleep. Finally, the use of ketamine-xylazine anesthesia as a model of SWS comprise some differences, among them are a more regular slow oscillation pattern, more uniform slow waves across cortical areas, and an increase in the gamma frequency power. However, the basic mechanisms of generation and propagation of slow waves were similar in both preparations.

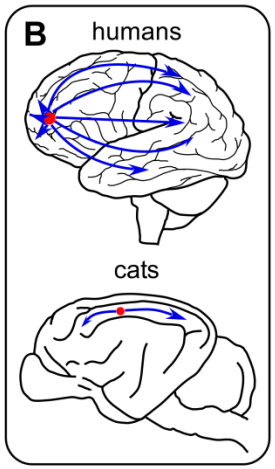
B
humans
cats

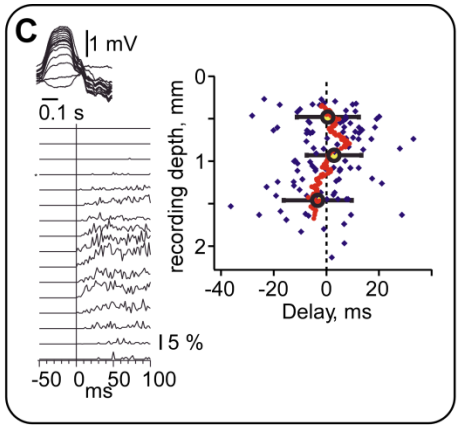
C
1 mV
0.1 s
5 %
-50 0 50 100
ms
recording depth, mm
0
1
2
-40 -20 0 20
Delay, ms

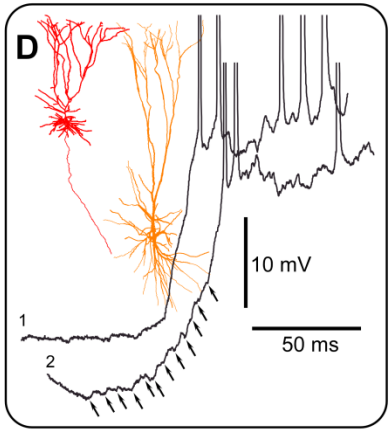
D
10 mV
50 ms
1
2

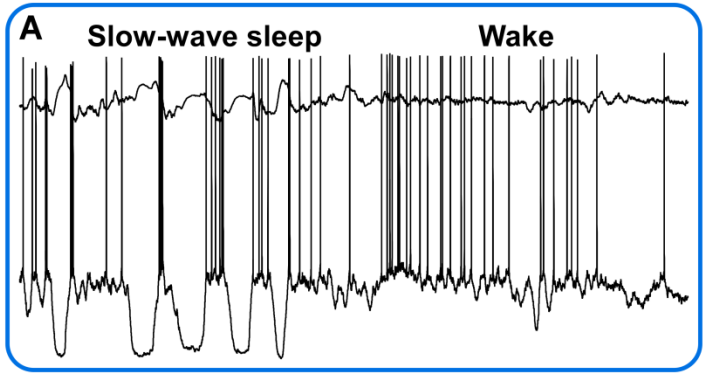
A
Slow-wave sleep
Wake

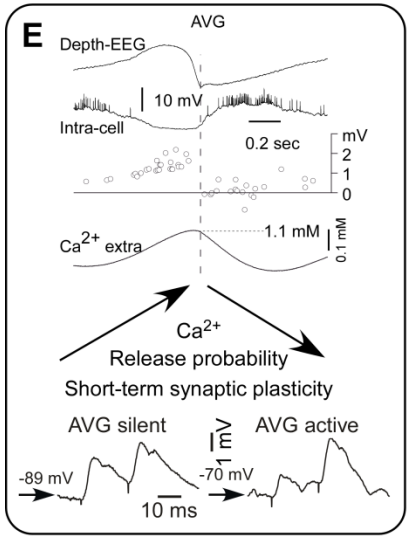
E
AVG
Depth-EEG
10 mV
Intra-cell
0.2 sec
mV
2
1
0
Ca2+ extra
1.1 mM
0.1 mM
Ca2+
Release probability
Short-term synaptic plasticity
AVG silent
AVG active
1 mV
-89 mV
-70 mV
10 ms

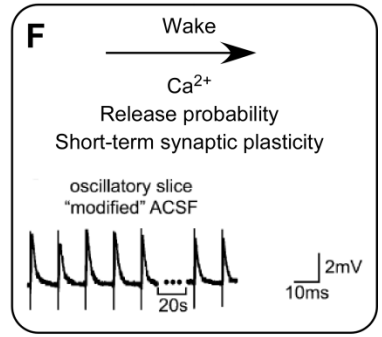
F
Wake
Ca2+
Release probability
Short-term synaptic plasticity
oscillatory slice
"modified" ACSF
20s
2mV
10ms

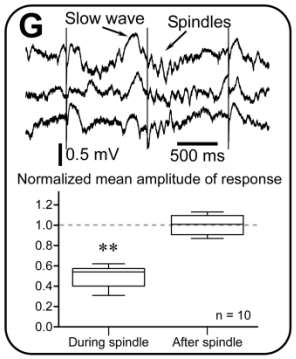
G
Slow wave
Spindles
0.5 mV
500 ms
Normalized mean amplitude of response
1.2
1.0
0.8
0.6
0.4
0.2
0.0
**
n = 10
During spindle
After spindle

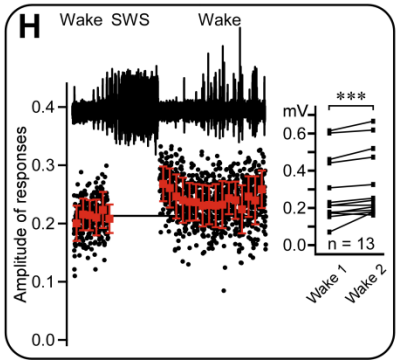
H
Wake SWS
Wake
Amplitude of responses
0.4
0.3
0.2
0.1
0.0
mV
0.6
0.4
0.2
0.0
***
n = 13
Wake 1
Wake 2

Figure VII-1 Slow-wave sleep modulates synaptic properties; concluding figure

A. Segment of local field potential and intracellular recording during a transition from SWS to waking state (modified from cerebral cortex cover page, November 2010). **B**. Horizontal propagation of slow waves. Drawing of a human and of a cat brain, showing the location of the foci (red dot) with the highest probability for the generation of slow waves. Blue arrows represent the direction of propagation for slow waves. (modified from (Timofeev and Chauvette, 2011)). **C**. Vertical propagation of slow waves. The left panel shows a superimposition of one cycle of a slow wave recorded with a 16-channel silicon probe during natural slow-wave sleep. Lower panel represents the multiunit firing probability in relation to the recording depth. Right panel shows the dependence of the delay of activity onset in state clusters on intracellular recording depth in animal anesthetized with ketamine-xylazine. Each blue diamond symbol represents data for one cell. Running averages (red symbols) were calculated for sets of 17 neurons. Note that both preparations (natural slow-wave sleep and ketamine-xylazine anesthesia) points to an origin of active states in cortical layer 5 (modified from (Chauvette et al., 2010)). **D**. Left panel, two neurolucida reconstructed pyramidal neurons (red from layer II/III, orange from layer V). Right panel shows two different types of transition from silent to active state. Note the presence of many individual events (oblique arrows) in the onset with slow development of depolarization (2) and a smooth slope of a rapid transition (1) (modified from (Chauvette et al., 2010)). **E**. Wave-triggered average of EEG, intracellular activities, and $[Ca^{2+}]_o$ as well as amplitude of intracellular events (responses and failures) triggered by microstimuli applied during different phases of the slow oscillation. The first maximum of EEG-depth negativity was taken as 0 time. Lower panel, averaged paired-pulse responses (all stimuli) of a neuron during active and silent network states in the ketamine-xylazine anaesthetized cat (modified from (Crochet et al., 2005)). **F**. Scheme showing that during wake, $[Ca^{2+}]_o$ remains stable, the release probability is stable, and there would be very little short-term plasticity (modified from (Reig et al., 2006)). **G**. Somatosensory evoked potentials elicited by medial lemniscus stimuli, recorded during spindles oscillations and outside spindles. Lower panel shows that somatosensory evoked potential are strongly reduced when stimuli occurred during spindles (modified from (Ferecsko et al., in preparation for submission)). **H**. Left panel, segment of local field potential recorded during a wake – SWS – wake

transition. Black dots represent the amplitude of individual somatosensory evoked potentials and red symbols are the running average for 60 consecutive evoked potentials. Note that no stimulations occurred during SWS and that responses are enhanced in the second wake episode. The right panel shows that in all cases, responses are enhanced in a wake episode following SWS as compared to the previous wake episode (modified from (Chauvette et al., 2012)).

8.0 General bibliography

Achermann P, Borbely AA (1997) Low-frequency (< 1 Hz) oscillations in the human sleep electroencephalogram. Neuroscience 81:213-222.

Achermann P, Borbely AA (2003) Mathematical models of sleep regulation. Front Biosci 8:s683-693.

Aladjalova NA (1957) Infra-slow rhythmic oscillations of the steady potential of the cerebral cortex. Nature 179:957-959.

Aladjalova NA (1962) Slow electrical processes in the brain. Moscow: Acad Sci USSA.

Alam MN, Szymusiak R, Gong H, King J, McGinty D (1999) Adenosinergic modulation of rat basal forebrain neurons during sleep and waking: neuronal recording with microdialysis. The Journal of physiology 521 Pt 3:679-690.

Allen PJ, Fish DR, Smith SJ (1992) Very high-frequency rhythmic activity during SEEG suppression in frontal lobe epilepsy. Electroencephalogr Clin Neurophysiol 82:155-159.

Amitai Y, Friedman A, Connors BW, Gutnick MJ (1993) Regenerative activity in apical dendrites of pyramidal cells in neocortex. Cereb Cortex 3:26-38.

Amzica F, Steriade M (1995) Disconnection of intracortical synaptic linkages disrupts synchronization of a slow oscillation. J Neurosci 15:4658-4677.

Amzica F, Steriade M (1998) Electrophysiological correlates of sleep delta waves. Electroencephalogr Clin Neurophysiol 107:69-83.

Andrillon T, Nir Y, Staba RJ, Ferrarelli F, Cirelli C, Tononi G, Fried I (2011) Sleep Spindles in Humans: Insights from Intracranial EEG and Unit Recordings. The Journal of Neuroscience 31:17821-17834.

Avendano C, Rausell E, Perez-Aguilar D, Isorna S (1988) Organization of the association cortical afferent connections of area 5: a retrograde tracer study in the cat. The Journal of comparative neurology 278:1-33.

Avramescu S, Nita DA, Timofeev I (2009) Neocortical post-traumatic epileptogenesis is associated with loss of GABAergic neurons. Journal of neurotrauma 26:799-812.

Azouz R, Gray CM (2000) Dynamic spike threshold reveals a mechanism for synaptic coincidence detection in cortical neurons in vivo. Proceedings of the National Academy of Sciences of the United States of America 97:8110-8115.

Baillarger J (1840) Recherches sur la structure de la couche corticale des circonvolutions du cerveau. Mémoires de l'Académie royale de médecine, Paris 8:149 -183.

Bal T, McCormick DA (1993) Mechanisms of oscillatory activity in guinea-pig nucleus reticularis thalami in vitro: a mammalian pacemaker. The Journal of physiology 468:669-691.

Bal T, McCormick DA (1996) What stops synchronized thalamocortical oscillations? Neuron 17:297-308.

Ball GJ, Gloor P, Schaul N (1977) The cortical electromicrophysiology of pathological delta waves in the electroencephalogram of cats. Electroencephalogr Clin Neurophysiol 43:346-361.

Barbara JG, Auclair N, Roisin MP, Otani S, Valjent E, Caboche J, Soubrie P, Crepel F (2003) Direct and indirect interactions between cannabinoid CB1 receptor and group II metabotropic glutamate receptor signalling in layer V pyramidal neurons from the rat prefrontal cortex. The European journal of neuroscience 17:981-990.

Barbaresi P, Bernardi S, Manzoni T (1989) Callosal connections of the somatic sensory areas II and IV in the cat. The Journal of comparative neurology 283:355-373.
Barbaresi P, Minelli A, Manzoni T (1994) Topographical relations between ipsilateral cortical afferents and callosal neurons in the second somatic sensory area of cats. The Journal of comparative neurology 343:582-596.
Barth AL, Poulet JFA (2012) Experimental evidence for sparse firing in the neocortex. Trends in Neurosciences 35:345-355.
Battaglia FP, Sutherland GR, McNaughton BL (2004) Hippocampal sharp wave bursts coincide with neocortical "up-state" transitions. Learn Mem 11:697-704.
Bazhenov M, Timofeev I (2006) Thalamocortical oscillations. In: http://www.scholarpedia.org/article/Thalamocortical_Oscillations.
Bazhenov M, Rulkov NF, Timofeev I (2008) Effect of synaptic connectivity on long-range synchronization of fast cortical oscillations. Journal of neurophysiology.
Bazhenov M, Timofeev I, Steriade M, Sejnowski TJ (1998a) Cellular and network models for intrathalamic augmenting responses during 10-Hz stimulation. Journal of neurophysiology 79:2730-2748.
Bazhenov M, Timofeev I, Steriade M, Sejnowski TJ (1998b) Computational models of thalamocortical augmenting responses. J Neurosci 18:6444-6465.
Bazhenov M, Timofeev I, Steriade M, Sejnowski TJ (1999) Self-sustained rhythmic activity in the thalamic reticular nucleus mediated by depolarizing GABAA receptor potentials. Nature neuroscience 2:168-174.
Bazhenov M, Timofeev I, Steriade M, Sejnowski T (2000) Spiking-bursting activity in the thalamic reticular nucleus initiates sequences of spindle oscillations in thalamic networks. Journal of neurophysiology 84:1076-1087.
Benardo LS, Masukawa LM, Prince DA (1982) Electrophysiology of isolated hippocampal pyramidal dendrites. J Neurosci 2:1614-1622.
Berger H (1933) Uber das Elektrenkephalogramm des Menschen Sechste Mitteilung. Zeitschrift für die gesamte Neurologie und Psychiatrie 99:555-574.
Bergmann TO, Mölle M, Diedrichs J, Born J, Siebner HR (2012) Sleep spindle-related reactivation of category-specific cortical regions after learning face-scene associations. Neuroimage 59:2733-2742.
Binder S, Baier PC, Mölle M, Inostroza M, Born J, Marshall L (2012) Sleep enhances memory consolidation in the hippocampus-dependent object-place recognition task in rats. Neurobiology of Learning and Memory 97:213-219.
Blake H, Gerard RW (1937) Brain potentials during sleep. Am J Physiol 119:692-703.
Blethyn KL, Hughes SW, Crunelli V (2008) Evidence for electrical synapses between neurons of the nucleus reticularis thalami in the adult brain in vitro. Thalamus & Related Systems 4:13-20.
Blethyn KL, Hughes SW, Toth TI, Cope DW, Crunelli V (2006) Neuronal basis of the slow (<1 Hz) oscillation in neurons of the nucleus reticularis thalami in vitro. J Neurosci 26:2474-2486.
Blitz DM, Foster KA, Regehr WG (2004) Short-term synaptic plasticity: a comparison of two synapses. Nature reviews 5:630-640.
Bonjean M, Baker T, Lemieux M, Timofeev I, Sejnowski T, Bazhenov M (2011) Corticothalamic Feedback Controls Sleep Spindle Duration In Vivo. The Journal of Neuroscience 31:9124-9134.

Bonjean M, Baker T, Bazhenov M, Cash S, Halgren E, Sejnowski T (2012) Interactions between Core and Matrix Thalamocortical Projections in Human Sleep Spindle Synchronization. The Journal of Neuroscience 32:5250-5263.

Borg-Graham LJ, Monier C, Fregnac Y (1998) Visual input evokes transient and strong shunting inhibition in visual cortical neurons. Nature 393:369-373.

Born J, Wilhelm I (2012) System consolidation of memory during sleep. Psychol Res 76:192-203.

Born J, Rasch B, Gais S (2006) Sleep to remember. Neuroscientist 12:410-424.

Borst JGG (2010) The low synaptic release probability in vivo. Trends in Neurosciences 33:259-266.

Boucetta S, Crochet S, Chauvette S, Seigneur J, Timofeev I ((in press)) Extracellular Ca^{2+} fluctuations in vivo affect afterhyperpolarization potential and modify firing patterns of neocortical neurons. Experimental Neurology.

Bouyer JJ, Montaron MF, Rougeul A (1981) Fast fronto-parietal rhythms during combined focused attentive behaviour and immobility in cat: cortical and thalamic localizations. Electroencephalogr Clin Neurophysiol 51:244-252.

Bragin A, Mody I, Wilson CL, Engel J, Jr. (2002) Local generation of fast ripples in epileptic brain. J Neurosci 22:2012-2021.

Bragin A, Engel J, Jr., Wilson CL, Fried I, Mathern GW (1999a) Hippocampal and entorhinal cortex high-frequency oscillations (100--500 Hz) in human epileptic brain and in kainic acid--treated rats with chronic seizures. Epilepsia 40:127-137.

Bragin A, Engel J, Jr., Wilson CL, Fried I, Buzsaki G (1999b) High-frequency oscillations in human brain. Hippocampus 9:137-142.

Branco T, Staras K (2009) The probability of neurotransmitter release: variability and feedback control at single synapses. Nature reviews 10:373-383.

Bressler SL (1990) The gamma wave: a cortical information carrier? Trends Neurosci 13:161-162.

Brumberg JC, Nowak LG, McCormick DA (2000) Ionic mechanisms underlying repetitive high-frequency burst firing in supragranular cortical neurons. J Neurosci 20:4829-4843.

Budde T, Biella G, Munsch T, Pape HC (1997) Lack of regulation by intracellular Ca2+ of the hyperpolarization-activated cation current in rat thalamic neurones. The Journal of physiology 503 (Pt 1):79-85.

Buhl EH, Tamas G, Szilagyi T, Stricker C, Paulsen O, Somogyi P (1997) Effect, number and location of synapses made by single pyramidal cells onto aspiny interneurones of cat visual cortex. The Journal of physiology 500 (Pt 3):689-713.

Buonomano DV (1999) Distinct functional types of associative long-term potentiation in neocortical and hippocampal pyramidal neurons. J Neurosci 19:6748-6754.

Buxhoeveden DP, Casanova MF (2002a) The minicolumn and evolution of the brain. Brain Behav Evol 60:125-151.

Buxhoeveden DP, Casanova MF (2002b) The minicolumn hypothesis in neuroscience. Brain 125:935-951.

Buzsaki G (1989) Two-stage model of memory trace formation: a role for "noisy" brain states. Neuroscience 31:551-570.

Buzsaki G (1998) Memory consolidation during sleep: a neurophysiological perspective. Journal of sleep research 7 Suppl 1:17-23.

Calvin WH, Sypert GW (1976) Fast and slow pyramidal tract neurons: an intracellular analysis of their contrasting repetitive firing properties in the cat. Journal of neurophysiology 39:420-434.

Cardin JA, Palmer LA, Contreras D (2005) Stimulus-dependent gamma (30-50 Hz) oscillations in simple and complex fast rhythmic bursting cells in primary visual cortex. J Neurosci 25:5339-5350.

Cash SS, Halgren E, Dehghani N, Rossetti AO, Thesen T, Wang C, Devinsky O, Kuzniecky R, Doyle W, Madsen JR, Bromfield E, Eross L, Halasz P, Karmos G, Csercsa R, Wittner L, Ulbert I (2009) The human K-complex represents an isolated cortical down-state. Science (New York, NY 324:1084-1087.

Castelo-Branco M, Neuenschwander S, Singer W (1998) Synchronization of visual responses between the cortex, lateral geniculate nucleus, and retina in the anesthetized cat. J Neurosci 18:6395-6410.

Castillo PE (2011) Presynaptic LTP and LTD of Excitatory and Inhibitory Synapses. Cold Spring Harbor Perspectives in Biology.

Castro-Alamancos MA, Connors BW (1996a) Short-term plasticity of a thalamocortical pathway dynamically modulated by behavioral state. Science (New York, NY 272:274-277.

Castro-Alamancos MA, Connors BW (1996b) Cellular mechanisms of the augmenting response: short-term plasticity in a thalamocortical pathway. J Neurosci 16:7742-7756.

Chagnac-Amitai Y, Luhmann HJ, Prince DA (1990) Burst generating and regular spiking layer 5 pyramidal neurons of rat neocortex have different morphological features. The Journal of comparative neurology 296:598-613.

Chauvette S, Volgushev M, Timofeev I (2010) Origin of Active States in Local Neocortical Networks during Slow Sleep Oscillation. Cerebral Cortex 20:2660-2674.

Chauvette S, Seigneur J, Timofeev I (2012) Sleep Oscillations in the Thalamocortical System Induce Long-Term Neuronal Plasticity. Neuron 75:1105-1113.

Chauvette S, Volgushev M, Mukovski M, Timofeev I (2007) Local origin and long-range synchrony of active state in neocortex during slow oscillation. In: Mechanisms of spontaneous active states in the neocortex (Timofeev I, ed), pp 73-92. Kerala, India: Research Signpost.

Chauvette S, Crochet S, Volgushev M, Timofeev I (2011) Properties of Slow Oscillation during Slow-Wave Sleep and Anesthesia in Cats. The Journal of Neuroscience 31:14998-15008.

Chen C, Blitz DM, Regehr WG (2002) Contributions of receptor desensitization and saturation to plasticity at the retinogeniculate synapse. Neuron 33:779-788.

Chen J-Y, Chauvette S, Skorheim S, Timofeev I, Bazhenov M (2012) Interneuron-mediated inhibition synchronizes neuronal activity during slow oscillation. The Journal of physiology 590:3987-4010.

Chevaleyre V, Takahashi KA, Castillo PE (2006) Endocannabinoid-mediated synaptic plasticity in the CNS. Annu Rev Neurosci 29:37-76.

Chistiakova M, Volgushev M (2009) Heterosynaptic plasticity in the neocortex. Experimental Brain Research 199:377-390.

Chrobak JJ, Buzsaki G (1996) High-frequency oscillations in the output networks of the hippocampal-entorhinal axis of the freely behaving rat. J Neurosci 16:3056-3066.

Cirelli C, Tononi G (2000a) Differential expression of plasticity-related genes in waking and sleep and their regulation by the noradrenergic system. J Neurosci 20:9187-9194.
Cirelli C, Tononi G (2000b) Gene expression in the brain across the sleep-waking cycle. Brain research 885:303-321.
Cirelli C, Pompeiano M, Tononi G (1996) Neuronal gene expression in the waking state: a role for the locus coeruleus. Science (New York, NY 274:1211-1215.
Cirelli C, Gutierrez CM, Tononi G (2004) Extensive and divergent effects of sleep and wakefulness on brain gene expression. Neuron 41:35-43.
Cirelli C, Huber R, Gopalakrishnan A, Southard TL, Tononi G (2005) Locus ceruleus control of slow-wave homeostasis. J Neurosci 25:4503-4511.
Cisse Y, Grenier F, Timofeev I, Steriade M (2003) Electrophysiological properties and input-output organization of callosal neurons in cat association cortex. Journal of neurophysiology 89:1402-1413.
Cisse Y, Crochet S, Timofeev I, Steriade M (2004) Synaptic enhancement induced through callosal pathways in cat association cortex. Journal of neurophysiology 92:3221-3232.
Clemens Z, Fabo D, Halasz P (2005) Overnight verbal memory retention correlates with the number of sleep spindles. Neuroscience 132:529-535.
Clemens Z, Molle M, Eross L, Jakus R, Rasonyi G, Halasz P, Born J (2011) Fine-tuned coupling between human parahippocampal ripples and sleep spindles. The European journal of neuroscience 33:511-520.
Collingridge GL, Isaac JT, Wang YT (2004) Receptor trafficking and synaptic plasticity. Nature reviews 5:952-962.
Collins DR, Lang EJ, Pare D (1999) Spontaneous activity of the perirhinal cortex in behaving cats. Neuroscience 89:1025-1039.
Connors BW, Gutnick MJ (1990) Intrinsic firing patterns of diverse neocortical neurons. Trends Neurosci 13:99-104.
Connors BW, Gutnick MJ, Prince DA (1982) Electrophysiological properties of neocortical neurons in vitro. Journal of neurophysiology 48:1302-1320.
Contreras D, Steriade M (1995) Cellular basis of EEG slow rhythms: a study of dynamic corticothalamic relationships. J Neurosci 15:604-622.
Contreras D, Llinas R (2001) Voltage-sensitive dye imaging of neocortical spatiotemporal dynamics to afferent activation frequency. J Neurosci 21:9403-9413.
Contreras D, Timofeev I, Steriade M (1996a) Mechanisms of long-lasting hyperpolarizations underlying slow sleep oscillations in cat corticothalamic networks. The Journal of physiology 494 (Pt 1):251-264.
Contreras D, Destexhe A, Steriade M (1997) Intracellular and computational characterization of the intracortical inhibitory control of synchronized thalamic inputs in vivo. Journal of neurophysiology 78:335-350.
Contreras D, Destexhe A, Sejnowski TJ, Steriade M (1996b) Control of spatiotemporal coherence of a thalamic oscillation by corticothalamic feedback. Science (New York, NY 274:771-774.
Cragg BG (1967) The density of synapses and neurones in the motor and visual areas of the cerebral cortex. J Anat 101:639-654.
Creutzfeldt OD (1995) Cortex cerebri : performance, structural, and functional organization of the cortex. New York: Oxford University Press.

Crill WE (1996) Persistent sodium current in mammalian central neurons. Annu Rev Physiol 58:349-362.
Crochet S, Petersen CC (2006) Correlating whisker behavior with membrane potential in barrel cortex of awake mice. Nature neuroscience 9:608-610.
Crochet S, Chauvette S, Boucetta S, Timofeev I (2005) Modulation of synaptic transmission in neocortex by network activities. The European journal of neuroscience 21:1030-1044.
Crochet S, Fuentealba P, Cisse Y, Timofeev I, Steriade M (2006) Synaptic plasticity in local cortical network in vivo and its modulation by the level of neuronal activity. Cereb Cortex 16:618-631.
Csercsa R et al. (2010) Laminar analysis of slow wave activity in humans. Brain 133:2814-2829.
Csicsvari J, Hirase H, Czurko A, Mamiya A, Buzsaki G (1999a) Fast network oscillations in the hippocampal CA1 region of the behaving rat. J Neurosci 19:RC20.
Csicsvari J, Hirase H, Czurko A, Mamiya A, Buzsaki G (1999b) Oscillatory coupling of hippocampal pyramidal cells and interneurons in the behaving Rat. J Neurosci 19:274-287.
Cunningham MO, Whittington MA, Bibbig A, Roopun A, LeBeau FE, Vogt A, Monyer H, Buhl EH, Traub RD (2004) A role for fast rhythmic bursting neurons in cortical gamma oscillations in vitro. Proceedings of the National Academy of Sciences of the United States of America 101:7152-7157.
Czarnecki A, Birtoli B, Ulrich D (2007) Cellular mechanisms of burst firing-mediated long-term depression in rat neocortical pyramidal cells. The Journal of physiology 578:471-479.
De Gennaro L, Ferrara M (2003) Sleep spindles: an overview. Sleep Medicine Reviews 7:423-440.
DeFelipe J, Farinas I (1992) The pyramidal neuron of the cerebral cortex: morphological and chemical characteristics of the synaptic inputs. Prog Neurobiol 39:563-607.
Destexhe A, Contreras D, Sejnowski TJ, Steriade M (1994) A model of spindle rhythmicity in the isolated thalamic reticular nucleus. Journal of neurophysiology 72:803-818.
Destexhe A, Hughes SW, Rudolph M, Crunelli V (2007) Are corticothalamic 'up' states fragments of wakefulness? Trends Neurosci 30:334-342.
Diekelmann S, Born J (2010) The memory function of sleep. Nature reviews 11:114-126.
Djonlagic I, Saboisky J, Carusona A, Stickgold R, Malhotra A (2012) Increased Sleep Fragmentation Leads to Impaired Off-Line Consolidation of Motor Memories in Humans. PloS one 7:e34106.
Dossi RC, Nunez A, Steriade M (1992) Electrophysiology of a slow (0.5-4 Hz) intrinsic oscillation of cat thalamocortical neurones in vivo. The Journal of physiology 447:215-234.
Douglas RJ, Martin KA (2004) Neuronal circuits of the neocortex. Annu Rev Neurosci 27:419-451.
Douglas RJ, Martin KA (2007) Recurrent neuronal circuits in the neocortex. Curr Biol 17:R496-500.
Doyon J, Benali H (2005) Reorganization and plasticity in the adult brain during learning of motor skills. Curr Opin Neurobiol 15:161-167.
Draguhn A, Traub RD, Schmitz D, Jefferys JG (1998) Electrical coupling underlies high-frequency oscillations in the hippocampus in vitro. Nature 394:189-192.

Eder M, Zieglgansberger W, Dodt HU (2002) Neocortical long-term potentiation and long-term depression: site of expression investigated by infrared-guided laser stimulation. J Neurosci 22:7558-7568.

Egger V, Feldmeyer D, Sakmann B (1999) Coincidence detection and changes of synaptic efficacy in spiny stellate neurons in rat barrel cortex. Nature neuroscience 2:1098-1105.

Ego-Stengel V, Wilson MA (2010) Disruption of ripple-associated hippocampal activity during rest impairs spatial learning in the rat. Hippocampus 20:1-10.

Eschenko O, Molle M, Born J, Sara SJ (2006) Elevated sleep spindle density after learning or after retrieval in rats. J Neurosci 26:12914-12920.

Eschenko O, Magri C, Panzeri S, Sara SJ (2012) Noradrenergic Neurons of the Locus Coeruleus Are Phase Locked to Cortical Up-Down States during Sleep. Cerebral Cortex 22:426-435.

Euston DR, Tatsuno M, McNaughton BL (2007) Fast-forward playback of recent memory sequences in prefrontal cortex during sleep. Science (New York, NY 318:1147-1150.

Faraguna U, Vyazovskiy VV, Nelson AB, Tononi G, Cirelli C (2008) A causal role for brain-derived neurotrophic factor in the homeostatic regulation of sleep. J Neurosci 28:4088-4095.

Feldman DE (2009) Synaptic Mechanisms for Plasticity in Neocortex. Annual Review of Neuroscience 32:33-55.

Feldmeyer D, Egger V, Lubke J, Sakmann B (1999) Reliable synaptic connections between pairs of excitatory layer 4 neurones within a single 'barrel' of developing rat somatosensory cortex. The Journal of physiology 521 Pt 1:169-190.

Ferecsko AS, Seigneur J, Chauvette S, Kovacs K, Lajeunesse F, Sik A, Timofeev I (in preparation for submission) Low-threshold calcium spike dependent gating in thalamus.

Fioravante D, Regehr WG (2011) Short-term forms of presynaptic plasticity. Current Opinion in Neurobiology 21:269-274.

Fischer S, Hallschmid M, Elsner AL, Born J (2002) Sleep forms memory for finger skills. Proceedings of the National Academy of Sciences of the United States of America 99:11987-11991.

Fisher RS, Webber WR, Lesser RP, Arroyo S, Uematsu S (1992) High-frequency EEG activity at the start of seizures. J Clin Neurophysiol 9:441-448.

Fogel SM, Smith CT (2006) Learning-dependent changes in sleep spindles and Stage 2 sleep. Journal of sleep research 15:250-255.

Foster KA, Kreitzer AC, Regehr WG (2002) Interaction of postsynaptic receptor saturation with presynaptic mechanisms produces a reliable synapse. Neuron 36:1115-1126.

Freeman WJ (1991) The physiology of perception. Sci Am 264:78-85.

Fries P, Nikolic D, Singer W (2007) The gamma cycle. Trends Neurosci 30:309-316.

Fuentealba P, Timofeev I, Bazhenov M, Sejnowski TJ, Steriade M (2005) Membrane bistability in thalamic reticular neurons during spindle oscillations. Journal of neurophysiology 93:294-304.

Fuentealba P, Crochet S, Timofeev I, Bazhenov M, Sejnowski TJ, Steriade M (2004) Experimental evidence and modeling studies support a synchronizing role for electrical coupling in the cat thalamic reticular neurons in vivo. The European journal of neuroscience 20:111-119.

Gais S, Born J (2004a) Low acetylcholine during slow-wave sleep is critical for declarative memory consolidation. Proceedings of the National Academy of Sciences of the United States of America 101:2140-2144.
Gais S, Born J (2004b) Declarative memory consolidation: mechanisms acting during human sleep. Learn Mem 11:679-685.
Gais S, Molle M, Helms K, Born J (2002) Learning-dependent increases in sleep spindle density. J Neurosci 22:6830-6834.
Gais S, Rasch B, Wagner U, Born J (2008) Visual-procedural memory consolidation during sleep blocked by glutamatergic receptor antagonists. J Neurosci 28:5513-5518.
Galarreta M, Hestrin S (1999) A network of fast-spiking cells in the neocortex connected by electrical synapses. Nature 402:72-75.
Galarreta M, Hestrin S (2001a) Electrical synapses between GABA-releasing interneurons. Nature reviews 2:425-433.
Galarreta M, Hestrin S (2001b) Spike transmission and synchrony detection in networks of GABAergic interneurons. Science (New York, NY 292:2295-2299.
Gentet LJ, Avermann M, Matyas F, Staiger JF, Petersen CC (2010) Membrane potential dynamics of GABAergic neurons in the barrel cortex of behaving mice. Neuron 65:422-435.
Gibson JR, Beierlein M, Connors BW (1999) Two networks of electrically coupled inhibitory neurons in neocortex. Nature 402:75-79.
Gibson JR, Beierlein M, Connors BW (2005) Functional properties of electrical synapses between inhibitory interneurons of neocortical layer 4. Journal of neurophysiology 93:467-480.
Girardeau G, Benchenane K, Wiener SI, Buzsaki G, Zugaro MB (2009) Selective suppression of hippocampal ripples impairs spatial memory. Nature neuroscience 12:1222-1223.
Golshani P, Liu XB, Jones EG (2001) Differences in quantal amplitude reflect GluR4-subunit number at corticothalamic synapses on two populations of thalamic neurons. Proceedings of the National Academy of Sciences of the United States of America 98:4172-4177.
Gray CM, McCormick DA (1996) Chattering cells: superficial pyramidal neurons contributing to the generation of synchronous oscillations in the visual cortex. Science (New York, NY 274:109-113.
Gray CM, Konig P, Engel AK, Singer W (1989) Oscillatory responses in cat visual cortex exhibit inter-columnar synchronization which reflects global stimulus properties. Nature 338:334-337.
Greene CM, Bellgrove MA, Gill M, Robertson IH (2009) Noradrenergic genotype predicts lapses in sustained attention. Neuropsychologia 47:591-594.
Grenier F, Timofeev I, Steriade M (2001) Focal synchronization of ripples (80-200 Hz) in neocortex and their neuronal correlates. Journal of neurophysiology 86:1884-1898.
Grenier F, Timofeev I, Steriade M (2003a) Neocortical very fast oscillations (ripples, 80-200 Hz) during seizures: intracellular correlates. Journal of neurophysiology 89:841-852.
Grenier F, Timofeev I, Crochet S, Steriade M (2003b) Spontaneous field potentials influence the activity of neocortical neurons during paroxysmal activities in vivo. Neuroscience 119:277-291.

Groh A, de Kock CP, Wimmer VC, Sakmann B, Kuner T (2008) Driver or coincidence detector: modal switch of a corticothalamic giant synapse controlled by spontaneous activity and short-term depression. J Neurosci 28:9652-9663.

Gruner JE, Hirsch JC, Sotelo C (1974) Ultrastructural features of the isolated suprasylvian gyrus in the cat. The Journal of comparative neurology 154:1-27.

Hale MW, Lowry CA (2011) Functional topography of midbrain and pontine serotonergic systems: implications for synaptic regulation of serotonergic circuits. Psychopharmacology (Berl) 213:243-264.

Hanlon EC, Faraguna U, Vyazovskiy VV, Tononi G, Cirelli C (2009) Effects of skilled training on sleep slow wave activity and cortical gene expression in the rat. Sleep 32:719-729.

Hanlon EC, Vyazovskiy VV, Faraguna U, Tononi G, Cirelli C (2011) Synaptic Potentiation and Sleep Need: Clues from Molecular and Electrophysiological Studies. Current Topics in Medicinal Chemistry 11:2472-2482.

Hasselmo ME (1999) Neuromodulation: acetylcholine and memory consolidation. Trends Cogn Sci 3:351-359.

Hasselmo ME, McGaughy J (2004) High acetylcholine levels set circuit dynamics for attention and encoding and low acetylcholine levels set dynamics for consolidation. Prog Brain Res 145:207-231.

Hassler R, Muhs-Clement K (1964) Architektonisjer Aufbau des sensorimotorischen und parietalen cortex der Katze. j Hirnforschung 6:377-422.

Heinemann U, Lux HD, Gutnick MJ (1977) Extracellular free calcium and potassium during paroxsmal activity in the cerebral cortex of the cat. Exp Brain Res 27:237-243.

Hirsch JA, Alonso JM, Reid RC, Martinez LM (1998) Synaptic integration in striate cortical simple cells. J Neurosci 18:9517-9528.

Holz J, Piosczyk H, Feige B, Spiegelhalder KAI, Baglioni C, Riemann D, Nissen C (2012) EEG sigma and slow-wave activity during NREM sleep correlate with overnight declarative and procedural memory consolidation. Journal of sleep research:no-no.

Houser CR, Vaughn JE, Barber RP, Roberts E (1980) GABA neurons are the major cell type of the nucleus reticularis thalami. Brain research 200:341-354.

Houweling AR, Bazhenov M, Timofeev I, Steriade M, Sejnowski TJ (1999) Cortical and thalamic components of augmenting responses: A modeling study. Neurocomputing 26–27:735-742.

Houweling AR, Bazhenov M, Timofeev I, Grenier F, Steriade M, Sejnowski TJ (2002) Frequency-selective augmenting responses by short-term synaptic depression in cat neocortex. The Journal of physiology 542:599-617.

Huber R, Ghilardi MF, Massimini M, Tononi G (2004) Local sleep and learning. Nature 430:78-81.

Huber R, Ghilardi MF, Massimini M, Ferrarelli F, Riedner BA, Peterson MJ, Tononi G (2006) Arm immobilization causes cortical plastic changes and locally decreases sleep slow wave activity. Nature neuroscience 9:1169-1176.

Hughes SW, Blethyn KL, Cope DW, Crunelli V (2002) Properties and origin of spikelets in thalamocortical neurones in vitro. Neuroscience 110:395-401.

Huguenard JR (1996) Low-threshold calcium currents in central nervous system neurons. Annu Rev Physiol 58:329-348.

Isomura Y, Sirota A, Ozen S, Montgomery S, Mizuseki K, Henze DA, Buzsaki G (2006) Integration and segregation of activity in entorhinal-hippocampal subregions by neocortical slow oscillations. Neuron 52:871-882.

Jahnsen H, Llinas R (1984) Electrophysiological properties of guinea-pig thalamic neurones: an in vitro study. The Journal of physiology 349:205-226.

Jankel WR, Niedermeyer E (1985) Sleep spindles. J Clin Neurophysiol 2:1-35.

Jenkins JG, Dallenbach KM (1924) Obliviscence during Sleep and Waking. The American Journal of Psychology 35:605-612.

Ji D, Wilson MA (2007) Coordinated memory replay in the visual cortex and hippocampus during sleep. Nature neuroscience 10:100-107.

Joliot M, Ribary U, Llinas R (1994) Human oscillatory brain activity near 40 Hz coexists with cognitive temporal binding. Proceedings of the National Academy of Sciences of the United States of America 91:11748-11751.

Jones EG (1985) The thalamus. New York: Plenum.

Jones EG (2001) The thalamic matrix and thalamocortical synchrony. Trends Neurosci 24:595-601.

Jones EG (2002) Thalamic circuitry and thalamocortical synchrony. Philos Trans R Soc Lond B Biol Sci 357:1659-1673.

Jones EG (2007) The Thalamus, 2nd Edition. New York: Cambridge University Press.

Jones MS, Barth DS (1999) Spatiotemporal organization of fast (>200 Hz) electrical oscillations in rat Vibrissa/Barrel cortex. Journal of neurophysiology 82:1599-1609.

Jones MS, MacDonald KD, Choi B, Dudek FE, Barth DS (2000) Intracellular correlates of fast (>200 Hz) electrical oscillations in rat somatosensory cortex. Journal of neurophysiology 84:1505-1518.

Jones MV, Westbrook GL (1996) The impact of receptor desensitization on fast synaptic transmission. Trends Neurosci 19:96-101.

Kaas JH (2012) Evolution of columns, modules, and domains in the neocortex of primates. Proceedings of the National Academy of Sciences 109:10655-10660.

Kandel A, Buzsaki G (1997) Cellular-synaptic generation of sleep spindles, spike-and-wave discharges, and evoked thalamocortical responses in the neocortex of the rat. J Neurosci 17:6783-6797.

Kandel ER, Spencer WA (1961) Electrophysiology of hippocampal neurons. II. After-potentials and repetitive firing. Journal of neurophysiology 24:243-259.

Kattler H, Dijk DJ, Borbely AA (1994) Effect of unilateral somatosensory stimulation prior to sleep on the sleep EEG in humans. Journal of sleep research 3:159-164.

Kim U, Bal T, McCormick DA (1995) Spindle waves are propagating synchronized oscillations in the ferret LGNd in vitro. Journal of neurophysiology 74:1301-1323.

Knott GW, Quairiaux C, Genoud C, Welker E (2002) Formation of dendritic spines with GABAergic synapses induced by whisker stimulation in adult mice. Neuron 34:265-273.

Korman M, Doyon J, Doljansky J, Carrier J, Dagan Y, Karni A (2007) Daytime sleep condenses the time course of motor memory consolidation. Nature neuroscience 10:1206-1213.

Krimer LS, Goldman-Rakic PS (2001) Prefrontal microcircuits: membrane properties and excitatory input of local, medium, and wide arbor interneurons. J Neurosci 21:3788-3796.

Kurth S, Ringli M, Geiger A, LeBourgeois M, Jenni OG, Huber R (2010) Mapping of Cortical Activity in the First Two Decades of Life: A High-Density Sleep Electroencephalogram Study. J Neurosci 30:13211-13219.

Lahl O, Wispel C, Willigens B, Pietrowsky R (2008) An ultra short episode of sleep is sufficient to promote declarative memory performance. Journal of sleep research 17:3-10.

Landisman CE, Long MA, Beierlein M, Deans MR, Paul DL, Connors BW (2002) Electrical synapses in the thalamic reticular nucleus. J Neurosci 22:1002-1009.

Larkum ME, Zhu JJ (2002) Signaling of layer 1 and whisker-evoked Ca2+ and Na+ action potentials in distal and terminal dendrites of rat neocortical pyramidal neurons in vitro and in vivo. J Neurosci 22:6991-7005.

Leresche N, Lightowler S, Soltesz I, Jassik-Gerschenfeld D, Crunelli V (1991) Low-frequency oscillatory activities intrinsic to rat and cat thalamocortical cells. The Journal of physiology 441:155-174.

Lisman J, Yasuda R, Raghavachari S (2012) Mechanisms of CaMKII action in long-term potentiation. Nature reviews 13:169-182.

Liu XB, Jones EG (1999) Predominance of corticothalamic synaptic inputs to thalamic reticular nucleus neurons in the rat. The Journal of comparative neurology 414:67-79.

Liu XB, Honda CN, Jones EG (1995a) Distribution of four types of synapse on physiologically identified relay neurons in the ventral posterior thalamic nucleus of the cat. The Journal of comparative neurology 352:69-91.

Liu XB, Warren RA, Jones EG (1995b) Synaptic distribution of afferents from reticular nucleus in ventroposterior nucleus of cat thalamus. The Journal of comparative neurology 352:187-202.

Llinas R, Jahnsen H (1982) Electrophysiology of mammalian thalamic neurones in vitro. Nature 297:406-408.

Llinas R, Ribary U (1993) Coherent 40-Hz oscillation characterizes dream state in humans. Proceedings of the National Academy of Sciences of the United States of America 90:2078-2081.

Llinas RR (1988) The intrinsic electrophysiological properties of mammalian neurons: insights into central nervous system function. Science (New York, NY 242:1654-1664.

Loomis AL, Harvey EN, Hobart G (1935) Potential Rhythms of the Cerebral Cortex during Sleep. Science (New York, NY 81:597-598.

Luthi A, Bal T, McCormick DA (1998) Periodicity of thalamic spindle waves is abolished by ZD7288,a blocker of Ih. Journal of neurophysiology 79:3284-3289.

Lytton WW, Sejnowski TJ (1991) Simulations of cortical pyramidal neurons synchronized by inhibitory interneurons. Journal of neurophysiology 66:1059-1079.

Magee JC, Johnston D (1995) Synaptic activation of voltage-gated channels in the dendrites of hippocampal pyramidal neurons. Science (New York, NY 268:301-304.

Malenka RC, Bear MF (2004) LTP and LTD: An Embarrassment of Riches. Neuron 44:5-21.

Malinow R, Malenka RC (2002) AMPA receptor trafficking and synaptic plasticity. Annu Rev Neurosci 25:103-126.

Markram H, Tsodyks M (1996) Redistribution of synaptic efficacy between neocortical pyramidal neurons. Nature 382:807-810.
Markram H, Lubke J, Frotscher M, Sakmann B (1997a) Regulation of synaptic efficacy by coincidence of postsynaptic APs and EPSPs. Science (New York, NY 275:213-215.
Markram H, Lubke J, Frotscher M, Roth A, Sakmann B (1997b) Physiology and anatomy of synaptic connections between thick tufted pyramidal neurones in the developing rat neocortex. The Journal of physiology 500 (Pt 2):409-440.
Markram H, Toledo-Rodriguez M, Wang Y, Gupta A, Silberberg G, Wu C (2004) Interneurons of the neocortical inhibitory system. Nature reviews 5:793-807.
Marshall L, Born J (2007) The contribution of sleep to hippocampus-dependent memory consolidation. Trends Cogn Sci 11:442-450.
Marshall L, Helgadottir H, Molle M, Born J (2006) Boosting slow oscillations during sleep potentiates memory. Nature 444:610-613.
Massimini M, Amzica F (2001) Extracellular calcium fluctuations and intracellular potentials in the cortex during the slow sleep oscillation. Journal of neurophysiology 85:1346-1350.
Massimini M, Huber R, Ferrarelli F, Hill S, Tononi G (2004) The sleep slow oscillation as a traveling wave. J Neurosci 24:6862-6870.
Matsumura M (1979) Intracellular synaptic potentials of primate motor cortex neurons during voluntary movement. Brain research 163:33-48.
Matveev V, Zucker RS, Sherman A (2004) Facilitation through buffer saturation: constraints on endogenous buffering properties. Biophys J 86:2691-2709.
McCormick DA (1992) Neurotransmitter actions in the thalamus and cerebral cortex and their role in neuromodulation of thalamocortical activity. Prog Neurobiol 39:337-388.
McCormick DA, Pape HC (1990) Properties of a hyperpolarization-activated cation current and its role in rhythmic oscillation in thalamic relay neurones. The Journal of physiology 431:291-318.
McCormick DA, Bal T (1997) Sleep and arousal: thalamocortical mechanisms. Annu Rev Neurosci 20:185-215.
McCormick DA, Connors BW, Lighthall JW, Prince DA (1985) Comparative electrophysiology of pyramidal and sparsely spiny stellate neurons of the neocortex. Journal of neurophysiology 54:782-806.
Mednick S, Nakayama K, Stickgold R (2003) Sleep-dependent learning: a nap is as good as a night. Nature neuroscience 6:697-698.
Mednick SC, Nakayama K, Cantero JL, Atienza M, Levin AA, Pathak N, Stickgold R (2002) The restorative effect of naps on perceptual deterioration. Nature neuroscience 5:677-681.
Meier-Koll A, Bussmann B, Schmidt C, Neuschwander D (1999) Walking through a maze alters the architecture of sleep. Percept Mot Skills 88:1141-1159.
Metherate R, Ashe JH (1993) Ionic flux contributions to neocortical slow waves and nucleus basalis-mediated activation: whole-cell recordings in vivo. J Neurosci 13:5312-5323.
Metherate R, Cox CL, Ashe JH (1992) Cellular bases of neocortical activation: modulation of neural oscillations by the nucleus basalis and endogenous acetylcholine. J Neurosci 12:4701-4711.

Molle M, Born J (2009) Hippocampus whispering in deep sleep to prefrontal cortex--for good memories? Neuron 61:496-498.
Molle M, Marshall L, Gais S, Born J (2002) Grouping of spindle activity during slow oscillations in human non-rapid eye movement sleep. J Neurosci 22:10941-10947.
Molle M, Bergmann TO, Marshall L, Born J (2011) Fast and slow spindles during the sleep slow oscillation: disparate coalescence and engagement in memory processing. Sleep 34:1411-1421.
Molle M, Yeshenko O, Marshall L, Sara SJ, Born J (2006) Hippocampal sharp wave-ripples linked to slow oscillations in rat slow-wave sleep. Journal of neurophysiology 96:62-70.
Mölle M, Born J (2011) Slow oscillations orchestrating fast oscillations and memory consolidation. In: Progress in Brain Research (Eus J.W. Van Someren YDVDWPRRHDM, Fernando HLDS, eds), pp 93-110: Elsevier.
Morin A, Doyon J, Dostie V, Barakat M, Hadj Tahar A, Korman M, Benali H, Karni A, Ungerleider LG, Carrier J (2008) Motor sequence learning increases sleep spindles and fast frequencies in post-training sleep. Sleep 31:1149-1156.
Morison RS, Dempsey EW (1942) A study of thalamo-cortical relations. Am J Physiol 135:281-292.
Morison RS, Bassett DL (1945) Electrical activity of the thalamus and basal ganglia in decorticate cats. Journal of neurophysiology 8:309-314.
Mountcastle VB (1957) Modality and topographic properties of single neurons of cat's somatic sensory cortex. Journal of neurophysiology 20:408-434.
Mountcastle VB (1997) The columnar organization of the neocortex. Brain 120 (Pt 4):701-722.
Mountcastle VB (1998) Perceptual Neuroscience, The cerebral cortex. Cambridge, Massachusetts: Harvard University Press.
Mukovski M, Chauvette S, Timofeev I, Volgushev M (2007) Detection of active and silent states in neocortical neurons from the field potential signal during slow-wave sleep. Cereb Cortex 17:400-414.
Murthy VN, Fetz EE (1992) Coherent 25- to 35-Hz oscillations in the sensorimotor cortex of awake behaving monkeys. Proceedings of the National Academy of Sciences of the United States of America 89:5670-5674.
Nadasdy Z, Hirase H, Czurko A, Csicsvari J, Buzsaki G (1999) Replay and time compression of recurring spike sequences in the hippocampus. J Neurosci 19:9497-9507.
Neher E (1998) Vesicle pools and Ca2+ microdomains: new tools for understanding their roles in neurotransmitter release. Neuron 20:389-399.
Neher E, Sakaba T (2008) Multiple roles of calcium ions in the regulation of neurotransmitter release. Neuron 59:861-872.
Nishida M, Walker MP (2007) Daytime naps, motor memory consolidation and regionally specific sleep spindles. PloS one 2:e341.
Nishida M, Pearsall J, Buckner RL, Walker MP (2009) REM sleep, prefrontal theta, and the consolidation of human emotional memory. Cereb Cortex 19:1158-1166.
Nishikawa K, MacIver MB (2000) Excitatory synaptic transmission mediated by NMDA receptors is more sensitive to isoflurane than are non-NMDA receptor-mediated responses. Anesthesiology 92:228-236.

Nita DA, Vanhatalo S, Lafortune FD, Voipio J, Kaila K, Amzica F (2004) Nonneuronal origin of CO2-related DC EEG shifts: an in vivo study in the cat. Journal of neurophysiology 92:1011-1022.

Noda H, Adey WR (1970) Firing of neuron pairs in cat association cortex during sleep and wakefulness. Journal of neurophysiology 33:672-684.

Nunez A, Amzica F, Steriade M (1993) Electrophysiology of cat association cortical cells in vivo: intrinsic properties and synaptic responses. Journal of neurophysiology 70:418-430.

O'Neill J, Pleydell-Bouverie B, Dupret D, Csicsvari J (2010) Play it again: reactivation of waking experience and memory. Trends Neurosci 33:220-229.

Oertel WH, Graybiel AM, Mugnaini E, Elde RP, Schmechel DE, Kopin IJ (1983) Coexistence of glutamic acid decarboxylase- and somatostatin-like immunoreactivity in neurons of the feline nucleus reticularis thalami. J Neurosci 3:1322-1332.

Okun M, Naim A, Lampl I (2010) The subthreshold relation between cortical local field potential and neuronal firing unveiled by intracellular recordings in awake rats. J Neurosci 30:4440-4448.

Palva JM, Lamsa K, Lauri SE, Rauvala H, Kaila K, Taira T (2000) Fast network oscillations in the newborn rat hippocampus in vitro. J Neurosci 20:1170-1178.

Pape HC (1996) Queer current and pacemaker: the hyperpolarization-activated cation current in neurons. Annu Rev Physiol 58:299-327.

Payne JD, Stickgold R, Swanberg K, Kensinger EA (2008) Sleep preferentially enhances memory for emotional components of scenes. Psychol Sci 19:781-788.

Payne JD, Tucker MA, Ellenbogen JM, Wamsley EJ, Walker MP, Schacter DL, Stickgold R (2012) Memory for Semantically Related and Unrelated Declarative Information: The Benefit of Sleep, the Cost of Wake. PloS one 7:e33079.

Peigneux P, Laureys S, Fuchs S, Collette F, Perrin F, Reggers J, Phillips C, Degueldre C, Del Fiore G, Aerts J, Luxen A, Maquet P (2004) Are spatial memories strengthened in the human hippocampus during slow wave sleep? Neuron 44:535-545.

Peyrache A, Khamassi M, Benchenane K, Wiener SI, Battaglia FP (2009) Replay of rule-learning related neural patterns in the prefrontal cortex during sleep. Nature neuroscience 12:919-926.

Pfurtscheller G, Neuper C (1992) Simultaneous EEG 10 Hz desynchronization and 40 Hz synchronization during finger movements. Neuroreport 3:1057-1060.

Plihal W, Born J (1997) Effects of Early and Late Nocturnal Sleep on Declarative and Procedural Memory. Journal of Cognitive Neuroscience 9:534-547.

Porter LL, White EL (1986) Synaptic connections of callosal projection neurons in the vibrissal region of mouse primary motor cortex: an electron microscopic/horseradish peroxidase study. The Journal of comparative neurology 248:573-587.

Poulet JF, Petersen CC (2008) Internal brain state regulates membrane potential synchrony in barrel cortex of behaving mice. Nature 454:881-885.

Rall W (1977) Core conductor theoryand cable properties of neurons. In: Handbook of physiology, Sec 1, The nervous system (Kandel ER, ed), pp 39-97. Bethesda, MD: American Physiological Society.

Rasch B, Buchel C, Gais S, Born J (2007) Odor cues during slow-wave sleep prompt declarative memory consolidation. Science (New York, NY 315:1426-1429.

Rasch B, Pommer J, Diekelmann S, Born J (2009) Pharmacological REM sleep suppression paradoxically improves rather than impairs skill memory. Nature neuroscience 12:396-397.

Reig R, Sanchez-Vives MV (2007) Synaptic transmission and plasticity in an active cortical network. PloS one 2:e670.

Reig R, Gallego R, Nowak LG, Sanchez-Vives MV (2006) Impact of Cortical Network Activity on Short-term Synaptic Depression. Cereb Cortex 16:688-695.

Renger JJ, Hartman KN, Tsuchimoto Y, Yokoi M, Nakanishi S, Hensch TK (2002) Experience-dependent plasticity without long-term depression by type 2 metabotropic glutamate receptors in developing visual cortex. Proceedings of the National Academy of Sciences of the United States of America 99:1041-1046.

Ribeiro S, Goyal V, Mello CV, Pavlides C (1999) Brain gene expression during REM sleep depends on prior waking experience. Learn Mem 6:500-508.

Ribeiro S, Mello CV, Velho T, Gardner TJ, Jarvis ED, Pavlides C (2002) Induction of hippocampal long-term potentiation during waking leads to increased extrahippocampal zif-268 expression during ensuing rapid-eye-movement sleep. J Neurosci 22:10914-10923.

Ribeiro S, Gervasoni D, Soares ES, Zhou Y, Lin SC, Pantoja J, Lavine M, Nicolelis MA (2004) Long-lasting novelty-induced neuronal reverberation during slow-wave sleep in multiple forebrain areas. PLoS Biol 2:E24.

Ribeiro S, Shi X, Engelhard M, Zhou Y, Zhang H, Gervasoni D, Lin SC, Wada K, Lemos NA, Nicolelis MA (2007) Novel experience induces persistent sleep-dependent plasticity in the cortex but not in the hippocampus. Front Neurosci 1:43-55.

Riedner BA, Vyazovskiy VV, Huber R, Massimini M, Esser S, Murphy M, Tononi G (2007) Sleep homeostasis and cortical synchronization: III. A high-density EEG study of sleep slow waves in humans. Sleep 30:1643-1657.

Rizzoli SO, Betz WJ (2005) Synaptic vesicle pools. Nature reviews 6:57-69.

Rosanova M, Ulrich D (2005) Pattern-specific associative long-term potentiation induced by a sleep spindle-related spike train. J Neurosci 25:9398-9405.

Rougeul-Buser A, Bouyer JJ, Buser P (1975) From attentiveness to sleep. A topographical analysis of localized "synchronized" activities on the cortex of normal cat and monkey. Acta Neurobiol Exp (Wars) 35:805-819.

Rudolph M, Pospischil M, Timofeev I, Destexhe A (2007) Inhibition determines membrane potential dynamics and controls action potential generation in awake and sleeping cat cortex. J Neurosci 27:5280-5290.

Rulkov NF, Timofeev I, Bazhenov M (2004) Oscillations in large-scale cortical networks: map-based model. J Comput Neurosci 17:203-223.

Sakata S, Harris KD (2009) Laminar structure of spontaneous and sensory-evoked population activity in auditory cortex. Neuron 64:404-418.

Sanchez-Vives MV, McCormick DA (2000) Cellular and network mechanisms of rhythmic recurrent activity in neocortex. Nature neuroscience 3:1027-1034.

Sanchez-Vives MV, Reig R, Winograd M, Descalzo VF (2007) An active cortical network in vitro. In: Mechanisms of spontaneous actrive states in neocortex (Timofeev I, ed), pp 23-44. Kerala, India: Research Signpost.

Sanchez-Vives MV, Descalzo VF, Reig R, Figueroa NA, Compte A, Gallego R (2008) Rhythmic spontaneous activity in the piriform cortex. Cereb Cortex 18:1179-1192.

Scheibel ME, Scheibel AB (1966) The organization of the nucleus reticularis thalami: a Golgi study. Brain research 1:43-62.
Schmitz D, Schuchmann S, Fisahn A, Draguhn A, Buhl EH, Petrasch-Parwez E, Dermietzel R, Heinemann U, Traub RD (2001) Axo-axonal coupling. a novel mechanism for ultrafast neuronal communication. Neuron 31:831-840.
Schwindt PC, Crill WE (1995) Amplification of synaptic current by persistent sodium conductance in apical dendrite of neocortical neurons. Journal of neurophysiology 74:2220-2224.
Sejnowski TJ, Destexhe A (2000) Why do we sleep? Brain research 886:208-223.
Sheer DE (1989) Focused arousal and the cognitive 40-Hz event-related potentials: differential diagnosis of Alzheimer's disease. Prog Clin Biol Res 317:79-94.
Sherman SM (2005) Thalamic relays and cortical functioning. Prog Brain Res 149:107-126.
Siapas AG, Wilson MA (1998) Coordinated interactions between hippocampal ripples and cortical spindles during slow-wave sleep. Neuron 21:1123-1128.
Silva AJ (2003) Molecular and cellular cognitive studies of the role of synaptic plasticity in memory. J Neurobiol 54:224-237.
Singer W, Gray CM (1995) Visual feature integration and the temporal correlation hypothesis. Annu Rev Neurosci 18:555-586.
Sirota A, Csicsvari J, Buhl D, Buzsaki G (2003) Communication between neocortex and hippocampus during sleep in rodents. Proceedings of the National Academy of Sciences of the United States of America 100:2065-2069.
Soltesz I, Lightowler S, Leresche N, Jassik-Gerschenfeld D, Pollard CE, Crunelli V (1991) Two inward currents and the transformation of low-frequency oscillations of rat and cat thalamocortical cells. The Journal of physiology 441:175-197.
Somogyi P, Tamas G, Lujan R, Buhl EH (1998) Salient features of synaptic organisation in the cerebral cortex. Brain Res Brain Res Rev 26:113-135.
Spencer WA, Kandel ER (1961) Electrophysiology of hippocampal neurons IV. Fast prepotentials. Journal of neurophysiology 24:225-242.
Squire LR (1992) Memory and the hippocampus: a synthesis from findings with rats, monkeys, and humans. Psychol Rev 99:195-231.
Steriade M (1992) Basic mechanisms of sleep generation. Neurology 42:9-17; discussion 18.
Steriade M (2001a) The intact and sliced brain. In: The intact and sliced brain, The MIT Press Edition (press TM, ed), p 366. Cambridge, Massachusetts.
Steriade M (2001b) Impact of network activities on neuronal properties in corticothalamic systems. Journal of neurophysiology 86:1-39.
Steriade M (2004) Neocortical cell classes are flexible entities. Nature reviews 5:121-134.
Steriade M (2006) Grouping of brain rhythms in corticothalamic systems. Neuroscience 137:1087-1106.
Steriade M, Deschenes M (1984) The thalamus as a neuronal oscillator. Brain Research Reviews 8:1-63.
Steriade M, Llinas RR (1988) The functional states of the thalamus and the associated neuronal interplay. Physiol Rev 68:649-742.
Steriade M, Amzica F (1998) Coalescence of sleep rhythms and their chronology in corticothalamic networks. Sleep Res Online 1:1-10.

Steriade M, Timofeev I (2003) Neuronal plasticity in thalamocortical networks during sleep and waking oscillations. Neuron 37:563-576.
Steriade M, McCarley RW (2005) Brainstem Control of Wakefulness and Sleep. New York: Plenum.
Steriade M, Jones EG, Llinas R (1990) Thalamic oscillations and signaling. New York: John Wiley & Sons.
Steriade M, Nunez A, Amzica F (1993a) A novel slow (< 1 Hz) oscillation of neocortical neurons in vivo: depolarizing and hyperpolarizing components. J Neurosci 13:3252-3265.
Steriade M, McCormick DA, Sejnowski TJ (1993b) Thalamocortical oscillations in the sleeping and aroused brain. Science (New York, NY 262:679-685.
Steriade M, Amzica F, Contreras D (1996a) Synchronization of fast (30-40 Hz) spontaneous cortical rhythms during brain activation. J Neurosci 16:392-417.
Steriade M, Jones EG, McCormick DA (1997) Thalamus: organization and function. Kidlington, Oxford: Elsevier Science Ltd.
Steriade M, Timofeev I, Grenier F (2001) Natural waking and sleep states: a view from inside neocortical neurons. Journal of neurophysiology 85:1969-1985.
Steriade M, Deschenes M, Domich L, Mulle C (1985) Abolition of spindle oscillations in thalamic neurons disconnected from nucleus reticularis thalami. Journal of neurophysiology 54:1473-1497.
Steriade M, Domich L, Oakson G, Deschenes M (1987) The deafferented reticular thalamic nucleus generates spindle rhythmicity. Journal of neurophysiology 57:260-273.
Steriade M, Contreras D, Amzica F, Timofeev I (1996b) Synchronization of fast (30-40 Hz) spontaneous oscillations in intrathalamic and thalamocortical networks. J Neurosci 16:2788-2808.
Steriade M, Timofeev I, Grenier F, Durmuller N (1998a) Role of thalamic and cortical neurons in augmenting responses and self-sustained activity: dual intracellular recordings in vivo. J Neurosci 18:6425-6443.
Steriade M, Amzica F, Neckelmann D, Timofeev I (1998b) Spike-wave complexes and fast components of cortically generated seizures. II. Extra- and intracellular patterns. Journal of neurophysiology 80:1456-1479.
Steriade M, Timofeev I, Durmuller N, Grenier F (1998c) Dynamic properties of corticothalamic neurons and local cortical interneurons generating fast rhythmic (30-40 Hz) spike bursts. Journal of neurophysiology 79:483-490.
Stickgold R (2005) Sleep-dependent memory consolidation. Nature 437:1272-1278.
Stickgold R, James L, Hobson JA (2000) Visual discrimination learning requires sleep after training. Nature neuroscience 3:1237-1238.
Strecker RE, Morairty S, Thakkar MM, Porkka-Heiskanen T, Basheer R, Dauphin LJ, Rainnie DG, Portas CM, Greene RW, McCarley RW (2000) Adenosinergic modulation of basal forebrain and preoptic/anterior hypothalamic neuronal activity in the control of behavioral state. Behav Brain Res 115:183-204.
Stuart GJ, Hausser M (2001) Dendritic coincidence detection of EPSPs and action potentials. Nature neuroscience 4:63-71.
Sun Y, Olson R, Horning M, Armstrong N, Mayer M, Gouaux E (2002) Mechanism of glutamate receptor desensitization. Nature 417:245-253.
Sutherland GR, McNaughton B (2000) Memory trace reactivation in hippocampal and neocortical neuronal ensembles. Curr Opin Neurobiol 10:180-186.

Szentagothai J (1965) Degeneration patterns in the nervous system, progress in brain research. Amsterdam: Elsevier.

Takashima A, Petersson KM, Rutters F, Tendolkar I, Jensen O, Zwarts MJ, McNaughton BL, Fernandez G (2006) Declarative memory consolidation in humans: a prospective functional magnetic resonance imaging study. Proceedings of the National Academy of Sciences of the United States of America 103:756-761.

Thomson AM, Bannister AP (2003) Interlaminar connections in the neocortex. Cereb Cortex 13:5-14.

Thomson AM, Lamy C (2007) Functional maps of neocortical local circuitry. Front Neurosci 1:19-42.

Thomson AM, West DC, Deuchars J (1995) Properties of single axon excitatory postsynaptic potentials elicited in spiny interneurons by action potentials in pyramidal neurons in slices of rat neocortex. Neuroscience 69:727-738.

Thomson AM, West DC, Wang Y, Bannister AP (2002) Synaptic connections and small circuits involving excitatory and inhibitory neurons in layers 2-5 of adult rat and cat neocortex: triple intracellular recordings and biocytin labelling in vitro. Cereb Cortex 12:936-953.

Timofeev I (2011) Neuronal plasticity and thalamocortical sleep and waking oscillations. In: Progress in Brain Research (Van Someren EJW, Van Der Werf YD, Roelfsema PR, Mansvelder HD, Lopes Da Silva FH, eds), pp 121-144: Elsevier.

Timofeev I, Steriade M (1996) Low-frequency rhythms in the thalamus of intact-cortex and decorticated cats. Journal of neurophysiology 76:4152-4168.

Timofeev I, Steriade M (1997) Fast (mainly 30-100 Hz) oscillations in the cat cerebellothalamic pathway and their synchronization with cortical potentials. The Journal of physiology 504 (Pt 1):153-168.

Timofeev I, Steriade M (1998) Cellular mechanisms underlying intrathalamic augmenting responses of reticular and relay neurons. Journal of neurophysiology 79:2716-2729.

Timofeev I, Bazhenov M (2005) Chapter I: Mechanisms and biological role of thalamocortical oscillations. In: Trends in Chronobiology Research (Columbus F, ed), pp pp. 1-47: Nova Science Publishers, Inc.

Timofeev I, Chauvette S (2011) Thalamocortical Oscillations: Local Control of EEG Slow Waves. Current Topics in Medicinal Chemistry 11:2457-2471.

Timofeev I, Grenier F, Steriade M (2000a) Impact of intrinsic properties and synaptic factors on the activity of neocortical networks in vivo. J Physiol Paris 94:343-355.

Timofeev I, Grenier F, Steriade M (2001a) Disfacilitation and active inhibition in the neocortex during the natural sleep-wake cycle: an intracellular study. Proceedings of the National Academy of Sciences of the United States of America 98:1924-1929.

Timofeev I, Bazhenov M, Sejnowski TJ, Steriade M (2001b) Contribution of intrinsic and synaptic factors in the desynchronization of thalamic oscillatory activity. Thalamus & related Systems 1:53-69.

Timofeev I, Grenier F, Bazhenov M, Sejnowski TJ, Steriade M (2000b) Origin of slow cortical oscillations in deafferented cortical slabs. Cereb Cortex 10:1185-1199.

Timofeev I, Grenier F, Bazhenov M, Houweling AR, Sejnowski TJ, Steriade M (2002) Short- and medium-term plasticity associated with augmenting responses in cortical slabs and spindles in intact cortex of cats in vivo. The Journal of physiology 542:583-598.

Tononi G (2009) Slow wave homeostasis and synaptic plasticity. J Clin Sleep Med 5:S16-19.
Tononi G, Cirelli C (2003) Sleep and synaptic homeostasis: a hypothesis. Brain Res Bull 62:143-150.
Tononi G, Cirelli C (2006) Sleep function and synaptic homeostasis. Sleep Med Rev 10:49-62.
Traub RD, Whittington MA, Stanford IM, Jefferys JG (1996) A mechanism for generation of long-range synchronous fast oscillations in the cortex. Nature 383:621-624.
Traub RD, Schmitz D, Jefferys JG, Draguhn A (1999) High-frequency population oscillations are predicted to occur in hippocampal pyramidal neuronal networks interconnected by axoaxonal gap junctions. Neuroscience 92:407-426.
Traub RD, Buhl EH, Gloveli T, Whittington MA (2003) Fast rhythmic bursting can be induced in layer 2/3 cortical neurons by enhancing persistent Na+ conductance or by blocking BK channels. Journal of neurophysiology 89:909-921.
Traub RD, Spruston N, Soltesz I, Konnerth A, Whittington MA, Jefferys GR (1998) Gamma-frequency oscillations: a neuronal population phenomenon, regulated by synaptic and intrinsic cellular processes, and inducing synaptic plasticity. Prog Neurobiol 55:563-575.
Trussell LO, Zhang S, Raman IM (1993) Desensitization of AMPA receptors upon multiquantal neurotransmitter release. Neuron 10:1185-1196.
Tucker MA, Hirota Y, Wamsley EJ, Lau H, Chaklader A, Fishbein W (2006) A daytime nap containing solely non-REM sleep enhances declarative but not procedural memory. Neurobiol Learn Mem 86:241-247.
Tully K, Bolshakov VY (2010) Emotional enhancement of memory: how norepinephrine enables synaptic plasticity. Mol Brain 3:15.
Turner RW, Meyers DE, Richardson TL, Barker JL (1991) The site for initiation of action potential discharge over the somatodendritic axis of rat hippocampal CA1 pyramidal neurons. J Neurosci 11:2270-2280.
Turrigiano GG (2000) AMPA receptors unbound: membrane cycling and synaptic plasticity. Neuron 26:5-8.
Vanhatalo S, Palva JM, Holmes MD, Miller JW, Voipio J, Kaila K (2004) Infraslow oscillations modulate excitability and interictal epileptic activity in the human cortex during sleep. Proceedings of the National Academy of Sciences of the United States of America 101:5053-5057.
Villablanca J, Salinas-Zeballos ME (1972) Sleep-wakefulness, EEG and behavioral studies of chronic cats without the thalamus: the 'athalamic' cat. Arch Ital Biol 110:383-411.
Volgushev M, Chauvette S, Timofeev I (2011) Long-range correlation of the membrane potential in neocortical neurons during slow oscillation. In: Progress in Brain Research (Van Someren EJW, Van Der Werf YD, Roelfsema PR, Mansvelder HD, Lopes Da Silva FH, eds), pp 181-199: Elsevier.
Volgushev M, Chauvette S, Mukovski M, Timofeev I (2006) Precise long-range synchronization of activity and silence in neocortical neurons during slow-wave oscillations [corrected]. J Neurosci 26:5665-5672.
Volgushev M, Mukovski M, Chauvette S, Timofeev I (2007) Detection of active and silent states in neocortical networks. In: Mechanisms of spontaneous active states in the neocortex (Timofeev I, ed), pp 93-122. Kerala, India: Research Signpost.

von Krosigk M, Bal T, McCormick DA (1993) Cellular mechanisms of a synchronized oscillation in the thalamus. Science (New York, NY 261:361-364.

Vyazovskiy V, Borbely AA, Tobler I (2000) Unilateral vibrissae stimulation during waking induces interhemispheric EEG asymmetry during subsequent sleep in the rat. Journal of sleep research 9:367-371.

Vyazovskiy VV, Tobler I (2008) Handedness leads to interhemispheric EEG asymmetry during sleep in the rat. Journal of neurophysiology 99:969-975.

Vyazovskiy VV, Cirelli C, Tononi G (2011a) Electrophysiological correlates of sleep homeostasis in freely behaving rats. In: Progress in Brain Research (Van Someren EJW, Van Der Werf YD, Roelfsema PR, Mansvelder HD, Lopes Da Silva FH, eds), pp 17-38: Elsevier.

Vyazovskiy VV, Welker E, Fritschy JM, Tobler I (2004) Regional pattern of metabolic activation is reflected in the sleep EEG after sleep deprivation combined with unilateral whisker stimulation in mice. The European journal of neuroscience 20:1363-1370.

Vyazovskiy VV, Riedner BA, Cirelli C, Tononi G (2007) Sleep homeostasis and cortical synchronization: II. A local field potential study of sleep slow waves in the rat. Sleep 30:1631-1642.

Vyazovskiy VV, Cirelli C, Pfister-Genskow M, Faraguna U, Tononi G (2008) Molecular and electrophysiological evidence for net synaptic potentiation in wake and depression in sleep. Nature neuroscience 11:200-208.

Vyazovskiy VV, Olcese U, Hanlon EC, Nir Y, Cirelli C, Tononi G (2011b) Local sleep in awake rats. Nature 472:443-447.

Vyazovskiy VV, Olcese U, Lazimy YM, Faraguna U, Esser SK, Williams JC, Cirelli C, Tononi G (2009) Cortical firing and sleep homeostasis. Neuron 63:865-878.

Wadiche JI, Jahr CE (2001) Multivesicular release at climbing fiber-Purkinje cell synapses. Neuron 32:301-313.

Wagner U, Gais S, Born J (2001) Emotional memory formation is enhanced across sleep intervals with high amounts of rapid eye movement sleep. Learn Mem 8:112-119.

Walker MP, Brakefield T, Hobson JA, Stickgold R (2003a) Dissociable stages of human memory consolidation and reconsolidation. Nature 425:616-620.

Walker MP, Brakefield T, Seidman J, Morgan A, Hobson JA, Stickgold R (2003b) Sleep and the time course of motor skill learning. Learn Mem 10:275-284.

Wallace CS, Withers GS, Weiler IJ, George JM, Clayton DF, Greenough WT (1995) Correspondence between sites of NGFI-A induction and sites of morphological plasticity following exposure to environmental complexity. Brain Res Mol Brain Res 32:211-220.

Walling SG, Harley CW (2004) Locus ceruleus activation initiates delayed synaptic potentiation of perforant path input to the dentate gyrus in awake rats: a novel beta-adrenergic- and protein synthesis-dependent mammalian plasticity mechanism. J Neurosci 24:598-604.

Wang SS, Denk W, Hausser M (2000) Coincidence detection in single dendritic spines mediated by calcium release. Nature neuroscience 3:1266-1273.

Wang XJ (1999) Fast burst firing and short-term synaptic plasticity: a model of neocortical chattering neurons. Neuroscience 89:347-362.

Wang Z, McCormick DA (1993) Control of firing mode of corticotectal and corticopontine layer V burst-generating neurons by norepinephrine, acetylcholine, and 1S,3R-ACPD. J Neurosci 13:2199-2216.

Waters J, Helmchen F (2004) Boosting of action potential backpropagation by neocortical network activity in vivo. J Neurosci 24:11127-11136.

Wester JC, Contreras D (2012) Columnar Interactions Determine Horizontal Propagation of Recurrent Network Activity in Neocortex. The Journal of Neuroscience 32:5454-5471.

Wierzynski CM, Lubenov EV, Gu M, Siapas AG (2009) State-dependent spike-timing relationships between hippocampal and prefrontal circuits during sleep. Neuron 61:587-596.

Williams SR, Toth TI, Turner JP, Hughes SW, Crunelli V (1997) The 'window' component of the low threshold Ca2+ current produces input signal amplification and bistability in cat and rat thalamocortical neurones. The Journal of physiology 505 (Pt 3):689-705.

Wilson MA, McNaughton BL (1994) Reactivation of hippocampal ensemble memories during sleep. Science (New York, NY 265:676-679.

Winer JA, Larue DT (1989) Populations of GABAergic neurons and axons in layer I of rat auditory cortex. Neuroscience 33:499-515.

Wong RK, Prince DA, Basbaum AI (1979) Intradendritic recordings from hippocampal neurons. Proceedings of the National Academy of Sciences of the United States of America 76:986-990.

Wright KP, Lowry CA, LeBourgeois MK (2012) Circadian and Wakefulness-Sleep Modulation of Cognition in Humans. Frontiers in Molecular Neuroscience 5.

Xu-Friedman MA, Regehr WG (2003) Ultrastructural contributions to desensitization at cerebellar mossy fiber to granule cell synapses. J Neurosci 23:2182-2192.

Yen CT, Conley M, Hendry SH, Jones EG (1985) The morphology of physiologically identified GABAergic neurons in the somatic sensory part of the thalamic reticular nucleus in the cat. J Neurosci 5:2254-2268.

Ying SW, Futter M, Rosenblum K, Webber MJ, Hunt SP, Bliss TV, Bramham CR (2002) Brain-derived neurotrophic factor induces long-term potentiation in intact adult hippocampus: requirement for ERK activation coupled to CREB and upregulation of Arc synthesis. J Neurosci 22:1532-1540.

Ylinen A, Bragin A, Nadasdy Z, Jando G, Szabo I, Sik A, Buzsaki G (1995) Sharp wave-associated high-frequency oscillation (200 Hz) in the intact hippocampus: network and intracellular mechanisms. J Neurosci 15:30-46.

Zucker RS, Regehr WG (2002) Short-term synaptic plasticity. Annu Rev Physiol 64:355-405.